LATE QUATERNARY PALAEOENVIRONMENTAL RECORDS FROM THE GEOCHEMISTRY OF SPELEOTHEMS, NORTH-WEST NELSON, NEW ZEALAND

By

JOHN CHARLES HELLSTROM

A thesis submitted for the degree of Doctor of Philosophy of the Australian National University

September, 1998

Statement

The analytical data, interpretations and conclusions presented in this thesis are my own except where otherwise acknowledged. The work is based on research carried out at the Research School of Earth Sciences between October 1994, and September 1998.

John Hellstrom 22/9/98

Acknowledgments

I am grateful to Malcolm McCulloch for his supervision, and for offering myself and this project a place at RSES. His support and advice, and that of my advisers Linda Ayliffe, John Stone and Brad Pillans, has been of great assistance. I particularly thank Brad for steering me in the direction of this project in the first place. I have also benefited from conversations with John Chappell and Michael Bird.

Graham Mortimer, Les Kinsley and Joe Cali have provided me with invaluable training and technical assistance over the course of this project, for which I am most grateful. I also thank Gael Watson for technical assistance, and Mike Shelly for his work on aspects of the RSES LA-ICPMS system that made analysis of speleothem samples possible.

Conversations with my fellow students Jol Desmarchelier, Dan Sinclair, Pyramo Marianelli and Tim Barrows have helped greatly in the formation of a number of the arguments and ideas expressed herein. Jol's collaboration in the development of straw speleothem ICPMS analysis techniques has been particularly helpful. I thank Dan for suggesting many last-minute diversions, particularly in the field of wavelet analysis, and am sorry he will have to keep the slippers.

Removal of core samples from deep vertical caves was a difficult task, and would have been impossible without assistance from members of Victoria Cavers, the National University Caving Club, and Wellington Caving Group. The New Zealand Department of Conservation are thanked for their permission to remove speleothem samples from what is now Kahurangi National Park, as are the Institute of Geological and Nuclear Sciences for their help in supplying a replacement core drill at very short notice.

Finally, many thanks to Jenny O'Connell, Sherry Mayo, Mark Bown and Linda Ayliffe for help with proofreading.

Abstract

A detailed investigation of speleothems from beneath Mt Arthur, in the northwestern corner of New Zealand's South Island gives considerable insight into the nature of environmental changes there, over the last 31,000 years. In particular, a flowstone core sample, MD3, from Nettlebed cave is found to have grown continuously over the last 31,000 years, and provides detailed records of changes in local temperature, precipitation, and forest productivity, and the extent of South Island glaciation.

It is argued that the ^{18}O content, $\delta^{18}O$, of these speleothems changes in response to a number of environmental parameters, most notably to changes in the intensity of westerly atmospheric circulation over the Tasman Sea, and thus is a proxy indicator of periods of conditions favourable for glacier advance. The ^{13}C content, $\delta^{13}C$, has been very strongly influenced by changes in organic activity above the cave, and thus of forest extent, shown to closely follow changes in local temperature.

Trace element concentration changes in speleothems are shown to be useful indicators of palaeoenvironmental change. In particular, barium is found to closely correspond to changes in the $\delta^{13}C$ record, and thus to the environmental parameters that $\delta^{13}C$ reflects. The concentration of magnesium, and the ratios of uranium and strontium isotopes, are found to vary in response to groundwater residence times above the cave, and thus are a proxy for past changes in the amount of precipitation.

The temperature at Mt Arthur is found to have increased very suddenly from glacial to warm Holocene conditions at 15,000 cal yr B.P., coincident with the same event in Greenland. There is no temperature depression associated with the Younger Dryas-aged event recorded in the speleothem record. A glacier advance at this time is instead attributed to increased precipitation and westerly winds. A sudden increase in precipitation at 13,000 cal yr B.P. reflects warming of the Southern Ocean at this time.

Laser-ablation ICPMS analysis is tested as a means of investigating very fine-scale changes in speleothem trace element concentrations. "Soda straw" stalactites are found to contain cyclic variations in their trace element concentrations, in phase with annual banding sometimes visible on their surfaces, indicating their potential use in constructing annually-resolved climate records.

Table of Contents

Chapter 1. Introduction

It is generally accepted by researchers in the field of Quaternary palaeoclimatology that the climate of the last few hundred thousand years has been dominated by a series of glacial-interglacial cycles (e.g., Broecker and Denton, 1989; Imbrie *et al.*, 1993b; Winograd *et al.*, 1992). Much remains to be understood about the processes behind these cycles, a knowledge of which is critical to our interpretation of the workings of the earth's climate, and consequently our ability to predict future change. Ongoing research is focussed on determining the timing, magnitude and global extent of individual events during this period, in order to constrain, and test, the various models which attempt to explain Quaternary climate change.

Quaternary climate change is currently thought by most researchers to be largely driven by changes in oceanic circulation and ice cover in high northern latitudes, in particular in the North Atlantic (e.g., Broecker, 1994; Keigwin and Jones, 1994; Koç and Jansen, 1994). Consequently, much research has focused on that region, where the relationships between terrestrial and marine climate change now appear to be relatively well understood over the last glacial cycle of 120,000 years or so. Outside of this region, and particularly in the Southern Hemisphere, long duration Quaternary climate records are considerably fewer, and often of lower temporal resolution. In particular, there are few published terrestrial records capable of addressing the exact nature and timing of climate changes such as the termination of the last glaciation to precisions of better than a few thousand years.

New Zealand, an island group in the south-west Pacific Ocean, centred on ca. 41°S, has a strongly maritime climate, which is representative of mid-latitude Southern Hemisphere climate generally (Pillans, 1991; Salinger, 1983). Terrestrial records of environmental change from these islands are thus likely to provide significant insights into the history of hemispheric, and possibly global, climate. By utilising the extremely precise chronology afforded by U-series dating of speleothems, and the detailed palaeoenvironmental records

that they often contain, the aim of this study is to improve our knowledge of late Quaternary climate change in New Zealand and the Southern Hemisphere, and thus to provide new constraints on the nature of global Quaternary climate.

Global Quaternary palaeoclimate

Current theories of climate change

Foremost amongst recent explanations of Pleistocene glaciation is the Milankovitch theory of orbitally induced climate change (Hays *et al.*, 1976; Imbrie *et al.*, 1984; Milankovitch, 1930). This theory proposes that global climate is directly controlled, or at least very strongly influenced by, periodic variations in summer solar insolation at high northern latitudes. The Northern Hemisphere is considered to play the dominant role in controlling global temperature, on the basis that the combined ice cover of Antarctica and other southern land masses has not significantly changed in extent over the Quaternary. In contrast, the Northern Hemisphere continental landmasses, currently largely ice-free, potentially exert immense control over global temperature, albedo and sea level. Cooling of these land masses in response to an initial reduction in insolation is expected to lead to an increase in snow and ice cover, and thus increased albedo, so providing a positive feed-back leading to the build-up of extremely large continental ice sheets in high northern latitudes. Support for the Milankovitch theory comes from the similarity of records of global ice volume, as reconstructed from records of oxygen isotope variation in deep-sea cores, to insolation at 65°N reconstructed from known orbital variations (Imbrie *et al.*, 1992; Martinson *et al.*, 1987).

Unfortunately, support for this theory is often of a somewhat circular nature, as the ocean cores from which most support for this hypothesis is derived generally lack any independent chronology. They are generally dated by "tuning" to known orbital variations, on the assumption that those orbital variations are directly responsible for the isotope variations recorded in the cores (e.g., Black *et al.*, 1988; Martinson *et al.*, 1987). Independently dated

chronologies are few, and are variable in their support of this theory. The Devil's Hole vein calcite record (Winograd *et al.*, 1992), for instance, one of few long records with a reliable independent chronology (Ludwig *et al.*, 1992), provides little support for Milankovitch theory, although the significance of this is disputed (Imbrie *et al.*, 1993b). Conversely, there is excellent support for the orbital hypothesis from the Vostok Ice Core, in the form of atmospheric oxygen isotope variation (Jouzel *et al.*, 1993), although the Vostok chronology is by comparison less reliable, and has been tweaked such that it supports an orbital chronology (Jouzel *et al.*, 1996).

The Milankovitch theory predicts as a basic premise that global climate change is driven from high northern latitudes, and thus requires that consequent change elsewhere on earth should be subject to some degree of lag and attenuation. One problem that the theory does not easily explain, is that temperatures in the Southern Hemisphere appear to cool by similar amounts to Northern Hemisphere temperatures during glacial periods, and appear to do so in a roughly synchronous fashion (e.g., Hendy and Hendy, 1997). This is despite apparently much smaller temperature changes in the tropics during the same periods, raising the question of how Northern Hemisphere cooling might propagate to the Southern Hemisphere (Broecker and Denton, 1989). Investigation of the precise timing of major climatic events, such as the glacial terminations, between the two hemispheres is a powerful way of testing the Milankovitch theory - to date there are few published records of sufficient precision to allow this, particularly in the Southern Hemisphere. The antarctic ice cores (Blunier *et al.*, 1998) are notable exceptions.

Broecker and Denton (1989) argued that the apparent global synchroneity, and hemispheric symmetry, of global glaciation precludes orbital variation as a dominant direct control on Quaternary palaeoclimate. Instead, they proposed sudden changes between glacial and interglacial climate to be caused by rapid shifts between two stable modes of the global ocean-atmosphere system, which are probably modulated by insolation-driven changes in Northern Hemisphere seasonality. Pivotal to this theory is the role of the global thermohaline oceanic circulation (e.g., Broecker *et al.*, 1985;

Keigwin *et al.*, 1994), particularly as manifested in the North Atlantic ocean. Thermohaline circulation occurs where dense, super-chilled brines, produced during the formation of sea-ice, sink and flow equator-ward over the sea floor, inducing relatively warm water to be drawn pole-ward on the surface of the ocean. This "oceanic conveyor belt" is credited with significantly warming the high latitudes of the Northern Hemisphere, and, were it to slow or stop, could result in severe climate change in that region.

It has been proposed that much of the sudden change seen in North Atlantic palaeoclimate, recorded in the ocean as Heinrich events (Heinrich, 1988) and in ice cores as Dansgaard-Oeschger events (Bond *et al.*, 1993), has been caused by massive discharges of icebergs and melt-water there (Broecker, 1994; Lindstrom and MacAyeal, 1993). While the most profound effects of these events would have been felt locally, their effect of inhibiting the formation of North Atlantic Deep Water (Broecker and Denton, 1989), and thus their effect on Atlantic and global thermohaline circulation, would have had global ramifications. So, it can be seen that instabilities of Northern Hemisphere ice sheets may have had significant influence on global climate changes. Other suggested causes of glacial-interglacial climate change have included significant changes in atmospheric content of water vapour, and of dust (Thompson *et al.*, 1995), which heat and cool the earth respectively.

Existing records of global climate change

What could now be called the traditional view of Quaternary climate change, centred about the Milankovitch theory, is focussed on, and gains most support from, oxygen isotope analysis of foraminifera obtained from deep ocean cores distributed about the globe (e.g., Chappell and Shackleton, 1986; Imbrie *et al.*, 1993a). Generally, these data are "tuned" to the earth's orbital frequencies, as in most cases independent chronologies are not easily obtainable. While such records have been instrumental in constraining the history of global ice cover over hundreds of thousands to millions of years, they are rarely useful in addressing fine-scale climatic changes, or indeed in investigating the precise timing of major events such as glacial terminations.

This is due to a combination of factors related to most ocean cores, including bioturbation, coarse sampling rate, and temporal aliasing in the sampled data (Broecker, 1986).

In addition to these marine data, there are many sources of data on terrestrial climate change over the Quaternary. Unfortunately, with the exception of ice core records, it is rare for terrestrial data to be temporally continuous to anything approaching that of records from marine cores. Coupled with their relatively discontinuous nature, terrestrial records have also often suffered from poor chronologies, making precise reconstruction of the nature and timing of climatic events such as the Younger Dryas in many cases very difficult. This is despite the presumably large impact left by these events on the terrestrial environment (Wohlfarth, 1996). Some excellent terrestrial records have been produced, often from loess stratigraphy or from uplifted marine terrace sequences, but these usually still suffer from inadequate resolution with respect to differentiating between the different climate models addressed above. Pollen records have much potential, as strong palaeoenvironmental inferences can be derived from them, but, particularly in the Southern Hemisphere, they generally suffer from low resolution sampling, and are often sparsely dated.

A third class of existing climate records is that of ice cores, which, with few exceptions are from the polar ice sheets of Greenland and Antarctica. These records enjoy extremely high resolution, and mostly span tens to hundreds of thousands of years (e.g., Greenland Ice-core Project Members, 1993; Lorius *et al.*, 1985). In the case of the Greenland cores, extremely good chronologies have been produced back to 15,000 years or so by annual layer counting (Stuiver *et al.*, 1995). Beyond this age they are based on less accurate ice flow models, as are most Antarctic ice cores over their entire lengths (Dansgaard *et al.*, 1993, but see also Blunier *et al.*, 1998). The few ice core records available from temperate regions (Thompson, 1998; Thompson *et al.*, 1995) do not extend as far back in time, and generally suffer from poorly constrained ages. Interpretation of isotopic data from tropical ice cores is more ambiguous than

is the case for polar cores, although considerable effort is being invested into calibrating these records against modern data (Thompson, 1998).

The Northern Hemisphere high-resolution records

As investigation of the global cycles of Pleistocene glaciation has focussed on high northern latitudes, particularly in the North Atlantic region, where there are now detailed records of marine and terrestrial palaeoclimate. Not only are these records often extremely detailed (e.g., McManus *et al.*, 1994), but in many cases they have extremely precise chronologies, particularly where counting of annual rings or layers is possible, as is the case for the Greenland ice cores and for some varved sediment records. In addition to this, many marine and terrestrial records have detailed radiocarbon chronologies (e.g., Bard *et al.*, 1987), which as a result of increasingly well defined calibration curves, may now be considered in absolute terms. These high-resolution records, particularly those spanning the period since the last glacial maximum, show major climatic events, particularly Dansgaard-Oeschger events, to have been regionally synchronous, implicating instabilities in large ice bodies as a catalyst of major changes in climate (Bond *et al.*, 1993).

Speleothem records

A class of terrestrial records, which appear to have much unrealised potential, are those derived from speleothems. As these records are described in great detail elsewhere in this work, only a brief synopsis of their implications on a global basis follows. In Europe, speleothem growth rates have been linked to known sequences of both short and long-term climate change, by assuming that very cold or dry conditions must inhibit speleothem growth (Baker *et al.*, 1995; Baker *et al.*, 1993b; Henning *et al.*, 1983). These studies, while conforming to what is known from other sources, have as yet been of little use in further refining this knowledge. In general, despite arguably having great potential, speleothems cannot be said to have contributed greatly to the study of Quaternary climate, except where they have been put to use in dating other records. These include glacial deposits (Williams, 1996), uplifted marine

terrace sequences (Williams, 1982), and where they have been used to constrain the history of sea-level changes (e.g., Li *et al.*, 1989; Richards *et al.*, 1994).

Southern Hemisphere palaeoclimate

Climatic changes in the Southern Hemisphere are generally far less well constrained than is the case in the Northern Hemisphere, as the available marine and terrestrial records of climate change over this period are mostly of comparatively low resolution, and are relatively few in number. The only currently available high-resolution records continuous over tens of thousands of years are from Antarctic ice cores (e.g., Lorius *et al.*, 1985), which indicate that Antarctic climate broadly covaried with North Atlantic climate over the last glacial cycle, but did not show the short-duration events seen there. This implies that the Antarctic is buffered from transient shifts in Northern Hemisphere climate (Dansgaard *et al.*, 1993), leaving open the question of whether climate change in central southern latitudes is more closely related to that in the Northern Hemisphere, or to that experienced by Antarctica. This question is crucial to our understanding of the mechanisms behind Pleistocene climate change (Broecker *et al.*, 1985), in that it can directly address the question of lag and smoothing of climatic signals between the hemispheres.

There is a clear need for high-resolution, well-dated records of climate change from the largely marine Southern Hemisphere. Results from Southern Hemisphere continental land-masses show temperatures to have been considerably lower during the last glacial maximum (LGM) than they are today, (e.g., Miller *et al.*, 1997; Thompson *et al.*, 1995). However, the extent to which continental climate was influenced by local factors, such as greatly increased aridity, is unclear. In contrast, records from regions dominated by a maritime climate might be expected to show variations more representative of marine, and thus hemispheric, climate change (Salinger, 1983).

The Younger Dryas

In trying to determine the global extent and influence of the well-documented northern climate change sequence, attention has focused on the Younger Dryas event, a distinctive cold event centred in the North Atlantic region, that occurred from 12,900 to 11,700 cal yr B.P. (Stuiver *et al.*, 1995). Currently there is much debate as to how, if at all, this event was manifested in the Southern Hemisphere (e.g., Clapperton *et al.*, 1997; Denton and Hendy, 1994; Hansen, 1995). The records from ocean cores are generally of too low a resolution to address this question, and the temperate terrestrial records usually lack continuity over this period. The Antarctic Cold Reversal (ACR) is a cold event seen during the last deglaciation in Antarctic ice core records (Jouzel *et al.*, 1992), and has often been associated with the Younger Dryas, although their temporal relationship has been uncertain (Jouzel *et al.*, 1993). Recent attempts to calibrate the chronologies of Antarctic ice cores to Greenland ice cores by comparison of atmospheric gas records have yielded considerably more precise Antarctic chronologies, which show the ACR to have preceded the Younger Dryas by several centuries (Blunier *et al.*, 1998).

The last glacial termination

Another event that can be identified in many climate records is Termination I, the end of the last glaciation (Wohlfarth, 1996), the relative timing of which around the world is also of critical importance, and has yet to be convincingly dated in the Southern Hemisphere. The first appearance of organic sedimentation in pollen records from New Zealand and South America is often taken as corresponding to this event (e.g., Singer *et al.*, 1998; Heusser and Rabassa, 1987). Unfortunately, this is often not sufficiently accurate to give a precise chronology, or to address how rapid the changes were. Excellent coral records exist for the sudden sea level rise associated with this event (Blanchon and Shaw, 1995; Chappell and Polach, 1991), but the record of terrestrial temperature change over this period, particularly in the temperate Southern Hemisphere, is limited.

The last glaciation

Extreme variations of temperature inferred from Greenland Ice cores during the last glaciation are also seen in North Atlantic oceanic cores (Keigwin and Jones, 1994), but are considerably less pronounced (especially for periodicities of under 5,000 yr) in the Antarctic Vostok ice core (Dansgaard *et al.*, 1993). Corresponding variations are not evident in most oceanic cores, presumably because both ice volume and deep ocean temperature are buffered from rapid change. A question which must be addressed in the temperate Southern Hemisphere is thus the degree of climatic variation that occurred during this period, and whether it coincided with the northern Hemisphere variations. Whilst evidence in the Southern Hemisphere is of many glacial advances (e.g., Burrows, 1979; Suggate, 1990), it is not known to what extent those advances can be correlated on a regional, let alone hemispheric basis, nor is the degree to which climate ameliorated between individual advances.

New Zealand as a recorder of hemispheric climate change

The islands of New Zealand are well-positioned to record the effects of mid-latitude climate change in the Southern Hemisphere, as they lie across 13° of latitude, including the oceanic Subtropical Front (STF; e.g., Belkin and Gordon, 1996) and the associated subtropical high and westerly wind belt (Sturman and Tapper, 1996). New Zealand's weather is dominated by the westward movement of low pressure systems over the Tasman Sea, and is sensitive to changes in the nature of this movement (Salinger, 1983). As such, terrestrial records of climate change from New Zealand can be expected to reflect changes in regional maritime climate, itself presumably responding to changes in the general climate of central southern latitudes (Gordon, 1985).

The Subtropical Front

The Subtropical Front separates the Subtropical Water in the north, from the Subantarctic Water in the south. It passes beneath both Tasmania and Stewart Island, and bows to the north in the Tasman Sea, currently as far as 44°S

(Heath, 1985). To the east of New Zealand, it follows the bathometric high of the Chatham Rise, and continues beyond into the Pacific Ocean. In modern times, latitudinal changes in the position of the STF are correlated with changes in the strength of the prevailing south-westerly winds reaching southern New Zealand, and with changes in precipitation and temperature in the western South Island (Fitzharris *et al.*, 1992). Northward movement of the STF, such as occurs during an El Niño phase of the Southern Oscillation, causes wind and precipitation in the western South Island to increase, and temperatures there to drop. Such conditions have been shown to greatly favour glacial advance in the Southern Alps (Gellatly and Norton, 1984; Hessell, 1983), dramatically illustrated by the advance of the South Island's West Coast glaciers during the 1990s in response to persistent El Niño conditions.

To explain reconstructed terrestrial palaeoclimates for the last glaciation in New Zealand, it has been argued by a number of researchers investigating Quaternary palaeoclimate in New Zealand (e.g., Fenner *et al.*, 1992; McGlone *et al.*, 1993), that the STF in the Tasman Sea moved several degrees to the north during the last glacial maximum. In contrast to previously published interpretations of ocean core oxygen isotope records from around New Zealand (Head and Nelson, 1994; Nelson *et al.*, 1994), it has recently been shown that deep sea cores in the Tasman Sea strongly support the idea that the STF moved to the north during the LGM (T. Barrows, in preparation). This implies that its modern relationship to climate and glacier mass balance in the western South Island is also applicable throughout the late Quaternary.

The potential of speleothems from North-West Nelson

North-West Nelson, which is almost entirely incorporated into the Kahurangi National Park, is a region of several hundred thousand hectares occupying the north-western corner of the South Island. Its climate is similar to that of the West Coast (Garnier, 1958), in that it is a mountainous region to which the prevailing westerly weather arrives from the Tasman Sea. Mt Arthur is a peak of 1795 metres, located 50 km from the coast, and is underlain by some

of New Zealand's largest and deepest cave systems (Ravens, 1986; Ravens, 1992). It shall be argued herein that the climate of Mt Arthur is essentially a maritime one, and that any palaeoclimate records obtained from its caves will reflect changes predominantly in maritime climate, and hence will be of regional significance.

Two of Mt Arthur's cave systems, both over 20 km in length, have been found to contain in places massive speleothems, assumed to have grown continuously over tens to hundreds of thousands of years. This project concentrates on core samples taken from speleothems in each cave, in both cases in ancient, stable passages at depths of 200 metres below the surface. It will be shown that geochemical variations in these speleothems contain records of local palaeoenvironmental conditions, spanning tens of thousands of years, that provide constraints on the timing and magnitude of regional climatic events.

Summary - Aims of this project

The primary objective of this endeavour is to produce well-dated, continuous and high-resolution records of palaeoenvironmental change spanning the last few tens of thousands of years, by measurement and interpretation of geochemical variations preserved within speleothems from North-West Nelson, New Zealand. From these records, it is shown that additional constraints can be placed on the mechanisms by which global climate changes might occur on a glacial-interglacial basis, principally through reducing uncertainties in the relative timing and magnitudes of such changes between the Northern and Southern Hemispheres. In this study emphasis is placed on oxygen isotope stages 1 and 2, spanning the last ca. 27,000 years, the periods best constrained by existing climate records in both hemispheres.

Chapter 2. Speleothems as environmental recorders

Introduction

Speleothems, secondary calcite deposits formed in caves, have long been used to infer climate histories. Initial attention was centred on making climatic inferences from their geographic distribution, and from their physical mineralogy, but this was hampered by a lack of real understanding of the timespan over which they had grown. Relatively accurate dating of speleothems, at first by the radiocarbon method, and more recently using uranium-series disequilibria, has since allowed changes in cave, and thus external, environments to be investigated as a function of time. Palaeoenvironmental changes are recorded versus time in speleothems by a number of variables, most notably by changes in their trace element and stable isotopic compositions.

Speleothems are capable of continuous growth over tens, or theoretically hundreds, of thousands of years. As they can now be dated extremely accurately, back to several hundred thousand years before present, they are of particular interest in studies of Quaternary climate variation. A disadvantage of speleothems, common to many other recorders of Quaternary environmental variation, is that as yet no quantitative method of resolving palaeoenvironmental changes in variables such as temperature versus time has been developed. Regardless of this, because speleothems can now be so accurately dated, qualitative records of environmental change can be constructed as a function of time, potentially allowing the timing of specific events such as the last glacial maximum to be precisely determined.

The development of laser-ablation analysis techniques, with spatial resolutions currently as low as five microns, potentially allows records of environmental change to be constructed over monthly or even weekly timescales for some speleothems. This method also allows autocalibration dating, that is, dating by counting of annual cycles along a speleothem

(Roberts *et al.*, 1998). This enables very young speleothems to be compared with the relatively short modern instrumental record of climate change, and thus they may be used to extend this record into prehistory.

Growth of speleothems

Speleothems (Moore, 1952) are secondary mineral formations, usually calcite ($CaCO_3$), found in natural caves. While speleothems have been observed in other situations, the vast bulk of them are formed in caves found in carbonate parent rock, specifically in limestones and marbles. Speleothems are formed by aqueous dissolution and precipitation of calcium carbonate, from the limestone parent rock into the cave below.

As water sinks through the soil above a cave, it absorbs CO_2 and equilibrates with the elevated CO_2 levels found in the soil atmosphere, forming weak carbonic acid. The acidified water then reacts with calcium and carbonate ions from carbonate rock below the soil horizon (Schwarcz, 1986):

$$CaCO_3 + CO_2 + H_2O \leftrightarrow Ca^{2+} + 2HCO_3^- \qquad (2.1)$$

The acidified water sinks through the porous host rock, usually being fully saturated with carbonate by the time it enters a cave below. On contact with the cave atmosphere, which generally has a similar CO_2 concentration to that of outside air (Hendy, 1970) the seepage water loses CO_2 as it moves towards equilibration with the cave air. In losing CO_2, the equilibrium in the seepage water shifts in favour of solid carbonate (equation 2.1), causing the deposition of calcite from the water onto surfaces within the cave (fig. 2.1). Thus, over time, speleothems build up in layers, each layer corresponding to a specific time horizon.

Following from this, it can be seen that speleothems will generally only form beneath soils where sufficient vegetation exists to elevate soil CO_2 levels, and where water is able to seep to the cave below, (e.g., Baker *et al.*, 1993b).

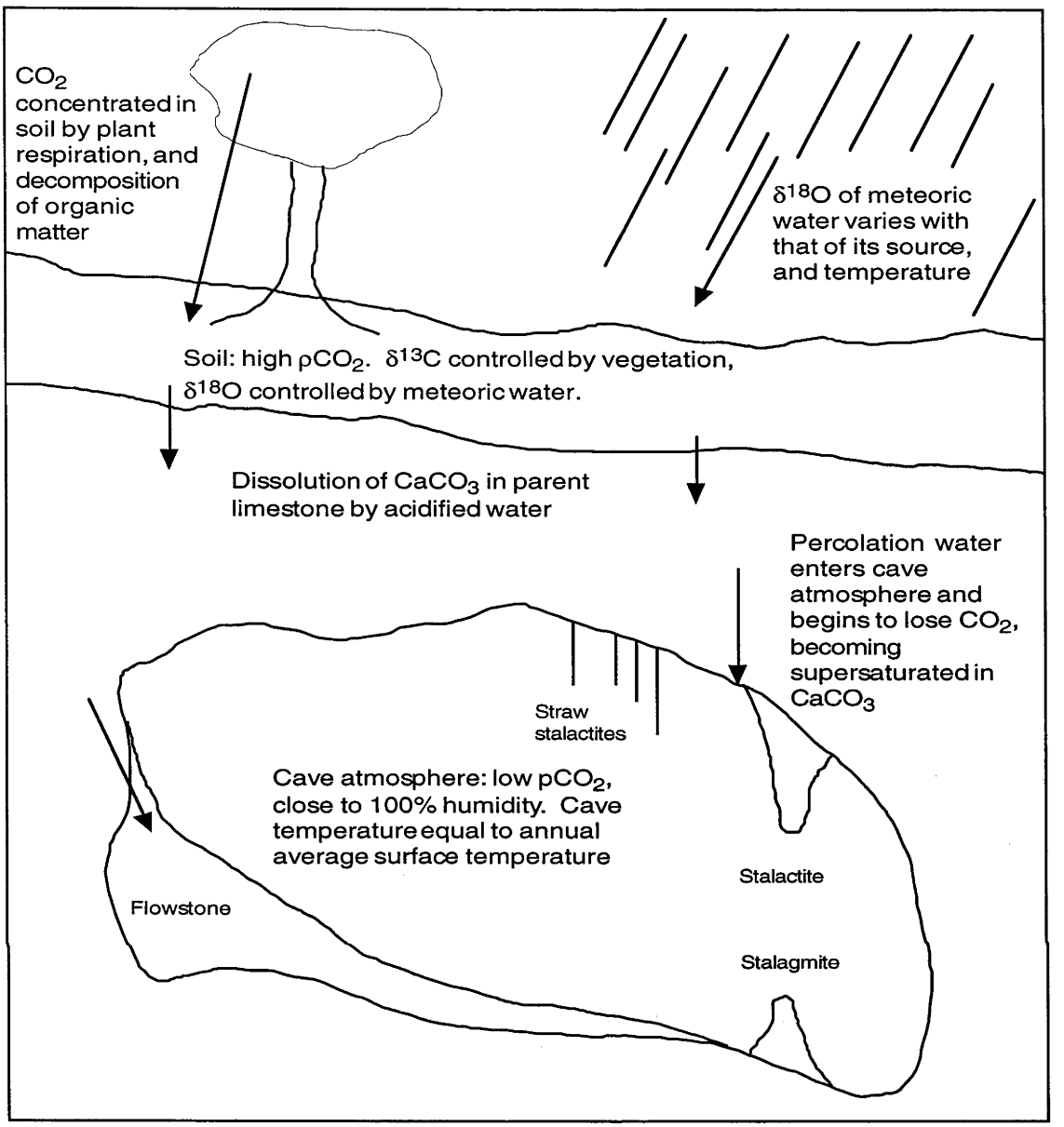

Fig. 2.1. A schematic diagram of the processes associated with the formation of speleothems. Cave environments are very stable compared to those on the surface above them. Changes in the stable isotope and trace element geochemistry of speleothems are predominantly the response of seepage water chemistry to changing conditions on the surface and in the soil.

Alternative mechanisms by which calcite speleothems might form have been proposed (e.g., Dreybrodt, 1982), but are not considered significant in the context of this work.

The morphology of calcite speleothems varies greatly, being directly dependent on the nature of the water flow from which they are deposited. Stalactites form where water seeps from cracks or pores in the cave ceiling, and at first generally take the form of "straws," which resemble thin glass tubes, formed by progressive addition of calcite as water drops ooze from a growing tip. Blocking of the central conduit of a straw leads to water flow over its exterior causing thickening, ultimately to form a classic, tapered, stalactite. Stalagmites form where a drip stream from above meets the cave floor, sometimes growing up to the point where they form a continuous column with a paired stalactite from above. Flowstones are an important variety of speleothem growth, forming where a film of water flows over an area of a cave wall or floor. There are many other speleothem morphologies, comprehensively reviewed in Hill and Forti (1997), and not discussed here.

History of speleothem research

Research before 1900 AD (abridged from Shaw, 1992)

As early as the first century AD, classical scholars thought that speleothems formed through the petrification of seeping water. There was little advancement on this until the 16th and 17th centuries, when various theories converged about solidification of some material carried in the flowing water. Over the following two centuries it was realised first that the calcite was somehow carried in solution in the water, and finally, in 1812, that carbonic acid was responsible, via the chemistry of equation 2.1. Other theories came and went over this time too, such as formation by plant-like vegetative growth.

Palaeoenvironmental inferences from speleothems were few prior to the 20th century, being limited to discussion of the effects of changes in the surface

vegetation, and of air circulation within the cave, on speleothem growth rate. The growth rate of speleothems itself received much attention, particularly during the 19th century, as it was rightly thought to have considerable implication for the antiquity of the earth. Despite much investigation, the only conclusion was that speleothem growth rates are greatly variable.

Speleothem research since 1900

Allison (1923) measured the growth of stalactites and their corresponding stalagmites beneath a cement ceiling in a United States mine, deducing a set of rules by which a speleothem's age might be inferred from its physical dimensions. Unfortunately, the chemistry by which calcite forms beneath concrete is very different from that which governs the growth of speleothems, and he overestimated growth rates by a factor of 25 or more (Moore, 1962). Since this time, little attempt has been made to estimate the ages of speleothems based only on their physical size, and growth rate can be shown to be highly variable, even for a single speleothem (e.g., Harmon *et al.*, 1978b).

Moore (1956) found evidence to suggest that aragonite speleothems currently form only in warm areas of the United States, and concluded that the presence of fossil aragonite speleothems in colder regions demonstrated climate there to have once been warmer than today. Subsequent work, however (Siegel and Dort, 1966), suggests aragonite speleothems are formed in dry, rather than warm, cave air. While still suggesting the presence of aragonite might be a useful palaeoclimatic indicator, this research was apparently not followed up.

The first measurement of long-term speleothem growth rates was by Broecker *et al.* (1960), who used radiocarbon dating to show a stalagmite had grown at an average 60 microns per year over a 1,400 year period. Many other authors have since used radiocarbon dating to estimate ages and growth rates of speleothems, although this method is subject to error in speleothems due to incorporation of ancient carbon at time of formation (this issue was comprehensively examined by Hendy, 1970).

Rosholt and Antal (1962), made the first attempts to date speleothems using the $^{230}Th/^{234}U$ method, but these met with little success, and until 1970 it was generally thought that speleothems were unsuitable for uranium-series dating (Gascoyne, 1984). Duplessy *et al.* (1970) first reported successful uranium-series ages (by alpha spectrometry), and by 1983 at least 660 such dates had been published by many researchers. Using these, Henning *et al.* (1983) were able to estimate the timing of major events in the last glacial/interglacial cycle, by assuming periods of low or zero speleothem formation to correspond to glacial periods.

Hendy and Wilson (1968) first used the stable isotope ratios of oxygen and carbon in speleothems as a proxy for past climate, and presented a record of temperature versus time during the late Pleistocene, constrained by 5 radiocarbon ages. Although many similar papers have been published since, the "preliminary" data of Hendy and Wilson, from two speleothems in the North Island of New Zealand, still comprise one of the clearest and most significant speleothem records reported. Recognising that extraction of quantitative temperature histories from speleothem stable isotope data may not be possible, attempts have been made (e.g., Harmon and Schwarcz, 1981; Harmon *et al.*, 1979; Schwarcz *et al.*, 1975) to supplement this data with isotopic analyses of fluid inclusions trapped within the speleothem calcite. As yet these studies have met with little success, however recent work by Rowe *et al.* (1998) and others suggests this method may yet develop to the point where it can produce quantitative temperature records.

A field in which speleothems have been used to place quantitative constraints on Quaternary environmental changes is the study of past sea levels. Spalding and Mathews (1972) used uranium-series and radiocarbon ages of currently submerged speleothems to show that sea-level 22,000 years ago was at least 37 feet lower than present. Since then many other dates have been published from submerged speleothems (e.g., Richards *et al.*, 1994), constraining maximum sea-level, and providing a complimentary method to the dating of corals (e.g., Chappell, 1983; Edwards *et al.*, 1993) as indicators of minimum sea-level.

Thermal ionisation mass spectrometry was applied to uranium-series dating of speleothems by Li *et al.* (1989), significantly improving the precision and range of the method. Other dating methods, such as electron spin resonance (e.g., Geyh and Henning, 1986), amino acid racemisation (Lauritzen *et al.*, 1994), thermoluminescence (Wintle, 1978) and palaeomagnetism (e.g., Latham *et al.*, 1979; Morinaga *et al.*, 1985) have also been applied to speleothems, with varying degrees of success.

Gascoyne, (1983) proposed using temporal variations in the trace element concentrations (particularly of magnesium) of speleothems as a palaeothermometer, but recognised that the method faced considerable difficulties. Goede (1994) found agreement between magnesium content and the carbon isotopic composition of a Tasmanian speleothem, but considered magnesium unsuitable as a speleothem palaeothermometer. Roberts *et al.* (1998) recently reported annually banded trace element variations in a Holocene speleothem, and speculated that it might become a powerful new tool for autocalibration dating.

Speleothem research has also proceeded on a number of other fronts. Lauritzen *et al.* (1990) used pollen and soot extracted from a Norwegian speleothem as indicators of palaeoenvironmental variation. Annual banding, as well as longer period variations, in the ultra-violet luminescence of speleothems has been reported by Baker *et al.* (1993a), and Shopov *et al.* (1994). Both groups speculated that this might eventually allow autocalibration dating of speleothems, producing calender ages for late Holocene samples. Visible annual banding has been reported in some speleothems (Genty *et al.*, 1996), and is apparently visible with the naked eye in straw stalactites from both New Zealand and Tasmania (this work; J. Desmarchelier, unpublished data).

While speleothems occur in a stunning array of forms (Hill and Forti, 1997), attention so far has focussed largely on records from single stalagmites, for which discontinuous growth is a potential problem. Stalagmites are usually fed by single drips, and are thus sensitive to microscale changes in the paths

taken by seepage waters, which can conceivably cause discontinuous growth independent of any variations in external climate. By contrast, flowstones, massive sheet speleothems which form on cave walls and floors, are often fed by many independent sources of seepage water, and thus are more likely to grow continuously over long periods of time. To date, few records have been published from flowstones, due partly to the relative ease of recovering stalagmite samples from caves.

Uranium-series dating

Uranium-series dating of speleothems is achieved by measuring disequilibria of the ^{238}U-^{234}U-^{230}Th decay chain. This is made possible by the extremely low solubility of thorium, and the relatively high solubility of uranium, in cave seepage waters. The method thus assumes that uranium is incorporated into speleothems as they are precipitated from cave percolation water, but that thorium remains in the weathering zone of the host limestone, and is not incorporated into speleothems (e.g., Gascoyne, 1984; Schwarcz, 1989). Following from this assumption, any ^{230}Th present in a speleothem at a given time, should have originated from the decay of its parent uranium isotopes, over the life of that speleothem.

Measurement of the relative concentrations of ^{230}Th, ^{234}U and ^{238}U allows the determination of a speleothem's age, for speleothems younger than several hundred thousand years, using the equation (Schwarcz, 1986):

$$\left[\frac{^{230}Th}{^{234}U}\right]_{act} = \left[\frac{^{238}U}{^{234}U}\right]_{act}\left(1-e^{-\lambda_{230}t}\right)+\frac{\lambda_{230}}{\lambda_{230}-\lambda_{234}}\left(1-\left[\frac{^{238}U}{^{234}U}\right]_{act}\right)\left(1-e^{-(\lambda_{230}-\lambda_{234})t}\right) \quad (2.2)$$

where λ_{234} and λ_{230} are the decay constants of ^{234}U and ^{230}Th, respectively, and *act* denotes activity ratio. This form of the ^{238}U-^{234}U-^{230}Th age equation is commonly used where the activity ratios have been determined by α-spectrometry (c.f. equation 5.1). Before calculating an age using the ^{238}U-^{234}U-^{230}Th method, the ^{232}Th content of the speleothem is also examined, as ideally there should be none of this isotope present (^{232}Th not being a decay product

of any natural isotope). Speleothem ^{232}Th can only have been derived from a detrital (usually silicate) contaminant phase, and if present must have been accompanied by some amount of ^{230}Th at the time of deposition, potentially negating the assumptions on which this dating method is based. Detrital contamination of the measured ^{230}Th in a sample has normally been considered a problem if the $^{230}Th/^{232}Th$ activity ratio is less than 20 (Schwarcz, 1989), although the increased precision of mass-spectrometric dating has required re-evaluation of this figure.

Due to the asymptotic nature of equation 2.2, it is not possible to accurately determine U-series ages of much more than 500,000 years, even when measurement of the uranium-series isotopes is made using a thermal ionisation mass spectrometer. The ^{238}U-^{234}U-^{230}Th method is commonly used for dating of marine corals, which typically have uranium contents in excess of 2000 ppb. By contrast, speleothems, commonly containing uranium at a few tens to a few hundreds of parts per billion (Gascoyne, 1984; Schwarcz, 1989), are difficult to analyse and generally produce less precise ages. Two-sigma errors of a few percent are commonly reported for TIMS dates of speleothems.

Application

The most prevalent application of U-series speleothem dating has probably been in the investigation of the temporal distribution of speleothem growth periods (e.g., Atkinson *et al.*, 1986; Baker *et al.*, 1995; Harmon *et al.*, 1977; Thompson *et al.*, 1974; Thompson *et al.*, 1976). By assuming that speleothems grow only when sufficient vegetation and water exist on the surface above, it is possible to define periods of relative dryness, or of ice sheet cover above the cave, based on periods of low or zero speleothem growth in a region. An advancement of this approach is the stacking of the age distribution curves of tens or tens or hundreds of individual dates, producing a stacked growth frequency curve for a region (Ayliffe *et al.*, 1998; Baker *et al.*, 1993b; Henning *et al.*, 1983; Hercman and Walanus, 1996). Speleothem growth periods have also been used to constrain maximum sea level versus time, as they can only have

formed while above sea-level (e.g., Gascoyne *et al.*, 1979; Harmon *et al.*, 1981; Richards *et al.*, 1994).

As well as being used to date growth periods, U-series dates are commonly used to apply accurate chronologies to the growth histories of individual speleothems, such that other parameters measured within the speleothem may be placed in a chronological framework. While many such records in the past have relied on chronologies obtained by interpolation of two or three dates, a realisation that growth rates can be highly variable, even within individual speleothems, has led to more comprehensively dated records (e.g., Bar-Matthews and Ayalon, 1997; Dorale *et al.*, 1992; Lauritzen and Lundberg, 1998).

Oxygen isotope records

Most attempts to reconstruct palaeoclimate from speleothems have relied on oxygen isotope measurements (e.g., Goede *et al.*, 1990; Harmon *et al.*, 1978b; Lauritzen, 1995; Thompson *et al.*, 1974). Oxygen isotope variation in carbonates is usually expressed as parts per mil deviation from the composition of the PDB standard (Pee Dee Belemnite; Craig, 1957), and is hereafter reported as:

$$\delta^{18}\mathbf{O} = 1000\frac{{}^{18}O/{}^{16}O_{Sample} - {}^{18}O/{}^{16}O_{PDB}}{{}^{18}O/{}^{16}O_{PDB}} \qquad (2.3)$$

Oxygen isotope fractionation occurs during speleothem formation, between the speleothem calcite and the drip-water from which it forms. The degree of this fractionation is sensitive to temperature, and thus under ideal conditions it can record cave temperature changes in the calcite, at a rate of -0.24‰/°C (Hendy, 1971; Hendy and Wilson, 1968). Unfortunately, these ideal conditions are very rarely attained, as they include the requirement that the $\delta^{18}O$ of the cave waters must be precisely known through time.

Cave seepage water has been shown to be generally of the same isotopic composition as the meteoric water from which it was derived (Schwarcz,

1986), and so changes in the $\delta^{18}O$ of meteoric waters will directly affect the $\delta^{18}O$ of any speleothems forming below. The $\delta^{18}O$ of waters reaching the cave interior, and therefore of the speleothems formed from them, will thus reflect changes in the $\delta^{18}O$ of the oceans, in conditions at the source area from which the meteoric waters were derived, and in local climate above the cave. Under adverse conditions speleothem $\delta^{18}O$ may also vary independently of both temperature and seepage water $\delta^{18}O$, due to non-equilibrium fractionation of ^{18}O between the water and calcite. This may be caused by loss of CO_2 by rapid degassing of the seepage water or when calcite is precipitated due to evaporation of the seepage water (Hendy, 1971).

Application

Most published records of oxygen isotope variation in speleothems have been interpreted by one means or another as being proxies for local temperature change above the cave, through time (e.g., Duplessy *et al.*, 1970; Goede *et al.*, 1990; Harmon *et al.*, 1978a; Lauritzen, 1995). It appears to be universally recognised that the $\delta^{18}O$ of meteoric waters cannot have been constant through time, and a number of approaches have been taken to correcting for this, none of them completely robust. One such approach has been to use the modern global relationships of meteoric $\delta^{18}O$ versus temperature, reported by Dansgaard (1964), to model changes in ancient meteoric waters, (e.g., Gascoyne *et al.*, 1980; Harmon *et al.*, 1978b; Hendy and Wilson, 1968). The subsequent realisation that such modelling can not generally be considered reliable, lead to a number of attempts to measure the $\delta^{18}O$ of old meteoric waters directly, from inclusions trapped within the speleothem calcite (Harmon and Schwarcz, 1981; Harmon *et al.*, 1979; Schwarcz *et al.*, 1975; Thompson *et al.*, 1974). This approach that has so far met with little success, due to difficulties extracting inclusion water from speleothems without fractionating it in the process, although recent results are encouraging (Rowe *et al.*, 1998).

Other attempts to correct for changes in meteoric water have included analysis of ancient ground-waters (Talma and Vogel, 1992), and projection of

modern local drip-water $\delta^{18}O$ to temperature relationships into the past (Bar-Matthews and Ayalon, 1997; Goede *et al.*, 1982; Harmon *et al.*, 1978a; Millen and Dickey, 1987). In general, while many workers still represent speleothem $\delta^{18}O$ as being a proxy for temperature, few of them now attempt to apply any absolute temperature scales to such records.

Carbon isotope records

The carbon isotopic composition of speleothem calcite has received less attention than have the oxygen isotopes, and studies were initially directed at determining the suitability of speleothems for oxygen isotope analysis, or for calculating correction factors for radiocarbon dating. Later work on carbon isotopes has focused on the inference of palaeovegetation changes (Brook *et al.*, 1990; Dorale *et al.*, 1992; Talma and Vogel, 1992), although problems with this approach have since been highlighted (Baker *et al.*, 1997; Goede, 1994). As is the case with oxygen isotopes, the carbon isotope content of carbonates is expressed relative to the Pee Dee Belemnite standard (Craig, 1957), as:

$$\delta^{13}\mathbf{C} = 1000\frac{{}^{12}C/{}^{13}C_{\text{Sample}} - {}^{13}C/{}^{12}C_{\text{PDB}}}{{}^{13}C/{}^{12}C_{\text{PDB}}} \qquad (2.4)$$

Unlike oxygen, which is buffered from isotopic fractionation by being the major constituent of water, only a very small amount of carbon is present in cave waters. It is thus susceptible to significant isotopic fractionation at all stages of its transport from soil organic matter to speleothem calcite (e.g., Hendy, 1971). As such, while it can be relatively easy to predict the $\delta^{13}C$ of soil CO_2 for any given vegetation type and environmental setting, (e.g., Bird *et al.*, 1996; Cerling *et al.*, 1989; Dulinski and Rozanski, 1990), prediction of the $\delta^{13}C$ of speleothems derived from this soil CO_2 is in most cases not possible (Baker *et al.*, 1997).

Application

Carbon isotope variation in speleothems has commonly been interpreted as being in response to changes in the relative abundance of plants above the cave using the C_4 photosynthetic pathway, to those using the C_3 pathway. In such cases, it has been assumed that migrations of different vegetation zones (generally forest and grassland), in response to changes in regional climate, are responsible for the observed $\delta^{13}C$ variation. Unfortunately, as asserted above, inorganic processes acting on soil CO_2 during transport and speleothem formation can potentially have even greater effects on $\delta^{13}C$ than can C_3/C_4 vegetation changes. These inorganic effects include changes in the partial pressure of soil CO_2, in the amount of soil atmosphere in contact with the seepage water during carbonate deposition, and in the rate of seepage water flow over the speleothem surface (Baker *et al.*, 1997; Dulinski and Rozanski, 1990; Hendy, 1970). While these effects may completely mask changes in soil $\delta^{13}C$, they are also likely to vary in intensity as a result of environmental changes, thus potentially recording such changes in speleothem calcite (see chapter 6).

Other palaeoenvironmental recorders in speleothems

Ultra-violet luminescence

Ultra-violet luminescence of speleothems is thought to be influenced by organic acids incorporated into the calcite during speleothem growth, which vary in response to changes in the activity of, and rate of decomposition of, surface vegetation (Baker *et al.*, 1993a; Shopov *et al.*, 1994). Variations in the intensity of this effect have been observed in bands parallel to growth layering in speleothems, with periods ranging from months to hundreds of thousands of years (Shopov *et al.*, 1994). Published work to date has emphasised annual luminescence banding, focussing on its potential as a dating tool, and for examining fine-scale changes in annual growth rate. Supporting the inference that speleothem $\delta^{13}C$ and ultra-violet luminescence might both be influenced

by vegetation and soil conditions, Shopov *et al.* (1994) found good agreement between the two variables in a speleothem, over a 100,000 yr period. Changes in the ultra-violet luminescence of a speleothem may be related to the type or extent of vegetation above the cave, the growth rate of the speleothem, and other undetermined factors.

Trace element variation

Gascoyne (1983) suggested that the magnesium content of calcite may potentially be useful as a palaeothermometer, due to the strong temperature-dependency of magnesium's calcite-water distribution coefficient, which he was able to demonstrate in speleothems. He also noted that the potential of this approach was low, as the magnesium to calcium activity ratio in cave seepage water is unlikely to remain constant through time. González *et al.* (1992) observed the magnesium content of speleothems to strongly correlate with magnesium to calcium concentration ratios in their parent seepage waters, over three orders of magnitude of magnesium concentration, implying this to be the dominant control on magnesium content. Goede (1994) found the magnesium content of a Tasmanian speleothem to vary from 240 to 640 ppm over a 35,000 yr period, in good agreement with the carbon isotopic record along the same speleothem. The strontium content of this speleothem varied from 40 to 140 ppm over the same period, showing no relationship to the magnesium concentration or carbon isotope records, but showing similarities to features of the $\delta^{18}O$ record.

Gascoyne (1983) expressed hope that some other trace element might be found, with a constant activity ratio to magnesium in cave waters, but with a temperature-independent distribution coefficient (such as that exhibited by strontium), by which means palaeotemperatures could be determined. Unfortunately, no such pair of trace elements has been forthcoming, and there seems little reason to suspect one may exist. Morse and Bender (1990) note that the activities and partition coefficients of trace elements into calcite from solution may be strongly influenced not only by their concentration in solution, but by the concentrations of other species (both organic and

inorganic), and by the calcite growth rate. In addition, Reeder, (1996) found that different trace elements favour inclusion onto different faces of growing calcite crystals, which implies trace element variation independent of growth layering may be a problem in speleothems.

Despite this pessimistic outlook, hope remains that trace elements in speleothems may be of use as palaeoenvironmental indicators (Gascoyne, 1992), if only because of the relative ease by which a great number of them may be measured. The results reported by Roberts *et al.* (1996) indicate, pending a greatly enhanced understanding of many of the processes involved, that trace element concentration variations in speleothems are unlikely to be of use as a quantitative indicator of palaeoenvironmental conditions. They discovered that analyses of contemporaneous speleothems from the same cave chamber can give conflicting results. However, they also showed that speleothem trace element content can vary on an annual timescale, suggesting application at least as a method of producing accurate annually resolved timescales.

Other

Pollen has been extracted from a number of speleothems (Brook *et al.*, 1990; Lauritzen *et al.*, 1990; Schwarcz, 1986), potentially combining established pollen palaeoclimate reconstruction methods with the absolute chronology afforded by speleothems. Unfortunately, most speleothems forming in such a setting as to entrain useful quantities of pollen are also likely to suffer from contamination by detrital silicates, making U-series dating difficult or impossible. Similarly, charcoal dust has been found in speleothems, interpreted as indicating the timing of past fires (Lauritzen *et al.*, 1990), and apparently capable of reaching speleothems some distance from the nearest cave entrance.

Broecker *et al.* (1960) reported finding an annual periodicity in the visible banding of a speleothem. While such banding might be useful as a means of autocalibration dating, and of investigating variation in annual growth rate

versus time, it would presumably first have to be established in each case that the banding was annual, by an independent means. González *et al.* (1992) found the crystal habits of speleothems to be influenced by growth rate, and by seepage water flow rates, potentially meaning inferences might be made about palaeoclimate from the physical appearance of a speleothem. Little such use of variation in fabric has been made to date.

Chapter 3. The late Quaternary in New Zealand

Introduction

New Zealand (fig. 3.1) is richly endowed with a diverse and extensive range of late Quaternary deposits, so pervasive as to often be the bane of geologists seeking to study older, hidden, strata. Deep, active sedimentary basins contain detailed stratigraphic records, while elsewhere rapid uplift rates record every transgression of sea level or river aggradation as terraces or terrace remnants. Loess layers interspersed with paleosols mantle much of the landscape, recording climate-related changes in landscape stability, while widespread swamps and lakes accumulate pollen and organic matter as records of changing vegetation patterns. South Island glaciers have repeatedly advanced, leaving a variety of deposits as indicators of their timing and extent.

As elsewhere in the world, the expansion and retreat of ice, and the associated major fluctuations in sea level, climate and vegetation have dominated the Quaternary in New Zealand. As noted by Pillans (1991), New Zealand's isolation, span of 13° of latitude, and immense variety of modern environmental conditions, means it should be highly sensitive to, and well-placed to record, changes in global climate. As such, the wealth of palaeoenvironmental information contained within its Quaternary stratigraphic record is of global relevance and interest.

Great progress has been made in linking marine and terrestrial records of glacial-interglacial cycles throughout the late Quaternary (Pillans, 1994). However, dating is not yet of sufficient precision or resolution to address the exact timings of such events as glacial terminations, nor to test the Milankovitch theory of climate change (e.g., Imbrie *et al.*, 1992). Although high-resolution records of New Zealand palaeovegetation since the LGM have

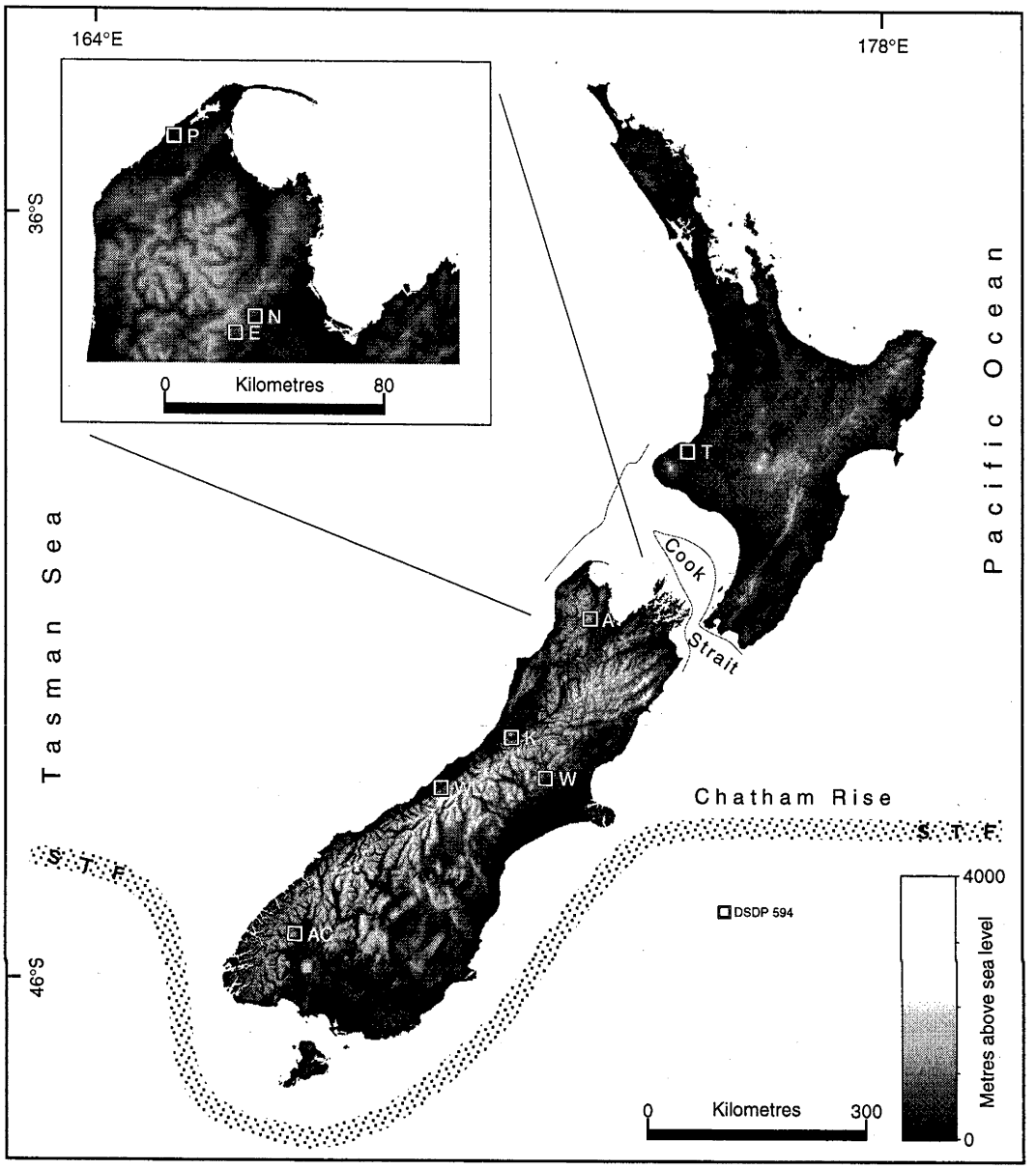

Figure 3.1. Relief map of New Zealand, showing locations mentioned in the text. The 125 metre bathometric contour is shown in the vicinity of Cook Strait, indicating the approximate location of the shoreline at 19,000 cal yr B.P.. T: Taranaki loess record; A: Mt Arthur; K: Kumara glacier advance sequence; W: Waimakariri glacier advance sequence; WL: Waiho Loop moraine, Franz Josef Glacier; AC: Aurora Cave, Fiordland; P: Patarau; N: Nettlebed; E: Exhaleair; STF: Subtropical Front.

been obtained in recent years (McGlone, 1995; McGlone *et al.*, 1993), these often suffer from sparse dating, while direct records of glacial advance are scattered, and generally poorly dated (Pillans, 1991; Suggate, 1990).

This chapter constitutes a broad overview of the dating methods used in the New Zealand late Quaternary, and the palaeoenvironmental records they are used to constrain. It then continues to briefly cover mechanisms potentially influencing and controlling the glacial/interglacial cycle in New Zealand, and examines the effects of human occupation over the last ca. 850 yr.

Dating palaeoenvironmental records

Tephrostratigraphy

The Central Volcanic Region, occupying much of the central North Island, is an area of intensive volcanism marking the southward extension onto land, of back-arc spreading associated with the Tonga-Kermadec trench. Eruptions from a series of volcanic centres have produced predominantly rhyolitic tephra which blanket much of the North Island, and sometimes beyond, over much of the Quaternary (Froggatt, 1983). A detailed stratigraphy of these tephra has been compiled (Froggatt, 1983; Froggatt and Lowe, 1990), particularly covering the last 50,000 years. While not all of the tephra have been dated, their sequence is known, and most can be uniquely identified by geochemical means.

Tephra thus form an invaluable tool for correlating and dating North Island sediments (e.g., Alloway *et al.*, 1992; Pillans, 1988), and in some cases also South Island (e.g., McIntosh *et al.*, 1990) and offshore deposits (e.g., Nelson *et al.*, 1985; Wright *et al.*, 1995). Two widespread tephra of critical importance in this respect, are the Rangitawa Tephra (ca. 340,000 yr B.P.; Alloway *et al.*, 1993; Pillans *et al.*, 1996) and the Kawakawa Tephra (Pillans *et al.*, 1993). The Kawakawa Tephra, erupted at ca. 26,500 cal yr B.P., is present near the base of oxygen isotope stage 2 in many late Quaternary deposits, and is thus a very important marker for the LGM in New Zealand.

Carbon-14 dating

Radiocarbon dating has been used widely in New Zealand Quaternary stratigraphy, often forming a foundation for other dating methods, such as tephrostratigraphy, weathering rind dating, etc. Radiocarbon dating first became available in New Zealand in 1951, and the first dates for glacial features in North Westland were obtained shortly thereafter (Gage, 1985; Gage and Suggate, 1958). Due to New Zealand's high rainfall, contamination of samples by modern carbon can be a problem (Pillans, 1991; Suggate, 1990), sometimes giving artificially young ages. Because of this, unsupported single radiocarbon dates must be treated with some caution.

The chronologies of most New Zealand records younger than 30,000 yr are based on the radiocarbon method, including those dated by tephrostratigraphy or other correlation methods. Because of this, most workers present chronologies in terms of the radiocarbon time-scale, rarely giving calibrated ages. The 1993 radiocarbon calibration of Stuiver and Reimer (1993) enables radiocarbon ages of up to 19,000 ^{14}C yr B.P. to be calibrated to calender years, allowing direct comparison with ages determined using absolute dating methods such as U-series disequilibria (Bartlein *et al.*, 1995). Herein, all radiocarbon dates are reported in their calibrated form, using the 1993 calibration (Stuiver and Reimer, 1993) to 19,000 ^{14}C yr B.P., and thereafter by adding 4,000 yr, based on the data of Bard *et al.* (1993).

Other dating methods

On a global basis, deep ocean cores are usually dated using various "orbital tuning" methods, based on the assumption that global ice volume is very strongly influenced by variations in the earth's orbital parameters (Imbrie *et al.*, 1984; Martinson *et al.*, 1987). Much of New Zealand's Pleistocene chronology is partially or fully derived from this technique, by correlation with ocean core records thus dated (e.g., Pillans *et al.*, 1994). Unfortunately, a limitation of the orbital tuning method is that the ca. 30,000 yr period at each end of a given record cannot be tuned (e.g., Waelbroeck *et al.*, 1995). This

makes meaningful comparison of many published ocean core records (e.g., DSDP 594; Black *et al.*, 1988; Nelson *et al.*, 1985) to Quaternary terrestrial records difficult or impossible over the last 30,000 years.

Uranium-series disequilibrium dating of speleothems has been used to constrain the ages of a number of New Zealand late Quaternary stratigraphic records (Lyons, 1996; Williams, 1982; Williams, 1996). In all cases, the ages were obtained by alpha counting, resulting in a generally lower precision than that now obtainable by thermal ionisation mass spectrometry. Earlier speleothem dating (Hendy, 1970; Hendy and Wilson, 1968; Wilson *et al.*, 1979) was by the radiocarbon method which, due to the uncertain contribution of ancient carbon, is now generally considered to be give inaccurate age estimates from speleothems.

A number of other dating methods have been used to constrain ages in the New Zealand late Quaternary, most of them attempting to target the period beyond the useful range of radiocarbon dating. These methods include amino acid racemization (Pillans, 1983), magnetostratigraphy (Pillans *et al.*, 1994), biostratigraphy (Beu and Edwards, 1984), fission track dating of tephra (Alloway *et al.*, 1993), thermoluminescence dating of loess (Berger *et al.*, 1992), and weathering rind dating of glacial tills (Chinn, 1981). None of these methods have both the precision and resolution required to accurately discriminate between events of only a few thousand years' duration.

Palaeoenvironmental records

New Zealand Quaternary palaeoenvironmental records can be divided into two categories, being longer records addressing the global glacial—interglacial cycle over much or all of the Quaternary, and records largely or entirely within the range of radiocarbon dating, addressing often fine-scale local changes. The latter category, of short, relatively high-resolution records is herein given the most attention, as being most relevant to the Mt Arthur speleothem records.

Oceanic cores

DSDP 594 (Nelson *et al.*, 1986; Nelson *et al.*, 1985), off the eastern South Island, is widely considered to contain a proxy record for South Island glacial extent, through the middle and late Quaternary (Suggate, 1990). As many as 12 episodes of glacial advance are inferred over the last 730,000 years, from variations of the $CaCO_3$ percentage in the core, far more episodes than can be found in the New Zealand terrestrial record. The upper 160,000 yr of the record has been investigated at the relatively high resolution of ca. 500 years, by Nelson *et al.* (1993), but the chronology, being based on orbital tuning (Black *et al.*, 1988), suffers from poor age control over the last few tens of thousands of years. The distinctive feature of the last glacial cycle in this record, is the large increase in $CaCO_3$ at ca. 15,000 cal yr B.P., implying a major glacial retreat at this time (the end of oxygen isotope stage 2). Analysis by Heusser and Van De Geer, (1994) of pollen contained in the upper section of the core is considered below. DSDP 593 (Head and Nelson, 1994), while usefully positioned to the West of New Zealand, unfortunately suffers from extremely low temporal resolution.

A number of other ocean cores lie off the east coast of New Zealand, mostly covering only a few tens of thousands of years, at relatively high resolutions. Marine cores on the Chatham Rise (Fenner *et al.*, 1992) show the Subtropical Front did not move to the north of the rise during the last glaciation. They also show upwelling over the rise to have been much stronger then, due to considerably stronger westerly winds. Three deep-sea sediment cores off northeast New Zealand (Wright *et al.*, 1995) give a high-resolution record of palaeoceanographic changes in the north of New Zealand, dated by tephrostratigraphic means. These data imply the LGM in northern New Zealand, while a time of persistent westerly winds, was only ca. 2°C cooler than today. Pollen data from these cores is considered below.

Compared to Northern Hemisphere regions, the few published marine core records in the vicinity of New Zealand are of low resolution and are poorly dated over the last few tens of thousands of years. Nonetheless, taken

together, they provide important information about changes in the configuration of regional oceanic water masses, the nature of palaeowinds, and the magnitude of sediment fluxes from the Islands of New Zealand. Nelson *et al.* (1994) found that, while the STF has remained locked to its current position by the bathometry of the Chatham Rise, the water immediately to its south became very much colder. They noted that a greatly increased latitudinal and longitudinal temperature gradient over the South Island would have resulted, causing strong, cold winds. T. Barrows (in preparation) finds that the colder temperatures and increased thermal gradient to the east of the South Island were caused by northward migration of the Sub-Antarctic Front to within as little as one degree south of the STF. He also finds the LGM position of the STF in the Tasman Sea, and of its associated westerly wind belt, to have been as much as four degrees to the north of its present position.

Pollen records

Many records of pollen accumulation have been obtained covering oxygen isotope stage 1, and to a lesser extent stage 2, in New Zealand. Although these records often suffer from inadequate dating, there is currently a good understanding of New Zealand vegetation changes since the LGM (McGlone *et al.*, 1993). Generally, the pollen records are obtained from bogs or lakes, and are dated by some combination of radiocarbon dating and tephrostratigraphy. Records of vegetation patterns from changes in the nature of the pollen flux reaching offshore sites have also been published, covering periods extending beyond the LGM (Heusser and Van De Geer, 1994; Wright *et al.*, 1995). While pollen records can useful indicators of vegetation changes over time, they can not yet be used as quantitative proxies for past changes in environmental variables in New Zealand (McGlone *et al.*, 1993). However, useful qualitative inferences about changes in variables such as temperature, wind strength, storm frequency and rainfall have been made, from the timing and nature of vegetation changes implied by the pollen data.

The first major post-glacial increase in arboreal pollen may be taken as an indicator of the time of climatic amelioration and reafforestation throughout the country (McGlone, 1988), following a LGM climate devoid of widespread forest (Pillans *et al.*, 1993). The timing of this event varies with latitude in New Zealand, with vegetation patterns consistent with cold conditions seemingly ending at ca. 20,000 cal yr B.P. in the far north (Dodson *et al.*, 1988), and at ca. 11,000 cal yr B.P. in the far south (McGlone *et al.*, 1993) of the country. As a broad generalisation, this initial reafforestation is followed throughout the country by several thousand years of warm, wet climate, corresponding to a change to vegetation of greater biomass (McGlone, 1988). Over the remainder of the Holocene, NZ climate became slowly drier and cooler, favouring expansion of forest dominated by *Nothofagus* species.

New Zealand pollen data are not necessarily diagnostic of the presence or absence of conditions favouring glacial advance. McGlone (1995) noted that during the Younger Dryas Stadial, a time at which there is now considerable evidence that a significant glacial advance occurred in New Zealand (Denton and Hendy, 1994; this work), there is no sign in the vegetation record of a cooling. Indeed, Denton and Hendy (1994) were able to date the advance of the Franz Josef Glacier at this time using remains of the lowland wet temperate rain forest it swept through. McGlone (1995) noted that glacier advance on the West Coast of the South Island is not necessarily dominated by temperature effects (this point has been the subject of considerable debate; Gellatly and Norton, 1984; Hessell, 1983; Salinger *et al.*, 1983). He instead proposed a period of increased cloudiness and precipitation as an explanation for the advance. With this in mind, it is worth noting that conditions favourable to glacier advance, and conditions favourable to extensive forest growth, are not necessarily mutually exclusive in the South Island.

Pollen data from the central West Coast of the South Island (Moar and Suggate, 1996) show climate there to have favoured sparse, lowland forest and shrubland during oxygen isotope stage 3, with a change to grassland and shrubland representing a cold, windy climate during stage 2. Data from the North-West Nelson region (Worthy and Mildenhall, 1989) indicate that while

coastal forest was restricted to low-lying sheltered areas, substantial remnants existed throughout the LGM, with the first signs of climatic amelioration occurring at ca. 17,000 cal yr B.P. The results of Singer *et al.* (1998) from the Cobb Valley, ca. 10 km to the northwest of Mt Arthur, show a sudden return of forest to grassland areas at 15,000 cal yr B.P.

Pollen data from the marine core DSDP 594 (Heusser and Van De Geer, 1994) span the last ca. 350,000 yr, and indicate the eastern South Island to have been considerably cooler during glacial times, although possibly not significantly drier than today. In particular, herbaceous pollen levels from this site strongly correlate with fluctuations in oceanic $\delta^{18}O$ in the same core, linking on a coarse timescale climatic conditions in the South Island to the global oceanic ice volume signal. Wright *et al.* (1995) examined the record of pollen accumulation in four deep marine cores east of northern New Zealand, dated at a relatively high resolution by tephrostratigraphic means. Their data imply that full conifer-hardwood forest conditions in northern New Zealand prior to 47,000 cal yr B.P., and then a vegetation assemblage implying cooler and drier conditions until 14,000 cal yr B.P. From this time, there was a rapid return to full Holocene forest conditions.

Loess records

Episodes of loess deposition have been used to infer times of glacial climate in New Zealand, in particular in the North Island, where extensive and well-dated tephras place good constraints on ages through tephrostratigraphic correlation (Pillans, 1991). Loess accumulates during glacial periods in New Zealand, due to a combination of increased wind velocity, lowered sea-level exposing the silt-laden continental shelf, and greatly increased fluvial and glacial erosion leading to high sediment production rates in both islands (e.g., Alloway *et al.*, 1992; Pillans, 1988). The resulting loess units, forming continuous horizons on a regional scale, are separated by paleosols, creating a continuous record of glacial-interglacial transitions, of 500,000 years or more in some locations (Pillans and Wright, 1990). The loess stratigraphy of the southwest North Island, in particular, forms an important part of the New

Zealand late Quaternary stratigraphic timescale (Pillans, 1991; Pillans, 1994; Pillans, 1988).

Taranaki, in the southwestern North Island, is a region dominated by andesitic input from the volcano Mt Taranaki. Alloway *et al.* (1992) were able to obtain a high-resolution record of loess accumulation rate during oxygen isotope stage 2, by examining the quartz loess content of andesitic airfall tephra beds in north Taranaki, thus producing a proxy record for the severity of glacial conditions over oxygen isotope stage 2. Thiede (1979), by examining terrestrial dust content in a number of deep ocean cores, inferred past changes in the strength and direction of winds at the LGM. He found westerly winds to have been stronger, due to the westerly wind belt in the Tasman Sea shifting considerably to the north at this time.

Glacier deposits

Direct records of late Quaternary glaciation in New Zealand are mostly in the form of glacial deposits in the South Island, and are generally poorly dated and fragmentary (Pillans, 1991). While the mountainous regions were heavily glaciated during oxygen isotope stage 2, the extensive tills are not easily dated, and correlation even between adjacent valleys is difficult. Radiocarbon dating, and other methods calibrated on the basis of radiocarbon ages, form the framework of much of the available chronology, and are limited by problems such as contamination of samples by modern carbon (Pillans, 1991). Additionally the temporal relationships between dated organic samples and associated glacier advances is sometimes uncertain (e.g., McSaveney and Whitehouse, 1989). The Fiordland glacier advances dated by Williams (1996), using the uranium-series alpha-counting method, can be considered the most accurately dated direct glacial chronology available, although as always, this chronology may have limited significance beyond the local or regional level.

The most widely quoted general glacial chronology for New Zealand is that of Suggate (1965), which sub-divides oxygen isotope stage 2 (the Otiran glaciation) into the Kumara 2_2, and Kumara 3 advances. This chronology

records the advances of large glaciers on the West Coast of the South Island, which descended steeply from the Southern Alps and flowed across the plains to the west during glacial periods. These glaciers are likely to have been highly sensitive to changes in the nature of the westerly atmospheric circulation over the Tasman Sea (Chinn, 1995; Fitzharris *et al.*, 1992; Gellatly and Norton, 1984; McGlone, 1995). Their sequence of advances is taken by most authors as being representative at least of glaciation on the West Coast, and by some as being representative of South Island or New Zealand glaciation generally.

Other South Island records of glacial advance are difficult to correlate to the Kumara record, but this can be explained at least in part by relatively poor dating of these sequences (Gellatly *et al.*, 1988; Pillans, 1991; Suggate, 1990). Despite this, and the fragmentary nature of many records, correlations between East and West Coast glaciers have been attempted covering the last ca. 25,000 ^{14}C yr B.P. (Gellatly *et al.*, 1988; Suggate, 1990), although the question whether glacier advances are synchronous over the island has yet to be answered either way. The Waimakariri glacial sequence (Gellatly *et al.*, 1988) is important in any attempts at correlation, as a representative East Coast sequence, geographically close to the West Coast Kumara sequence.

Based on the reconstructed timings and extents of glacial advances through the late Quaternary, various reconstructions of glacial climate in New Zealand have been attempted. Some of the assumptions on which these reconstructions are based remain controversial, in particular the question of whether modern (and thus ancient) glaciers are controlled more closely by changes in temperature, or by changes in precipitation (Gellatly and Norton, 1984; Hessell, 1983; Salinger *et al.*, 1983). Most authors, however tend to agree that, by whichever mechanism, glacier advance in modern times is correlated with changes in the strength and prevalence of westerly winds reaching the South Island (Gellatly and Norton, 1984; Gordon, 1985; McGlone, 1995). Based on the modern relationship in New Zealand of the snowline to altitude, and on a LGM snowline generally 850 metres or so lower than it is today, Soons (1979) concluded that temperature at the LGM was probably 4.5°C

colder than today in the eastern South Island. Gage (1965) noted, on the basis of glacier deposits in north Westland, that precipitation there during the LGM may have been similar to, or possibly greater than today. Glacier expansion was instead likely to have been largely as a result of short, cold, and cloudy summers reducing summer ablation of the ice.

As previously discussed, the Younger Dryas Stadial, a time of glacier readvance in the North Atlantic region, is a period of intense interest on a global basis. It is an event that may help to elucidate both the degree to which global climate is driven from high northern latitudes, and the rate at which sudden climate changes propagate about the Earth. Equivocal evidence existed for such an advance in New Zealand (e.g., Gellatly *et al.*, 1988), until Denton and Hendy (1994) presented evidence for a major advance of the West Coast's Franz Josef Glacier at 13,800 cal yr B.P. This is exactly equivalent to the timing of the Younger Dryas in Northern Europe and Greenland (e.g., Stuiver *et al.*, 1995). While the significance of this advance of the Franz Josef Glacier has since been questioned (McGlone, 1995), it nonetheless invites closer investigation of its timing and duration, and of the nature of the conditions that caused its advance.

Speleothems

Hendy and Wilson (1968) examined oxygen isotope variation in two speleothems from the Waitomo region of the western North Island, and concluded that isotope maxima at ca. 24,000 and 30,000 cal yr B.P. were consistent with temperatures 5–6°C colder than the present. This finding relied on a greatly simplified model of isotope fractionation in meteoric waters, and on the assumption that the tropical oceans were 4–5°C cooler than today (a contentious issue to this day, e.g. Broecker, 1986; Guilderson *et al.*, 1994). Hendy (1970) later found that, typically, New Zealand LGM speleothem calcite was 1‰ heavier than it is today, and noted this may be due to some combination of changes in local temperature, oceanic surface water composition, and latitudinal temperature gradient. Despite the now flawed premises (see chapter 6) of the temperature curve of Hendy and Wilson,

(1968), it has been used in more recent composite New Zealand palaeotemperature reconstructions, such as that of Salinger (1983).

Wilson and Hendy (1971) derived a short-term temperature curve for central New Zealand, based on a radiocarbon-dated speleothem from Patarau, North-West Nelson. By assuming that the oxygen isotopic composition of the meteoric waters was constant over the lifetime of the speleothem, they attributed $\delta^{18}O$ variation entirely to temperature change, at a rate of 0.24‰/°C. They found support for this approach in the instrumental record of local temperature variation over the last century, although given the low sampling resolution and large relative errors involved, this support is not strong. Nonetheless, they found their record agreed with the historic temperature curve from England, and interpreted a sharp rise in $\delta^{18}O$ at 500 cal yr B.P. as corresponding to the initiation of the Little Ice Age in Europe.

Two other published New Zealand speleothem records have relied on speleothem dates to constrain the ages of other stratigraphic features, and thus of events responsible for their formation. Williams (1982) applied U-series dating to speleothems in order to constrain late Quaternary uplift rates at two sites on the South Island's West Coast, noting that speleothems, both at Patarau, and further south at Westport, appeared to have been growing during the LGM. This implies that vegetation was present above the caves at this time (consistent with Worthy and Mildenhall, 1989). Williams (1996) also used speleothems dated by U-series disequilibria, to constrain ages of stratigraphic horizons in a very detailed investigation of Aurora Cave, Fiordland. Using the premise, supported by their positions in the stratigraphy of cave infill deposits, that speleothems grew only while the surface above the cave was free of ice, he identified six major glacial advances during the last 90,000 cal yr B.P.

Mechanisms of climate change in New Zealand

A number of mechanisms by which New Zealand's climate may vary on a Quaternary timescale have been proposed, in particular that it responds in

some way to global climate change. That global temperature is subject to significant variation, at least in the temperate (e.g., Kukla, 1987) and polar (e.g., Johnsen *et al.*, 1992; Jouzel *et al.*, 1987) regions, is now well accepted. However, the degree to which equatorial temperature may have changed remains highly controversial (e.g., Broecker, 1986; Guilderson *et al.*, 1994; McCulloch *et al.*, 1996; Miller *et al.*, 1997; Thompson *et al.*, 1995; Thunell *et al.*, 1994). The 4.5–5.5°C glacial-interglacial temperature change typically estimated for New Zealand (McGlone *et al.*, 1993) is consistent with most models of global climate, but the local chronology of climate change is not yet tightly enough constrained to discriminate between them.

As previously discussed, temperature is not necessarily the strongest control on New Zealand's climate, and indeed may only exert minor influences on the state of glacier advance, one of the more visible manifestations of local climate change. A number of workers have proposed that New Zealand's climate might be dominated by the strength of local winds (Gordon, 1985; McGlone, 1988; Nelson *et al.*, 1994). It has also been shown that mid to high-latitude Southern Hemisphere winds were considerably stronger during the LGM (Petit *et al.*, 1981; Thiede, 1979), linking New Zealand's climate with changes in atmospheric and oceanic circulation in mid to high southern latitudes.

Although New Zealand climate change might be explained largely in terms of regional changes in atmospheric circulation, presumably due to changes in the nature of hemispheric atmospheric circulation, associated changes in the nature of global oceanic circulation should also be considered. Major changes in global oceanic circulation, particularly those originating in the North Atlantic region, are commonly proposed as a significant component of the "engine" that drives global climate (e.g., Broecker *et al.*, 1985; Heinrich, 1988; Keigwin and Jones, 1994; Porter and An, 1995). Such changes can ultimately influence the oceanography local to New Zealand (Heath, 1985; Stanton, 1973), thus affecting its climate (Nelson *et al.*, 1993; Wright *et al.*, 1995).

Indeed, and perhaps most importantly in the context of this work, small changes in local oceanography alone may conceivably have had large and

sudden effects on the climate of New Zealand as a whole, most specifically in the South Island. Nelson *et al.* (1994) noted that latitudinal movement of oceanic fronts in the vicinity of New Zealand would have lead to greatly increased latitudinal and longitudinal temperature gradients over the South Island, resulting in lower temperatures and stronger winds there, whilst affecting the North Island to a much lesser degree. Evidence from other ocean cores proximal to New Zealand reinforces this (Fenner *et al.*, 1992; Wright *et al.*, 1995). The milder changes inferred for the North Island are consistent with terrestrial pollen records from the far north of the country (Dodson *et al.*, 1988).

A number of workers have now proposed that New Zealand's climate, in particular that of the South Island, is quite specifically dominated by changes in the position of the Subtropical Front (STF; Fenner *et al.*, 1992; McGlone *et al.*, 1993), and the associated westerly wind belt and sub-tropical high (T. Barrows, in preparation; Fitzharris *et al.*, 1992). Such latitudinal changes in the position of the STF and westerly wind belt have potentially major influence on New Zealand's climate, based on observations of modern climate (Gordon, 1985; Sturman and Tapper, 1996), and on records of ancient climate (T. Barrows, in preparation). The STF is thus a mechanism capable of linking (and amplifying) changes in global oceanic and atmospheric conditions to New Zealand climate. A striking illustration of this mechanism can be found in the modern behaviour of Tasman Sea atmospheric circulation, and thus of New Zealand climate, in response to the Southern Oscillation (Gordon, 1985), the El Niño phase being analogous to mild glacial conditions.

Human occupation

The earliest human settlement in New Zealand appears to have been ca. 700 years before present (McGlone *et al.*, 1994), although there is strong evidence that humans at least visited both main islands as early as ca. 2000 cal yr B.P. (Holdaway, 1996). Almost immediately on settling in New Zealand, humans began hunting the herbivorous avian megafauna, in particular the various species of moa (Dinornithiformes), some of which reached up to 300 kg in

weight, and which are believed to have had considerable influence on the character of New Zealand's forest flora (Wardle, 1991). Shortly thereafter, a major forest clearance phase began over the country, ending at a similar time to the extinction of most moa species, ca. 400 years ago (McGlone *et al.*, 1994, based on evidence from palaeovegetation, palaeontological and archaeological studies).

It is inferred that the extinction of the Moa is likely to have lead to considerably more vigorous forest growth throughout the country (Wardle, 1991). This is now illustrated by the considerable difference between the mainland forest, and that on offshore islands free of browsing animals (now being mammals such as goats and deer, introduced by European explorers and colonists). Major forest clearance was restricted in pre-European times to those parts of New Zealand over which forest could be easily burned, in particular the eastern parts of the country (McGlone *et al.*, 1994).

Chapter 4. Setting, fieldwork and sample preparation

Setting

Mount Arthur (fig. 4.1) is a prominent peak of 1795 metres, positioned in the Arthur Range of North-West Nelson, South Island, New Zealand. It has formed from the uplift of one of a number of discrete bodies of Ordovician marble found in the north-western corner of the South Island, which has a surface extent of about 30 square kilometres. Beneath the mountain are known to lie a number of large cave systems, the longest and deepest of which are Nettlebed and Exhaleair, the two caves from which samples were obtained for this study. Mt Arthur is within the borders of Kahurangi National Park, and its immediate environment has never been subjected to significant human modification.

The cave systems of Mt Arthur were chosen as a field area because they were inferred to be capable of supporting continuous speleothem growth, over long periods of time. Thick flowstone sequences exist in passages inferred to be hundreds of thousands of years in age, and the deep and wet nature of the caves implies indicates they are suitable for stable isotope palaeotemperature determination from speleothems. Mt Arthur's position close to the West Coast of the South Island means its climate is strongly influenced by oceanic climate. This increases the likelihood that changes in its local environment, as recorded in the speleothems of the caves below, will strongly reflect changes in the regional climate of the Tasman Sea.

Physical setting

North-West Nelson is a geologically complex region of predominantly Paleozoic strata and granitic batholiths (Suggate *et al.*, 1978). The Ordovician Arthur Marble (Grindley, 1961) is the principal member of the Mount Arthur Group, and is exposed throughout the region, dominantly in the east, where

Fig. 4.1. Topographic map (part NZMS 260 sheet M27 Mt Arthur) of Mt Arthur, showing Nettlebed and Exhaleair caves, and their relationship to the modern treeline. The locations of core samples MD3 and ED1 are shown, both of which are ca. 200m below the surface. Contours are in Metres, and north is to the top left of the figure. Cave outlines are from Ravens (1986; 1992).

Mt Arthur is a major outcrop. The marble varies from impure dark grey siliceous marbles, through to pure white calcite marble (Suggate *et al.*, 1978), cave development usually being in the less siliceous strata. Throughout Nettlebed, massive blue-grey marble is typical, grading upwards into less pure micaceous marble containing layers of quartzite boudin, in the higher regions of the cave (Wright, 1981). The lower passages of Exhaleair relevant to this study seem to be developed largely in the massive blue-grey marble.

The Ellis Karst, the surface expression of the Arthur Marble in the Mt Arthur area, covers some 30 square kilometres of the Arthur Range, roughly centred on the mountain (Johnston, 1973). The Karamea Fault, which has uplifted impermeable silicate rocks to the west of the karstfield, apparently forces about 25 square kilometres of this area to drain to the north and east, through cave systems to the Pearse Resurgence, the source of the Pearse River, at an altitude of 269 metres. Caves presumed to drain to the Pearse Resurgence have been discovered as high as 1750 metres above sea level, and up to 7 kilometres from the Pearse Resurgence.

Nettlebed, at 889 metres, is the deepest known cave in the karstfield, and consists of over 24 km of surveyed passage (Ravens, 1986), making it the second longest. The Ellis Basin cave system, six kilometres to the southwest, is currently surveyed to 30 km in length, and is over 700 m deep (Ravens, 1992). There are three other major cave systems known beneath the mountain, and numerous smaller caves, predominantly deep shafts choked with fallen rubble. The region above the caves is predominantly forested with *Nothofagus* species, with some conifer and broadleaf species at lower altitudes. A generally sharp treeline ranges in altitude from 1100 to 1300 metres, above which scattered low scrub grades upwards into alpine *Chionochloa* tussock grasses. Above 1500 metres, bare rock is prevalent, in the form of marble bluffs, pavements and screes.

Synoptic climatology

Mt Arthur receives precipitation predominantly from westerly airflow (Garnier, 1958), which first crosses 50 km of mountainous country from the coast, including the Arthur Range at ca. 1600 metres above sea level. Annual precipitation in the region is over 2500 mm, and annual average temperature at sea level nearby is 12°C (Garnier, 1958). The climate of the Mt Arthur area is also influenced by the proximity of Cook Strait, the only break in the 1600 km length of New Zealand's main islands. Here, the southwesterly winds dominant to the north and in the south are replaced by northwesterly winds formed as westerly airflow funnels between the islands (Garnier, 1958). At the last glacial maximum Cook Strait was mostly dry, and the North and South Islands were possibly connected as a single body of land (Lewis and Carter, 1994), a change which must be considered likely to have had a considerable influence on the local climate.

Sample sites (site selection)

The two speleothem samples on which most of this study is based were collected at elevations of 390 m (core MD3, Nettlebed) and 685 m (core ED1, Exhaleair), and are both located ca. 200 m beneath the surface, under the eastern and southern flanks of the mountain, respectively. In both cases, apparently thick flowstone deposits partially fill abandoned phreatic passages, the sites being chosen as the best candidates for obtaining long flowstone cores samples. It is assumed in each case that the percolation water reaching the caves is sinking from the surface approximately above the site, due to the highly fractured nature of the host marble.

Nettlebed

Nettlebed (fig. 4.2) is a three-dimensional maze of active and abandoned phreatic tubes, of up to 10 m in diameter, whose development has generally been structurally controlled, by a combination of transposed bedding and

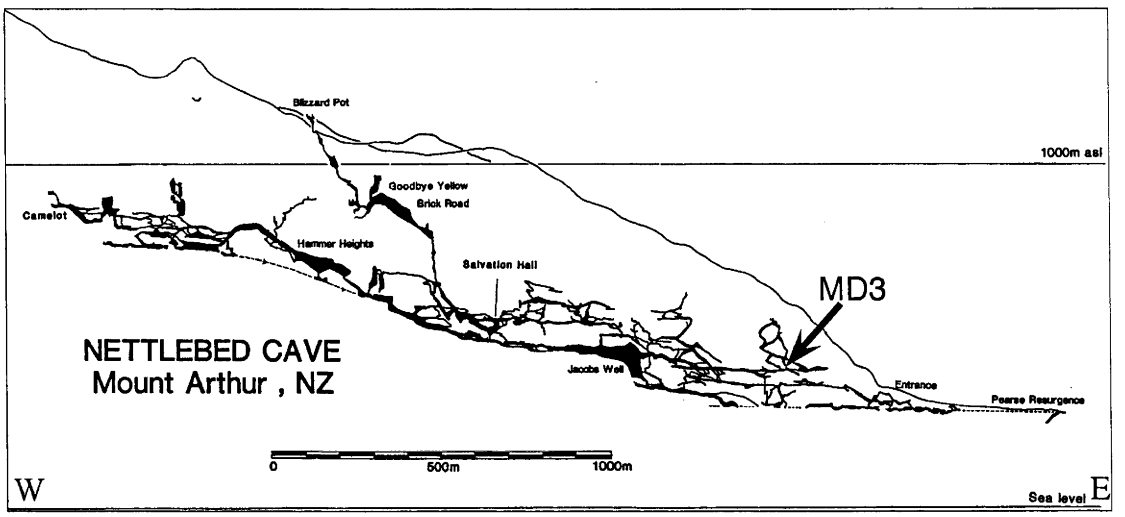

Fig. 4.2. Projected elevation of the major passages of Nettlebed Cave (Ravens, 1986), showing its relationship to the surface above. The section is projected west-east. The location of core sample MD3 is shown.

fractures (Wright, 1981). Superimposed upon the four or more abandoned phreatic levels are more recently developed vadose rifts. The phreatic and rift passages rise to over 800 metres above sea-level by the back of the known cave, which is some two kilometres west of the main entrance (Ravens, 1986). A narrow shaft near the Mt Arthur treeline was connected to Nettlebed in 1986, making it at the time the deepest known cave in the Southern Hemisphere. The main entrance to Nettlebed, 301 metres above sea level, appears to be a fossil resurgence of, and in high flood is still a source of, the Pearse River. The development of the nearby Pearse Resurgence has lowered the average water table to 25 metres below the cave entrance, allowing access through dry phreatic passages in all but extreme flood conditions.

Percolation water and active speleothem growth are common throughout the cave above the maximum flood level, and are prevalent in passages closest to the surface (Wright, 1981). In some of the higher passages near the entrance, flowstones have completely blocked tubes of over 5 metres in diameter, and sometimes extend for many tens of metres down-slope. Most parts of the cave experience some degree of air movement, usually very faint in large or blind passages, but reaching an extreme of 50 km/h (Cody, 1981) in one constriction near the entrance. Air temperatures in the lower regions of the cave range from 7 to 10 degrees (Cody, 1981).

The site chosen for the main core sample in Nettlebed is at the foot of The Meltdown, a massive flowstone sequence steeply descending from what is interpreted as a blocked fossil resurgence of the Pearse River. The core samples were taken where the flowstone intersects a large horizontal passage, spreading out over the silt floor. Airflow in this passage is very slight, and all surfaces are damp. The temperature at The Meltdown was measured in February 1995 as 8.3°C. The nearest known cave entrance is the main entrance, some 800 metres away by the shortest known route.

Exhaleair

Exhaleair, discovered in 1989, is part of the Ellis Basin cave system (Ravens, 1992). Most of the cave consists of a maze-like main phreatic level, overlying an active rift system 50 metres below. The main phreatic levels are generally 200 to 300 metres below the surface, and can be reached by several vertical shafts from the surface. The water in the active rift passages is considered by cavers to contribute the bulk of the flow of the Pearse River. Unfortunately, downstream exploration towards the Pearse Resurgence and Nettlebed (some 5 kilometres away) has been restricted by an unacceptably high risk of death by drowning.

While speleothem formation is common in the phreatic levels of Exhaleair, it is neither as prolific nor as massive as in Nettlebed. This may be due to the higher altitude of the cave (the 300 metre series of abseils into the cave starts at about 900 metres above sea level), or the greater depth below the surface of most of the passage. Subjectively, Exhaleair is several degrees colder than the lower levels of Nettlebed.

The site chosen in Exhaleair is in the main phreatic levels, in the downstream region of the cave. The flowstone here is not as thick as at the Nettlebed site, and descends ca. 15 metres down a sloping wall before spreading over the floor, where the core sample was taken. There is some air movement at the site, almost certainly as part of a closed circuit driven by the pumping action of rapids and waterfalls in the main streamway of the cave, which passes some 50 metres beneath the site in a large rift passage. The cave walls, roof and floor in the vicinity are all saturated with water, indicating very high humidity. The nearest known entrance is 700 metres away, and almost 300 metres above (Ravens, 1992).

Fieldwork

A total of four trips have been made to Nettlebed, and one to Exhaleair, to collect samples, between August 1994 and February 1996. On each occasion,

the drilling equipment, caving equipment, tents and food were flown by helicopter to a camp site near the cave entrance, from which the fieldwork was based. The single sampling trip to Exhaleair, in the Ellis Basin, was made in conjunction with a National University Caving Club caving expedition, and was made possible by the use of ropes and equipment placed in the cave by that expedition.

August—September 1994

Due to difficulties in freighting drilling equipment from Australia, the only available drill for this trip was a 20 mm core drill borrowed from the Institute of Geological and Nuclear Sciences in Wellington, which was powered by an 23 cc petrol engine. A preliminary investigation of the chosen site at The Meltdown was made, and two core samples were taken from a flat-lying section of the flowstone, on the passage floor. Three core samples were also taken from the Headsnapper Passage, close to the cave entrance, when high water levels prevented access to The Meltdown for the first two days. Members of the Victoria Cavers and Wellington Caving Group provided assistance in the field.

March 1995

An attempt was made to drill a 50 mm core at the Meltdown, using an RSES drill powered by a 60 cc petrol engine. After drilling to 20 cm, an adaptor on the core barrel broke, halting work. A number of water samples, and fragments of already broken speleothems, were collected, again with the assistance of VC and WCG members. A second trip to Nettlebed was made once a replacement drill adaptor had been sent to New Zealand from Canberra, and the Meltdown core sample, MD3, was continued to a depth of 1.10 metres. A shorter parallel core was also drilled (MD8).

January—February 1996

By taking advantage of an expedition organised to the Ellis Basin on the southern side of Mt Arthur, by the National University Caving Club, access

was gained to Exhaleair, allowing the sampling of core ED1. This was followed by a final trip to Nettlebed cave, during which several "live" straw stalactites were collected, and a final core, MD10, was sampled from The Meltdown.

Sampling permits

As Nettlebed is located within Kahurangi National Park, permission to remove speleothem samples was sought from the Nelson regional office of the New Zealand Department of Conservation. Permission was granted on three occasions to remove speleothem core samples, subject to a number of environmental considerations and to the condition that material remaining after analysis is to be made available to other researchers. Permission was also granted to remove a number of previously broken speleothems, and samples of modern calcite growing on plastic tape in the cave. Speleothems were removed under Department of Conservation permit numbers GEO/94/1, SPE 95/1 and SPE 96/1.

Site access constraints

Both the size and weight of the drilling equipment had to be restricted, as access to the drill sites was difficult. In Nettlebed, a prolonged constriction near the entrance is as narrow as 25 cm by 50 cm. Included in the 1.5 km journey to The Meltdown are steep handlines, rock climbs, wire ladders, deep pools of water and traverses over shafts in the floor. Travel was therefore slow, requiring the fixing of ropes in places, and that packs be hauled and ferried past different obstacles. Coupled with the cold, wet and generally oppressive nature of the cave, this made the fieldwork physically and psychologically difficult. Access to the Ellis Basin site includes a technically difficult 250 metre vertical abseil from the surface, but beyond this point was somewhat easier than Nettlebed. It was not feasible to separately haul equipment back up the entrance shaft, so weight was limited to what could be carried back to the surface by individual cavers as they ascended the ropes.

The entire drilling system, including tools, collected cores, polythene bags and groundsheets, fits into 5 manageable (smaller than torso sized) PVC packs, for a total weight of approximately 80 kg. To facilitate this, the motor and gearbox had to be carried separately, and re-assembled in the cave. The 50 cm steel drill barrels were carried inside lengths of 80 mm PVC drainpipe, to protect both their threads and the PVC packs. Core samples were transported inside the drill barrels, wrapped in layers of clingfilm.

Drill set-up/core recovery

The 75 mm drill bit (50 mm core diameter) is driven by a 60 cc two-stroke engine mounted on a 9:1 reduction gearbox. Using the three 50 cm drill barrels, a core length of 1.7 metres is theoretically possible. The drill barrel is flushed with water using a gravity-fed system consisting of a fifteen-litre water container and ten metres of plastic tubing. A extension to the engine's exhaust was made using stainless steel tubing and a length of radiator hose, to allow the gas to be piped into polythene bags for later gradual release, a condition of the sampling permit. Tools and spares for the motor were carried, along with large strap wrenches for disconnecting core barrels from the bit and from each other.

Drilling generally required at least 3 people: one handling the drill, and two others handling the water and exhaust systems. For the first drilling trip, in August 1994, a similar set-up was used, with a 23 cc drill driving a 20 mm core barrel (this system could only drill to a depth of 200 mm). Core recovery was in most cases 100%, but, for both the 20 mm and 50 mm cores, no individual core segment was longer than 100 mm. This fracturing of the core was partly due to significant judder of the core barrel (presumably due to a misalignment of the gearbox, or of the adaptor to the core barrel), and partly due to the large crystal size of the flowstone allowing fracturing along calcite cleavage planes. The orientation and sequence of individual segments was recorded as they were recovered, for later reconstruction of the cores.

Environmental concerns

The main environmental impact addressed was that of engine emissions upon the cave environment. Two-stroke exhaust contains unburnt oil, which could potentially coat cave walls and speleothems, and leave an unpleasant smell. To address this problem, the exhaust was piped into large polythene bags during drilling, which were sealed and left for a minimum of 24 hours. The gas was subsequently gradually released by puncturing the bags, and was found to be clear and comparatively odourless, although presumably with a considerable carbon monoxide content. The polythene bags, the insides of which were had become coated with oil and carbon, were then removed from the cave.

A condition of the permit to drill in the cave was that fuels and oils were to be used and transported with utmost care while inside the cave. Fuel was carried into the cave in a 600 ml aluminium fuel bottle, wrapped in a number of layers of plastic. No fuel was transported inside the motor's tank, and the motor was wrapped in multiple layers of plastic bubble wrap. Refuelling was conducted over two layers of plastic tarpaulin, with no spillage.

Despite precautions such as scrubbing boots before walking on it, the flowstone around the drill site usually became contaminated with some mud, as well as by a considerable volume of finely ground calcite from the drill bit. This was removed by scrubbing the flowstone immediately after drilling. Drill-holes were plugged or covered with fragments of marble or speleothem from nearby, and will eventually be concealed by continued growth of the flowstone.

Collection of other samples

A number samples were collected for trace element and stable isotope analysis of seepage waters, in most cases by placing a bottle under an active drip. Samples for trace element analysis were collected into 125 ml plastic bottles, and acidified with several ml of concentrated nitric acid. Stable

isotope water samples were also collected into 125 ml bottles, but not acidified, and the caps sealed with electrical tape. In addition, two one-litre bottles of drip-water were collected for U-series analysis by isotope dilution, also into pre-acidified bottles. A 20 cm broken stalagmite, RK1, was collected from close to The Meltdown, as were a number of broken straw stalactites and other small samples of modern speleothem. Five active, or "live" straw stalactites were collected from the vicinity of The Meltdown, then broken into 10 cm lengths and carefully packed into a hard plastic container for transport.

Samples collected

August 1994

Three 20 mm cores of up to 150 mm in length, designated HS1, HS2 and HS3, were drilled in the Headsnapper passage, near the Nettlebed entrance. 20 mm cores MD1 and MD2 were drilled at the base of a massive flowstone in The Meltdown, 800 metres into the cave, both ca. 195 mm in length. A small sample of the marble host rock, EK1, was also taken, from outside the cave entrance.

December 1994

A number of small speleothem fragments were removed from the floors of caves on the Nullarbor Plain, Western Australia. Most notable is the sample AM1, apparently a section of subaqueous calcite rind from an abandoned cave lake.

March 1995

50 mm cores MD3 (1.1 m) and MD8 (0.25 m) were drilled in the base of the Meltdown flowstone. A 200 mm broken stalagmite (RK1) was collected, along with a number of straw stalactite fragments. In addition, samples of seepage water and the modern calcite growing from it were taken from several locations in the cave. A sample of fluvial cave sediment was taken from an undisturbed section of the floor in The Meltdown.

February—March 1996

40 cm of 50 mm core (ED1) was recovered from a flowstone in the central phreatic levels of Exhaleair cave. In Nettlebed, MD10 (65 cm) was drilled higher on the Meltdown flowstone than the earlier cores. Six actively growing straw stalagmites, of up to 50 cm in length, were removed from The Meltdown passage in 10 cm sections.

Descriptions of all samples

50 mm cores

Examination of the upper section of core MD3 from Nettlebed Cave, the main focus of this research, showed it to consist over most of its 587 mm length of large (up to 50 mm in diameter) crystals of clouded calcite, with faint growth banding defined by layers of fine fluid inclusions. From 100 to 290 mm depth in the core, the calcite crystals are irregular and elongated, with a jumbled appearance (growth banding is still defined by fluid inclusions, but the layering is irregular). It appears that the parallel elongate crystals correspond to the period of slowest growth rate, and the irregular elongate crystals to the period of fastest growth rate in the core (see chapter 5).

On examination under both visible and UV light, a single possible growth hiatus in core MD3, a sharp, light brown band, was identified at 457 mm depth (on the assumption that any significant hiatus in growth is likely to be visible in the flowstone; see Baker *et al.*, 1995, for instance). Dating immediately above and below this band (samples MD3A7 and MD3A9, chapter 5) showed it not to represent a measurable break in speleothem deposition, strongly implying that the upper 587 mm of the core grew continuously. Below 587 mm, core MD3 shows evidence of post-depositional alteration, in the form of sponge-like cavities in the original crystals, rimmed with microcrystalline calcite. This section also has several muddy hiatuses, including one short (estimated 25 mm) silt interval. The consistently large

crystal size, preservation of growth layering, and clean nature of the core above 587 mm precludes any post-depositional alteration of the speleothem.

The Exhaleair core, ED1 (235 mm long), was found to have several hiatuses below 172 mm. Above this, the core consists entirely of large clouded crystals similar to those in MD3, except with a faint orange colouration. Core ED1 shows no sign of post-depositional alteration at any depth. Core MD8, taken about 30 cm from MD3, has identical stratigraphy to the upper section of MD3, over its 25 cm length. MD10, taken approximately 10 metres higher up the flowstone from MD3, suffered significant fragmentation during drilling, and achieved less than 90 percent core recovery. Of significance in this core is a zone of obvious secondary alteration of the calcite, at ca. 30 cm depth.

20 mm cores

Cores HS1, HS2 and HS3, from the Headsnapper passage, were all drilled into a gently sloping flowstone floor, within 20 cm of each other. As such, their stratigraphy is very similar. HS1 reached a depth of 130 mm below the surface, where it intercepts a muddy layer, with some evidence of post-depositional alteration. It ranges from white through cream to light brown over its length, the colour variation apparently being defined by detrital silicate content. The colour is finely laminated in places, but there are no obvious hiatuses. Two very fine black bands are closely spaced at a depth of 105 mm. Cores HS2 and HS3 reached 52 mm and 73 mm respectively.

Cores MD1 and MD2, from a horizontal section at the base of the Meltdown flowstone, were taken within 30 cm of each other, and show very similar stratigraphy. Both cores are of pure white calcite for the upper 120 mm, and cream in colour below this depth. Both cores also show a thin band of detrital material, representing a likely hiatus in deposition, at a depth of 165 mm. MD1 intercepts a small lens of detrital material at a depth of 190 mm, before terminating at 195 mm. MD2 intercepts marble host rock at 175 mm, presumably a fallen clast embedded in the flowstone rather than the cave

floor, which is inferred to be silt. The speleothem calcite in both cores is clear, consisting of parallel elongated crystals of calcite, with few fluid inclusions.

Other calcite/sediment

Modern calcite samples were collected at a number of points in Nettlebed, complementary to each water sample. These consisted of crystals growing on the walls of pools in flowstone floors, the tips of small stalactites, and of flowstone that had begun to form on plastic flagging tape placed on the cave floor by explorers in the early 1980s. RK1, a 20 cm stalagmite found broken on the route into the cave, contains a brown detrital layer at its base, but is otherwise composed of large, pure white calcite crystals. A sediment sample collected from the floor of The Meltdown passage consists of grey silt, interpreted as fluvial sediment deposited by ancient floodwaters.

Many fragments of straw stalactite were collected on the route from The Meltdown to the cave entrance, from straws presumably broken by the first explorers of the cave (sample PV1). These fragments, from 40 mm to 100 mm in length, typically resemble 5 mm glass tubing, although some have a greater or lesser diameter. On a number of straws, a ribbed outer surface is apparent, suggestive of regular annual banding. Sample MD9 consists of six actively growing straw stalactites from the Meltdown area, from 150 to 400 mm in length, collected in 70-150 mm segments. While broadly similar to the straw fragments of PV1, these straws are in some cases overgrown in their upper sections by younger calcite, and one is pure white for part of its length (suggesting a high density of fluid inclusions). Two of the MD9 straws have highly regular surface ribbing over their lengths, suggesting an annual growth rate of the order of 150 microns per year.

Water samples

A one litre water sample, MD4, was collected for U-series analysis, beneath one of the principal drips onto the Meltdown flowstone, about two metres "up-flow" of the location of core MD10. 125 ml samples were taken at the same location, for stable isotope and trace element analysis. A similar set of

water samples, with a corresponding modern calcite sample was taken from a pool near to Rockfall 'K,' 500 metres further into the cave. Samples for stable isotope and trace element analysis were also taken from a pool at The Oubliette, close to The Meltdown, with a modern calcite sample. Water was collected from the Pearse Resurgence, as a representative sample of river water in the caves, for trace element and stable isotope analysis. The samples for U-series and trace element analyses were acidified during collection.

Sample preparation

50 mm Cores

For the 50 mm cores, segment order and orientation was recorded in the cave. Core MD3, the longest core recovered, has a total length of 1100 mm, in seventeen sections. The first eleven sections were found, by careful matching of the crystal faces of adjacent segments, to form a continuous length. From the twelfth section onwards there are a number of hiatuses, a silt section and some post depositional alteration, and the individual sections cannot be reconstructed into a single core.

Binding

To best sample the cores they had to be re-assembled as complete lengths. The two main options investigated were setting the sections in a bed of plaster of Paris, and binding the sections with fibreglass tape. Fibreglass was chosen on the basis that it is stronger, and can be used to assemble a core with minimal contamination of the calcite (ICPMS analysis showed epoxy resin to contain no appreciable uranium or thorium, an important consideration for U-series dating). A strong red pigment was used in the epoxy resin, to enable later visual identification of, and removal or avoidance of, any contaminated calcite.

The seven sections of the shorter core MD8 were re-assembled as a continuous length. Fibreglass tape soaked in epoxy resin was laid along the sides of the core and allowed to set. The core was then rotated 90° and two additional

tapes were set. It was found that the reconstructed core could now be split along its axis, and was considerably more robust than had it been a continuous length of speleothem core sample to start with. Further longitudinal splitting of one of the half cores was attempted, producing two full-length quarter cores.

The upper 587 mm of the longer core MD3 was then assembled using a similar procedure. It was decided to also split this core into one half-round and two quarters.

Samples for uranium-series dating

The half core of MD3 was backed with a length of heavy aluminium extrusion, allowing slices to be removed for dating, while still preserving the exact relative positions of the remaining sections of the core. 2 mm slices were cut from the half-round using a diamond glass-cutting saw, parallel to the growth laminae (i.e. subnormal to the core axis), giving sample weights of approximately 10 grams for U-series dating (which were later halved, to allow for duplicate 5 g samples).

Microcarbonate device/ICPMS sample milling

An issue that had to be addressed before sampling any core for trace element or stable isotope analysis was whether to use homogenised adjacent increments of the core, or to sample discrete points along the core. In favour of taking discrete samples at a high resolution is the ability to investigate a sequence at low resolution by skipping samples, before returning to analyse intermediate samples in the regions of greatest interest. Outweighing this advantage, though, is the problem of aliasing, that is, of spurious low frequency signals resulting from the sampling of signals with a wavelength of less than twice the sampling interval. Modelling of synthetic speleothem records showed adjacent samples to give significantly more accurate results than discrete samples, which in some cases gave quite misleading results (fig. 4.3). Because of this, it was decided to sample adjacent increments, and to

later re-sample at higher resolutions where required (again, using adjacent increments of the sample).

One of the quarter sections of MD3, backed with a section of aluminium extrusion, was mounted on a computerised milling machine. 117 increments, each of 5 mm in thickness, were milled from a 1 mm by 1 mm groove along the corner of the section, corresponding to the central axis of the core. These samples, each of ca. 5 mg, were homogenised, and stored in a silica gel desiccator for later analysis. The positions of the 5 mm increments were marked on the core, to enable accurate repeat sampling of some sections at much higher resolutions. Later, the basal 150 mm of MD3 was re-sampled in this manner, at a 2 mm interval, and the interval from 435 to 535 mm was re-sampled at a 1 mm interval.

LA-ICPMS slides

One of the quarter-rounds of core MD3 was glued to a 40 mm by 600 mm section of 2.5 mm glass sheet using epoxy resin (again with a red tracer dye). The core was then sliced off the glass with a diamond saw, leaving a 1 mm slice of core on the glass, of the length of the original core. A ca. 5 mm strip of this slice was taken, approximately corresponding to the central axis of the core, and cut into 50 mm lengths. These lengths were mounted side-by-side onto 25 mm by 64 mm glass slides, and then in each case abraded to a planar surface and polished, ready for laser ablation. A second ca. 5 mm strip was cut from the glass-backed slice of MD3, parallel to and adjacent to the first. This section was also cut into 50 mm segments, but with the cuts offset by 25 mm from those in the first slice, to produce overlapping segments. The segments from the second section were also mounted on slides for laser ablation.

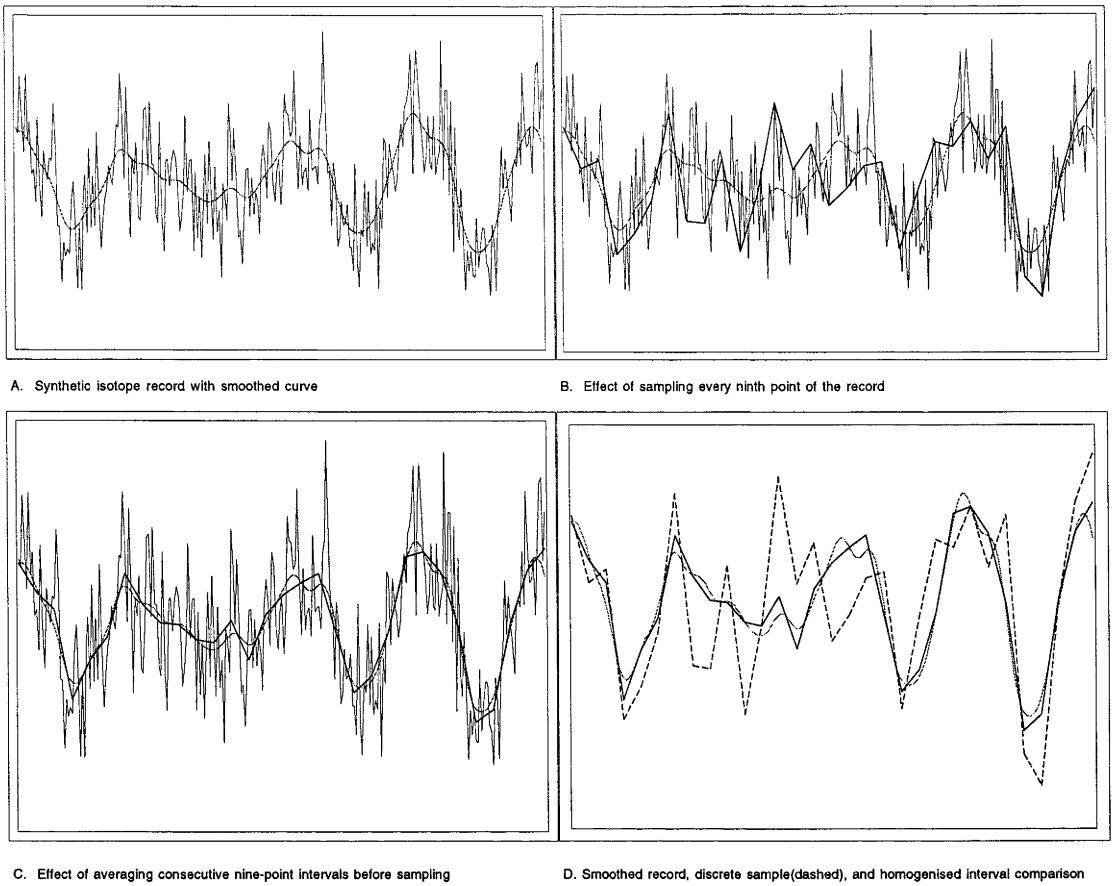

Fig. 4.3. A synthetic speleothem oxygen isotope record, showing the degree to which drilling discrete samples can bias results. Panel A shows the original isotope signal versus distance, and a smoothed version, which it is generally assumed sampling at a lower resolution will reflect. Panel B shows the effect of taking discrete samples at regular intervals along the speleothem, as is commonly done for speleothem records. Panel C shows the effect of homogenising adjacent sections of the speleothem, as has been the practice for this project. Panel D compares the methods, showing discrete sampling to seriously misrepresent the original signal.

Other

25 mm cores

The 25 mm cores, each up to 180 mm long in several sections, have not been re-assembled, although it is possible to match the individual sections, and verify that the cores are complete. A number of these sections have been split into half-rounds, and ten 4 mm increments of these have been used for U-series dating. A 1 mm longitudinal slice of core HS2 was mounted on a glass slide and finished with a one-micron polish, for examination by microscope, and for preliminary LA-ICPMS analysis.

Straws

Some straw speleothem fragments from this sample were used to investigate the best method of milling straws for analysis. Based on this investigation, a 20 mm length of straw PV1 was mounted onto a perspex block, using epoxy resin, and mounted on a computerised milling machine. This straw (sample PV1.1) was then milled, in 0.5 mm homogenous increments (each producing about 3 mg of calcite), for analysis by solution introduction ICPMS. Two further straws from this sample (pv1.2 and pv1.3) were mounted on a glass slide and slightly abraded to form planar surfaces, for experimental laser ablation ICPMS analysis. Subsequent LA-ICPMS analysis of straws has been by temporarily mounting them on a glass slide, and ablating the outer surface with no prior preparation of the sample.

Stalagmite and modern calcite samples

The 20 cm stalagmite RK1 was split along its axis, into one half section and two quarter sections. A 10 mm slice was taken from one quarter section for experimental sampling with the milling machine. The base of this slice was also sampled for U-series dating. Modern calcite samples were cleaned and dated as five-gram samples.

Australian samples

The calcite sample AM1, from the Nullarbor Plain, presumed to have formed as a subaqueous rind, has been prepared as a standard for both solution introduction and laser ablation ICPMS. A stock solution (AM1.1) was made by dissolving one gram of this sample in 100 ml of weak nitric acid, which was then calibrated against the BHVO igneous standard. AM1.1 has since been used, diluted a further ten times, as an analytical standard for all Nettlebed speleothem ICPMS analyses. A solid standard, AM1.2, was prepared by cutting a 10 mm by 7 mm rod of AM1, normal to its growth layering, and polishing one surface. LA-ICPMS traverses of AM1.2 have been calibrated against NBS 610 standard glass, and it is now used as a standard for ICPMS analysis of other speleothem samples.

A pure white section of macrocrystalline calcite was cut from a block of flowstone, previously collected from Yarangobilly Caves by John Stone. This white horizon, thought to be ca. 25,000 cal yr in age, was cut into 2 kg of 30 mm cubic blocks using a rock saw, which were then ultrasonically cleaned in acetone and deionised water. The blocks were then broken into smaller fragments, and shuffled, before being crushed in a tungsten mill. The resulting powder was sieved through a 30-micron mesh, producing ca. 1.5 kg of fine powder (sample YB1), for use as an internal speleothem standard for Uranium-series dating.

Chapter 5. Uranium series dating of speleothems

Introduction

Arguably the most compelling property of speleothems as indicators of past environments is that they can be precisely dated on an absolute timescales. This chapter examines the theoretical background of the uranium-series method by which this is possible, and discusses the practicalities of applying it to low-uranium speleothems such as those found beneath Mt Arthur. The results of uranium-series dating of Mt Arthur speleothems are reported, and the implications of these ages for the environmental history of the region are discussed.

Theory

^{238}U-^{234}U-^{230}Th dating of speleothems is made possible by the very low solubility of thorium, and the relatively high solubility of uranium, in natural waters (e.g., Schwarcz, 1989). The method assumes that uranium is incorporated into speleothems as they precipitate from cave seepage waters, but that thorium remains behind in the weathering zone of the host limestone (e.g., Schwarcz, 1986). It follows from this assumption that any ^{230}Th present in a speleothem at a given time must have resulted from the decay of its parent uranium isotopes in that speleothem. Using the known decay rates of ^{230}Th and ^{234}U, it is possible to accurately determine the age of a speleothem, back to a practical limit of 400,000—600,000 years, depending on the uranium content of the sample.

U-series disequilibrium

In an undisturbed sample of several million years' age, ^{238}U, ^{234}U and ^{230}Th will be in secular equilibrium, that is, the activities of all three isotopes will be the same, and the relative abundance of each isotope shall be proportional to its half-life. The chemical processes leading to the formation of a speleothem

disturb this equilibrium in a predictable fashion, and thus the age of a speleothem may be inferred by the degree to which equilibrium has been restored in that speleothem (e.g., Ivanovich, 1982). In addition to the disequilibrium caused by the exclusion of thorium during speleothem formation, speleothems at time of formation reflect the $^{238}U/^{234}U$ disequilibrium present in natural waters, which results from increased mobility of ^{234}U in weathering host rocks (Gascoyne, 1982). This increased mobility was originally thought to be due to ^{234}U occupying sites in the crystal lattices of host minerals damaged by emission of α and β-particles during the decay of its parent ^{238}U (Cherdyntsev, 1971; Cherdyntsev *et al.*, 1965). It now appears that alpha recoil of ^{234}U from solid into solution may be a more important factor (Osmond and Cowart, 1982; see also chapter 7). As two decay systems are present, one of them with an unknown degree of disequilibrium, an iterative calculation for age is required. An equation by which achieves this was derived by Kaufman and Broecker (1965):

$$\left[\frac{^{230}Th}{^{238}U}\right]_{act} = 1 - e^{-\lambda_{230}t} + \left(\left[\frac{^{234}U}{^{238}U}\right]_{act} - 1\right)\left(\frac{\lambda_{230}}{\lambda_{230} - \lambda_{234}}\right)\left(1 - e^{(\lambda_{234} - \lambda_{230})t}\right) \qquad (5.1)$$

where *act* denotes activity ratio, *t* denotes age in years and the decay constants λ_{230} and λ_{234} are the reciprocals of the half lives 352,740±710 yr and 108,750±850 yr, respectively (Edwards *et al.*, 1987). Alternatively, equation 2.2 may be used. As neither form of the equation can be expressed in terms of time, an iterative technique must be used to resolve an age for each sample that is dated.

It can be seen that this method relies on the speleothem in question acting as a closed system over its life, and that no initial ^{230}Th is incorporated at its time of formation. The assumption that speleothems act as closed systems seems justified, as long as care is taken to select samples of non-porous, macrocrystalline calcite, as post-depositional alteration of such samples is very easily identified. The second assumption above can be tested for in each sample, as any initial incorporation of ^{230}Th will be as common thorium, which is predominantly composed of ^{232}Th. Detrital silicate phases are the

predominant source of detrital ^{232}Th (Ivanovich, 1982). Attempts have been made to correct for such contamination based on the amount of ^{232}Th present in a sample and on an assumed $^{232}Th/^{230}Th$ ratio in the contaminant phase (e.g., Dorale *et al.*, 1992). Such corrections are by nature crude, as a degree of ^{238}U and ^{234}U contamination must also be assumed and addressed (e.g., Slowey *et al.*, 1996). The correction of badly contaminated samples has been addressed using isochron methods (Bischoff and Fitzpatrick, 1991; Luo and Ku, 1991), but these methods by nature involve analysing several samples to attain one date, and assume uniform contamination, so in most cases are difficult to justify in speleothems. By careful selection of samples, that is, by avoiding visibly "dirty" calcite, it is generally possible to date samples where detrital contamination is negligible. That is, where the measured $^{230}Th/^{232}Th$ activity ratio of the sample is greater than 20 (Schwarcz, 1989), or, more preferably for TIMS dates, greater than 100 (Li *et al.*, 1989).

Isotope dilution

To accurately date a sample, the $^{230}Th/^{238}U$ activity ratio must be determined as precisely as is possible. As uranium and thorium are chemically different, they respond in different ways to any chemical procedure required to prepare them for measurement, and so will fractionate relative to each other in an unpredictable fashion during this chemistry. To counter this, a known amount of ^{233}U and ^{229}Th, both isotopes that do not occur in nature, is added (spiked) to each sample immediately on its dissolution, such that the natural uranium and thorium isotopes respectively can be measured relative to these isotopes. Thus their absolute and relative concentrations in the speleothem can be determined, regardless of any chemical fractionation occurring during the chemistry and mass spectrometry. While most U-series dates reported to date have been measured using α-spectrometry, and many labs still use this procedure, a considerably more precise procedure is measurement by mass spectrometry. Uranium and thorium fractions of the spiked sample are isolated using cation exchange resins, and are analysed separately, using thermal ionisation mass spectrometry (TIMS).

Comparison to ^{14}C records - calibration curves

Equation 5.1 gives ages in terms of *t*, that is years before the sample was dated. Unfortunately, many other Quaternary dating methods, most notably the radiocarbon method, are not absolute methods, making direct comparisons of results from different methods in some cases difficult, or even meaningless. In the case of radiocarbon dating, a calibration curve has been developed to counter this, by radiocarbon dating of many samples of known age. Initially these samples were independently dated using dendrochronology, but the curve has since been extended to 22,000 cal yr B.P., by dating Pleistocene coral samples using both the radiocarbon and ^{238}U-^{234}U-^{230}Th methods (Bard *et al.*, 1990). The high-resolution section of the calibration curve has now been extended beyond 14,000 cal yr B.P. by dating varved lake deposits, in which annual layers may be counted (Hughen *et al.*, 1998). The Grip Ice core has also been used to add to the curve, in a similar fashion (Stuiver *et al.*, 1995). By using this curve, it is now possible to calibrate radiocarbon ages such that they are directly comparable to calender or U-series ages. All radiocarbon ages quoted in this work are thus calibrated, using the 1993 calibration curve of Stuiver and Reimer (1993), and by adding 4,000 years to radiocarbon ages beyond the reach of this, on the basis of data in Bard *et al.* (1993).

U/Th at RSES

Chemistry

The procedures used at the Research School of Earth Sciences to spike, separate and concentrate uranium and thorium isotopes for U-series dating of carbonates are described in detail by Stirling *et al.* (1995) and Stirling (1996), and so are only briefly covered herein. The chemical procedure used is broadly based on that of Chen *et al.* (1986).

A few milligrams of each sample are removed before dissolution to allow determination of their uranium content by solution ICPMS analysis, which

enables calculation of an appropriate ^{233}U /^{229}Th spike weight. This step is required due to the large and unpredictable variation of uranium content in speleothems, and to the requirement that the $^{233}U/^{235}U$ ratio in a sample is close to 1. Two to five gram samples of speleothem are then ultrasonically washed in acetone and deionised water (a pre-wash step in dichloromethane is added for samples taken from fibreglass-bound cores, to remove any traces of epoxy resin), and air dried.

As ^{230}Th must in some cases be measured in concentrations as low as tens of parts per quadrillion to date speleothems, it is essential that the chemical procedure does not introduce contaminants to the samples at any stage. Work is conducted in laminar flow work-stations, using equipment cleaned with AR-grade acids and high-purity deionised water. Reagent acids are distilled from AR-grade acid in quartz-glass stills, and diluted where required with deionised water. Procedural blanks are measured with each batch of five samples, and typically indicate that error due to contamination is two to three orders of magnitude lower than the precision to which samples are measured.

The air-dried samples are weighed into 60 ml teflon vials, covered with water, and then dissolved by step-wise addition of concentrated HNO_3. Immediately after dissolution, samples are spiked according to their uranium content with a known amount of a pre-mixed $^{233}U/^{229}Th$ spike. Hydrogen peroxide is then added to the sample to destroy any organic compounds trapped in the speleothem, and the sample is left to allow full equilibration with the spike.

After evaporation to near dryness, the samples are diluted with weak HNO_3, and a small amount of iron chloride added. The pH is then progressively raised by addition of ammonium hydroxide until an iron hydroxide precipitate forms, scavenging the uranium and thorium from the sample. The remaining fluid, containing the bulk of the carbonate sample is discarded, and the washed precipitate dissolved in HNO_3 and loaded into a prepared ion exchange column. The uranium and thorium fractions are collected separately, and each fraction further purified using smaller ion-exchange columns. Samples are collected in Teflon vials and evaporated to dryness (a

small amount of suspended graphite is sometimes added before drying the samples down, to aid in later location of the dried sample on the base or sides of the vial).

Mass spectrometry

Both uranium and thorium are analysed on a Finnigan MAT 261 thermal ionisation mass spectrometer, again following the procedures used at RSES for the dating of corals on this machine (Stirling, 1996; Stirling *et al.*, 1995). An attempt was made by T. Esat to analyse the thorium fraction from one of the Nettlebed samples (MD3A8) using charge-collection mass spectrometry (see Stirling *et al.*, 1995, for details of method). Unfortunately it was found that the ^{230}Th level in this sample (and thus in young speleothems generally) was very close to the background levels typical of this method. Because of this, Th from speleothem samples has since instead been measured on the RSES MAT 261, using a peak-hopping method on the analogue secondary electron multiplier (SEM). The Finnigan has proved considerably more accurate at very low thorium beam currents, due lower background counts, and greater sensitivity to very low intensity ion beams.

The RSES procedure for uranium measurement is a type of static multi-collection, where ^{233}U, ^{235}U and ^{238}U are measured in faraday cups, while ^{234}U is simultaneously measured in an analogue SEM. Data is collected in blocks, between which the SEM is calibrated against the faraday cups using the natural ^{238}U/^{235}U ratio of 137.88. This ratio is also used to measure mass fractionation of uranium, avoiding the need for a double uranium (^{233}U/^{236}U) spike. Thorium measurement is very difficult for young speleothems, due to the extremely low levels of ^{230}Th present, and so ^{232}Th is generally only measured against ^{230}Th and ^{229}Th for two or three blocks of data, after which the ^{230}Th and ^{229}Th peaks are alternately measured until the sample is exhausted.

Error calculation

The ion and activity ratios from the MAT 261 output, corrected by its online software for mass fractionation and according to the spike isotope ratios, are entered into a Microsoft Excel spreadsheet. Ages are calculated by solving equation 5.1 for each sample, using an iterative method. While calculation of ages from the isotope data is thus straightforward, calculation of their associated errors is considerably more complex. Whilst some authors have treated this subject rigorously (e.g., Edwards *et al.*, 1987; Ludwig *et al.*, 1992), many others do not mention how their age errors were calculated (e.g., Atkinson *et al.*, 1978; Falguères *et al.*, 1992; Ford *et al.*, 1993).

Error propagation

For young (less than 100,000 yr) ages, or ages where the error is very small as a percentage of the age, the errors on a ^{238}U-^{234}U-^{230}Th age may be considered symmetrical about that age. In such cases, the assumptions underlying conventional error propagation hold true, namely that the percentage error is small, and that the probability distribution of the age is symmetrical about its mean (i.e. where the mean and median of the distribution are the same). The error associated with a U-series date may be split into three components: systematic error, from the uncertainty in the known decay constants; error derived from uncertainty in the measurement of the isotopic ratios for any given sample; and potential error resulting from failures in the assumptions of the method (such as inclusion of ^{230}Th in the sample at the time of formation, or post-depositional alteration of the speleothem).

While others have propagated the systematic error associated with the decay constants when calculating errors for ^{238}U-^{234}U-^{230}Th dates (e.g., Stirling *et al.*, 1995), it is not considered necessary in this study. As the error is systematic, and even in samples of 100,000 years in age contributes less than 1,000 years to the total age error (Stirling, 1996), it is here considered counterproductive to factor it into the error calculation. Doing so would unnecessarily reduce the relative precision of U-series ages, a relative precision that is becoming

increasingly important in studies of the late Quaternary. The absolute precision of these ages is of lesser interest, as over most of the last 500,000 years there are few other dating methods which approach the precision of the ^{238}U-^{234}U-^{230}Th method. Where other dating methods are sufficiently precise, it should be remembered that the absolute precision of U-series ages lags slightly behind their relative precision.

Error derived from potential failures of the assumptions explicit in the ^{238}U-^{234}U-^{230}Th method is also ignored herein, in that it is extremely difficult to quantify this error. As such, rather than attempting to correct for such effects, results from samples which prove to contain significant concentrations of thorium, or which show any signs of post-depositional alteration, are not considered here. The error addressed for ages in this study is thus that which derives from the determination of the U-series activity ratios within any given sample, based on the counting statistics reported by the MAT 261 mass spectrometer. As addressed above, this error may be propagated through equation 5.1, for young or very precise ages, but becomes increasingly inaccurate as the percentage error increases (i.e. for older samples).

Monte Carlo simulation

Monte Carlo simulation allows calculation of an error where error propagation or calculation by other means is difficult or impossible. Each input variable to the age equation is randomised (in this case treating the decay constants as constant), such that after enough iterations its mean and standard deviation correspond to its reported value and reported error respectively. By doing this for very many instances of the age equation, the (skewed) distribution of the resulting ages is made to reflect the true precision of the date. For ages with near-symmetric errors as discussed above, Monte Carlo simulation and error propagation produce indistinguishable results. For older or less precise ages, error propagation overestimates the lower error and underestimates the upper error, relative to the errors produced by Monte Carlo simulation.

Monte Carlo age calculation spreadsheet

A Microsoft Excel spreadsheet was written to calculate ^{238}U-^{234}U-^{230}Th ages and their associated errors using Monte Carlo simulation. While this is an inefficient way of achieving this, using a spreadsheet enabled easy debugging of the algorithm, the graphical environment facilitates a better understanding of the calculation, and the spreadsheet can be run on most desktop computers. The spreadsheet is based about a macro which generates one thousand rows on a spreadsheet, each row containing all of the inputs to the age equations, randomised as above for those inputs with associated errors.

The macro solves each row for time (equation 5.1) using an iterative method, also determining an initial $\delta^{234}U$ for each row. The 1000 ages are then ranked from youngest to oldest, and the 25th youngest and 25th oldest samples are recorded as the lower and upper 95% errors respectively. The initial $\delta^{234}U$ is treated similarly. The median age for any sample corresponds to the age calculated using equation 5.1. The same spreadsheet also calculates errors based on error propagation (using partial derivatives of the age equation, based on a spreadsheet by P. Marianelli), and compares them to the Monte Carlo errors.

Histogram stacking

The capacity to export the column of 1000 ages calculated for each sample was added to the spreadsheet above, so that their distribution could be viewed as a histogram. Such histograms can be stacked for many individual samples on a regional basis, giving a cumulative speleothem growth frequency curve. A similar approach has been used in the past (Baker *et al.*, 1993b; Henning *et al.*, 1983), except based on stacking normal distribution curves for each date. As noted by Hercman and Walanus (1996), the latter method can only be approximate, particularly for old ages, as it assumes a normally distributed confidence interval for each sample. Hercman and Walanus (1996) stacked Monte Carlo-derived histograms for 75 Polish speleothems. Ayliffe *et al.* (1998) stacked 44 speleothem age determinations from Naracoorte Caves,

South Australia, using histograms derived from the spreadsheet described above, the highest growth frequencies correlating with times of relatively high effective precipitation in the region.

A potential problem with the cumulative probability method described above follows from its implicit assumption that cave scientists sample speleothems of random ages. There is an obvious bias towards younger ages apparent in all such records, presumably reflecting progressive burial or removal of older speleothems by cave processes. Presumably other less obvious factors also bias sample selection. The most convincing features of the record of Ayliffe *et al.* (1998) are the marked periods completely free of speleothem growth. It seems that the dating of the prominent hiatuses present in many speleothems (i.e. dating of the time of cessation and resumption of growth) on a regional basis, and stacking of the results, might give a clearer and less biased picture of the timing of regional slowings in growth.

"Graphical" solutions

The Monte Carlo spreadsheet discussed above has been adapted to produce a high-resolution map of the ^{238}U-^{234}U-^{230}Th age equation (equation 5.1), giving time as a function of [$^{230}Th/^{238}U$]act versus [$^{234}U/^{238}U$]act. Further adaptation of the spreadsheet, such that it can solve equation 5.1 for variables other than time, has been also been used to produce isochron diagrams of the solution to equation 5.1, allowing crude age and error estimates to be calculated graphically (fig. 5.1).

Following from this graphical approach, it is possible to mathematically describe error ellipses on the surface of a time versus [$^{230}Th/^{238}U$]act and [$^{234}U/^{238}U$]act graph, from equation 5.1. If an age error ellipse is thus described, using 2σ errors, the maximum and minimum ages found on the circumference of the ellipse will be the plus and minus 2σ errors respectively for that age determination. For a given [$^{234}U/^{238}U$]act determination,

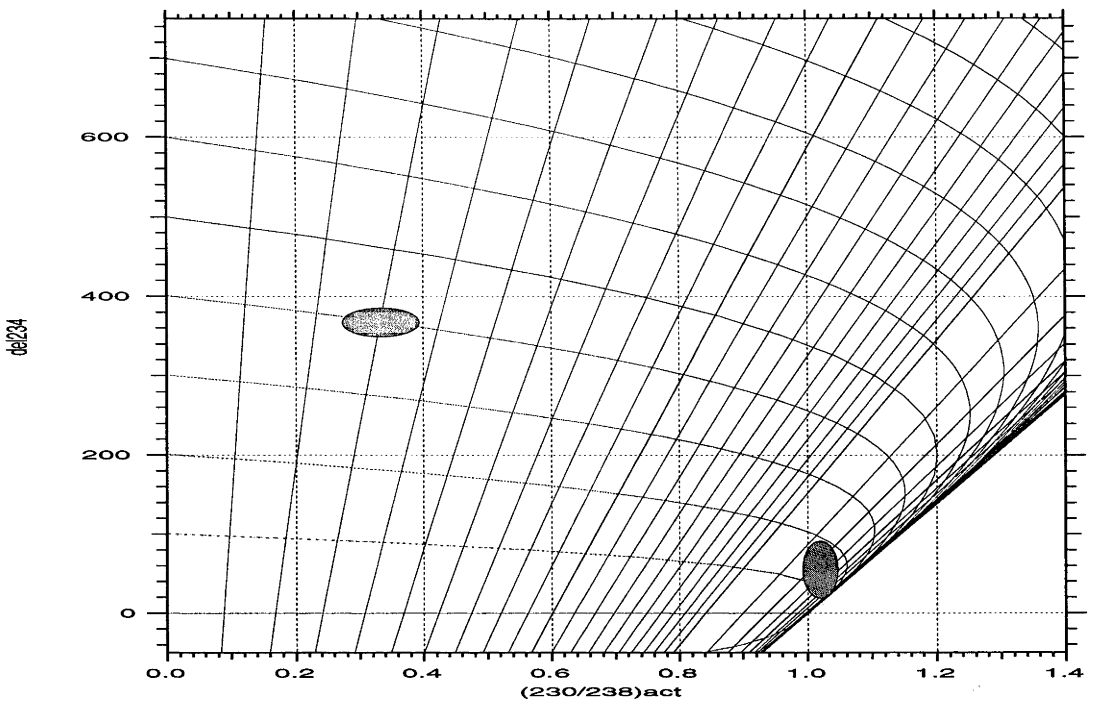

Fig. 5.1. The area of the $\delta^{234}U(T)$ vs. ($^{230}Th/^{238}U$)act isochron plot that is occupied by most speleothem samples. The straight diagonal lines are isochrons, the black lines being every 50,000 yr, increasing from zero age at the far left. Two example error ellipses are shown, illustrating that the youngest and oldest points within an ellipse are both on its circumference, an assumption implicit to error calculation methods using equations 5.2—5.4. The older ellipse also illustrates the asynchronous nature of errors associated with some U-series dates, being aged 325,000 (+600,000 –75,000) cal yr. The plot was created by iteratively solving equation 5.1 for fixed values of time and $\delta^{234}U(T)$.

$[^{234}U/^{238}U]act_{mean}$, with associated error $[^{234}U/^{238}U]act_{error}$, any given point on its error ellipse can have its $[^{234}U/^{238}U]act$ described in terms of the angle θ, from the centre of the ellipse:

$$\left[\frac{^{234}U}{^{238}U}\right]_{act} = \left[\frac{^{234}U}{^{238}U}\right]_{act_{mean}} + \left[\frac{^{234}U}{^{238}U}\right]_{act_{error}} \sin\theta \tag{5.2}$$

Similarly, for $[^{234}U/^{238}U]act$:

$$\left[\frac{^{230}Th}{^{238}U}\right]_{act} = \left[\frac{^{230}Th}{^{238}U}\right]_{act_{mean}} + \left[\frac{^{230}Th}{^{238}U}\right]_{act_{error}} \cos\theta \tag{5.3}$$

Substituting equations 5.2 and 5.3 into equation 5.1 gives:

$$\left(\left[\frac{^{230}Th}{^{238}U}\right]_{act_{mean}} + \left[\frac{^{230}Th}{^{238}U}\right]_{act_{error}} \cos\theta\right)$$
$$= 1 - e^{-\lambda_{230}t} + \left(\left[\frac{^{234}U}{^{238}U}\right]_{act_{mean}} + \left[\frac{^{234}U}{^{238}U}\right]_{act_{error}} \sin\theta - 1\right)\left(\frac{\lambda_{230}}{\lambda_{230} - \lambda_{234}}\right)\left(1 - e^{(\lambda_{234} - \lambda_{230})t}\right) \tag{5.4}$$

A second Microsoft Excel spreadsheet has been written, which calculates errors for any given ^{238}U-^{234}U-^{230}Th age, reporting upper and lower bounds, as plus and minus $n\sigma$ errors, or as plus and minus n% confidence intervals. To achieve this, a macro finds two nested iterative solutions: θ must be solved iteratively for the greatest and least values of time, and for each iteration of this solution, time must also be solved iteratively. This method has a considerable speed advantage over the Monte Carlo method, but more importantly produces more precise, fully repeatable results, as it has no dependence on random numbers. A disadvantage of this method is that it does not produce data suitable for stacking in a histogram, although it could be made to do so.

Results

A total of 39 Mt Arthur speleothem samples have been processed for U-series dating as part of this project, as have 9 procedural blanks. Of those 39 samples, five failed to register enough uranium in the collectors of the MAT 261 mass spectrometer during measurement. Five thorium fractions also failed to run, leaving only 32 which could be dated. The samples dated produced ages from 1745 to 158,000 years, covering a full glacial-interglacial cycle, although they are predominantly less than 50,000 years old. While generally very clean, the Mt Arthur samples have proved extremely difficult to date precisely, due both to their very low uranium levels, and to their young ages. $^{230}Th/^{232}Th$ activity ratios ranged from 10, at which samples must be considered marginally susceptible to problems with detrital thorium contamination (Schwarcz, 1989), to over 600, where such contamination is negligible.

It is difficult to explain why five thorium and five uranium fractions produced ion beams too small for measurement by the mass spectrometer. Other workers at ANU have also encountered this problem with speleothems. With some samples, particularly those with appreciable organic content, it is extremely difficult to induce a precipitate from the dissolved sample during the iron coprecipitation step of the chemical procedure. This is a potential cause of sample loss, which is apparently considerably reduced by combustion of samples at high temperature before dissolution, destroying any organic content. A second point at which uranium and thorium may be lost is during the ion-exchange column chemistry stage, possibly due to interference of organic molecules or very fine detrital material such as clay interfering with the exchange resin. Failure to fully load a sample onto a mass spectrometer filament can also cause low yields, as it is not always possible to confirm that the sample has been scavenged from the beaker in which it was dried down. That uranium loss was usually also accompanied by thorium loss implies that the problem lies during the chemical procedure, rather than during the mass spectrometry.

Speleothem standard YB1 has proved extremely difficult to date, although this may be mostly through bad luck, as others at RSES have not had such problems with the same sample. As such, the $^{234}U/^{238}U$ ratio of the standard is very well known, and the age somewhat less so, at 29,035 cal yr B.P., from six determinations (see appendix 4). Repeat measurements of this standard indicate that speleothem dates from the RSES laboratory have an external precision fully consistent with their reported errors, even through a change of $^{233}U/^{229}Th$ spike in the chemical procedure, and several replacement secondary electron multipliers on the Finnigan MAT 261.

Growth periods and rates

Cores MD3 and ED1

The raw activity ratios and calculated ages for the U-series dates are shown in table 5.1. Figure 5.2 shows depth versus age for cores ED1 and MD3, and the age/depth models used in this study. Both speleothems are actively growing today, as illustrated by incorporation of muddy boot-prints into the calcite surfaces since the discovery of the caves. Core MD3 grew continuously from 31,000 cal yr B.P. to the present, covering all of oxygen isotope stages 2 and 1, including the LGM, Termination I, and the period corresponding to the Younger Dryas. During this time, its growth rate varied by a factor of ten, from roughly 6 mm to 60 mm per year, illustrating the importance of dating multiple points along a speleothem. Core ED1 ceased growth between 73,000 cal yr B.P. and 16,000 cal yr B.P., and then grew continuously to the present.

Other cores from The Meltdown

Core MD1 is aged 34,756±413 cal yr B.P. at 125 mm depth, and the adjacent core MD2 is aged 36,282±1332 cal yr B.P. at 150 mm, in reasonable agreement with one another. A sharp band of detrital silicates, visible in both cores at 65 mm depth, is dated at 19,922±436 cal yr B.P. in core MD2. This band is likely to represent a slowing or cessation of growth at this time, and so the age

TABLE 5.1. U-SERIES DATA AND CALCULATED AGES FOR LOWER SECTIONS OF CORES MD3 AND ED1.

Sample	U (ppm)	Depth (mm)	$^{234}U/^{238}U$ activity	$^{230}Th/^{238}U$ activity	Age (yr)[a]	$^{230}Th/^{232}Th$ activity
MD3A1	0.052	105	1.370(0.044)	0.067(0.003)	5401(275)	82
MD3A5	0.049	297	1.355(0.004)	0.108(0.009)	9018(782)	10
MD3A6	0.091	374	1.362(0.007)	0.136(0.013)	11,382(1157)	564
MD3A7	0.113	451	1.410(0.013)	0.169(0.010)	13,850(878)	177
MD3A9	0.081	462	1.402(0.007)	0.176(0.004)	14,499(322)	260
MD3A19	0.092	486	1.413(0.005)	0.191(0.001)	15,699(145)	193
MD3A10	0.113	511	1.405(0.005)	0.244(0.020)	20,533(1868)	103
MD3A11	0.106	540	1.386(0.057)	0.313(0.021)	27,469(2417)	173
MD3.11C2	0.107	581	1.376(0.003)	0.345(0.004)	31,012(442)	85
ED1A1	0.073	103	1.246(0.010)	0.086(0.003)	7786(239)	15
ED1A2	0.068	173	1.225(0.030)	0.170(0.009)	16,216(980)	22
ED1A4	0.040	179	1.178(0.005)	0.583(0.014)	72,777(2501)	42

[a] Two-sigma errors (bracketed) are propagated by Monte Carlo simulation, and can be considered symmetrical (see text).

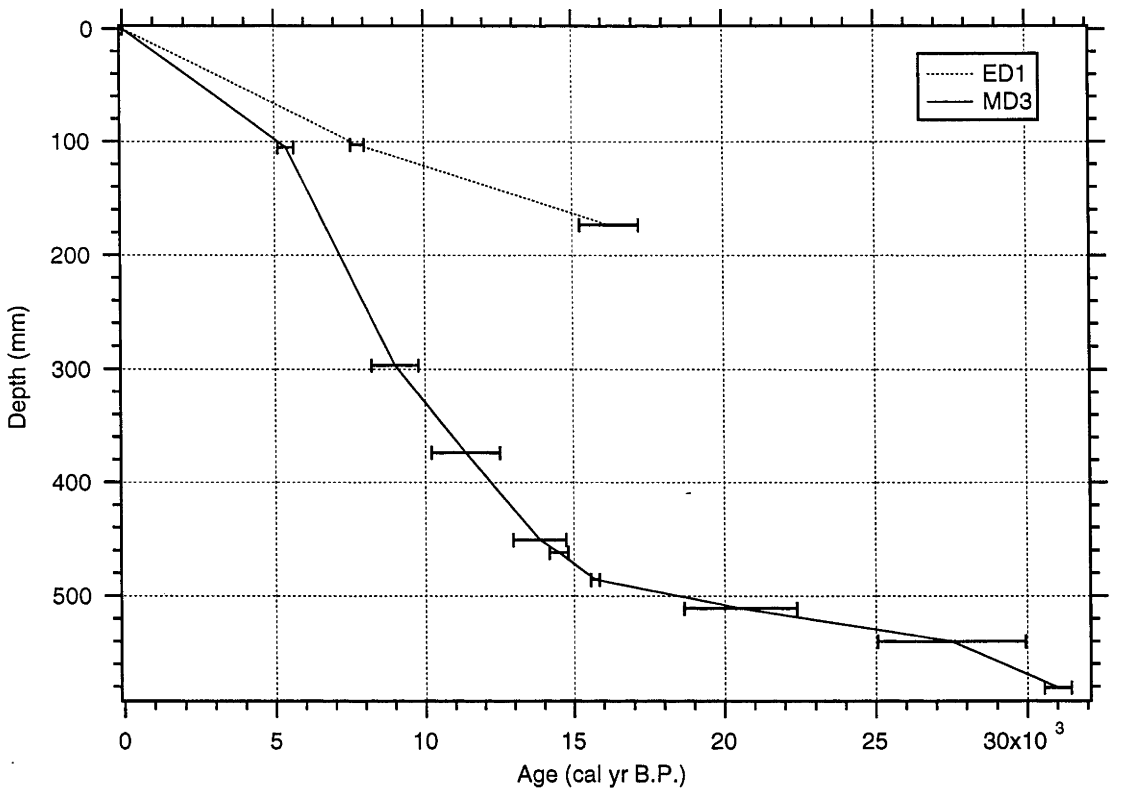

Fig. 5.2. Depth vs. age, for cores MD3 and ED1. The need to date speleothems at high resolutions is clearly illustrated by the large variations in growth rate of MD3 over 31,000 yr. The older sections of ED1 are not shown.

is probably an average of material deposited immediately before and after a hiatus in growth. Growth rates in these cores, both drilled into a horizontal flowstone floor, average from 3.2 to 4.1 microns per year.

Headsnapper passage

Age determinations from two cores show the flowstone at the Headsnapper passage to have grown for a minimum of 157,626±11,894 cal yr B.P. (sample HS1.6; appendix 3). Calcite of this age immediately overlies a muddy band in the base of the core, presumably emplaced the last time the cave flooded to the level of this flowstone. The modern maximum flood level in the cave is almost exactly 50 metres below this point, giving a crude estimate of the average rate of lowering of the water table local to Nettlebed, of 0.32 metres per thousand years. Using this rate of lowering, the last flooding of the location of core MD3 is likely to have been somewhat before 300,000 cal yr B.P.

The average growth rate of the Headsnapper flowstone over the last 160,000 years is slightly less than one micron per year (in core HS1), and appears to have slowed slightly over this period, based on two younger dates in the core. Two thin black bands at around 130,000 years may record forest fires outside the cave (a number of authors have previously reported soot preserved in speleothems; e.g., Lauritzen *et al.*, 1990), possibly representing a hot or dry period during the last interglacial. There are no visible hiatuses in core HS1, implying continuous, if extremely slow, growth over the period since the penultimate glaciation.

Climatic significance of flowstone growth periods

Currently, Mt Arthur flowstone speleothems grow only beneath forested areas, and all cave passage under areas of alpine scrub and grassland is devoid of modern flowstone growth (from Ravens, 1986; 1992, and from extensive field observations). The continuous growth of core MD3 over the last 31,000 years therefore implies that forest cover of some kind persisted on

the surface above the MD3 site over this period, giving a maximum treeline lowering locally of 600—700 m at the LGM. Similarly, the dated hiatus in core ED1 implies that from 73,000 to 16,000 cal yr B.P., throughout oxygen isotope stages 4—2, the treeline was locally at least 300—400 m below its present altitude. The apparently continuous growth of the Headsnapper flowstone over almost 160,000 years, implies the surface above this point, at 400 metres above sealevel, was continuously forested over this period.

An independent implication of the continuous growth of MD3 is that temperature cannot have been lower than today by more than the modern summer cave temperature of 8.3 °C, as it shows that the cave waters cannot have been frozen. This absolute limit on temperature drop at the LGM is consistent with existing estimates of 4.5-5.0 °C for post-LGM temperature rise in this part of New Zealand (McGlone, 1988; Soons, 1979). This provides further evidence that the extreme LGM temperature changes found in Southern Hemisphere continental regions (e.g., Miller *et al.*, 1997; Thompson *et al.*, 1995) cannot be applied to Southern Hemisphere maritime climates.

Chapter 6. Stable isotope variation

Introduction

The stable isotope ratios of oxygen and carbon, specifically $^{18}O/^{16}O$, and $^{13}C/^{12}C$, are the palaeoenvironmental indicators most often analysed in speleothems and reported versus time. Because oxygen and carbon are both major constituents of calcite, their isotope ratios are easily measured using stable isotope ratio mass spectrometry. In palaeoenvironmental studies, carbonate results are reported relative to the Pee Dee Belemnite standard (PDB; Craig, 1957), as $\delta^{18}O$ and $\delta^{13}C$ (equations 2.3 and 2.4).

Because light isotopes such as those of oxygen and carbon are fractionated by the physical and chemical processes in which they participate, changes in their relative abundances are affected by, and can sometimes be used to reconstruct, changes in environmental conditions. It is important to note that fractionations due to different physical or chemical processes are essentially additive, and as such it can be difficult or impossible to isolate from a final δ value the component of fractionation caused by any one process. This chapter briefly examines the background of stable isotope methods that are relevant to speleothems, and reports and discusses the results from stable isotope analyses of Mt Arthur speleothems.

Theory

Isotopes in global waters and precipitation

Dansgaard (1964) examined the patterns of oxygen ($\delta^{18}O$) and hydrogen (δD) isotopic variation in meteoric precipitation on a global basis, finding broad geographical correlations. Factors include a dependence on temperature (the "temperature effect"), and in some cases a dependence on the amount of rainfall (the "amount effect"). The temperature of vapour condensation controls the temperature effect, through progressive rainout of ^{18}O as distance

from the vapour source increases (Buchardt and Fritz, 1980). Comparing the global spatial relationship of average annual $\delta^{18}O$ in meteoric waters with that of annual average temperature, assuming that the $\delta^{18}O$ variation is primarily controlled by local temperature, gives a temperature effect of ca. 0.7‰/°C (many of the stations which strongly influence this figure are in polar regions). The amount effect is normally only considered significant in tropical precipitation (Dansgaard, 1964), and is known to be very weak in central and southern New Zealand (Taylor, 1990). An additional important effect on $\delta^{18}O$ in natural waters is the "altitude effect," which is strongly dependent on local topography and climate, but which typically causes $\delta^{18}O$ in meteoric waters to decrease by between 0.15 and 0.5‰ for every 100 metre increase in altitude (Gat, 1980). Note that δD and $\delta^{18}O$ in natural waters are normally expressed relative to the Standard Mean Ocean Water standard (SMOW; Craig, 1961b), where, for $\delta^{18}O$, $0‰_{SMOW}$ is equivalent to $-29.94‰_{PDB}$.

In general, Dansgaard (1964) found oxygen and hydrogen isotopes to covary along the meteoric water line, defined by Craig (1961a):

$$\delta D = 8\delta^{18}O + d \tag{6.1}$$

Where *d, deuterium excess,* is equal to 10. Departures of average natural waters at any given location from the meteoric water line can be attributed to kinetic processes, generally due to environmental conditions in the source regions of those waters favouring rapid evaporation (Johnsen *et al.*, 1989). Waters in rivers, aquifers and lakes reflect the isotopic compositions of the precipitation from which they were derived, except where significant evaporation has occurred from them (e.g., Fontes, 1980).

It is generally accepted that the $\delta^{18}O$ of the bulk oceans was between 1.1‰ and 1.3‰ heavier than today during the height of the last glacial maximum (e.g., Chappell *et al.*, 1996; Shackleton, 1987). At depths of greater than 500 m, the earth's oceans are essentially homogeneous with respect to $\delta^{18}O$, with modern $\delta^{18}O$ variation of the order of 0.3‰ (Ferronsky and Brezgunov, 1989). Variations versus time of the oxygen isotope ratios of benthic foraminifera in

deep ocean cores were initially taken as representative of past changes in deep ocean $\delta^{18}O$, on the assumption that abyssal temperatures have not varied significantly on a glacial-interglacial timescale (e.g., Pisias *et al.*, 1984; Shackleton and Opdyke, 1973). While this assumption has since been shown to be false (Chappell *et al.*, 1996; Chappell and Shackleton, 1986; Shackleton, 1987), the abyssal temperature change in some cases can be shown to have been minimal (Broecker, 1986). As such, the broad history of bulk oceanic $\delta^{18}O$ changes is reasonably well known, from the great number of deep ocean cores recovered, although temporal and spatial differences in oceanic mixing during sudden transitions such as Termination I remain a topic of lively discussion (e.g., Hendy and Hendy, 1997).

Compared to that of the bulk or deep oceans, the history of oxygen isotope changes in the surface oceans is considerably less well known. It is from the ocean surface that atmospheric water vapour is derived, meaning the ocean surface ultimately has a strong influence on the $\delta^{18}O$ of meteoric precipitation. Unless independent temperature constraints can be found for the ocean surface versus time, planktic foraminifera cannot be used to reconstruct surface $\delta^{18}O$, as both the temperature and the isotopic composition of water influence the $\delta^{18}O$ of foraminifera growing in it. Linsley (1996) argued that surface temperature in the Sulu Sea had not changed over the last glacial cycle, and thus that planktic foraminifera from ocean core ODP 769 constitute a high-resolution record of surface $\delta^{18}O$ change. No such records exist in the temperate Southern Hemisphere, although modelling by Juillet-Leclerc *et al.* (1997) indicates that ocean surface LGM $\delta^{18}O$ in central southern latitudes was probably ca. 1.3‰ lighter than at the present.

The stable isotopic composition of precipitation arriving at any given site on the surface of the earth is ultimately controlled by many fractionating processes acting during evaporation from an oceanic source, transport as water vapour, and precipitation as rain, hail or snow above the site. These processes are cumulative, progressively fractionating $\delta^{18}O$ and δD from their oceanic water starting point, and thus while they can be considered separately, it is difficult or impossible to deconvolve the effect of any one of

them. Precipitation falling over continental sites is subject to a greatly more complicated fractionation history, as some or all of its source water vapour may have been derived from terrestrial sources rather than from the ocean. This provides further reason to concentrate on island sites when attempting climate reconstructions from changes in the isotopic compositions of meteoric waters.

Carbon isotopes in soils

Soil CO_2 is derived from plant root respiration, and from microbial decay of soil organic matter (e.g., Trumbore *et al.*, 1996). The $\delta^{13}C$ of soil organic matter reflects the $\delta^{13}C$ of the atmosphere, and the photosynthetic pathway used by the vegetation growing in that soil (Bird *et al.*, 1996). The difference between dominance by plants using the C_3 (Calvin-Benson) and the C_4 (Hatch-Slack) photosynthetic pathways can potentially cause the bulk $\delta^{13}C$ of soil CO_2 to vary by as much as 14‰ (Deines, 1980). For purely C_3-derived soils, as is the case for New Zealand native vegetation (Wardle, 1991), soil CO_2 $\delta^{13}C$ is expected to depart by at most a few per mil from the expected value of -27‰ (Bird *et al.*, 1996). While soil temperature has a large influence on soil CO_2 production rates, which can vary by as much as an order of magnitude from summer to winter (Dörr and Münnich, 1986; Trumbore *et al.*, 1996), it has little if any effect on the isotopic values of that CO_2 (Bird *et al.*, 1996). A grassland may produce soil carbon 1.5‰ lighter than a C_3 forest in the same location (Bird *et al.*, 1996). Considerable variations in soil CO_2 $\delta^{13}C$ have been reported due to conditions of great aridity (Burns and Matter, 1995), an effect not considered significant at Mt Arthur.

Oxygen isotopes in speleothems

Cave seepage water has been shown to be of the same stable isotopic composition as the meteoric water from which it was derived (Duplessy *et al.*, 1970; Harmon and Schwarcz, 1981; Schwarcz, 1986). Thus, long-term changes in the $\delta^{18}O$ of meteoric water falling above a cave will be directly reflected by changes in the $\delta^{18}O$ of seepage waters in that cave. The $\delta^{18}O$ of speleothem

calcite precipitated from cave seepage water under conditions of isotopic equilibrium (that is, where loss of CO_2 from the water is slow), will be dependant only on the $\delta^{18}O$ of the water, and cave temperature at a rate of –0.24‰ per °C (Hendy and Wilson, 1968).

As the temperature deep within any given cave is generally considered to approximate average annual temperature on the surface above that cave (Wigley and Brown, 1976), it can be seen that under certain conditions it might be possible to reconstruct past temperatures from measurements of $\delta^{18}O$ in speleothem calcite. Unfortunately, to do so requires that the history of $\delta^{18}O$ change in local meteoric waters is either known or can be accurately modelled, and so temperature reconstruction by these means is rarely practicable.

A simple model of past meteoric water changes that may produce reliable temperature records from speleothems is to consider that meteoric water change is driven by oceanic $\delta^{18}O$ change and local temperature change alone. Variations on this have been attempted by a number of workers, including Gascoyne *et al.* (1981), Goede *et al.* (1986), Hendy and Wilson (1968), and Lauritzen (1995). This approach ignores many other potential effects leading to meteoric $\delta^{18}O$ change, some of which are discussed below, by assuming they are relatively small.

Carbon isotopes in speleothems

Cerling (1989) showed that the $\delta^{13}C$ of pedogenic carbonates is offset by a constant 14-16‰ from the $\delta^{13}C$ of associated soil organic matter. This has sparked interest in whether a similar offset could be applied to speleothem calcite and the soil beneath which it formed (e.g., Dorale *et al.*, 1992; Talma and Vogel, 1992). As observed by Baker *et al.* (1997), a careful reading of more fundamental literature (e.g., Dulinski and Rozanski, 1990; Hendy, 1971) shows that this is not the case. Baker *et al.* (1997) found significant $\delta^{13}C$ variation in speleothems formed purely from C_3 vegetation, in support of this argument.

For a given soil CO_2 $\delta^{13}C$, (ca. -27‰ in all C_3 vegetation contexts; Bird *et al.*, 1996), the most likely cause of $\delta^{13}C$ variation in speleothems derived from that soil are fractionation during the processes of dissolution, transport and precipitation of calcite. For a number of reasons the effects of these processes may be difficult or impossible to quantify (Baker *et al.*, 1997). In particular, speleothem $\delta^{13}C$ can vary by up to 10‰ due to changes in the rate of water flow, degree of air or water turbulence, and rate of precipitation at the speleothem surface (Hendy, 1971).

Methods

Measurement

Stable isotope data were obtained from homogenised adjacent increments of the cores, from 1 to 5 mm in length. 150 microgram portions of each homogenised sample were measured as CO_2, using a Finnigan Mat 251 mass spectrometer equipped with a Kiel carbonate-extraction device, and are reported relative to the PDB standard. In the Kiel device, dissolution in H_3PO_4 was performed at 90°C for 10 minutes. NBS 19 standards were measured at the beginning, middle and end of each run of 18 samples, and used to correct the data, such that for each NBS 19 measurement, $\delta^{18}O_{PDB}$ = –2.20‰ and $\delta^{13}C_{PDB}$ +1.95‰. Multiple portions of a number of samples were run, which indicated an external precision of better than 0.1‰. One sample (MD3B93) was repeated throughout the period of analysis of samples from core MD3, again indicating an external precision of better than 0.1‰.

Kinetic fractionation testing

Hendy (1971) found that for speleothems to be reliable indicators of palaeotemperatures or the $\delta^{18}O$ of meteoric waters, they must form in conditions of isotopic equilibrium. That is, the loss of CO_2 from solution during calcite precipitation must be sufficiently slow that isotopic equilibrium is maintained between the aqueous carbon dioxide, bicarbonate ions, and water. Under conditions where this does not hold true, kinetic fractionation is

likely to occur, meaning the deposited calcite is no longer in equilibrium with the water, and potentially producing fluctuations of $\delta^{13}C$ and $\delta^{18}O$ large enough to mask any variation due to changes in climatic variables. Hendy (1971) also calculated that any such kinetic fractionation would be expected to cause simultaneous enrichment of both ^{13}C and $\delta^{18}O$ in the calcite deposited, and noted that kinetic fractionation might be tested for by determining any such covariation.

Fantidis and Ehhalt (1970) confirmed these findings, both experimentally and from natural speleothems, finding kinetic fractionation to cause parallel variation of $\delta^{13}C$ and $\delta^{18}O$ along speleothem growth layers. However, they also found that kinetic fractionation could occur during the formation of a speleothem, yet still not be detected by testing for $\delta^{13}C/\delta^{18}O$ covariation versus time in that speleothem. That kinetic fractionation might be detected above other isotopic signals versus time in a speleothem requires that variation due to kinetic fractionation is significant when compared to other underlying isotopic variations. It can be argued, and can be shown by modelling of synthetic isotope records (fig. 6.1), that kinetic fractionation effects significant enough to mask climatic signals in a speleothem will cause measurable covariation between oxygen and carbon isotope ratios versus time. Unfortunately, testing for such covariation is not a useful test for kinetic fractionation, as carbon and oxygen isotopes may also covary in the absence of kinetic fractionation, due to linkages between the various environmental variables which influence oxygen and carbon isotopes respectively in speleothems.

A characteristic of kinetic fractionation is that if present, it should cause covariation of oxygen and carbon versus time at all frequencies, including at the highest frequency present in the record, that is the frequency defined by the temporal resolution at which the speleothem is sampled for stable isotope analysis. Conversely, it seems unlikely that the different environmental variables which influence $\delta^{13}C$ and $\delta^{18}O$ respectively will vary in concert over short timescales, in such a way as to cause high-frequency covariation of $\delta^{13}C$ and $\delta^{18}O$. Thus it seems that significant covariation at the highest frequency

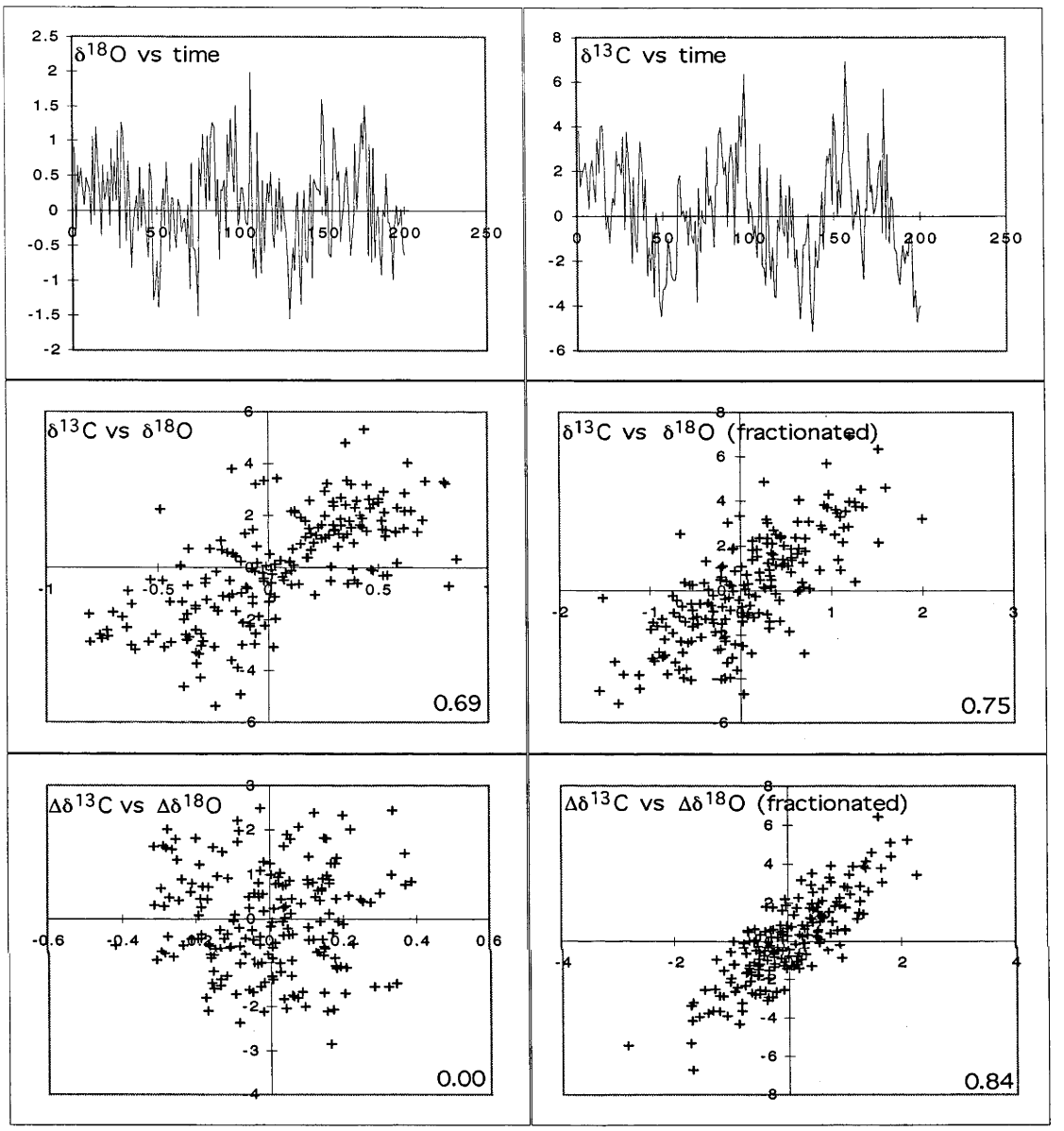

Fig. 6.1. A simulation of the effects of kinetic fractionation on oxygen and carbon isotope records. The top panels show two synthetic isotope records, to which the same random noise signal has been added, representing the effects of kinetic fractionation (such that the signal/noise ratio for $\delta^{18}O$ is 2, and the magnitude of the noise added to the $\delta^{13}C$ record is 2.5 times greater than that added to $\delta^{18}O$, as is commonly observed in real speleothems). The middle left plot shows that the records were correlated even before the addition of kinetic noise, as is the case for many speleothems, and the middle right plot shows an increased correlation after the addition of the noise. A characteristic of kinetic fractionation noise is that, unlike palaeoenvironmental signals, it is strongly correlated on all timescales. Thus, the 1st derivatives of the original noise-free records (lower left) show no correlation, and those of the fractionated records (lower right) are highly correlated. This suggests an effective test for kinetic fractionation, and several hundred repeats of the simulation indicated that records whose 1st derivatives have a correlation coefficient of less than 0.3 suffer from insignificant bias due to Kinetic fractionation. Correlation coefficients for each plot are shown in the lower right corners.

present in a speleothem record, that is, on a sample-to-sample basis, can be attributed to kinetic fractionation alone, suggesting a possible test for kinetic fractionation. By testing for covariation versus time between the first derivatives of $\delta^{13}C$ and $\delta^{18}O$, it should be possible to isolate variation due to kinetic fractionation alone, and thus test for it empirically. Modelling of synthetic speleothem records appears to confirm this (fig. 6.1), showing that variation due to kinetic fractionation, where strong enough to mask variation due to environmental changes, produces significant sample-to-sample covariation between $\delta^{13}C$ and $\delta^{18}O$ along a record. It should also be noted that kinetic fractionation is itself controlled by environmental conditions, and so may itself in some way record a response in the speleothem record to changes in these conditions (e.g., Polyak *et al.*, 1996).

Results

The stable isotope results from core MD3 and Core ED1 are shown versus depth in figure 6.2, using the age-depth model illustrated in figure 5.2. Recognising that much of the high-frequency noise in the record results from random error inherent in the analytical method, smoothing splines have been placed through the MD3 record, producing curves which are used in all subsequent discussions of the isotope records from this core.

Speleothem cores MD3 and ED1 show similar patterns of oxygen isotope variation over the last 16,000 years (fig. 6.2). Total variation of $\delta^{18}O$ in the Nettlebed flowstone over the last 31,000 years is 1.8‰, generally increasing from –5.5‰ at 31,000 cal yr B.P. to –4.2‰ at 19,000 cal yr B.P., then decreasing to ca. –6.0‰ by 7000 cal yr B.P. Seven short (one to two thousand year) positive excursions in $\delta^{18}O$, of up to 0.6‰ in magnitude, are identified along the record. Summer temperature was measured at the MD3 site as 8.3°C, and, while no temperature was recorded at the ED1 site (which is 300 m higher), it is noticeably colder. If $\delta^{18}O$ variation in the speleothems were controlled primarily by cave temperature, the ED1 record should then be displaced from MD3 in a positive sense. In fact, it is displaced in a negative sense, by 0.6‰,

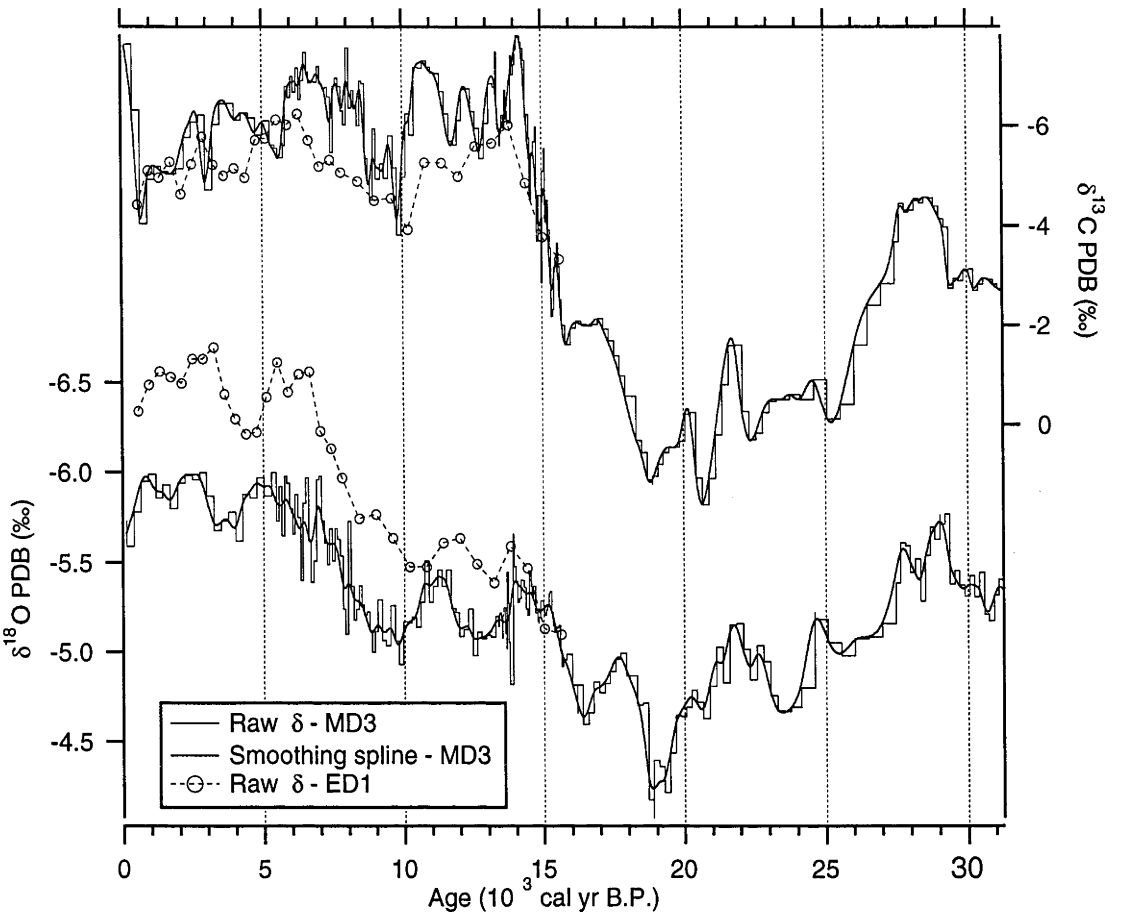

Fig. 6.2. $\delta^{18}O$ and $\delta^{13}C$ vs. time, for core MD3 and the upper section of core ED1. The MD3 and ED1 $\delta^{18}O$ records agree within the limits of their dating, strongly indicating forcing by a regional signal external to the cave environment. The smoothing splines derived here for MD3 are used to represent those records hereafter.

over much of its length, suggesting that variations in the $\delta^{18}O$ of these speleothems instead predominantly reflect changes in the $\delta^{18}O$ of the meteoric waters falling above the caves.

The MD3 and ED1 carbon isotope records broadly covary (fig. 6.2), but do not show the same degree of agreement as the oxygen records, probably due to local vegetation shifts causing the fine-scale variation. Total variation of $\delta^{13}C$ in the Meltdown flowstone over the last 31,000 years is almost 10‰, generally increasing from –4‰ at 31,000 cal yr B.P. to +2‰ at 21,000 cal yr B.P., then decreasing to –8‰ by 14,000 cal yr B.P. Broadly, $\delta^{13}C$ was high from 27,000 to 16,000 cal yr B.P., with a large and rapid fall centred on 15,000 cal yr B.P., from when it slightly increased to the present. The most striking feature of the MD3 $\delta^{13}C$ record is the extremely rapid shift to Holocene values at ca. 15,000 cal yr B.P., although the greatest individual fall in $\delta^{13}C$, of over 3‰, occurred approximately 700 years ago.

Interpretation - oxygen isotopes

It should be noted that all of the fractionating processes considered below as possible causes of $\delta^{18}O$ variation in the Mt Arthur speleothems are strictly additive, although the processes that cause them may in some cases interfere with each other, or be influenced by similar environmental changes. In this context, the processes are considered independently in the section below, followed by discussion of the likely relative importances of them.

Isotopic equilibrium

If a speleothem is not deposited under conditions of isotopic equilibrium, such as can be the case due to rapid degassing of CO_2 from the solution, kinetic fractionation can introduce unpredictable bias to the speleothem $\delta^{18}O$. As discussed, Hendy (1971) proposed a test for kinetic fractionation in speleothems by measuring $\delta^{18}O$ and $\delta^{13}C$ along a growth layer, but this test is unfortunately not possible for a core sample of only 50 mm diameter.

However, a comparison between the oxygen isotope records for cores ED1 and MD3 (figure 3) shows good agreement. This covariance between speleothems from opposite sides of a mountain, deposited in quite different settings, implies that kinetic fractionation during calcite precipitation is not in this case a significant factor affecting the $\delta^{18}O$ record.

While the ^{18}O and ^{13}C signals in MD3 do broadly covary (fig. 6.2), this can be explained in terms of both signals responding to similar climatic factors, as discussed below. The absence of significant fine-scale covariation between the two signals, as expected where significant kinetic fractionation is occurring, implies that kinetic fractionation during calcite precipitation was not a significant factor. Analysis of sample-to sample covariation of $\delta^{13}C$ and $\delta^{18}O$ in core MD3 shows an overall correlation coefficient of 0.3, while a running correlation coefficient along the record ranges between 0.2 and 0.5, the higher figure corresponding to the fastest growth period. Comparison of these results to those of isotope record modelling discussed above (fig. 6.1), implies that the highest growth-rate section of MD3 might have grown under conditions causing sufficient kinetic fractionation to at least partially obscure other climate-related signals.

Deposition by evaporation

In the event of relative humidity dropping below 100% in the cave, there will be some evaporation of seepage water from the surface of the speleothem, leading to supersaturation of calcite. Oxygen in calcite deposited in this manner will tend towards equilibrium with the cave atmosphere, and will be enriched in ^{18}O (Hendy, 1971). A regional climatic effect, probably lower rainfall, leading to lower relative humidity in the caves could this way cause higher $\delta^{18}O$ in both core samples. However, it is uncertain if lower rainfall when coupled with lower temperatures could cause this, as under these circumstances relative humidity in the cave would not necessarily fall. Hendy (1971) also proposed that, were significant evaporation to occur during deposition of a speleothem, a microcrystalline fabric would result, and concluded that evaporation of seepage waters was unlikely beyond the

entrance region of a cave. Evaporative effects seem unlikely to have been significant in the MD3 or ED1 speleothems, as they are both macrocrystalline, have comparatively low growth rates, and are located a considerable distance into the cave and beneath the earth's surface.

Temperature

The $\delta^{18}O$ of rainwater falling above the cave is dependant on local temperature, and on the $\delta^{18}O$ of the water vapour arriving in the region (Dansgaard, 1964). The temperature dependence of ^{18}O fractionation from cave seepage water into calcite is -0.24‰ per degree Celsius, while in modern New Zealand precipitation, $\delta^{18}O$ generally has a temperature dependence of roughly 0.19‰ per degree C, (Taylor, 1990). The temporal temperature gradient for New Zealand is here considered more applicable than the global spatial temperature gradient of 0.69‰/°C (Dansgaard, 1964). This is based on modelling of global meteoric isotope distribution reported by Jouzel (1998), but also because a gradient of more than ca. 0.3‰/°C would cause the MD3 record to indicate the LGM to have been warmer than today. A positive relationship between speleothem $\delta^{18}O$ and temperature, such as would be expected for a high meteoric precipitation $\delta^{18}O$ to temperature gradient, has however been reported for Tasmania (Goede *et al.*, 1986; Goede *et al.*, 1990)

At least for modern times, then, the speleothem $\delta^{18}O$ temperature effect largely cancels the local $\delta^{18}O$ temperature effect, as cave temperature is equal to average annual temperature on the surface above it. This renders the $\delta^{18}O$ of speleothem calcite essentially dependent on that of the water vapour arriving in the atmosphere above the cave. Assuming a temperature dependence of $\delta^{18}O$ in the meteoric water of 0.19‰ per °C, and that the LGM was 5°C colder than today (McGlone, 1988; Soons, 1979), temperature effects could account for very approximately 0.25‰ of the observed 1.9‰ change from the LGM to the present. This figure is a significant part of the ca. 0.6‰ excess (see following discussion) in MD3 $\delta^{18}O$ change at the LGM over that expected from oceanic $\delta^{18}O$ change alone.

Global ice volume

The $\delta^{18}O$ of the bulk oceans was ca. 1.2‰ higher than today during the LGM (e.g., Chappell and Shackleton, 1986), due to the preferential removal of ^{16}O to continental ice sheets. Precise local data for the Tasman sea or southern Ocean source areas for Mt Arthur water vapour is not available, due to the low temporal resolution of nearby ocean cores. Modelling by Juillet-Leclerc *et al.* (1997) indicates the increase in $\delta^{18}O$ of the mid-latitude Southern Hemisphere sea surface at the LGM would be ca. 1.3‰. Core ODP 769, from the Sulu sea, while being a long way from New Zealand, is the closest high-resolution core with a good chronology, and also shows a change of ca. 1.3‰ from the LGM to the present. A change of this magnitude in sea surface $\delta^{18}O$ in the source area, all other things remaining the same, would propagate through the atmosphere and result in calcite in LGM speleothems at Mt Arthur 1.3‰ heavier than today. By its similarity to existing records of oceanic $\delta^{18}O$ over the same time period (fig. 6.3), it seems likely that at least the low-frequency component of change seen in the MD3 record is largely due to the ice volume effect. This leaves a higher frequency component of up to 0.5‰ magnitude to be explained by other processes.

Local meteorology

As well as having a dependence on temperature, $\delta^{8}O$ in precipitation is inversely related to altitude ("altitude effect;" Dansgaard, 1964), and in some cases is related to the amount of precipitation ("amount effect;" Dansgaard, 1964). The magnitudes of these three effects are site-specific, depending on among other things local meteorology (Dansgaard, 1964; Gat, 1980). Any changes in the character of local meteorology over time could conceivably alter the magnitudes of these effects, causing variation in the speleothem $\delta^{18}O$ in the absence of change in the $\delta^{18}O$ of water vapour arriving over the South Island. The amount effect is generally weak in temperate regions (Dansgaard,

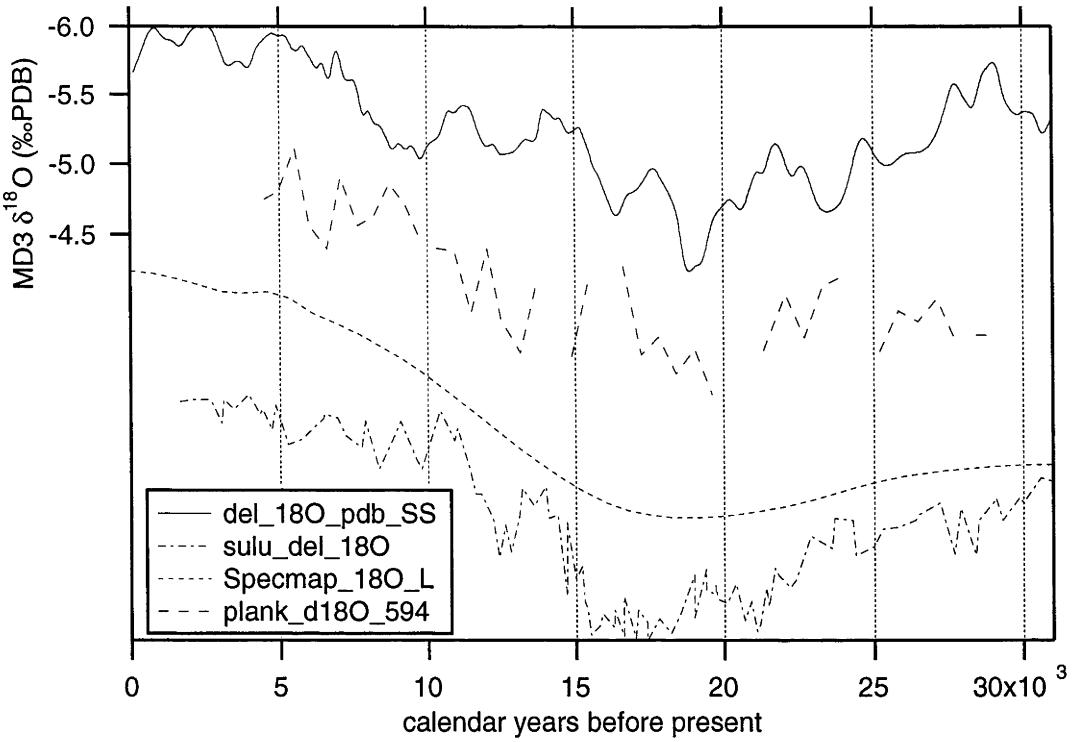

Fig. 6.3. The MD3 $\delta^{18}O$ record shown versus time with oceanic $\delta^{18}O$ records (the total variation in each record is similar, of the order of 1.5‰, and of the same polarity). Records from planktic foraminifera from DSDP 594 (off the east coast of the South Island; fig. 3.1) and ODP 769 in the equatorial Sulu Sea are shown, as is the SPECMAP composite record. These records show the oceanic signal which appears to be responsible for much of the long timescale variation in MD3.

1964), and correlation between precipitation amount and $\delta^{18}O$ in modern New Zealand meteoric precipitation is very weak (Taylor, 1990).

$\delta^{18}O$ in precipitation at a given site depends on the altitude of that site, typically changing at a rate of -0.15 to -0.5‰ per 100 metres above sea-level (Gat, 1980). The magnitude of this effect is also site-specific, depending on local climate and topography (Gat, 1980), and so may vary as local climate changes. Modern speleothems at Patarau, near sea level on the coast 70 km to the north-west of Mt Arthur, have a $\delta^{18}O$ of ca. 3.5‰ (Wilson *et al.*, 1979), compared to ca. 6.0‰ and ca. 6.5‰ for Nettlebed and Exhaleair respectively. If changing local meteorological conditions were to affect the local magnitude of the altitude effect, the $\delta^{18}O$ of ED1, the higher-altitude core, would be more strongly affected than that of MD3, which is in fact observed in the results (fig. 6.2). Curiously, the offset between the two records increases from 16,000 to 6000 yrs, and remains constant thereafter. This parallels the post-LGM sea-level rise, (e.g., Blanchon and Shaw, 1995) and therefore the re-filling of Cook Strait and coastal retreat (Lewis and Carter, 1994). The formation of a large body of water in Cook Strait would presumably have significantly affected local climate.

Season of maximum precipitation

The season of maximum precipitation is another variable that may have 0.5‰ or more influence on the average $\delta^{18}O$ of precipitation at Mt Arthur. From data in Taylor (1990), $\delta^{18}O$ in NZ precipitation is generally ca. 2‰ lower in the winter than the summer, meaning a change from dominantly winter precipitation to precipitation evenly spaced throughout the year would produce average meteoric waters ca. 0.5‰ heavier.

Deuterium excess, *d*, can be used to identify the type of oceanic water source from which precipitation was derived (Dansgaard, 1964; Johnsen *et al.*, 1989). Currently, westerly winds prevail along the West Coast of New Zealand (Garnier, 1958; Sturman and Tapper, 1996). In modern New Zealand precipitation, *d* indicates a sub-tropical source (d=10.2±0.7‰) in the north of

New Zealand, and a windy, sub-Antarctic source (d=4.5±1.5‰) in the south (d values from Taylor, 1990). This difference in source is associated with a gradation in season of precipitation in western New Zealand, from a winter maximum in the North, to a summer maximum in the south (Garnier, 1958). If, as seems very likely (T. Barrows, in preparation; McGlone, 1988), the STF and westerly wind belt moved north in the Tasman Sea during the LGM, the sub-Antarctic component would have become more dominant in Mt Arthur meteoric water, presumably coupled with a move towards summer maximum precipitation, and intensified westerly airflow. Such a change could result in average meteoric water ca. 0.5‰ heavier during the LGM. Similarly, it has been shown that the altitude effect can vary in strength from summer to winter, a study in Italy showing the summer gradient to be significantly lower (Fontes, 1980). This provides a second mechanism by which the altitude effect may have changed as discussed above, through changes in seasonality of precipitation, with the same sign to that observed at Mt Arthur.

Water vapour source area effects

A final possible cause of temporal variation in the $\delta^{18}O$ of speleothem calcite is change in the conditions at the source region of the water vapour arriving above the cave, including changes in the $\delta^{18}O$ of the bulk oceans, and changes in the configuration of oceanic water masses. Such variation should affect ED1 and MD3 by the same amount, as by their proximity they share the same distal water vapour source. Changes in source temperature, humidity and ocean surface roughness could affect the $\delta^{18}O$ of the initial water vapour by as much as +0.6‰ (calculated after Johnsen *et al.*, 1989; Merlivat and Jouzel, 1979). The precise contributions of these source effects to the 1.8‰ total variation in MD3 $\delta^{18}O$ cannot be uniquely determined, although the ca. –1.2‰ change in bulk ocean $\delta^{18}O$ since the LGM (Chappell *et al.*, 1996; Chappell and Shackleton, 1986) must contribute to the low-frequency component of the MD3 record. The sum of these effects may be responsible for some or all of the ca. 0.5‰ high-frequency variation in this record - any such influence is likely to have affected ED1 and MD3 by the same amount.

Discussion of possible effects on oxygen isotope record

Because the effects discussed above are cumulative, isolating the component of $\delta^{18}O$ change due to any one of them from the MD3 record is not currently feasible, with the probable exception of the oceanic $\delta^{18}O$ variation of ca. 1.2‰, which can be characterised from palaeoceanographic records. Broadly, the MD3 $\delta^{18}O$ signal corresponds to the global ice volume signal seen in records from ocean cores, but superimposed on this are a number of excursions towards higher $\delta^{18}O$ values, which may have been caused by any of a number of mechanisms. That these records reflect events external to the cave environment is very strongly supported by the similarity of the MD3 and ED1 signals, despite their different growth rates and their physical separation in different cave systems. The excursions are too rapid to be attributed to changes in sea level or in global ice volume, and so must be considered to be due to changes in local and Tasman Sea climate. This is considered here as likely to have been driven by latitudinal movement of the STF in the Tasman Sea. Such movement of the STF, through its effects on westerly winds and precipitation, would also strongly affect South Island glacial extent (McGlone *et al.*, 1993), linking the extent of south Island glaciation to Mt Arthur speleothem $\delta^{18}O$.

Of interest in the MD3 $\delta^{18}O$ record as indicators of local palaeoclimate, are the seven short positive excursions discussed above (fig. 6.4), hereafter referred to as MD3/1 through MD3/7. From the discussion above, these excursions seem likely to have resulted from northward migrations of the STF in the Tasman Sea, which would cause stronger westerly winds and lower temperatures in central and southern New Zealand (McGlone *et al.*, 1993). It has been shown that in historic times, stronger westerly atmospheric circulation over the Tasman Sea favours snowline lowering and glacial advance in the western South Island (Fitzharris *et al.*, 1992). There is also considerable evidence, from records of dust flux, marine $\delta^{18}O$ and pollen, that during the LGM westerly winds over the South Island were considerably

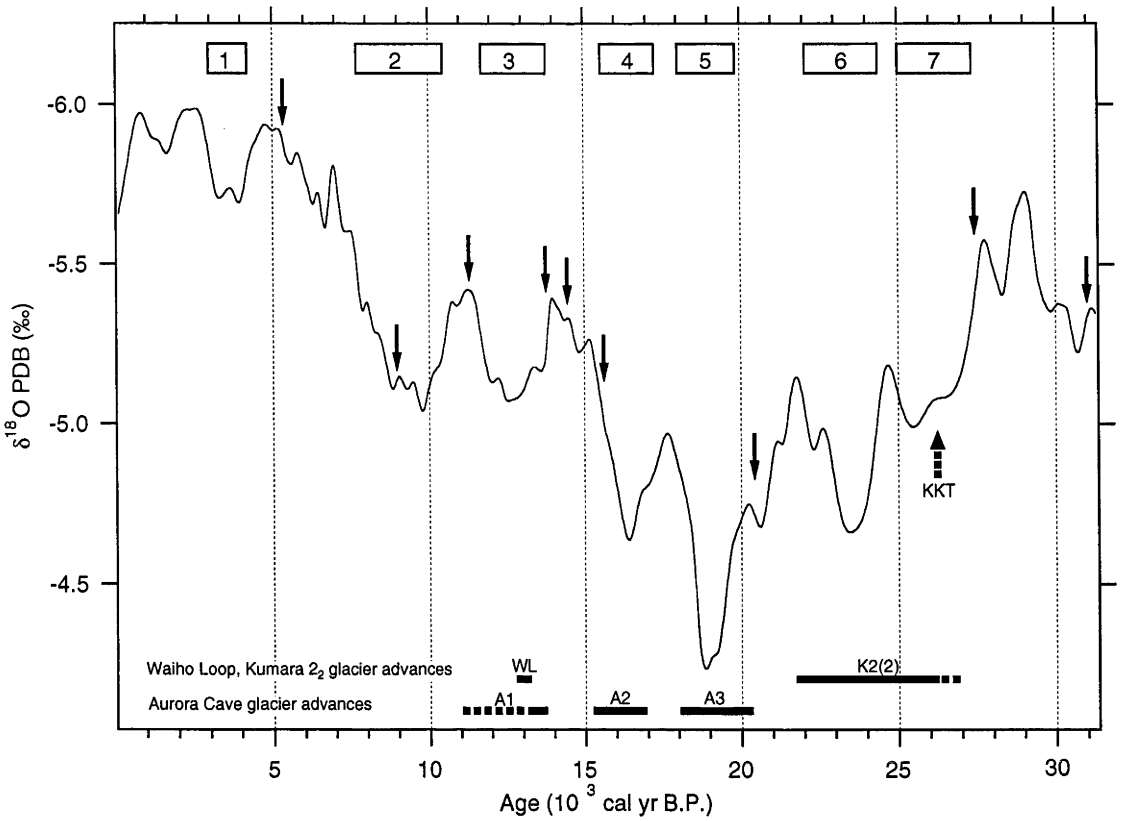

Fig. 6.4. The MD3 $\delta^{18}O$ record, shown against the best-confined periods of significant glacier advance in the South Island (black bars). The time of the eruption of the Kawakawa Tephra, an important stratigraphic marker for the initiation of oxygen isotope stage 2 glacial conditions in New Zealand, is arrowed, as are the locations of TIMS U-series dates in MD3. Shown at the top of the figure are the locations of the isotope excursions MD3/1 to MD3/9, as defined in the text.

stronger and more prevalent than today (Moar and Suggate, 1996; Nelson *et al.*, 1994; Thiede, 1979). Thus northward migration of the STF and westerly wind belt may be considered a mechanism strongly linked to both South Island glacial advances and to the MD3 isotope excursions.

Interpretation - carbon isotopes

Carbon isotope variation in speleothems is commonly interpreted as a response to changes in the relative abundance of plants above the cave using the C_4 photosynthetic pathway to those using the C_3 pathway. In many cases, it has been assumed that the resultant variations in soil $\delta^{13}C$ will be directly reflected in the speleothem calcite, (e.g., Dorale *et al.*, 1992; Talma and Vogel, 1992). The validity of this approach was recently challenged by Baker (1997), who observed that inorganic processes acting on soil CO_2 during transport and speleothem formation can have greater effects on $\delta^{13}C$ than can C_3/C_4 vegetation changes, which may be completely masked. These inorganic effects include changes in the partial pressure of soil CO_2, the amount of soil atmosphere in contact with the seepage water during carbonate deposition, and the rate of seepage water flow over the speleothem surface (Baker *et al.*, 1997; Dulinski and Rozanski, 1990; Hendy, 1970). All of these effects may vary in response to environmental changes, providing important information via the speleothem $\delta^{13}C$ record.

With only two exceptions (both salt-tolerant species absent from mountainous regions) no plant species native to New Zealand are known to use the C_4 photosynthetic pathway (Wardle, 1991). The 10‰ total variation in the MD3 carbon isotope record must therefore be accounted for in terms of inorganic processes acting on soil carbon dioxide derived from C_3 plants. The effect of lowered soil atmosphere CO_2 levels is to raise speleothem $\delta^{13}C$ (Dulinski and Rozanski, 1990), which is seen during the LGM in core MD3, and which is consistent with the known sparser vegetation during these times (McGlone *et al.*, 1993). Lower water flow rates over a speleothem surface will cause more calcite to have been lost from the fluid at any given point, thus precipitating

isotopically heavier calcite at that point (Dulinski and Rozanski, 1990). This effect is also consistent with the elevated values in core MD3 during the LGM, thought to have been drier than today (Pillans *et al.*, 1993). That growth rate, linked to the CO_2 flux from soil to cave, was low during the LGM implies soil ρCO_2 is the predominant effect forcing this record.

From the above, it would be expected that speleothem calcite growing beneath wet, dense lowland forest will be significantly depleted in ^{13}C compared to calcite formed beneath sparse sub-alpine forest. The MD3 $\delta^{13}C$ record is consistent with low forest productivity lasting from 27,000 to 16,000 cal yr B.P., followed by a very rapid increase in forest productivity in the Mt Arthur region, centred on 15,000 cal yr B.P. New Zealand has an especially rapid vegetation response time to climatic events when compared to continental climate records (McGlone *et al.*, 1993; Pillans, 1991), explaining the rapid change. That this vegetation change was so rapid implies that the associated climatic event was also very sudden, and that the event might be precisely dated by the vegetation response to it.

The carbon isotope record over the last 31,000 years (fig. 6.5) is thus interpreted as a proxy for forest extent versus time in the Mt Arthur area. Seen in this light, the $\delta^{13}C$ record shown in figure 6.5 is remarkably consistent with other records of palaeovegetation in the area, (e.g., Moar and Suggate, 1996; Pillans *et al.*, 1993; Singer *et al.*, 1998; Worthy and Mildenhall, 1989). In particular, the extremely rapid return of dense forest cover at 15,000 yr implied by the MD3 $\delta^{13}C$ data, also coinciding with a sudden increase in MD3 growth rate and the resumption of growth of ED1 (fig.3), is in very close agreement with that observed from nearby pollen records (Singer *et al.*, 1998). The LGM period of 27,000-15,500 cal yr defined by Pillans *et al.* (1993) for central New Zealand, on the basis of available pollen and geomorphic activity data, exactly coincides with the period of the highest values of $\delta^{13}C$ in MD3. Again as predicted by existing pollen data (McGlone *et al.*, 1993), the early

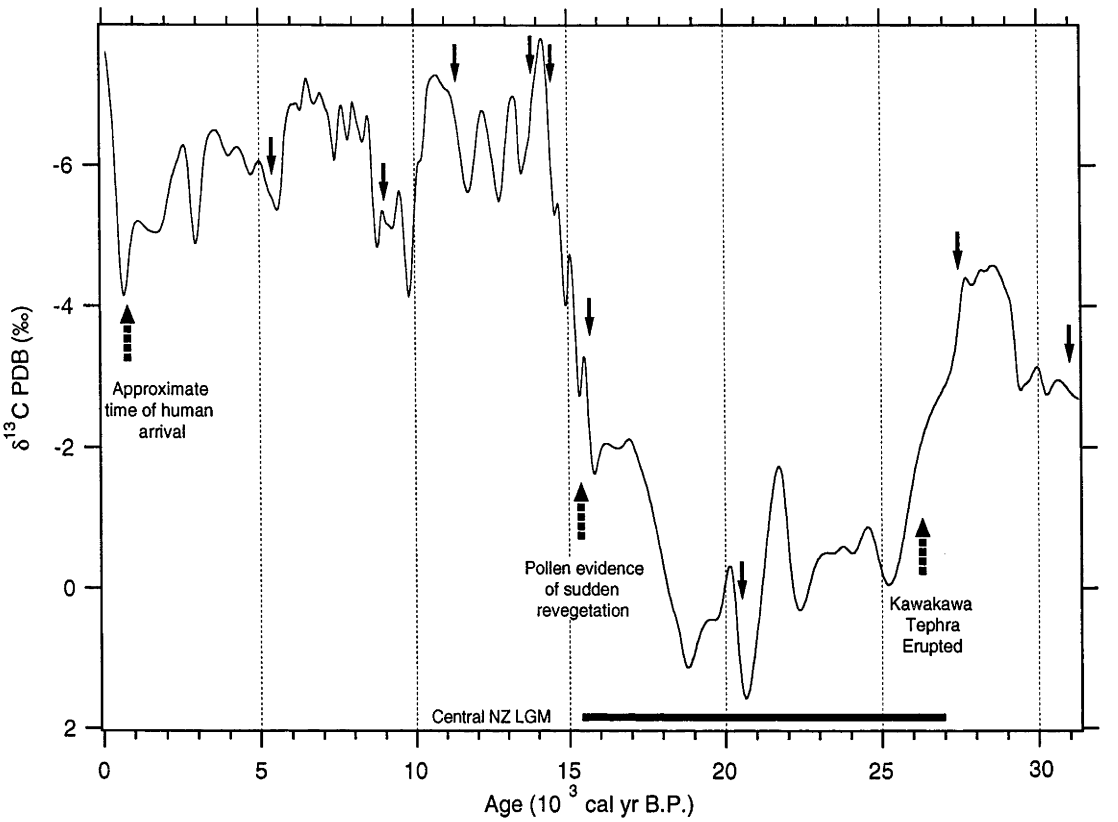

Fig. 6.5. The MD3 $\delta^{13}C$ record versus time. The period of the LGM for the central and southern North Island is shown, as defined by Pillans *et al.* (1993) on the basis of pollen and other data. The timing of the Kawakawa tephra is shown, as is the rapid revegetation observed near Mt Arthur starting at 15,500 cal yr B.P., reported by Singer *et al.* (1998), and the timing of the first evidence of significant human modification of forests in the Nelson region (McGlone *et al.* (1994). MD3 TIMS U-series dates are arrowed.

Holocene appears to have been the most favourable time for forest growth, with conditions degrading gradually through the late Holocene.

Reinforcing the likelihood that soil conditions driven by vegetation changes are the dominant forcing factor for the $\delta^{13}C$ record, is the very sudden rise in $\delta^{13}C$ at ca. 700 cal yr B.P. This is a time at which drastic climate-driven forest expansion seems unlikely, but which shortly post-dates the arrival of humans in New Zealand (McGlone *et al.*, 1994). The very sudden change to more vigorous forest growth indicated at this time is perhaps a result of the human extermination of New Zealand's browsing megafauna, thought to have had a major impact on the forest ecology (Wardle, 1991).

Chapter 7. Trace element geochemistry

Introduction

This chapter lays out the theoretical background for the study of minor and trace element concentrations in speleothems, with emphasis on their possible use as indicators of palaeoenvironmental conditions. Attention is brought to the many unquantified factors which might influence the trace element content of cave seepage waters, and the processes which might influence elemental partitioning between seepage waters and growing speleothems. Isotopic abundances of the trace elements strontium and uranium are also considered. The chapter goes on to examine solution introduction inductively coupled mass spectrometry (ICPMS) results from Mt Arthur speleothems, which are complemented with strontium and uranium isotope data from the same speleothems. Discussion of ultra-violet luminescence is also included here, on the basis that it may at least in part reflect speleothem trace element variations (Shopov *et al.*, 1994). Organic acids, the primary cause of speleothem ultra-violet luminescence (Baker *et al.*, 1993a; Ramseyer *et al.*, 1997; White *et al.*, 1995), can have a considerable influence on calcite growth (Lebron and Suarez, 1996). Laser-ablation ICPMS results from speleothems, still very much at a developmental stage, are reviewed separately in chapter 8.

ICPMS analysis was initially considered for this project as a means to easily determine the approximate uranium content of samples for U-series dating, in order to calculate appropriate ^{233}U -^{229}Th spike weights. A test on 40 consecutive calcite samples from straw speleothem PV1.1 later showed that the concentrations of many trace elements in Mt Arthur speleothems can vary with time, well in excess of the analytical errors associated with solution introduction ICPMS. On this basis, 117 homogenised adjacent samples from core MD3 were analysed for variation in a number of trace elements along its length. These results, despite very real theoretical barriers to the utility of trace element analyses of speleothems, imply that trace element variations may record recoverable palaeoenvironmental information.

Theoretical Background

While there has been some interest in trace and minor element variation in speleothems as indicators of palaeoclimate (Gascoyne, 1983; Goede, 1994; Goede and Vogel, 1991; Roberts *et al.*, 1998), it is recognised as an area as yet poorly investigated, but with considerable potential (e.g., Gascoyne, 1992). As such, there has been little published background investigation into the subject, such as systematic investigation of the composition of modern waters and calcite, especially relative to environmental variables such as temperature and rainfall (the work of Gascoyne, 1983, is a notable exception). Following from this, most of the literature reviewed in this section relates to inorganic marine carbonates, or to low-temperature calcite cements. Four subject areas are considered: likely variability in the trace element concentrations of soil waters and shallow ground waters; the behaviours and effects of trace element distribution coefficients in the water-calcite system; trace element isotopic ratio variations; and the applications to date of this knowledge to studies of speleothem trace element concentrations.

Trace element concentrations in shallow ground waters

Trace element variations in speleothems must ultimately reflect to some extent trace element variations in the waters from which they have grown. Cave seepage waters are ultimately derived from soil waters, and in many cases may have undergone significant subsequent chemical evolution during transport through pore space in the underlying carbonate rock. As such, the trace element contents of cave seepage waters are influenced by soil weathering processes, and by the subsequent dissolution of the host limestone above the cave. In this section, possible sources and causes of variation in the trace element content of cave seepage waters are addressed, under the major headings below. The headings are somewhat arbitrary in that each of the effects is to some extent interrelated with the others.

Partial pressure of soil CO_2

A dominant factor in soil chemistry, the partial pressure of CO_2 in the soil atmosphere directly affects the pH of soil waters, and thus the amount of organic and inorganic matter that they may dissolve. Soil CO_2 is sourced from microbial activity associated with the breakdown of soil organic matter and the respiration of plant roots (Dörr and Münnich, 1986). Both processes are strongest in spring and summer months, sometimes leading to summer-winter variations in soil CO_2 content of an order of magnitude or more (Dörr and Münnich, 1989). Significant changes in soil acidity might affect the absolute concentrations of dissolved mineral species in the soil waters, as well as their relative concentrations, because soil mineral phases have been shown to have differing bulk chemistry and surface cation exchange properties (e.g., Miller *et al.*, 1993).

As well as affecting soil chemistry, the pH of groundwaters directly affects the amount of carbonate rock they are capable of dissolving and carrying once beneath the soil horizon. This is likely to affect the relative rates at which different carbonate phases are dissolved, and the extent to which insoluble silicate phases are leached of trace elements (e.g., Drever and Vance, 1994). It also seems likely that groundwater pH will affect the nature of cation exchange effects on the surfaces of insoluble silicate minerals. While changes in soil temperature will influence a number of the variables considered in this section, it seems likely that the greatest effect of temperature change will be through its direct positive correlation with soil CO_2 concentration (e.g., Trumbore *et al.*, 1996).

Soil organic chemistry variation

Soil waters and waters derived from them contain dissolved organic matter, originating from biological activity in the soil. This organic matter has been shown to predominantly consist of dissolved fulvic and humic acids, generally sourced from vegetation activity and the decomposition of soil organic matter (Baker *et al.*, 1996; Drever and Vance, 1994). It has been shown

that these organic acids are capable of complexing with certain cation species, in some cases being the predominant mechanism by which these ions are carried in solution by natural waters. Conversely, binding by organic species is known to reduce the activity of some ions in solution, potentially isolating them from active participation in other groundwater chemical processes (Benedetti *et al.*, 1996). As such, the net effect of organic matter on trace element dissolution and transport in groundwaters is hard to accurately predict.

Soil water residence time

Similarly to the effect of increased soil water acidity, longer soil water residence times can lead to an increased relative contribution of dissolved metals derived from acid-resistant mineral phases. Where the bulk chemistry of such phases is significantly different from that of more easily dissolved or leached phases, the trace element chemistry of the derived soil waters will be affected by residence time. It has been shown that variation in the residence times of waters in karst aquifers affects the mineral phases from which dissolved carbonates are derived. In particular, longer residence times favour the dissolution of dolomite ($MgCO_3$) phases over calcite phases, increasing the concentration of magnesium, and possibly reducing those of trace elements such as strontium, which is present at relatively low concentrations in dolomite (Roberts *et al.*, 1998).

Changes in seepage water path

On leaving the base of a soil profile in a karst terrain, soil waters enter pore and facture space in the carbonate rock, and, even after reaching saturation with respect to calcium carbonate, may continue to dissolve carbonate minerals (Roberts *et al.*, 1998). It has been observed that changes in aquifer volume or flow rate are associated with changes in the trace element geochemistry of aquifer waters, perhaps due to changes in the nature of fluid transport. This could be from predominant flow through rock pore space, to, for increased water volumes, a greater dependence on migration through

fractures (e.g., Banner *et al.*, 1996). Such changes in transport, aside from potentially bringing the fluids into contact with chemically different sections of the aquifer rocks, can be thought of as effectively leading to lower average residence times for the waters. As such, the effects of changes in groundwater residence times considered above become important in these cases.

Trace element distribution coefficients in calcite

This section reviews what is known of the factors that influence the partitioning of various trace elements from aqueous solution into calcite. At its most simple level, the behaviour of a trace element in a solution from which a carrier mineral phase (e.g. calcite) is precipitating, is governed by the distribution coefficient, D, for that system (Henderson and Kracek, 1927):

$$D = \frac{(m_{Tr} / m_{Cr})_{solid}}{(m_{Tr} / m_{Cr})_{liquid}} \tag{7.1}$$

where m_{Tr} and m_{Cr} are the concentrations of trace (e.g. strontium) and carrier (calcium) metals respectively in solution and in the carbonate mineral. An intrinsic assumption of equation 7.1 is that the relative concentrations of the trace and carrier metals in solution do not change during precipitation due to preferential removal of one element from solution (e.g., Gascoyne, 1983). For most speleothems this would seem to be a sound assumption for any given point on the speleothem surface, as they rarely precipitate from a static body of water. There are, however, many factors which may affect the distribution coefficient of a given trace element into calcite, in many cases making it anything but constant (as reviewed in considerable detail by Morse and Bender, 1990). Those factors that are likely to apply to speleothem calcite are discussed in the sections below.

Changes in cation activities in solution

While equation 7.1 is expressed in terms of absolute concentrations, it is in fact the ratios of the activities of different elements in solution that affect their partitioning into the solid. Nominally, for an extremely dilute solution, the

activity coefficient for any given trace ion species is equal to one, that is, the activity of that ion is equivalent to its concentration in that solution (Sharp, 1983). However, even in the weak solutions typical of natural waters, activity coefficients can be highly variable. This means, for instance, that applying a distribution coefficient experimentally determined for sea water to a fresh water carbonate system can lead to errors of the order of 100% in calculated weight percent in the carbonate (Morse and Bender, 1990). For this reason, experimentally determined distribution coefficients for trace elements into calcite should ideally only be used for the precise conditions in which they were determined. At the very least an attempt to quantify changes in ion activity between the two settings should be made, and appropriate allowances applied (Morse and Bender, 1990).

In reality, it is difficult to calculate activity coefficients for natural systems, and so making such corrections may be considered difficult or impossible. Aside from total ionic strength of the solution, activity coefficients are affected by other variables, such as the presence of some organic compounds in solution (Benedetti *et al.*, 1996). In addition, solid phase activity coefficients, currently difficult to calculate in a precise manner, have a strong effect on calcite distribution coefficients. In particular, D_{Mg} at least in some cases has a strong negative dependence on mole percent $MgCO_3$ in solution, whereas D_{Sr} has a corresponding strong positive dependence on the same variable (Morse and Bender, 1990; Ohde and Kitano, 1984). This alone points to the need for considerable care to be taken when attempting to use distribution coefficients, to predict trace element concentrations in either solid or solution.

Changes in rate of calcite precipitation

It has now been shown for a number of trace elements in the calcite water system, that their partition coefficients, D, are variable depending on the rate of precipitation. This can be understood at a simple level by considering the difference between equilibrium fractionation, corresponding to precipitation at infinitesimally slow speeds, and kinetic fractionation, corresponding to rapid crystal growth. For equilibrium fractionation, ions are free to associate

and dissociate with the crystal surface as it grows, and will thus equilibrate according to their ideal, or thermodynamic equilibrium, distribution coefficient. In the case of kinetic fractionation, ions move in a unidirectional fashion from solution onto the rapidly growing crystal face, and the observed distribution coefficient will in many cases approach unity (that is, the trace element to calcium ratio in solid and solution will be the same; Lorens, 1981). While this effect is not significant for magnesium, over twelve orders of magnitude of rate (Morse and Bender, 1990), it exerts considerable influence on the distribution coefficient of strontium, and probably also of barium (Morse and Bender, 1990; Tesoriero and Pankow, 1996).

Because speleothems grow from continuously replenishing bodies of water, progressive changes in the composition of the parent solution, due to differential removal of components from that solution, is not likely to be a significant effect. None the less, this effect is likely to lead to progressive fractionation of seepage waters as they flow over a speleothem, and thus may be significant where the ratio of growth rate to water flow rate changes over time. For a given point on a speleothem surface, it is to be expected that a significant increase in growth rate relative to seepage water flow rate will lead to increased concentrations of trace elements with distribution coefficients smaller than unity (e.g. magnesium, strontium and barium) being deposited at that point.

The effect of temperature

For inorganic water-calcite systems, attention has focused on the potential of magnesium/calcium as a palaeothermometer, with a number of workers determining distribution coefficients as a function of temperature (e.g., Burton and Walter, 1991; Gascoyne, 1983). Unfortunately, as observed by Morse and Bender (1990), these distribution coefficients are generally unlikely to be applicable beyond the settings in which they were determined. D_{Mg} is consistently found to have a temperature dependence of the order of +0.001/°C (Gascoyne, 1983). Thus, while it may not be possible to precisely quantify this for all settings, it is apparent that temperature changes of only a

few degrees should be expected to significantly affect the magnesium content of calcite precipitated from a given solution. Conversely, D_{Sr} has not been found to have a measurable temperature dependence in inorganic natural systems (Gascoyne, 1983). While it is plausible that other trace elements have temperature-dependant partition coefficients in the calcite-water system, there is little published research in the area.

The effects of organic acids in solution

Organic acids in solution, specifically humic and fulvic acids, have been shown experimentally to exert major influences on calcite growth rate. While weak solutions of these organic species do not significantly affect calcite growth rate, it has been shown that increasing concentrations progressively inhibit calcite growth (Lebron and Suarez, 1996). The mechanism by which this occurs is coating of the crystal surface, such that few or no sites remain available for bonding with ions from solution (Lebron and Suárez, 1998). It seems possible that organic acids may preferentially coat certain sites, such as kinks and steps, on the crystal surface, and if so would discriminate against the inclusion of metal ions which preferentially bond to those sites (e.g., Reeder, 1996), effectively lowering the distribution coefficients for those ions.

The effect of crystal face zoning of trace elements

A particularly disturbing aspect of trace element partitioning into calcite, is the tendency of many metal ions to exhibit a preference to incorporate into certain crystal faces over other crystal faces (Reeder, 1996; Reeder and Grams, 1987). This leads to zoned crystals, whereby sectors of such crystals that were formed from growth on some faces exhibit greatly different trace element geochemistry from those formed on others. This has been described as being analogous to metals having different distribution coefficients for different calcite crystal faces, for growth from any one solution. Reeder (1996) interpreted this in terms of some ions preferring to incorporate onto flat crystal faces, while other ions, due to their size and charge differences from

calcite, are more likely to attach to the various step and kink sites present on other crystal face geometries.

While this is unlikely to present a problem to studies of trace elements in microcrystalline solids, it is potentially a major problem for the study of speleothems, which generally consist of calcite crystals millimetres to tens of millimetres across. Reeder and Grams (1987) observed variations between adjacent sectors of the same crystal of marine calcite cement, of up to 95% for magnesium, and 50% for strontium, along single growth horizons. Of all the effects mentioned above, this one is potentially the most difficult to address, as it is the only one which seems likely to introduce significant lateral variation along time horizons.

Trace element isotopic ratios in groundwater and speleothems

Unlike lighter isotopes, such as those of oxygen and carbon, the isotopes of elements with high mass numbers exhibit little or no mass fractionation during environmental processes (e.g., Bowen, 1988). In particular, the isotopes of strontium and uranium are not thought to undergo any measurable isotope fractionation during the growth of calcite crystals from solution, and thus they preserve in speleothems their ratio in the seepage waters from which those speleothems formed. Furthermore, the corrections that are made for instrumental fractionation during the measurement of these isotopes would eliminate the effects of any such natural fractionation. By a thoughtful analysis of how cave seepage waters acquire their strontium and uranium isotopic signals, and how this is likely to relate to the concentrations of these elements in the seepage waters, it may be possible to constrain the manner in which these elements partition from seepage waters into speleothems. Changes in the isotope ratios of these elements in cave seepage waters are also likely to have responded to palaeoenvironmental changes in their own right.

Strontium isotopes

A number of studies of the strontium isotopic compositions of natural carbonates have shown that they accurately reflect those of the waters from which they formed (Banner and Kaufman, 1994). As such, any study of strontium stable isotope variations in speleothems can be thought of as a direct study of the seepage waters from which those speleothems formed (as calcite excludes rubidium, the radioactive parent of ^{87}Sr; Bowen, 1988). The strontium isotopic characteristics of karst aquifers have received some attention in the past, as have those of soil waters, although there have been somewhat fewer published investigations of strontium isotopes in cave seepage waters or in speleothems.

The isotopic composition of strontium in waters derived from weathering of rock or sediments will reflect the time-integrated rubidium/strontium ratios of the parent materials, as well as the relative solubilities of the various minerals present (Bowen, 1988). The isotopic composition of such strontium will not be the same as that of the bulk parent material, because minerals bearing rubidium, and thus radiogenic ^{87}Sr, are more resistant to weathering (Bowen, 1988). It seems reasonable to assume that the degree of weathering, controlled by variables such as temperature, soil water residence time, and soil pH, will thus influence the isotopic composition of strontium derived from any given parent material. In addition to this effect, it has been shown that the strontium composition of soil waters can be influenced by changes in the relative inputs to soils from changing aeolian dust fluxes, airfall tephras, sea salt and meteoric waters. It has also been shown that changes in soil and seepage water chemistry can affect the amount of available strontium bound to organic substances in the soil, and alter the characteristics of ion exchange reactions occurring on the surface of clay particles in contact with the waters.

In summary, it can be seen that variation in the strontium isotopic composition of cave seepage waters, and thus of speleothems, at any one site will be controlled by some combination of effects. These include changing soil and host rock weathering characteristics, changing strontium inputs to the

soil profile above, and changes in seepage water chemistry and residence time affecting the relative strontium contributions from the soil and host carbonate rock.

Uranium isotopes

As well as being the principal means by which speleothems may be dated, uranium-series disequilibrium in speleothems must reflect that in the seepage waters from which they formed, at the time of formation. Because ^{234}U and ^{238}U are not stable isotopes, any disequilibrium between them in a speleothem sample must first be corrected for the age of the sample, using the equation (Edwards *et al.*, 1987):

$$\delta^{234}U(T) = \delta^{234}U(0)e^{\lambda_{234}T} \qquad (7.2)$$

$\delta^{234}U(T)$ and $\delta^{234}U(0)$ are the departures in parts per thousand of the $^{244}U/^{238}U$ activity ratio from equilibrium, at the time of sample formation and the time of sample analysis respectively, λ_{234} is the decay constant of ^{234}U, and T is the age of the sample. As uranium isotopes are known not to be fractionated by natural processes such as calcite precipitation from seepage water (e.g., Cherdyntsev, 1971), $\delta^{234}U(T)$ of a speleothem must exactly reflect that of the seepage waters from which it formed, and thus may be considered for use as a palaeoenvironmental indicator. Additionally, any such mass fractionation is removed during uranium isotope measurement, by correction to the natural $^{235}U/^{238}U$ ratio (see chapter 5).

The exact cause of the $^{234}U/^{238}U$ disequilibrium observed in natural waters (e.g., Cherdyntsev, 1971; Scott, 1982) appears to remain in dispute, although it is generally agreed that it is a consequence of the radiogenic origin of ^{234}U (Osmond, 1980). Two models are considered likely to be important in this process, being alpha recoil of ^{234}U into solution (e.g., Osmond and Cowart, 1982; Szabo and Rosholt, 1982), and preferential leaching of ^{234}U from crystal lattice sites damaged by alpha particle emission (e.g., Gascoyne, 1982; Rosholt, 1982).

Alpha recoil occurs where, as a consequence of the emission of an alpha particle during decay of ^{238}U to ^{234}Th, a nuclide is propelled backwards a few hundred angstrom units (Osmond and Cowart, 1982). In some cases, where the nuclide is close to a phase boundary, it may be propelled through that boundary, e.g. from a calcite crystal into surrounding fluids, where it decays to ^{234}U by rapid beta-decay events. It can be seen from this that, for adjacent high- and low-uranium phases, alpha recoil is likely to cause relative enrichment of ^{234}U in the uranium-poor phase, and depletion in the uranium-rich phase. It can also be seen that this process can only operate within a few hundred angstrom units of a mineral surface, and thus that the effect will be very much stronger for fine-grained materials. It is also evident that the magnitude of any such enrichment in fluid $\delta^{234}U$ will be strongly dependent on fluid residence time in the uranium source area (e.g., Osmond, 1980).

Preferential leaching of ^{234}U from a mineral lattice may occur where alpha decay and alpha recoil have led to fission track damage within that mineral. Because the ^{234}U occupies damaged lattice sites, it is more vulnerable to removal by leaching than is ^{238}U, which remains in intact sites within the crystal (Rosholt, 1982). Crystal damage from alpha particle emission can occur at any depth beneath a mineral surface, and so the magnitude of this effect is not dependent on grain size, so much as on chemical weathering rates. In the case of partial dissolution, this mechanism can be expected to lead to relative depletion of ^{234}U in the weathering mineral phase, and enrichment in surrounding fluids, whereas in the case of complete dissolution, the net $\delta^{234}U$ of the fluid should be zero. From this, it seems reasonable to assume that the magnitude of any isotopic differentiation due to preferential leaching from damaged lattice sites should be at its greatest for slow dissolution and long groundwater residence times, and approach zero for very fast dissolution rates.

Ultra-violet luminescence studies of speleothems

The luminescence exhibited by calcite speleothems on exposure to ultraviolet light has received considerable attention in recent years (Baker *et al.*, 1993a;

Denniston and Gonzalez, 1997; Shopov *et al.*, 1994; White *et al.*, 1995). Strictly speaking, while it has been noted that the presence of some trace elements could cause such luminescence (Shopov *et al.*, 1994), or indeed act to quench it (Baker *et al.*, 1996), it seems unlikely that trace metal content significantly influences it (Baker *et al.*, 1996). Instead, the UV luminescence of speleothems has been shown to be almost entirely due to organic acids incorporated from seepage waters during calcite precipitation (Baker *et al.*, 1996; Ramseyer *et al.*, 1997; White *et al.*, 1995). While UV luminescence may not directly reflect the trace element content of a speleothem, the effect of organic acids on the dissolution, transport and precipitation of these elements is likely to be significant. This, coupled with the relative ease with which UV luminescence is able to be measured, makes it a useful tool in attempting to understand trace element behaviour in speleothems.

Annual growth banding defined by ultra-violet luminescence was reported in speleothems by Baker *et al.* (1993a). Since then measurement of UV luminescence has been used as a means of counting annual bands by several authors, enabling them to construct long autocalibration chronologies for speleothem records (e.g., Jones *et al.*, 1995). Use of luminescence intensity as a palaeoenvironmental indicator in its own right has also received some attention. This follows from the reasonable assumption that organic acid incorporation into a speleothem at any given time is strongly related to the flux of organic acids from soil to cave, and thus to their production rate in the soil. Baker *et al.* (1996) found the UV luminescence intensity of a British Holocene speleothem to vary in agreement with pollen palaeovegetation records from the area. By using high-resolution laser-excitement methods, extremely high-resolution records have been produced, with sample intervals as short as six hours claimed (Shopov, 1996).

Initially thought to be caused by a combination of humic and fulvic acids incorporated into speleothem calcite, UV luminescence is now thought to be caused primarily by fulvic acids, with humic acids being responsible for much of the colouration observed in speleothems (White *et al.*, 1995). A number of workers have noted that dark, inclusion-free layers of calcite exhibit

considerably lower luminescence than cloudy, inclusion-rich layers (e.g., Genty *et al.*, 1996; Jones *et al.*, 1995). Scanning electron microscope analysis of speleothem samples by Ramseyer *et al.* (1997) confirmed this, showing the luminescing organic acids to be trapped within microscopic fluid inclusions, most likely by adsorbtion onto the walls of those inclusions. Ramseyer *et al.* (1997) also speculated that increased organic content in cave seepage waters favours fluid inclusion growth, by selectively blocking growth on the calcite surface, due to adsorbtion onto growth sites, and causing the crystal to grow around those sites. This is consistent with the observation by Lebron and Suarez (1996; 1998) that high concentrations of humic and fulvic acids in dripwater can completely halt calcite growth.

Previous trace element studies of speleothems

The first serious investigation of the potential of speleothem trace element variations as palaeoenvironmental indicators was that of Gascoyne (1983), who confirmed that the distribution coefficient of magnesium in the cave water-speleothem system appears to be temperature-dependent, and that the distribution coefficient of strontium is not. However, this study did not offer any hope for the use of speleothem magnesium content as a palaeothermometer, and the subject has received little attention since. Subsequent work by Goede (1994) and Goede and Vogel (1991) has offered hope that the concentrations of some trace elements, particularly magnesium, strontium and barium, may in at least some settings covary with aspects of climate change on a glacial-interglacial basis. More recently, Roberts *et al.* (1996) have shown that, at least over the range of environmental change known to have occurred over the Holocene, contemporaneous speleothems even from the same cave chamber can show incompatible records of trace element variation. Roberts *et al.* (1998) have found that very fine-scale trace element variations are likely to be of use as an annually resolved dating tool, in a similar fashion to UV luminescence records.

In conclusion, it must be said that the outlook, based on previous studies ,for meaningful interpretation of speleothem trace element variations does not

seem particularly promising. However, as observed by Roberts *et al.* (1996), it seems likely that, perhaps on a case-by-case basis, that calibration against other proxies or historic records might allow at least qualitative interpretation of trace element records from any given site.

Methods

ICPMS measurement procedure

Sample preparation for solution-introduction ICPMS

For the first speleothem samples analysed a two-step dissolution was used, in which samples were first dissolved in hydrochloric acid and evaporated to dryness, before being brought back into solution in 2% HNO_3. This is the medium used for solution introduction to the ICPMS, added such that each sample was diluted by a factor of 1000 times by weight. The dissolved samples were then spiked with an internal standard containing known concentrations of nine elements and enriched isotopes known not to be present in the sample at significant levels, following the procedure of Eggins *et al.* (1997b). Initial runs of speleothem samples were standardised to measurements of the BHVO-1 igneous standard. This was considered unsatisfactory for measurement of calcite, due to the likely effect of the difference in matrix on the tuning and mass response of the ICPMS.

A stock solution, sample AM1.1, was prepared from one gram of sample AM1, a uranium-rich speleothem from the Nullarbor Plain, Australia, and calibrated against the BHVO-1 standard. AM1.1 has since been used as a standard for all speleothem samples measured, the advantage of this approach being that results from individual runs may be quantitatively compared to each other. As absolute concentrations of trace elements in speleothem have turned out to be of little interest, no attempt has been made to improve the calibration of AM1.1, although this can be done at any time in the future, and appropriate corrections made to existing speleothem measurements calibrated to this standard.

After the first few ICPMS runs, the first dissolution step was discarded, as it has proved unnecessary. Beginning with analysis of samples from straw stalactite PV1.1, powdered samples were weighed directly into plastic centrifuge tubes, and dissolved in 10 ml of 2% HNO_3 pre-spiked with the internal standards. After testing of the AM1.1 standard at different dilution factors, it was found that the best results were attained by diluting samples to between two and five thousand times, by weight. The results of ICPMS analysis of straw stalactite PV1.1 later showed a dilution factor of 3,000 to produce the clearest results. More concentrated solutions than this suffer from considerable interferences due to calcium and its oxides, and more dilute solutions cause the signal intensities for some elements to drop close to their background levels. Analysis of 37 elements was attempted for straw PV1.1, and on the basis of the results obtained, subsequent analyses were restricted to 11 of these.

For analysis of samples from core MD3, approximately 3.3 milligrams of each homogenised powdered core increment were weighed into 10 ml tubes, and the spiked running solution added to fill the tube. Samples were left capped overnight to allow full equilibration with the spike before running. A drift monitor solution, sample OB3.2.1 was prepared from a speleothem sample, which, along with procedural blanks, was analysed several times, spaced throughout each run ICPMS of 40 to 50 samples. Standard AM1.1 was also measured during each run, and used for calibration of absolute concentrations. In retrospect, a more sensible approach would have been to use AM1.1 as the drift monitor as well as the concentration standard, as it is run at the same concentration as the other samples, spiked with the same internal standard.

ICPMS analytical procedure

Plastic centrifuge tubes containing the samples, standard, blanks and drift monitors were loaded into a Gilson auto-sampler, for introduction to a Fisons VG PlasmaQuad PQ2+ inductively coupled plasma mass spectrometer. After starting and tuning the spectrometer, sample and internal standard details

were entered into its control software, and the samples left to run overnight. A typical analysis run of fifty samples, seven blanks, seven drift monitors and one standard took approximately eighteen hours to complete.

Data processing

Data reduction using PlasmaQuad control software

For the initial samples, run for determination of their uranium content alone, dilution factors were entered into the ICPMS control software and all results were reported by the ICPMS as blank-subtracted solid concentrations. Uranium concentrations had an average analytical error of a few percent, and generally agreed within this error with subsequent values for the same samples determined by isotope dilution TIMS as part of the U-series dating procedure.

The data for the forty samples from straw PV1.1 were also reduced by the ICPMS, and reported as solid concentrations. The average of the reported calcium concentrations for the forty samples was 39.5%. This is extremely close to the expected value for calcite of 40.0%, especially when an allowance is made for the expected fluid inclusion content of a few parts per mil by weight (e.g., Dennis *et al.*, 1996; Schwarcz *et al.*, 1975). For most samples, the calcium concentration was within weighing error of the expected 40%, so all samples were normalised using a spreadsheet, such that calcium concentration was corrected to 40%.

Data reduction using Microsoft Excel spreadsheets

For samples measured subsequently to straw PV1.1, including all multi-element analyses of core MD3, absolute concentrations have been obtained by normalising all data such that calcium equals its expected value of 40%. This approach is justified by the precision with which fully quantitative calcium measurements corresponded to their expected values, and greatly simplifies sample preparation and data entry, as sample weights do not need to be recorded or entered.

Although the PlasmaQuad ICPMS can report blank-subtracted values, it is unable to interpolate between consecutive blanks in a run. For this reason, only the standard was blank-subtracted by the machine, and all other samples and standards were reported as raw concentrations in solution, to enable later background subtraction, where a better approximation of blank variation versus time could be determined. The limitation to this approach is that the machine is unable to correct as accurately for the effects of molecular interferences during a run, although this is not considered likely to be a significant effect in this context, for the elements measured. Except for the external standard (AM1.1), dilution factors were not entered into the ICPMS procedure, meaning the results were reported by the spectrometer as parts per billion concentrations in solution.

Data reduction was undertaken using an Excel spreadsheet, using raw concentration data transferred by floppy disk from the ICPMS. Firstly, the backgrounds determined by blank analyses were subtracted from the samples and drift monitors, by interpolating between the procedural blanks spaced through each run. For each isotope measured, the reported concentrations in the drift monitors were corrected to equal those in the first drift monitor of the run, and the resulting correction factors were interpolated between drift monitors and applied to all samples. The values resulting from this treatment were then normalised to the expected calcium concentration of 400‰. 117 samples spanning the length of core MD3, being 5 mm homogenised increments, were analysed over the course of three such ICPMS runs.

Trace element isotope measurement

Uranium isotopes

Uranium isotope measurements were made on two to five gram samples of speleothem, as part of the procedure for U-series dating. The method follows that of Stirling (1996), as described in chapter 5. $\delta^{234}U(T)$ was determined for each sample from its age and its $\delta^{234}U(0)$, using equation 7.2. For three samples from Core MD3, sample age could not be accurately determined, due

to poor or absent thorium isotope data, and in each of these cases, the age/depth model determined for MD3 in chapter 5 (fig. 5.2) was used to produce an interpolated age for use in equation 7.2.

Strontium isotopes

Strontium isotope measurements were made on 3 to 12 mg portions of 5 mm homogenised increments of core MD3, being the same samples from which stable isotope and ICPMS trace element measurements had been made, allowing direct comparison between the results. Samples were spiked on dissolution with a known amount of ^{84}Sr, and passed twice through cation exchange columns to extract the strontium fractions. The separated strontium samples were loaded onto tantalum single filaments, and run in a Finnigan MAT 261 mass spectrometer. $^{87}Sr/^{86}Sr$ results are reported as absolute ratios, corrected for mass fractionation by normalisation to the naturally occurring $^{86}Sr/^{88}Sr$ ratio of 0.1194.

Ultra-violet luminescence measurement

Split core samples were placed in a dark room, and illuminated by an ultra-violet fluorescent tube, placed parallel to the core, at a distance of ca. 100 mm. The resulting luminescence was photographed on 100 ASA colour positive transparency film, with a typical exposure time of one second. A telephoto lens (200 mm focal length) was used, to minimise distortion of the image, in conjunction with a "skylight" filter to block ultra-violet light, ensuring the film was exposed only by visible wavelengths. Magnification changes were achieved by varying the distance from sample to camera. Processed transparencies were scanned in 24-bit 3-channel colour, at ca. 3000 dots per inch, using a Nikon 35 mm transparency scanner. The blue channel was in each case discarded, and either the red or green channel used as an indicator of sample luminescence intensity (the red and green channels were found to be essentially indistinguishable in this regard, save for an absolute intensity difference).

The resulting 8-bit greyscale images were saved in uncompressed TIFF format, for export to the application NIH Image, where intensity profiles of each image were taken, parallel to the direction of growth. To reduce the effects of noise due to the grain of the film, profiles were generally taken as the average of a five to ten pixel-wide band, at each point along that band. Profile data were recorded on an arbitrary scale for each core, such that higher values corresponded to greater visible-light luminescence. These intensity data were exported as ASCII text, for import into spreadsheet and graphing software. It can be seen that a downside of this method is the lack of intra-sample repeatability or absolute calibration, but this is compensated by the ease with which ultra-violet luminescence data may be obtained, without the need for complex set-ups involving calibrated UV sources, filters, and microscopes. For direct comparison to other data for core MD3, the 3200-pixel luminescence record from this core was averaged into 5 mm intervals, carefully checked such that these increments physically corresponded as closely as possible with those samples obtained using the computer-controlled mill (see chapter 4).

Results

The methods described above have been used to produce results for a variety of speleothems, predominantly from Mt Arthur, descried in varying detail below. Particular attention is paid to results from core MD3, as many variables were analysed from portions of the same homogenised samples, providing a unique opportunity to improve the understanding of the significance of varying trace element contents of speleothems, over the full range of glacial—interglacial environmental changes. For this reason, the MD3 data trace element data is here compared only with data of the same spatial (5 mm) and temporal resolution, and discussion of the significance of higher resolution results is deferred to chapter 8.

Standard AM1

Speleothem standard AM1.1, prepared from a calcite sample from the Nullarbor Plain, Western Australia, was calibrated against the BHVO standard. As the latter is a silicate standard, it is possible that matrix differences may have led to small errors in the concentrations determined for some or all elements in this sample, and hence to all MD3 and other samples subsequently measured against it. This is not considered a significant problem, for, as mentioned, precise absolute trace element concentrations are not of great interest in this study, and if required they can easily be calculated in the future, by more accurate analysis of AM1.1, and subsequent recalculation of existing results. The AM1.1 standard was prepared from 1.2 grams of speleothem, enough for ca. 400 ICPMS internal standard measurements. It is, however, apparent that some elemental concentrations produced for AM1.1 are suspect, such as those for iodine, which, while apparently measured by solution-introduction ICPMS, is not expected in speleothem samples, and is not found by laser-ablation ICPMS analyses of the same samples (see chapter 8).

Absolute reliability of measurements

As discussed above, the uranium concentrations initially determined by fully quantitative ICPMS analysis generally agreed within their analytical errors with the intrinsically far more reliable isotope dilution TIMS results for the same samples (fig. 7.1). The fully quantitative thorium results showed less agreement, the differences implying that common thorium has a strongly heterogeneous distribution within the speleothems, perhaps due to its detrital origin. The uranium results determined for core MD3 by normalisation of each sample to the expected calcium content of 40%, as described above, are also in good agreement with those obtained by TIMS.

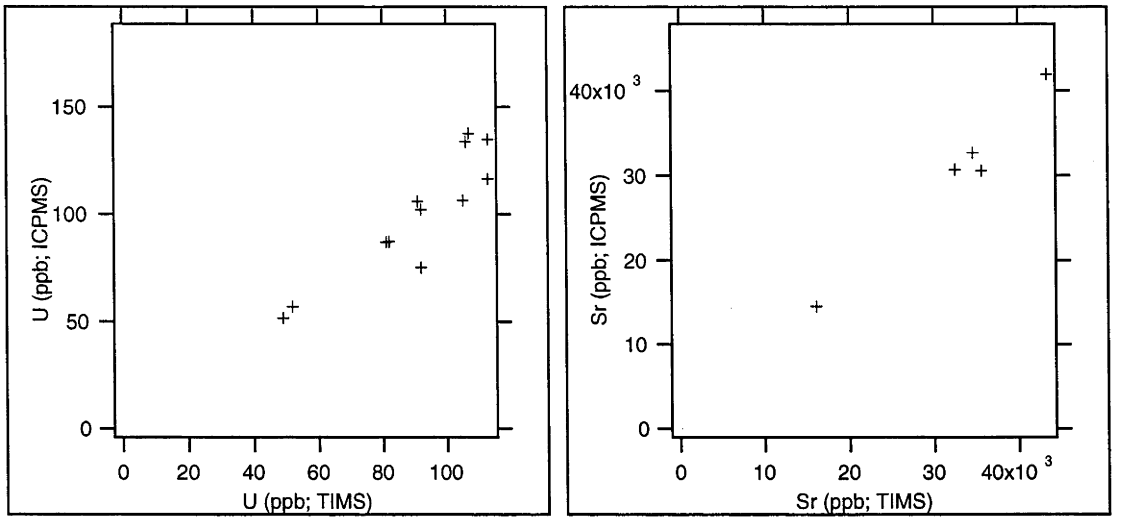

Fig. 7.1. A comparison of concentration determinations using ICPMS and TIMS, for uranium and strontium. Isotope dilution TIMS concentration determinations are intrinsically more accurate, providing an independent test of the ICPMS method in speleothem analysis. The Sr results are in very good agreement (with one outlier). The larger scatter in the U data is presumably due to the TIMS and ICPMS determinations not being made from exactly the same samples.

Whereas the uranium and thorium content determinations were determined on separate, approximately contemporaneous samples, TIMS strontium measurements were made from portions of the same homogenised increments of MD3 as the ICPMS measurements were, enabling direct comparison between the results. As can be seen (fig. 7.1), the strontium measurements using the two methods are in very close agreement. It appears from these results that the calcium-normalisation procedure described above is an accurate means of rapidly determining speleothem trace element content by ICPMS analysis.

Straw PV1.1

Of the 37 trace elements tested for in straw stalactite PV1.1, 28 were not considered to be reliably measurable, due to insufficient or unstable counts per second, leading to poor counting statistics, or due to low signal to background ratios. Of the 9 trace elements remaining, magnesium, strontium, barium and uranium appeared the most promising for measurement in speleothems, on the basis of both data quality, and of the nature of variability along the straw sample. ^{44}Ca, measured using the analogue mode of the ICPMS, appeared promising as a means of determining calcium concentration for normalisation purposes, although ^{43}Ca and ^{48}Ca are presumably more appropriate isotopes, as they can be measured using pulse-counting mode, as are all trace element isotopes. Iodine appears as a relatively stable signal along the length of the straw, although, as discussed above, it seems that this is probably due to an interference of some sort inherent to solution-introduction ICPMS, as no iodine is found by laser ablation methods. A notable feature of the ICPMS results is the very close covariance between strontium and barium ($r=0.98$) concentrations, implying their concentration changes, at least over relatively short periods, are driven by similar chemical processes.

Straw PV1.1 was milled at a resolution of 0.5 mm, being the shortest interval at which enough sample could be obtained to analyse by ICPMS,

predominantly to check for signs of periodic, presumably annual fluctuations in trace metal abundances. That these periodic fluctuations were not found is in hindsight not surprising, as subsequent work on Mt Arthur straws (see chapter 8) has shown that average growth rates of the order of a few hundred microns per year are common. Nonetheless, significant temporal variations in the concentrations of a number of elements were found from one end of the 20 mm straw section to the other, proving that such variations are measurable in speleothems at close to annual timescales. A lack of information about sample PV1.1, even such as which end is youngest (this sample was collected already broken, from the cave floor), precludes much meaningful analysis of the results. However, they were sufficiently encouraging that a more thorough investigation of variation along the much longer sample MD3 was undertaken, using the same methods.

Core MD3

Of the trace elements investigated, magnesium, strontium, barium and uranium show clear continuous records for the length of the core (fig. 7.2). Other elements measured, being iodine and several light rare earth elements, while appearing to produce good counting statistics, gave discontinuous records, or failed to give repeatable results for replicate analyses of individual samples. As such, attention is restricted here to the former four elements, each normalised to calcium. As well having analytical errors of only a few percent, these elements exhibit variance along the 31,000-year record of between 50 and 90 percent of their means, presumably driven by changing environmental conditions over this period.

Strontium and barium, as noted for straw PV1.1, again appear to produce closely related signals, implying similar processes influence their concentration changes in speleothems, over all timescales. The correlation does not appear to be linear, with strontium variation relative to barium being relatively large at low concentrations. Strontium concentration averages

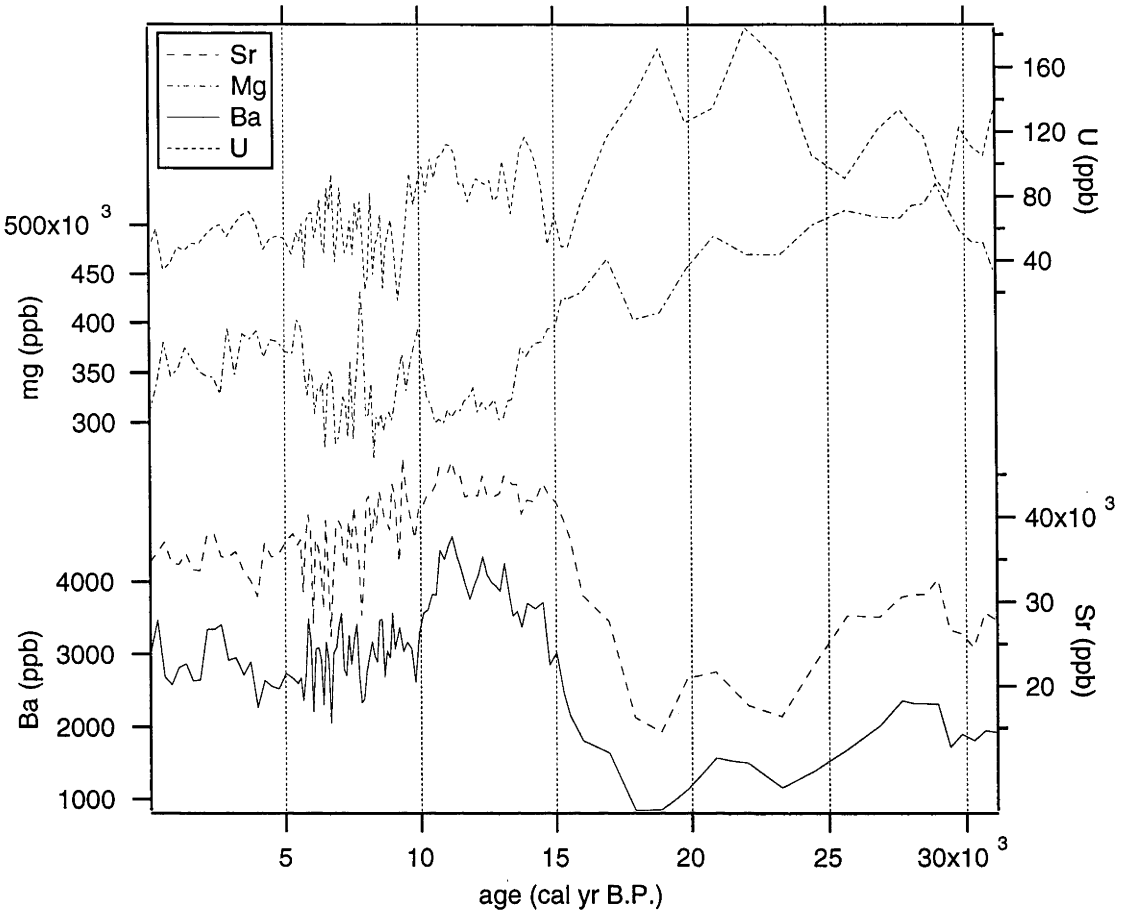

Fig. 7.2. Strontium, magnesium, barium and uranium versus time, core MD3. The relationships between these records are discussed in the text.

approximately 10 time the concentration of barium, throughout the record. Broadly, strontium and barium fall from concentrations of 25 and 2.5 ppm respectively, at 31,000 cal yr B.P., to 15 and 1 ppm at 19,000 cal yr B.P. This is followed by a rapid rise to the maximum values of both elements, of 45 and 4.5 ppm at ca. 14,000 cal yr B.P., and a subsequent decline over the Holocene, to modern values of 35 and 3 ppm. The distinctive feature of both records is the very rapid rise to higher concentrations seen at ca. 15,000 cal yr B.P.

The magnesium results are significantly different to the strontium and barium records, recording a gradual decline in concentration from over 500 ppm at 31,000 cal yr B.P., to 300 ppm by ca. 13,500 cal yr B.P, followed by little major variation over the course of the Holocene. A striking feature is the apparent fine-scale anticorrelation observed with strontium and barium, particularly over the Holocene. Prior to 15,000 cal yr B.P., the anticorrelation is less pronounced, with local minima in the magnesium data, at ca. 23,000 and 19,000 cal yr B.P., apparently matching the major concentration minima of both strontium and barium.

The uranium concentration in MD3 is highly variable, broadly decreasing form 31,000 cal yr B.P. to the present. Maxima at ca. 23,000 and 19,000 cal yr B.P. exactly coincide with minima in the other trace elements investigated. A surprising aspect of the uranium concentration record is its pronounced anticorrelation with the strontium and barium concentration records from 31,000 to 15,000 cal yr B.P., followed by a sudden polarity change to strong positive correlation with these records, from 15,000 cal yr B.P. to the present (figures 7.2 and 7.3). The change in phase notably coincides with the very sudden postglacial increases observed in strontium and barium, perhaps indicating significant changes in groundwater chemistry at this time.

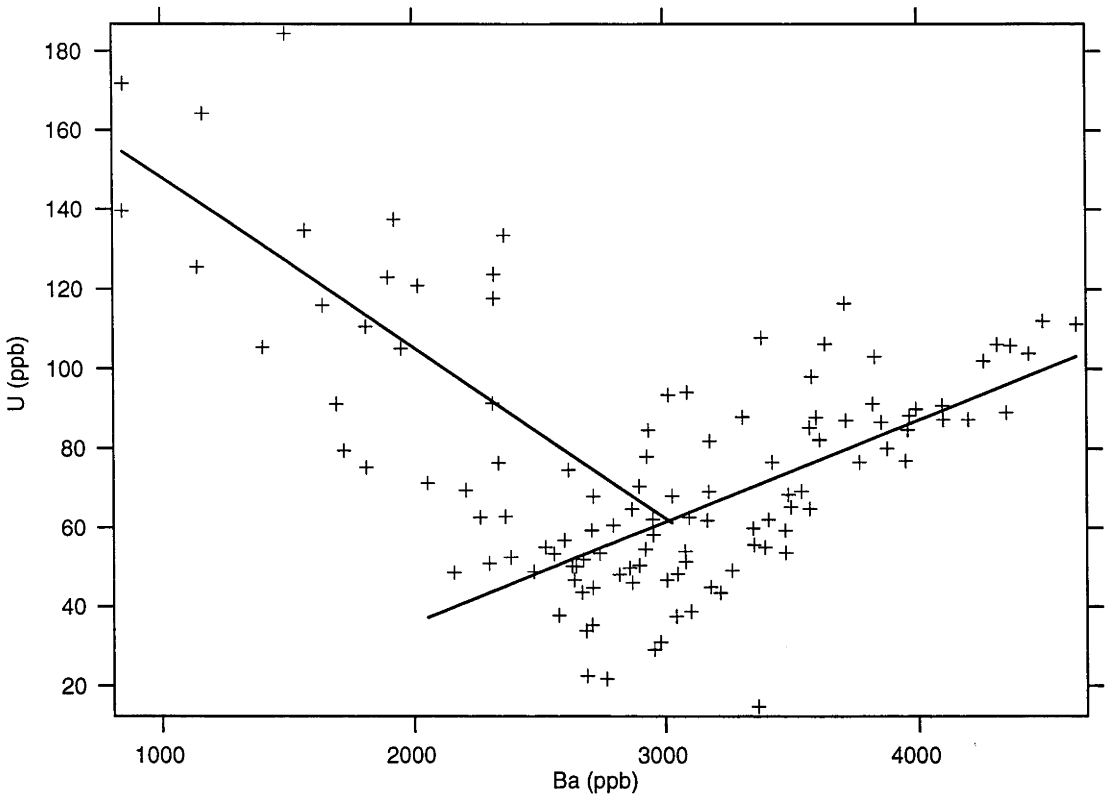

Figure 7.3. Uranium versus barium concentration, for MD3, showing the sudden change in behaviour of uranium relative to other variables at ca. 15,000 cal yr B.P. The left-hand line is the best fit (r=0.60) to points between 31,000 and 15,000 cal yr B.P., and the right-hand line is the best fit (r=0.66) to points younger than 15,000 cal yr B.P..

Uranium and strontium isotope results

Core MD3

Initial uranium isotope ($\delta^{234}U(T)$) data for core MD3 show significant variation versus time, relative to their analytical errors (fig. 7.4; table 7.1). Generally, $\delta^{234}U(T)$ increases slightly over the period from 31,000 to 13,000 cal yr B.P., from 420 to 440 delta units, before rapidly falling to a steady Holocene value of ca. 370 delta units. This sudden fall in $\delta^{234}U(T)$ postdates the sudden change seen in the strontium, barium and uranium contents of the MD3 speleothem sample, by 2,000 years, approximately coinciding with the less-rapid postglacial fall in magnesium concentration. It is not possible to make inferences as to the fine-scale variation, if any of $\delta^{234}U(T)$ in MD3, due to both relatively large errors, and to low temporal resolution of the data. Because of this, a simple model of steady glacial and Holocene values is adopted, with a step at 13,000 cal yr B.P. Uranium isotope data from MD3 show no correlation with uranium concentration data for the same samples.

Strontium isotope analysis of core MD3 is inconclusive, due to the low number of samples run, and the extremely limited range of isotopic variation. Samples were carefully chosen, such that they covered the full range of strontium concentration variation observed in this speleothem, on the assumption that any measurable isotope variation was likely to be in some way related to changes in concentration of the same element. This has not been the case, what little isotopic variation that is observed showing no such relationship. It appears that, whilst limited, strontium isotope changes are consistent with the behaviour of the uranium isotope data (fig. 7.4; table 7.1), with relatively steady values from 31,000 to 13,000 cal yr B.P., followed by a rapid rise to stable Holocene values, some 2,000 years after the sudden rise in trace element concentrations. As for the uranium isotope data, strontium isotope data show no correlation with strontium concentration for the same samples.

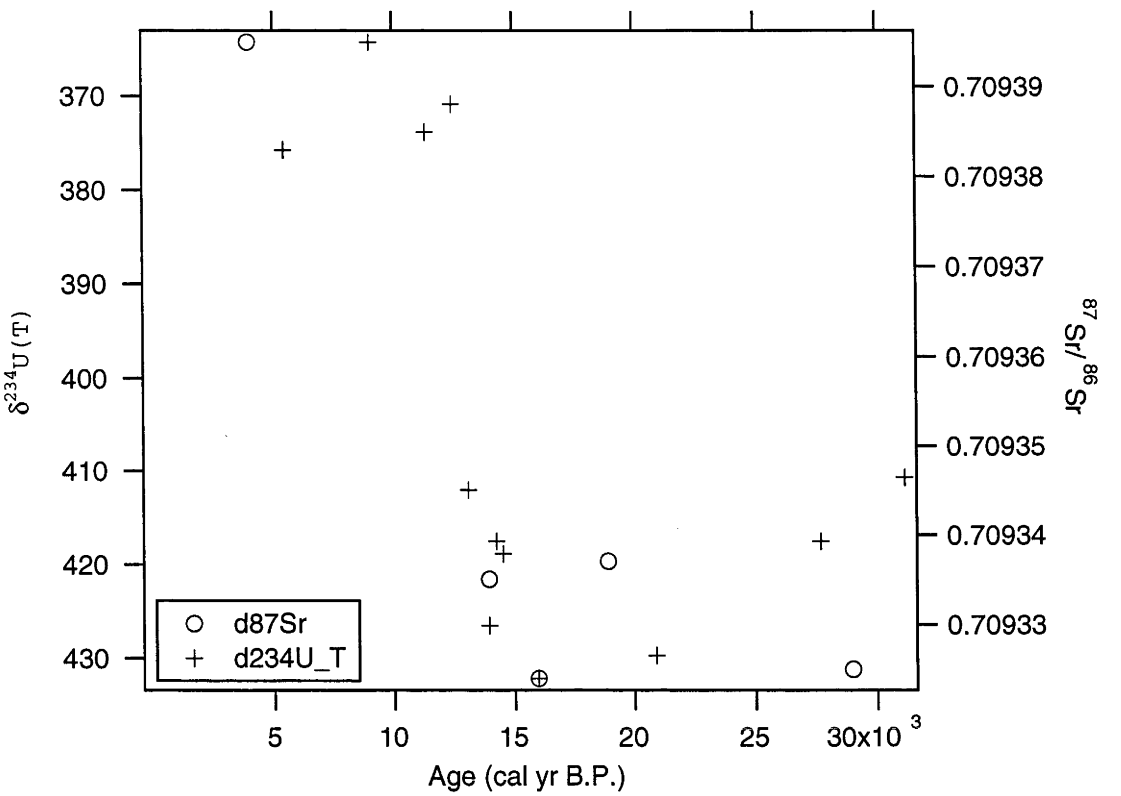

Fig. 7.4. $\delta^{234}U(T)$ and $^{87}Sr/^{86}Sr$ versus time, core MD3. The uranium data show a sharp jump at ca. 13,000 cal yr B.P. There are not enough points in the strontium curve to define or confirm similar behaviour at this time, but they do restrict any sudden rise to having occurred later than 14,000 cal yr B.P.. Error bars are omitted for clarity, but are typically ±10 and ±0.000015 for U and Sr, respectively (see table 7.1 for exact figures).

TABLE 7.1. URANIUM AND STRONTIUM TIMS CONCENTRATION AND ISOTOPIC DATA, CORE MD3.

Sample Name[a]	Depth (mm)	Age (yr)	$^{87}Sr/^{86}Sr$	$\pm^{87}Sr/^{86}Sr$	Sr (ppb)	$d^{234}U$ (0)	$\pm d^{234}U$	$d^{234}U$ (T)	U (ppb)
MD3B 102	77.5	3987	0.709395	0.000012	35600				
MD3B 096	107.5	5448				370	44	376	52
MD3B 058	297.5	9034				355	4	364	49
MD3B 043	372.5	11336				362	7	374	91
MD3B 036	407.5	12453				358	4	371	82
MD3B 032	427.5	13095				397	7	412	92
MD3B 027	452.5	13939	0.709335	0.000011	43400	410	13	427	113
MD3B 026	457.5	14234				401	24	418	105
MD3B 025	462.5	14522				402	7	419	81
MD3B 020	487.5	15991	0.709324	0.000018	32500	413	5	432	92
MD3B 017	502.5	18891	0.709337	0.000036	16100				
MD3B 015	512.5	20894				405	5	430	113
MD3B 009	542.5	27685				386	57	418	106
MD3B 006	557.5	28981	0.709325	0.000014	34600				
MD3B 001	582.5	31142				376	3	411	107

[a] Strontium data are from the same 5 mm milled MD3B samples as are the data in appendix 2. Uranium data are from much larger, 5 g samples cut from the core for U-series dating, and thus correspond to the named MD3B samples only to the nearest 5 mm, and are not directly comparable.

$\delta^{234}U(T)$ data from core ED1 are sparse, due to the lower resolution at which that core was dated. Variation is considerably greater than in core MD3, particularly in the lower sections, from 89,000 to 74,000 cal yr B.P., where a fall from 280 to 120 delta units is followed by a rise to 220 delta units. Again, it is not possible to determine whether this is a broad trend, or merely aliasing of higher-frequency variations in $\delta^{234}U(T)$. The apparently steady Holocene value of ca. 250 delta units appears to preclude a sudden fall in $\delta^{234}U(T)$ as seen in core MD3. There is no correlation between $\delta^{234}U(T)$ and uranium concentration observed in Mt Arthur samples, and nor are there any discernible patterns outside of intra-speleothem variations.

UV luminescence results

Core MD3

Ultra-violet luminescence data for MD3 are, in terms of relative luminescence, broadly proportional versus time to those obtained from ICPMS measurement of strontium and barium. As for those data, the broad trend in UV luminescence (fig. 7.5) is of a fall over the period from 31,000 to 19,000 cal yr B.P., to minimum values. This was followed by a rapid rise to maximum values at ca. 13,000 cal yr B.P., and a subsequent gradual fall in luminescence over the Holocene, to the present. The similarity of the luminescence record to the barium concentration record in particular is striking, at all scales (fig. 7.6).

Core ED1

UV luminescence in core ED1 is generally greater in the Holocene than in the older sections of the core, equivalent in age to oxygen isotope stage 5a. Because UV luminescence was not measured on an absolute scale, having

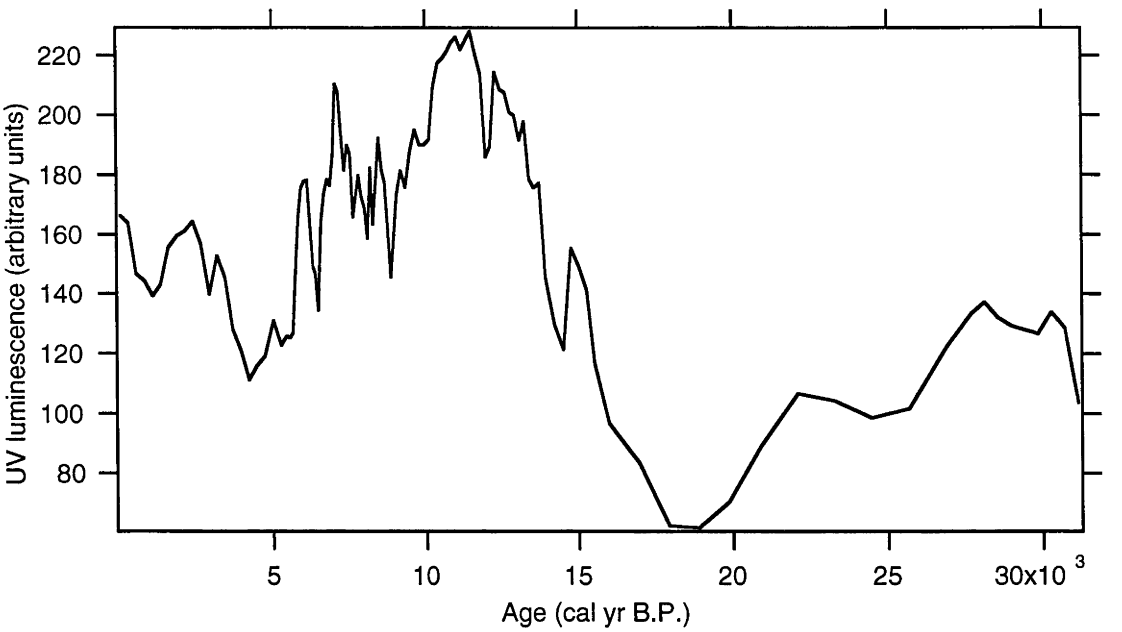

Fig 7.5. Ultra-violet luminescence versus time, core MD3. The units are arbitrary, higher values corresponding to greater luminescence under UV illumination (see text for method).

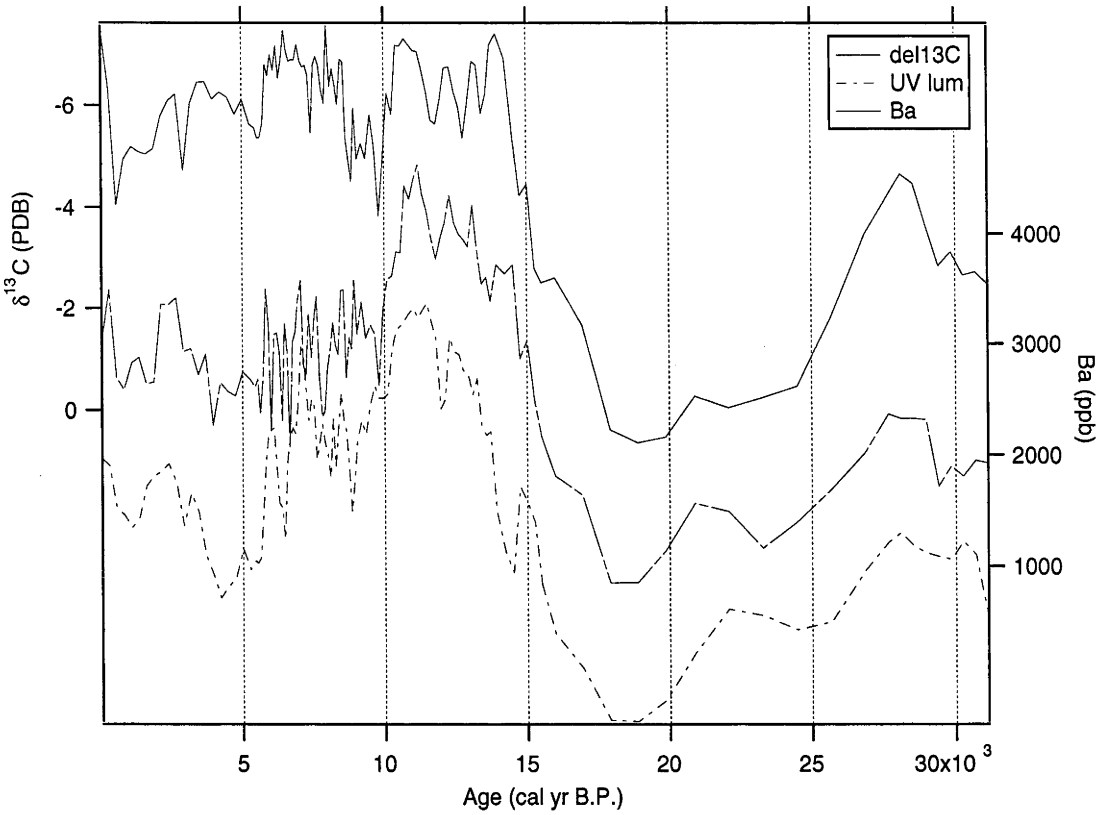

Fig. 7.6. $\delta^{13}C$, UV luminescence and barium concentration versus time, for core MD3. Note the sudden rise in all variables at ca. 15,000 cal yr B.P. A low-resolution version of the $\delta^{13}C$ record is used here, being the same 5mm intervals sampled for trace element analysis, to allow direct comparison between the records.

been subject to variable film exposure times, scanning parameters and digital image processing, these data cannot be compared with those from MD3 (this is not an inherent flaw in the method, as these parameters may be fixed at set values). Because of this, the significance of the greater magnitude of Holocene variability observed in this record cannot be quantitatively assessed.

Discussion

While it is apparent that a large number of elements are potentially measurable in speleothem calcite using ICPMS analysis, it can also be seen that only a few elements seem to be reliably measurable in most or all speleothems. Most of those are divalent metal ions thought to substitute for calcium in the calcite lattice. While other elements in some cases appear to be measurable, including sodium, aluminium, zinc, yttrium, lanthanum, and lead, they are not considered in this work. This is due partly to concerns as to the repeatability of such measurements, and partly to the currently sparse understanding of the nature of incorporation of these elements into environmental carbonates.

General discussion of trace element concentrations

As with the carbon isotope data, it can be seen that the most significant observation that may be made from stable isotope concentration changes, is that a sudden jump between two relatively stable states, the last glacial maximum and the Holocene, occurred at about 15,000 cal yr B.P. This is apparent not only from rapid increases in strontium and barium concentration at this time, but also from a sudden change in the behaviour of uranium, from a negative to positive correlation with presumed glacial-interglacial changes in major environmental variables such as temperature.

While it seems likely that $\delta^{18}O$ variation is at least indirectly related to local changes in temperature and rainfall (see chapter 6), it is dominated by meteoric water vapour effects, representing distal changes. $\delta^{13}C$ is a more appropriate variable with which to compare trace element behaviour versus

time, as soil chemistry, and thus vegetational activity seem amongst the most likely external environmental influences on trace element changes. It can be seen (fig. 7.6) that $\delta^{13}C$ changes are strongly inversely correlated with changes in barium concentration, and to a lesser degree with strontium concentration changes over the length of the record, implying a common control for much of the variation experienced by each of these variables. Uranium also very closely matches $\delta^{13}C$ over the period for which it appears to be positively correlated with strontium and barium.

From this it can be seen that, at least over the last 15,000 cal yr B.P., a common mechanism must be found which can address much or all of the variations in both the $\delta^{13}C$ and trace element geochemistry of forming speleothems. In Chapter six, it was argued that $\delta^{13}C$ must be strongly influenced by some combination of soil CO_2 partial pressure, and the flow rate of water over the speleothem surface. While many potential factors may control speleothem trace element chemistry, soil CO_2 partial pressure seems likely to be a strong factor influencing many of them. Changes in water flow rate may also have an effect, particularly by directly altering the degree of progressive enrichment of trace element content in solution with distance along an actively forming speleothem. Associated with any increase in soil CO_2 partial pressure is likely to be an increase in soil organic acid content, with a consequent decrease in soil pH and changes in other soil chemical characteristics.

Cave seepage water flow rate can be eliminated as a common influence on barium and strontium content changes (and thus, presumably as a major influence on either variable in this case). Slower flow rates, known to result in more calcite having been precipitated from solution on its reaching any given point along the speleothem surface, are argued to result in the precipitation of isotopically heavier carbon in the speleothem (high $\delta^{13}C$; e.g., Baker *et al.*, 1997), as is seen at the LGM in MD3. Conversely, any such increase in calcite precipitation prior to reaching a given point on a speleothem is expected to result in the precipitation of calcite relatively enriched in trace elements with distribution coefficients of significantly less than one. In particular, slower

water flow rates should thus be expected to produce calcite enriched in both $\delta^{13}C$ and in strontium and barium, whose distribution coefficients are very small. This effect is not observed in MD3, as $\delta^{13}C$ is anticorrelated with barium and strontium concentration, showing that changes in degree of progressive enrichment due to changing flow rates do not appear to have been significant in MD3.

The sudden change in the behaviour of uranium at ca. 15,000 cal yr B.P., is associated with sudden changes in both $\delta^{13}C$ and barium and strontium concentration, and is thus attributed to significant changes in soil chemistry. A possible cause for this change in behaviour is a sudden change in the oxidation state of uranium, from the U^{6+} state, capable of forming soluble complexes with carbonate ions, to the less soluble U^{4+} state (Osmond, 1980). The latter would lead to lower speleothem uranium concentrations, which might vary in concert with other trace elements, as observed. This could be caused by a move from oxidising conditions prior to 15,000 cal yr B.P., towards reducing conditions subsequent to this, perhaps in response to greater soil organic matter content at this time. More extreme glacial conditions, which lead to lower concentrations of strontium and barium, may through such a mechanism favour an increased availability of soluble uranium. Alternatively, the presence of more oxidising conditions during the last glacial maximum may have reduced the magnitude of the calcite surface uranium desorption effect noted by Morse *et al.* (1984). The potential effects of increased organic acid concentrations during the Holocene should also be considered, perhaps reducing the activity of uranium ions in solution by complexing with them.

Anticorrelation between magnesium with strontium and barium has been observed before, both in aquifer waters and in speleothems, and has been proposed as being due to changes in the residence time and flow paths of aquifer waters (Roberts *et al.*, 1998). Karst groundwaters reach saturation with respect to calcite before they reach saturation with respect to dolomite phases in the rock, and thus can continue to dissolve magnesium carbonate after reaching calcite saturation. As dolomite phases are generally lower in

strontium and barium than is associated calcite, this is a mechanism by which anticorrelation between these elements may be established in groundwaters and thus in speleothems. Correlations between magnesium content and water residence time have been previously noted in karst aquifers, and this mechanism used to explain magnesium anticorrelation with strontium and barium in speleothems (Roberts *et al.*, 1998). It seems then, that in the case of MD3, some or all of the observed variation in magnesium concentration might be attributable to changes in water residence time. It should be noted that the reduction in magnesium concentrations observed from the LGM to the Holocene, a transition associated with significant temperature increase (McGlone, 1988), rules out the effect of temperature on D_{Mg} as being a significant effect in this case.

The minor minima in magnesium concentration at ca. 19,000 and 23,000 cal yr B.P. imply either that water residence time increased at this time, implying higher rainfall, or that magnesium is influenced by variables other than water residence time alone. It is reasonable to assume that the concentration of any trace element in speleothems is subject to a number of significant controls, as discussed above. It may be that magnesium is subject to similar controls to those acting upon the concentrations of other trace elements investigated, in addition to the residence time effect discussed above. Similarly, it appears that the concentration records of barium and strontium, and of uranium during the Holocene, are predominantly influenced by vegetation and soil chemistry changes, as are carbon isotope ratios, upon which a smaller water residence time effect is superimposed, anticorrelated with the dominant magnesium signal.

Ultra-violet luminescence implications for soil and groundwater chemistry

That the UV luminescence record from core MD3 so strongly correlates with the $\delta^{13}C$ record and trace element records from the same speleothem, strongly implies that these records are dominantly forced by the same, or closely related, processes. UV luminescence is probably the proxy which can most

confidently be ascribed to a single forcing environmental variable, namely dripwater organic acid content (Baker *et al.*, 1996; Ramseyer *et al.*, 1997; White *et al.*, 1995), known to be closely related to the degree of organic activity on the surface above. $\delta^{13}C$ has been shown herein not to be significantly influenced by changes in seepage water flow rate, leaving the dominant control on this variable as changes in the partial pressure of soil CO_2, strongly related to organic activity and thus to organic acid production rate. Growth rate, which from equation 2.1 must be directly proportional to the seepage water-transmitted flux of CO_2 from soil atmosphere to cave atmosphere, and thus is strongly influenced by changes in soil CO_2 partial pressures, is also closely related to the UV luminescence and $\delta^{13}C$ records.

From these observations, it becomes apparent that biological activity in the soil, and on the surface above, is the dominant effect forcing these records, and thus is presumably also forcing the extremely similar trace element concentration records. While the means by which this environmental variable can influence $\delta^{13}C$, UV luminescence and growth rate are now reasonably well understood, the same cannot be said for its influence on trace metal concentration. The mechanism responsible could be as simple as lower soil water pH leading to increased weathering and leaching of silicate minerals in the soil, and consequently greater extraction of trace elements from those silicate phases. However, it could also be an indirect control, such as increased complexing, and concentration into the speleothem of, certain trace elements where organic acid concentrations in the seepage water increase.

Additional constraints from uranium and strontium isotopes

The uranium isotope data for core MD3 show a similar pattern to the records obtained from carbon isotope ratios, growth rate, and strontium and barium concentrations, except that the sudden step apparently associated with the end of glacial conditions occurred approximately 2000 years later. This offset is significant, and strongly implies that the uranium isotope ratios of the speleothem, and thus of cave waters, are influenced by factors not closely

related to those which influence the other records, considered above to be the intensity of biological activity in the soil.

If alpha recoil is considered to be the dominant mechanism by which uranium isotopes are fractionated into cave dripwaters, water residence time becomes a potentially important effect (Osmond, 1980). This would occur where slower flow rates, leading to longer residence times, cause an increase in the relative concentration of ^{234}U in the cave waters. If preferential leaching of ^{234}U from fission-damaged lattice sites is instead considered the most important uranium isotope fractionating mechanism, either longer water residence times or weathering by less aggressive waters can be considered potential mechanisms leading to increased $\delta^{234}U(T)$ in cave waters. An argument against more aggressive leaching of uranium after 13,000 cal yr B.P. being a significant factor in the observed reduction of $\delta^{234}U(T)$, is the lack of any increase in uranium concentration at this time. A significant change in the behaviour of uranium, associated with the large change in several other measured variables, instead occurred 2000 years prior to the increase in $\delta^{234}U(T)$, implying that changes in water residence time are of greatest significance.

The strontium isotope record from MD3 shows similar variation to that of the uranium isotope record, but is of lower resolution, and thus does not constrain whether the change from glacial to Holocene values was as sudden, nor if the Holocene values were as steady. However, the strontium isotope data do show that any increase to the higher value observed for the mid-Holocene, can have occurred no earlier than the sudden fall seen in $\delta^{234}U(T)$ at ca. 13,000 cal yr B.P. Again, it is hard to ascribe the change in strontium isotopic values to a change in the intensity of strontium weathering from the host rock, as changes in strontium concentration are totally independent of strontium isotopic variation.

Banner *et al.* (1996) proposed a model whereby the $^{87}Sr/^{86}Sr$ ratio of dripwaters and thus of speleothems vary in response to changes in the relative contribution of strontium from soil sources, to strontium from the host

limestone, thus recording changes in groundwater residence time. They found the strontium isotopic values to range towards a soil compositional end-member during wet periods, and a host limestone compositional member during periods of relatively low precipitation. By assuming a host limestone end-member $^{87}Sr/^{86}Sr$ of the order of 0.708 to 0.709, close to that of the Ordovician seawater from which it formed (Qing *et al.*, 1998), it can be argued that MD3 $^{87}Sr/^{86}Sr$ values closest to that end-member are indicative of longer groundwater residence times.

The uranium and strontium isotope data, then, appear to support the model of groundwater residence time variation versus time that can be inferred from the MD3 magnesium concentration record discussed above (fig. 7.7). This suggests that rainfall at Mt Arthur gradually increased throughout the last glacial maximum until a sudden increase at approximately 13,000 cal yr B.P., followed by a gradual decline over the Holocene. That this change in soil water residence time occurred significantly after the very sudden increase in vegetation activity at ca. 15,000 cal yr B.P., indicated by a number of measured MD3 variables, implies that the increase in biological activity was not caused by a significant increase in rainfall. This in turn suggests that rainfall in North-West Nelson was sufficient to maintain productive forests throughout the last glacial maximum. Consequently, the rapid return of interglacial vegetation centred on 15,000 cal yr B.P. must instead have been driven by a sudden change in some other major climatic variable, most likely an increase in regional temperature.

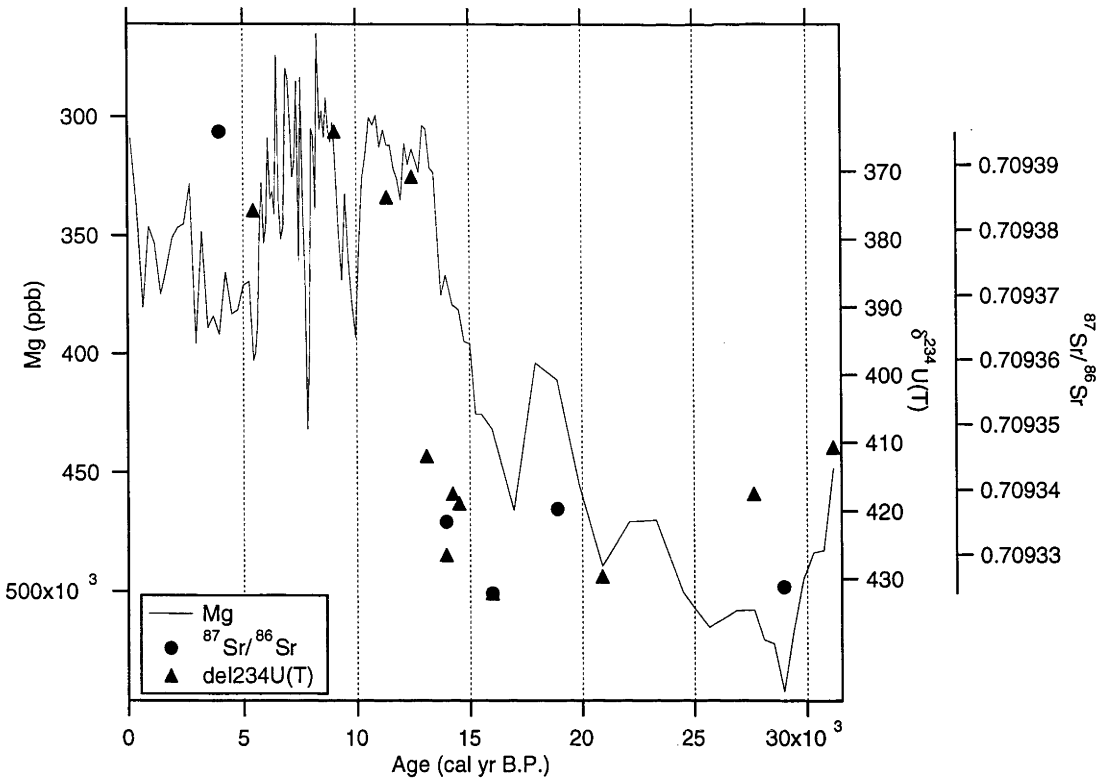

Fig. 7.7. Strontium and uranium isotopic data versus time, MD3. Also shown are magnesium concentration data for the length of the core. All three variables are thought to have responded to a reduction in groundwater residence times at ca. 13,000 cal yr B.P., corresponding to an increase in effective precipitation above the cave.

Chapter 8. Laser-ablation ICPMS analysis

Introduction

Building on the speleothem trace element concentration theory discussed and developed in chapter 7, this chapter reports the use of laser-ablation ICPMS methods for high-resolution trace element analyses. Emphasis is here placed on measuring relative concentration variation along individual speleothems, as accurate absolute concentration data has been shown to be of lesser interest for speleothem samples. High-resolution trace element data is reported spanning the length of core flowstone core sample MD3, as are attempts to resolve periodic annual variations using extremely high-resolution analytical methods.

Theory

Significance of trace element concentration variations

As discussed in chapter 7, there are many factors that might potentially cause trace element concentration variations versus distance in a speleothem, not all of them necessarily equating to variation versus time. Pending a detailed investigation of trace element concentrations in soils, groundwaters and the speleothems growing from them, and their relationships to environmental variables such as temperature and rainfall, it is likely to be difficult or impossible to discriminate between variations due many of these mechanisms. Nonetheless, it is possible, on the basis of relationships with other, better understood measured parameters, to at least broadly understand the palaeoclimatic implications of changes in trace element concentrations, even if the exact mechanisms by which these relationships occur are unknown. What is understood of the significance of concentration variations in several trace elements is summarised below.

Thorium is the best understood trace element that has been measured in Mt Arthur speleothems. As noted in chapter 5, thorium is insoluble in natural waters, and thus is not present in an ideal speleothem composed of 100% solution-derived carbonate. However, thorium often is found in speleothems, and is assumed to be derived from detrital silicate phases incorporated during calcite deposition. This assumption is supported by the coincidence of insoluble silicate residues after sample dissolution, with samples containing non-trivial amounts of ^{232}Th. Thus, thorium concentration is a direct proxy for the relative amount of silicate detrital material incorporated into speleothem at time of deposition. In the case of samples from The Meltdown, Nettlebed, detrital silicate was found to consist almost entirely of very fine white mica, strongly implying it is deposited onto the speleothem surface as dust, rather than being washed over the speleothem by cave seepage waters.

Magnesium, as argued in chapter 7, seems likely to be at least an approximate proxy for changes in the relative groundwater residence time of cave seepage waters. Progressive dissolution of more magnesium-rich carbonate phases within the host limestone are expected to lead to an increasing magnesium-calcium ratio with increasing groundwater age, with a corresponding, although at this stage unquantified, reduction in the relative concentration of some other trace elements, most notable barium and strontium. Magnesium is likely to be influenced by other factors as well as residence time, such as the changes in soil and groundwater pH discussed below. However, on the basis of its correlation with fluctuations in strontium and uranium isotopic ratios, also believed to correspond to changes in groundwater residence time, it seems likely that residence time, an inverse proxy for rainfall amount, is the predominant effect driving magnesium concentration.

Strontium and barium are here considered together because, whilst there may be some chemical differences (barium apparently corresponds more closely to changes in seepage water organic acid concentration, while strontium is more similar to the carbon isotope record of soil CO_2 partial pressure), they are chemically similar, and are highly correlated in records examined so far. The predominant forcing effect acting upon these trace element records appears to

be changes in the level of organic activity in the soils above, although the exact mechanism by which this occurs is still poorly understood. Increased biological activity leads to elevated soil CO_2 levels, and greater production rates of organic acids within the soil. This leads to a lower soil pH, by which greater quantities of strontium and barium might be leached from the host marble. Alternative mechanisms involve the effect of altered pH on the chemical behaviour of these elements, and potential effects of organic acids on the strengths of mechanisms by which they are dissolved, transported and deposited.

Uranium behaves very similarly to both barium and strontium during the Holocene section of the MD3 record, implying its concentration in speleothems is influenced by very similar processes related to vegetation on the surface above. However, before about 15,000 cal yr B.P., uranium concentration appears to behave in a completely different manner, its apparently negative correlation to these elements during glacial conditions illustrated by changes in its ratio to barium. The much greater concentration of uranium in the speleothems during times of low organic activity may indicate an inhibitory effect of organic acids in the soil and cave waters. Alternatively, it reflects a change towards more oxidising conditions during glacial times, leading to a relative increase in the proportion of soluble U^{6+} ions to relatively insoluble U^{4+} in the cave waters. If this is true, uranium concentration changes relative to strontium and barium may be a sensitive indicator of glacial stage environmental conditions on the surface above.

Why measure extremely fine-scale variations?

A general framework is now in place, within which to consider the likely causes and significance of temporal trace element concentration variations in speleothem calcite. It is hoped that greatly increasing the resolution at which these parameters can be measured might provide information about the nature of palaeoenvironmental changes over very short timescales. However, such fine-scale variation must be carefully evaluated against the many potential effects on speleothem trace element concentration (discussed in

chapter 7). Some of these effects might cause relatively high-amplitude variations at high frequencies, measurable by laser ablation, but not observed as significant factors influencing solution-introduction ICPMS measurements. In particular, variation due to the crystal zoning effect discussed in chapter 7 may become more significant at fine scales. This effect can be tested for though, by measurement of variation parallel to growth layers.

A particularly enticing possibility of this approach is the reliable measurement of trace element fluctuations on annual timescales, an obvious benefit of this being that it can potentially allow the construction of autocalibration chronologies, surpassing the precision of U-series dating. An immediate potential application of this is comparison of parameters measured from speleothems to instrumental records of climate change, and with other annually resolved records, such as those derived from tree rings. Even where absolute ages cannot be applied to measured annual cycles, perhaps due to discontinuous records, they can provide high-resolution data on changes in annual extension rate, itself a potentially important palaeoenvironmental indicator.

Methods

General LA-ICPMS theory and practice

The principles and advantages of ICPMS analysis are outlined in chapter seven, the most notable feature of this technique being the ability to simultaneously measure a great number of trace element concentrations from a single sample. Some downsides of ICPMS analysis are its relatively low sensitivity compared to thermal ionisation mass spectrometry, its susceptibility to molecular interferences at many mass numbers, and the tendency for both absolute and relative sensitivity of the instrument to drift during the course of an analytical run. Instrumental drift can be controlled by careful use of internal and external standards in the case of solution introduction ICPMS analysis only.

Laser ablation ICPMS analysis offers two great advantages over the solution introduction technique, namely very much higher sample throughput, and very much greater spatial analytical resolution. Its greatest disadvantage is its increased susceptibility to problems with ratio drift, as it is not possible to utilise internal standards as can be done with the solution introduction method. Also difficult is deriving absolute calibrations of signal intensity to trace element concentration in the ablated solid, due partly to problems with ratio drift, and partly to difficulties finding homogenous solid standards with similar matrix and trace element concentrations to the carbonates being measured.

The laser ablation technique employed at RSES utilises an argon fluoride excimer laser, which emits a 193 nm ultra-violet beam. The laser is nominally capable of a 60 W pulsed output, but is rarely used in this work at power outputs of more than 7.5 W, being 150 mJ pulses at 50 Hz. The beam is masked to the desired ablation spot geometry, before 20-times optical reduction to the sample surface, where the maximum possible beam size is approximately 1100 by 600 μm. Sample ablation, typically and ideally of polished planar sample surfaces, is in a cell containing an argon-helium mixture, at atmospheric pressure. Gas flow over the sample surface carries the ablated sample through a separate pulse-smoothing cell, and on to the same PlasmaQuad ICPMS used in this project for solution-introduction analysis. The RSES LA-ICPMS system is described by Eggins *et al.* (1997a), and Sinclair *et al.* (1998).

Initial exploratory analysis

Developmental work during the establishment of the RSES laser ablation hardware included analysis of coral and speleothem samples, by ablation of discrete fixed spots on the sample surface. As had been found for silicate and glass samples, a problem inherent to this approach is that mass signal intensities and ratios are susceptible to change as the ablation pit deepens, which is generally at a rate of the order of 0.1 μm per pulse, or 1 μm per second. Approaches to allowing for this are discussed the data reduction

section below, and, for large numbers of spot analyses, are computationally labour-intensive. A second problem with ablating discrete spots is the issue of spatial aliasing, discussed in detail in chapter 4, meaning the ablated spots should preferably be rectangular, and at the very least should be immediately adjacent to one another.

An obvious solution to the problems inherent with discrete spot ablation is to move to a continuous scanning model, whereby the ablation pit is always at the same depth below the sample surface, thus avoiding mass ratio variance with pit depth. Additionally, data can potentially be collected at a spatial resolution much greater than that inherent to the size of the sample ablation spot, meaning the record is effectively pre-filtered by the smoothing effect of the spot, before mass intensities are recorded as time slices by the ICPMS. An initial attempt to collect continuous time-resolved data was made by recording a 90-second traverse over 2 mm of polished speleothem sample, aligned normal to both the long axis of the 1000 by 100 μm laser spot, and to the growth horizons of the speleothem surface. The sample stage was moved within the ablation cell by turning one of its axial micrometers by hand, which produced surprisingly good results, based on the constancy of the calcium signal magnitude over this period.

Continuous scanning acquisition method

Results were sufficiently encouraging that a temporary DC electric motor and reduction assembly was constructed, such that the axial micrometer could be turned at a constant rate, resulting in a sample traverse rate in the range from 83 μms^{-1} to ca. 1.5 μms^{-1}. While it appears that the motor does not move the sample stage at a perfectly constant rate, it appears to be repeatable in either direction, and has produced no apparent artefacts in data collected from it over the course of two and a half years. The sample cell allows mounting of samples of up to 64 mm in length, but travel is restricted to 50 mm, giving a maximum sample size of 50 mm length by 50 mm width by 8 mm thickness. Both axial micrometers allow sample location precisions of the order of 5 to 10 mm, meaning error associated with relocating a typical ablation track of 70

μm width is insignificant. Following parallel method development by Sinclair *et al.* (1998), pre-ablation of sample tracks was adopted to remove surface contamination. Initially this was done using very wide spots and rapid pulse rates compared to those used for sample measurement. This approach was later moderated, subsequent pre-ablations using the same operating parameters as for sample acquisition, the advantage of this approach being that data could be acquired during pre-ablation runs, and that the instrument remained conditioned to input of ablated sample during these periods.

Straw speleothem analytical method

Unlike other speleothem samples, prepared as described in chapter 4 with polished planar surfaces normal to their growth horizons, straw stalactites have irregular curved surfaces, disrupting ideal gas flows over the ablating surface within the sample cell, and thus with the nature of ablation and transport of ablated material. Initial attempts to minimise these effects were by fixing straw samples to glass plates with epoxy resin, and very carefully abrading their surfaces with fine sandpaper to produce a planar surface between 1 and 2.5 mm in width, parallel to the basal glass plate for the length of the straw.

Straw speleothem PV1.2 was prepared this way, and ablated by continuous scanning to test this method. Results were encouraging, leading to the preparation and analysis of the youngest 13 mm of straw MD9.1 using the same method. Results from this sample were disappointing, leading to a temporary abandonment or straw analysis. Subsequent careful consideration of the stratigraphy of straw formation showed that any kind of physical abrasion of a straw surface prior to analysis may void the assumption that time horizons are being traversed in sequential order. Because straw surfaces are typically undulating, and because calcite is deposited within the straw as it continues to grow, abrasion of straw surfaces is likely to expose younger calcite, of variable ages. Subsequent straw analysis has been undertaken by ablating as closely as is possible to directly above the axis of each straw, aligned parallel to the base plate of the sample cell. It is recognised that the

irregular and curved nature of the straw surface may lead to some mass ratio drift, although the constancy of the calcium signal observed for most straw samples is encouraging, implying this effect is likely to be minor.

Raster scanning method

A largely untapped potential application of laser ablation ICPMS is the rasterisation of large areas of sample surface, to produce maps of trace element concentration in two dimensions. While this application ideally requires computer-control of the sample stage and laser trigger, it is possible with a lot of patience to produce such maps using the single axial DC motor set-up described above. A 5 by 3 mm section of the surface of sample AM1.2 was imaged at a spatial resolution of 83 by 100 μm, using the following procedure: The sample stage was set moving at 83 μms^{-1}, and a blank recorded. On passing a set distance threshold, the laser was triggered with a 70-μm circular spot, and run for 60 seconds, corresponding to 60 time slices and 5 mm of traverse. A blank was recorded over several seconds while the motor was reversed, and the same 5 mm ablated in the opposite direction. Following this, another blank was recorded as the stage was advanced 100 μm by hand, on the axis normal to scan direction, and the motor reversed to repeat the above procedure for a second adjacent strip. The procedure was repeated 30 times, and recorded as a single time-resolved data acquisition.

Ablation of wood sample

A sample of willow, *Salix* sp., was recovered from the stump of a freshly felled tree on the banks of Sullivan's Creek, ANU campus, to asses the viability of analysing coeval tree and straw stalactite trace element records from given areas. The principal attraction of such an approach is that it might further constrain the understanding of how speleothem trace element concentrations relate to the availability of those elements in the soil above. However, it also offers the potential of a combined approach to monitoring environmental contamination by heavy metals such as lead. The wood sample was abraded to a planar surface normal to growth ring surfaces with

fine sandpaper, ultrasonically washed in AR acetone, and dried. Because the surface of the tree still appeared to suffer from obvious contamination, the sample cell was disconnected from the ICPMS, and the sample pre-ablated at high power, using an 1100 by 600 rectangular spot. Sample acquisition was as for speleothems, with a 70-μm spot, but suffered from the presence in the wood of pores considerably larger than the spot size. While significant annual variation was found in many trace metals, it is not certain if they are driven by supply changes or by growth rate or metabolic changes, and there is unfortunately no easy way of calibrating the results

Data processing and calibration

Data reduction using Microsoft Excel

Spreadsheets were initially used to reduce all data. In general, the comma-delimited data exported from the ICPMS control software was manipulated to arrange data for each acquisition into blocks, each column of a block representing one measured mass number, and each row being one time slice of the acquisition. The blocks were then repeated from left to right across each spreadsheet, each subsequent data block representing one step in the data reduction procedure. The first step was background subtraction for each element, generally by interpolating background levels for each mass number between periods when the laser was not pulsing.

The next consecutive data block was normalised to calcium, initially to ^{46}Ca, but later to ^{48}Ca, or sometimes to a weighted average of ^{48}Ca and ^{43}Ca. Calcium-normalisation was used on the assumption that mass ratios remain constant with fluctuations in total signal strength, and that calcium content is always $4x10^8$ ppb (this assumption appears to be sound for most elements, uranium being an exception where some signal reduction occurs; Sinclair *et al.*, 1998). A downside of normalising to calcium is that the noise in each normalised record is increased through the addition of noise from the calcium signal. With very high-resolution data this is not a significant effect, as large

running means or other convolutions can be applied to smooth the resulting records.

In most cases, standards were measured at least at the beginning and end of each run, that is, between the sample cell being opened for sample changeovers. In these cases, drift in the ratios of trace elements to calcite could be quantified and corrected for, based on drift corrections interpolated in time from standard measurements. Drift-corrected count ratios could then be converted to absolute concentrations, although this was not usually done. Subsequent blocks of processed data in each acquisition spreadsheet generally included a three point running median filter, found by Sinclair *et al.* (1998) to be an effective means of removing the spurious single-point spikes which are frequently found in time-resolved data from the PlasmaQuad. This was followed by some kind of smoothing filter, usually a running box or triangular mean, of up to 15 points. Processed data were plotted versus distance or time, depending on sample chronological control

Data reduction for discrete spot ablation

Whilst this method was not continued beyond the first analysis of part of core HS2, an aspect of the processing method used has been of some use working with subsequent continuous scan data. The data series from this sample consists of 20 discrete sample acquisitions in one file, separated by backgrounds while the sample was being traversed to the next ablation spot. For the purposes of data reduction, the start and end time of each sample acquisition was precisely located, defined as being positive and negative peaks respectively in the first derivative of the ^{46}Ca time series. Because this method allows empirical definition of periods when the laser was active, each isotope could be averaged between these points to obtain signal and blank values, and then blank-subtracted. The values for each isotope were then normalised, such that its average concentration over the 20 ablations was equal to that known from straw PV1.1. The first derivative method of delineating periods of sample ablation in data files has been used extensively in subsequent analyses.

Calibration of mass ratio data to absolute concentrations

Initial attempts to calibrate speleothem LA-ICPMS data were by measurement of the NBS 612 silica glass standard at regular intervals during sample data acquisition. While this approach provided crude concentration numbers, it was abandoned as unsatisfactory, due to differences in both matrix type and absolute trace element concentration. In particular, while measuring trace elements from speleothems at very low concentrations, it appeared that after switching to a silicate matrix for short periods, machine sensitivity and background levels for some isotopes would only gradually return to their normal levels for speleothem calcite ablation. Because of this, and because absolute trace element concentrations in speleothems are of little interest compared to relative internal variation for any one speleothem, alternative approaches to concentration calibration have been attempted (note that in many cases data is simply reported as counts relative to a given calcium isotope).

Data reduction using Wavemetrics Igor Pro software

The production of very long data series, to date consisting of as many as 59,000 time slices, has meant that spreadsheet data processing is no longer a realistic option on desktop computers, due to constraints with both memory and operating speed. Wavemetrics Igor Pro, a signal-processing application, was found to be a solution to this problem, enabling rapid analysis and graphing of extremely large datasets. Due to constraints on the formats in which data files may be entered into this application, raw ICPMS data files were first processed in a text editing application, using a command macro that stripped out unnecessary headers and data, and formatted the raw count data into columns for each mass.

After this treatment, individual files were usually small enough to be imported into Microsoft Excel, where a template containing a running standard deviation filter was applied. This filter is a further development of the running median filter discussed above, and simply rejects any point lying

more than three standard deviations from the mean of the twenty points immediately adjacent to it. Rejected points are replaced with the mean value of the six points immediately adjacent. This filter has proven highly effective at removing spurious spikes from ICPMS datasets, without otherwise damaging those records. There is no reason in principle why a similar running standard deviation filter could not be written as a function for use in Igor, eliminating altogether the need to use Microsoft Excel.

After importation to Igor Pro, files representing individual segments, typically forty-minute data acquisitions, are joined to form long records. Background subtraction is no longer normally performed, particularly for straw speleothem analyses, as for most elements analysed the background intensities are typically two or more orders of magnitude lower than signal. For straw speleothems the only processing undertaken before smoothing operations is calcium-normalisation. Smoothing was initially undertaken with the aid of a smoothing spline, a least squares variant of a cubic spline, although attempts were also made at band-pass and low-pass filtering using fast Fourier transforms. Recent filtering has utilised wavelet convolutions, which have proven particularly effective at removing high-frequency noise without adversely distorting the underlying trace element signal.

The raster scan of part of the surface of sample AM1.2 was also processed using Igor Pro. Raw data were entered as a 6556-second time-resolved record for each measured element. Data were delineated using the first derivative of the calcium counts, as described above. Backgrounds, and the forward ablations, essentially pre-ablation treatments, were discarded, and the remaining second-ablation data merged to form a single series, 1800 points long, for each element. Data were then normalised to calcium, before being redimensioned to form 30- by 60-sample arrays, and plotted as images, where colour intensity corresponds to concentration for each trace element measured.

Calibration to a time-series standard

Sample AM1.2, a section through the speleothem from which the solution-introduction ICPMS standard AM1.1 was prepared, has been used as a standard for LA-ICPMS analysis. While this sample is by no means homogenous, it consists of a known time-series sequence from base to top, allowing calibration of other samples relative to it by traversal of this sequence. As can be seen in the results of the raster scan of this sample, it is not free of variation normal to its direction of growth, but nonetheless it provides a fast approximate means of assigning absolute concentrations to LA-ICPMS records from speleothems. Where repeats of the AM1.2 standard are made throughout an analysis run, the same ablation track is used for each traverse, allowing accurate internal drift correction over the course of that run.

Core sample MD3 was analysed over the course of 12 hours, including background determinations, sample changeovers, pre-ablation treatments and AM1.2 standard analyses. All data acquired over this period were pre-processed and imported to Igor Pro, where they were linked into a single 42,000-point datafile containing intensity versus time for each element analysed, for the entire 12-hour period. Background changes were interpolated throughout the 12 hours and subtracted, before calcium-normalisation. Using the 12 AM1.2 standards spaced throughout the run, a drift correction factor relative to the first standard measured was derived for each trace element, and interpolated to every time slice in the data series. These correction factors were then multiplied with the calcium-normalised counts for each trace element, removing the drift from each series (drift over the course of the 12 hour run was less than 25% for all elements). The ablation periods for each complete MD3 segment were then cut from the datafile and combined, to produce a complete record for each element (fig. 8.1). Also analysed during the same analysis run were eleven 20-mm ablations, made

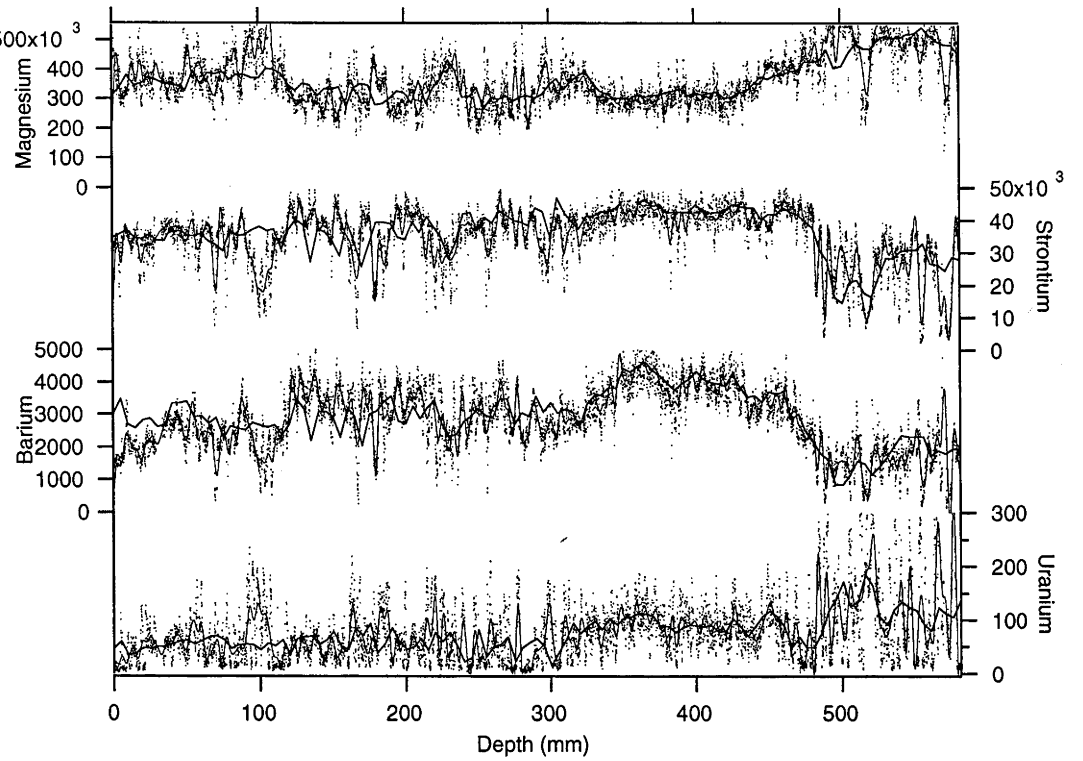

Fig. 8.1. Laser-ablation ICPMS data (parts per billion concentration) for magnesium, strontium, barium and uranium, versus depth in core MD3. The light line for each series is the output of a running gaussian mean, and the heavy lines are the results of solution-introduction ICPMS analysis.

approximately 5 mm from, and parallel to, the main analysis track. These ablations cover the joins between each 50 mm slide, and were taken from a second set of 50 mm slides cut parallel to the main set, but offset by 25 mm as described in chapter 4.

Calibration to existing solution data

In the case of Core MD3, a fully quantitative record of trace element concentrations had already been developed by solution-introduction, for 5-mm averages along its length. Because of this, the drift-corrected data above can be interpolated down to a suitable length and correlated with solution ICPMS data, deriving a correction factor for each element. This seems a most reliable method of concentration calibration, and the observed covariance reassures that both analytical methods are functioning to within their expected precisions.

Results and discussion

No attempt is made to report all Mt Arthur speleothem ICPMS results here. Many of the analyses undertaken, while of assistance in the ongoing development of analytical procedures, did not themselves constitute useful trace element records which can be used to further constrain what is known of the trace element characteristics of Mt Arthur speleothems. This is particularly true of many of the straw speleothems analysed, being broken fragments removed from cave floors with the intent of use in method development. The results reported here concentrate on a long record obtained for the full length of core MD3, after an earlier attempt produced results of slightly higher quality for half of the core. Also reported are recently acquired annually-resolved records from straw speleothems of known age, from Mt Arthur and from Frankcombe Cave, Tasmania.

Core MD3

As the principal focus of this project, the long core MD3 from The Meltdown, Nettlebed Cave, has been a high priority for high-resolution laser-ablation analysis. Because the core has already been analysed in detail using solution-introduction methods, the laser ablation data can be independently constrained and evaluated. A method of mounting the entire 600 mm core sample as 50 mm sections on glass slides was developed for this purpose, as described in chapter 4, forming the basis for two attempts at laser-ablation analysis of this core sample.

The first analysis attempt measured magnesium, calcium, strontium, barium, thorium and uranium versus distance over the basal half of the core, corresponding to the period ca. 30,000—20,000 cal yr B.P. A 70 μm diameter spot size was used, and the sample traversed at 25 μm/second, meaning three time slices of data were recorded in the time it took the spot to traverse its own width. The sensitivity of the ICPMS decayed throughout the day, as it had been decided not to retune the instrument over the course of the run, resulting in progressively poorer results for the very oldest section of the record. These initial data however agreed well with the lower-resolution solution introduction data for the same section of the core, as well as showing (for barium and strontium concentration) similar patterns of variation to the $\delta^{13}C$ record.

It was later decided to attempt to collect trace element results for the entire length of core MD3 over one day's operation of the ICPMS, in order to produce relative concentration data as precise as possible for each element. In order to achieve this while including a number of replicate analyses of standard AM1.2 throughout the run, the sample was traversed at the maximum available speed of 83 μms^{-1}, again using a 75-μm spot (this approach yields highly reproducible data for any given ablation track; fig. 8.2). The collected data for 14 main core sections, and 11 parallel overlap

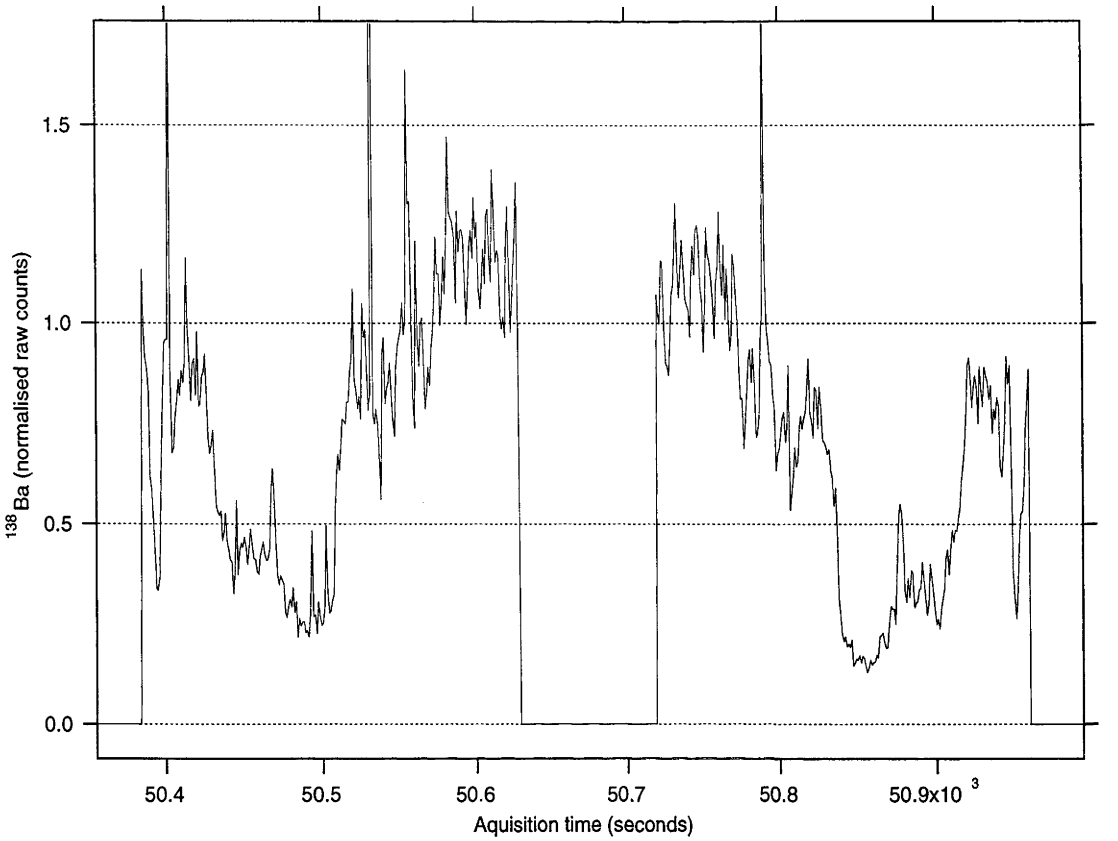

Fig 8.2. Barium results of a backward ablation (recorded as a pre-ablation step) of a section of MD3C, followed by a forward ablation following the same ablation track, showing excellent repeatability (the x-axis units are in seconds from the beginning of data acquisition). The section of MD3C shown corresponds to the overlap section from ca. 20,000—16,000 cal yr B.P., shown in figure 8.3.

sections of 20 mm, were blank-subtracted and normalised to calcium as one time series. The data were then normalised to drift factors interpolated from the AM1.2 standard measurements, to produce relative concentration data. Absolute concentration data were obtained by normalisation to the MD3 solution-introduction ICPMS data.

These data are in good agreement with existing solution-introduction data over most of the Holocene, but are in poor agreement during the last glacial maximum (fig. 8.3). The considerably higher-quality data for the lower section of MD3 reported above are in closer agreement with the solution data, suggesting that scanning at a slower rate produces better data for any given spot size. While not entirely intuitive, this may be a reflection of aliasing effects acting on high-frequency fluctuations in the trace-element data, as addressed in chapter four. A disturbing result of these data is the extremely poor agreement between the main scan data, and the eleven 20 mm parallel ablation tracks taken to enable better joining of them (fig. 8.3).

The lack of agreement between parallel sample traverses recorded only 5 mm apart is disturbing, and likely to be a combination of two factors. Retrospectively, it seems likely that allowing the sample to traverse a distance greater than the width of the ablating spot in the time taken to record a single data time slice may reduce the quality of that data. More significantly, trace element variation appears to occur along growth horizons, potentially voiding an assumption on which the utility of speleothem trace element data for palaeoclimate purposes is based. Because the solution-introduction data agree so well with other proxies such as $\delta^{13}C$ and growth rate, it is inferred that any such variation is fine-scale, and is largely averaged out by the ca. 5 mm^3 sample size used for the solution-introduction data. At the very least, this study shows that fine-scale variation in trace element data series should be interpreted with some considerable care.

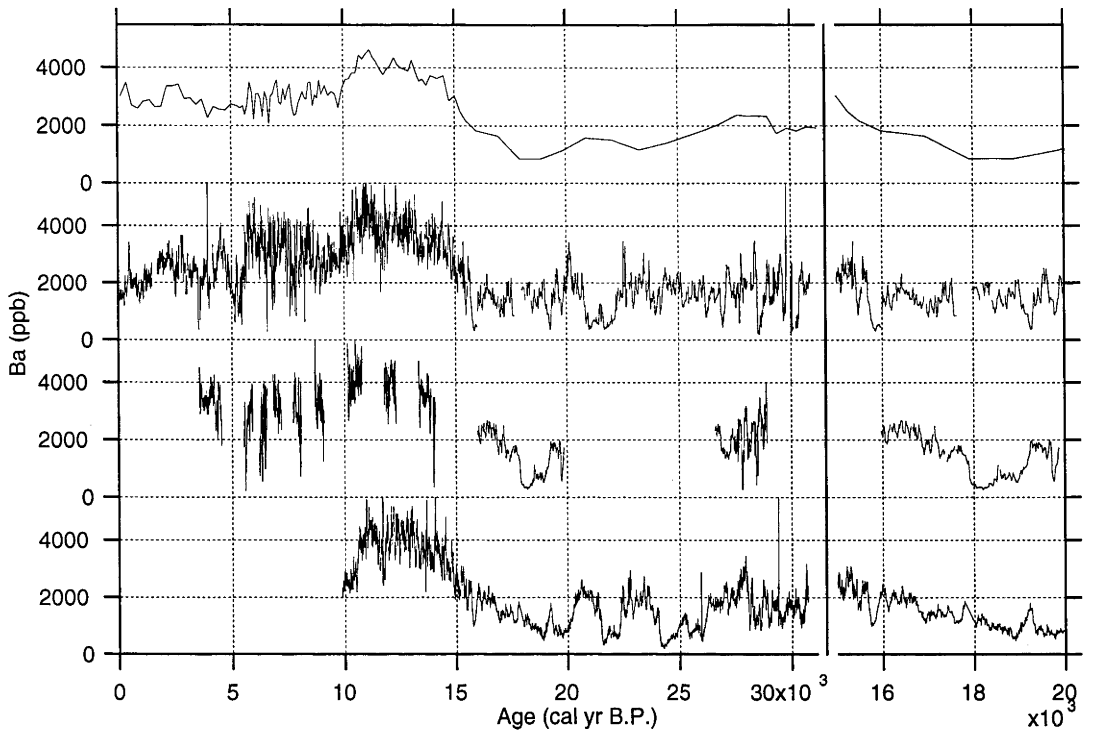

Figure 8.3. Barium concentration data from four traverses of core MD3. From the top down, the series are: 1) solution introduction data, 5mm resolution; 2) laser-ablation full-length scan; 3) 20-mm segments 5 mm from, and parallel to (2) above, to cover joins in that record; and 4) a higher-resolution record covering the lower 300mm of the core, taken parallel to, and 1—3 mm from the full MD3C series (2) above. The data are generally in good agreement, but not at scales of less than several millimetres The right-hand panel shows an enlargement of the interval 20,000—15,000 cal yr B.P., illustrating the fine-scale heterogeneity.

Straw stalactites

Straw speleothem PV1.2 was ablated using a rectangular beam size of 70 by 700 microns, recording one-second data time slices. Approximately 20 mm of sample was traversed over twenty minutes of signal acquisition, meaning at least five time slices were recorded in the time it took any point on the sample to traverse the width of the beam. The Ba concentration along ca. 5 mm of this stalactite shows a strong periodicity with a wavelength of a few hundred microns, implying an annual signal. This should however be interpreted with great care, as this straw was finished to a flat surface before analysis, voiding the assumption that ablated calcite progressively increases in age with distance from the straw tip. In smoothing the normally undulating surface of the straw, a complex pattern of time horizons is likely to have been exposed.

Straw stalactite MD9.1, ca. 180 mm in length, exhibits a periodic ribbing on it's surface, suggestive of annual growth rings about its circumference, at an average separation of ca. 160 μm. Based on the apparent success with straw PV1.2, several attempts have been made to detect any sort of periodic signal in sample MD9.1, particularly with a similar wavelength to the visible banding on the straw surface. Power spectral density analyses of high-resolution ICPMS scans of the 13 mm closest to the tip of this sample confirm there is a significant peak in spectral power at a wavelength of about 160 μm. It is apparent from the distance-resolved concentration data for strontium and magnesium that such a periodicity exists (fig. 8.4). Unfortunately, due to the low signal to noise ratio (a result of the very small ablation spot size required to resolve variations of this wavelength), it is not possible to reliably count these cycles by eye, nor to determine year-to-year changes in extension rate (fig. 8.4). Wavelet transform smoothing of the data is the only method that has yielded an obvious annual signal from this data. However, even then it can be seen that significantly higher-quality data will be needed to enable accurate autocalibration dating or growth rate variation records from this or from similar straw samples.

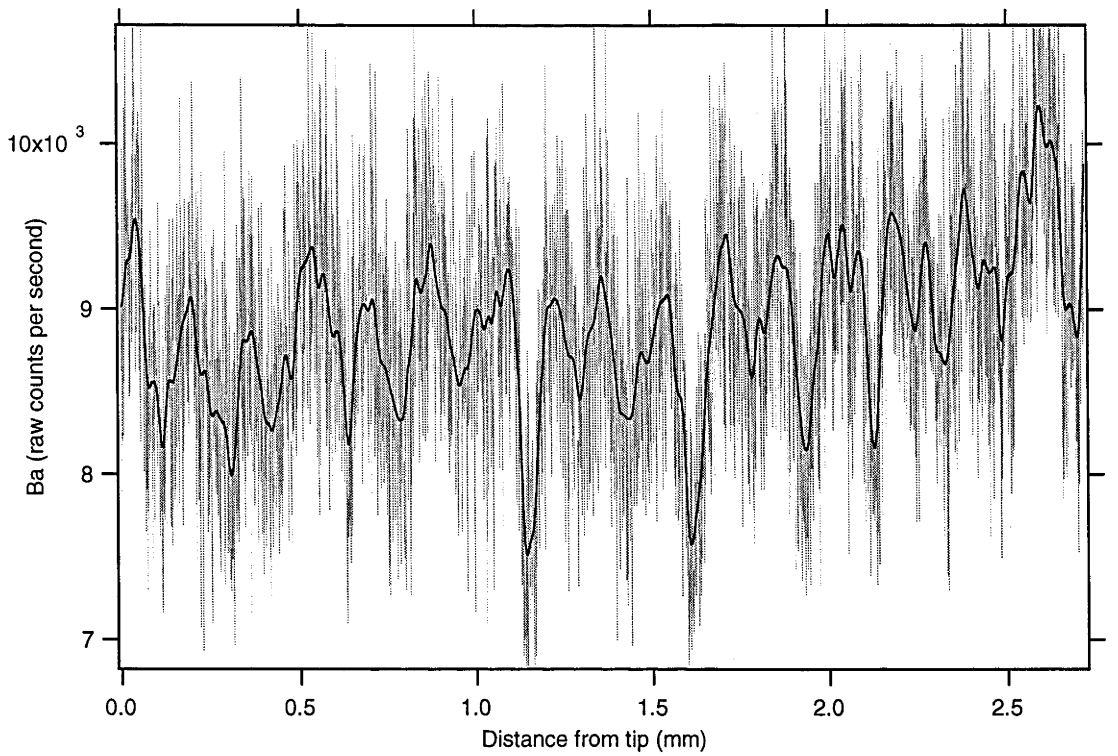

Fig. 8.4. Barium (raw counts per second) versus distance from the tip of straw MD9.1, taken from The Meltdown, Nettlebed. The heavy line has been smoothed using wavelet transforms, and shows a clear, apparently annual, banding with an average wavelength of ca. 170 μm.

Preliminary results from an analysis by J. Desmarchelier of a straw stalactite from Frankcombe Cave, Tasmania, are considerably more promising, exhibiting a pronounced periodicity in the concentrations of magnesium, barium and strontium, and less pronounced variation in that of uranium. These vastly clearer results (fig. 8.5) are exactly in phase with observed surface banding on the sample. Their clarity relative to data from Mt Arthur straws is thought to be due to a combination of the faster straw growth rate (ca. 1000 μm/yr), and greater seasonal precipitation variation in Tasmania. The pronounced troughs observed in strontium and barium content over each autumn and winter of the record presumably reflect greatly reduced soil CO_2 production rates, coupled with a slowing or cessation in growth. In contrast, the Mt Arthur straws are thought to grow at a similar rate throughout the year, due to the even distribution and reliability of rainfall in the region, with the minor variation observed being driven by soil temperature changes. The Frankcombe Cave sample indicates that accurate autocalibration dating of straws is possible using a combination of trace element concentration data and visible banding, offering the prospect of annually resolved palaeoclimate data from this source.

Two-dimensional surface map of section of sample AM1.2

In order to attempt to quantify the degree to which speleothem trace element concentrations can vary along time horizons, and the spatial extent over which any such effects are likely to be significant, a two-dimensional scan of part of the surface of speleothem standard AM1.2 was undertaken. A three by five millimetre section of the surface was imaged, and compared with a visible light photo of the same area (fig. 8.6). Most notable are the results for uranium, which exhibit a strong correspondence to a crystal fabric observable in the physical sample, and which is unrelated to, and crossed by, time horizons. A similar, but lesser effect is observed on the concentration data for strontium and magnesium, and a smaller still influence on barium concentration.

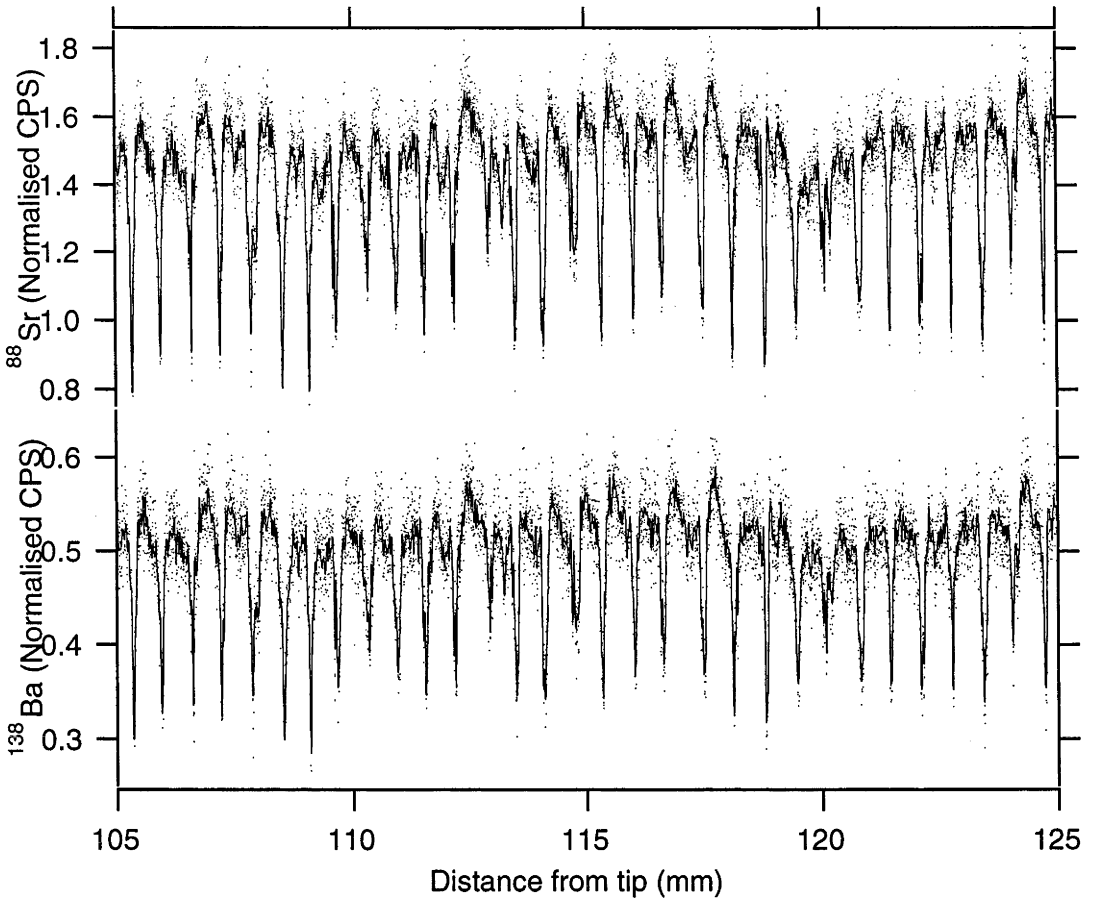

Fig 8.5. Strontium and barium data (normalised counts per second) versus distance from the tip of a section of straw speleothem from Frankcombe Cave, Tasmania (Jol Desmarchelier, unpublished data). The clearly annual signals are suggestive of an autumn/winter hiatus in growth, and allow the construction of accurate autocalibration chronologies, in this instance back to 1769±5 AD.

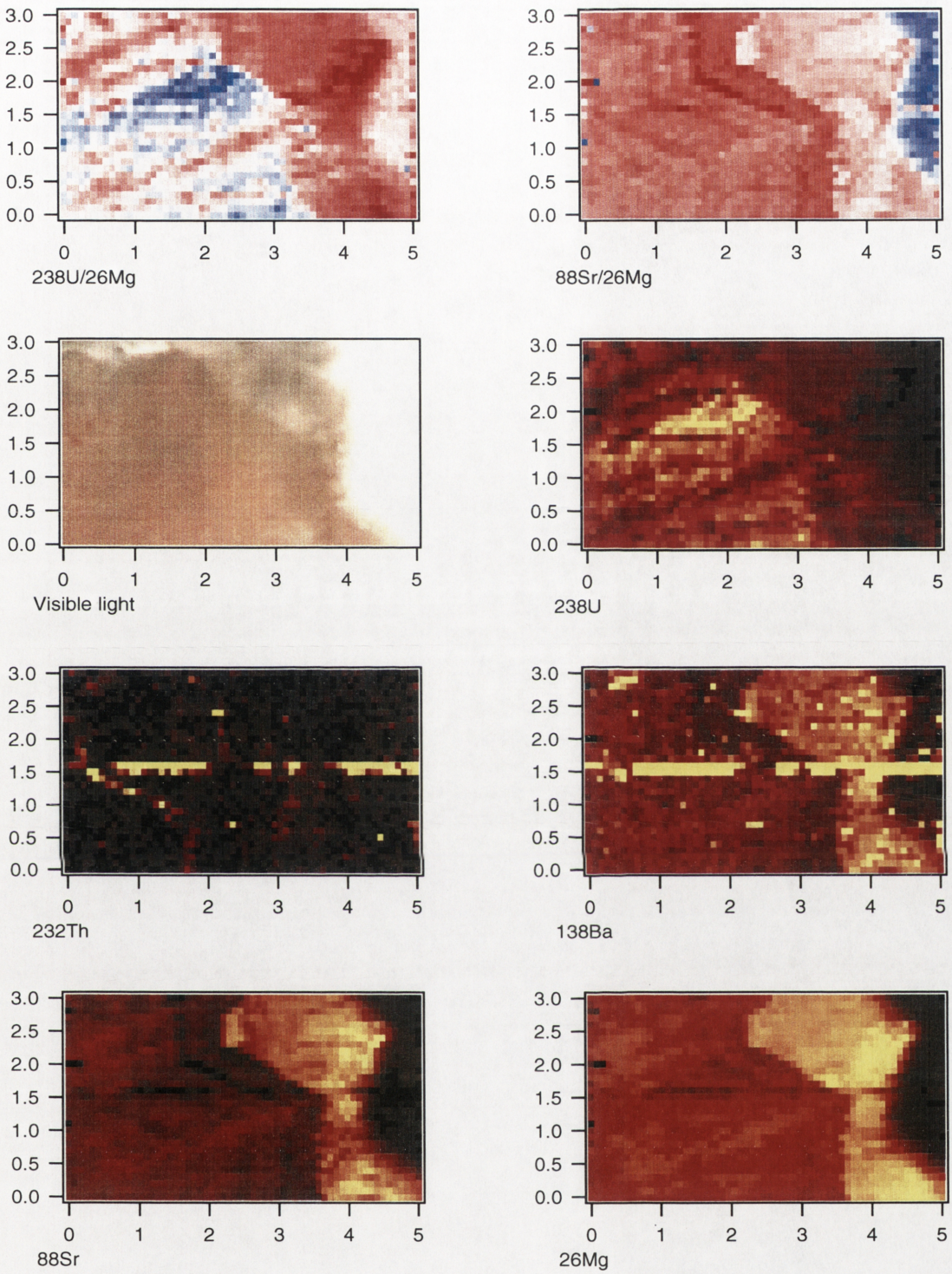

Fig. 8.6. Images of trace element concentrations over a 3- by 5-mm rectangle on the surface of sample AM1.2 (yellow indicates high concentrations, and black, low). A combination of growth banding and crystal fabric effects can be seen for each element analysed, the effect being exaggerated by the ratio of U to Mg, and subdued by the ratio of Sr to Mg. Uranium appears to suffer the greatest bias from this effect, and barium the least. The horizontal line in the centre of each image is due to a large number of previous linear ablations along a single track at that point.

Growth banding can be seen in all trace elements analysed, including thorium, in which they correspond to very faint red bands visible in the sample, indicative of slight detrital contamination of these growth surfaces, and further confirming that laser-ablation thorium analysis is an effective monitor of such contamination. Note that the thorium-rich bands correspond to reduced strontium concentrations, perhaps indicating a slowing or halting of growth associated with accumulation of the detrital material. Confirming results for core MD3, it appears that, while this crystal zoning effect is significant on small scales, the averaging of several cubic millimetres of material for solution-introduction analysis is likely to greatly reduce its effect. The effectiveness or utility of high-resolution laser-ablation analysis of speleothems is challenged by this, however, a problem which may possibly only be addressed by routinely imaging sample surfaces in two dimensions, enabling better identification of and correction for such effects. It should also be noted that this two-dimensional analysis has high-lighted apparent banding of growth horizons which might be too weak to show in a single one dimensional analysis of such a sample, but which may be clearly identified in the raster images. Such techniques may one day be of considerable use in the construction of very fine-scale trace element records.

Chapter 9. Discussion and Conclusions

Overview

Speleothem core sample MD3 from The Meltdown, Nettlebed Cave, has been shown by U-series dating to have grown continuously throughout the last 31,000 years. Analyses of change in measurable parameters along this sample have produced isotope and trace element records which can be interpreted in terms of local environmental change, and, less directly, in terms of regional climatic change. By careful consideration of the environmental factors most likely to influence each measured parameter, and of the relationships between those factors, it is in many cases possible to constrain each proxy record as responding predominantly to a single environmental factor. This chapter contains a summary and discussion of the significant results from this work, and explores their implications to the study of late Quaternary environmental change, at local, regional and global levels.

Speleothem growth rates and growth periods

Tree-line constraints

As summarised in chapter 4, the periods of growth of Mt Arthur speleothems have implications for the history of vegetation change on the surface above. In particular, it can be argued from their modern distribution beneath the mountain that massive speleothems such as flowstones cannot actively grow beneath alpine vegetation, and thus that periods of growth must coincide with the presence of some form of forest on the surface above. Following from this, it is likely that forest cover of some kind persisted on the surface above the MD3 site over the 31,000 yr period of continuous growth, restricting the local treeline during this time to at most 600—700 m lower than its present altitude. Similarly, the treeline above the ED1 site, on the southern side of the mountain, appears to have been locally at least 300—400 m lower than its current altitude over the period 73,000 to 16,000 cal yr B.P. A flowstone in the

Headsnapper passage, near the lower entrance of Nettlebed, appears to have grown continuously over the last ca. 160,000 years, implying that the treeline was never more than 900 m above lower than its current altitude, over the last full glacial-interglacial cycle.

Temperature constraints

Whilst some constraints on temperature change may be deduced from the inferred constraints on treeline changes, it must be remembered that treeline altitude is controlled by a combination of factors, including temperature, rainfall and wind velocity (McGlone, 1988). Nonetheless, crude estimates may be made, by assuming a vertical lapse rate of 0.5°C/100 m, the modern value for the central South Island (Soons, 1979). The same lapse rate is derived by assuming a modern sea-level temperature of 12°C (Garnier, 1958), and a zero degree isotherm of ca. 2400 m (fig. 3 in Chinn, 1995; fig. 2 in Soons, 1979). On this basis, surface temperature above the caves is approximately constrained to at least ca. 1.5°C colder than the present over the period 73,000 to 16,000 cal yr B.P. Similarly it can have been no more than ca. 4°C colder than today at any time over the last 31,000 years, and no more than ca. 5°C colder than today at any time over the last ca. 160,000 years.

An alternative approach is to use the ca. 800 m lowering of the 0°C isotherm argued by Soons (1979), and a 700 m lowering of the treeline, assumed to represent the 6°C isotherm, to derive a last glacial maximum temperature gradient (lapse rate) and intercept (sealevel temperature). The resulting 0°C isotherm of 1600 m and 6°C isotherm of 600 m give a lapse rate of 0.6°C/100 m, and a sealevel temperature of 9.6°C, ca. 2.5°C colder than today. The increased lapse rate is consistent with the findings of Soons (1979), and with the inference from Mt Arthur $\delta^{18}O$ records (see chapter 6) that local lapse rate must have increased during glacial times (see also Thunell *et al.*, 1994). The sealevel temperature drop is less than that found by other workers (e.g., Pillans *et al.*, 1993), possibly reflecting unusually favourable LGM conditions in the Pearse Valley, resulting in a higher treeline there. A completely independent control placed on the LGM temperature by the MD3 results is

that temperature cannot possibly have fallen by as much as 8.3°C, the modern cave temperature, as liquid water would in that case no longer be available for speleothem formation.

Vegetation productivity and rainfall inferences

While the timings of speleothem growth periods can place broad constraints on environmental conditions at times in the past, changes in speleothem growth rate during those periods of growth are also a potentially important palaeoenvironmental indicator. Calculations by Dreybrodt (1981) show that the growth rates of speleothems are controlled by some combination of the calcium ion concentration in solution, and the rate at which CO_2 can out-gas from seepage waters. In the case of slow, thin-moving films of water initial calcium ion concentration is the predominant effect controlling growth rate, which also accelerates as water flow over the speleothem becomes thicker and faster. Baker *et al.* (1998) found calcium ion concentration to be the more dominant effect, on the basis of observed growth rates from many speleothems.

On this basis, the growth rate history of core MD3 (fig. 9.1) implies that calcium ion concentrations, linked to the rate of carbonic acid production in the soils above (Dreybrodt *et al.*, 1996), were at their greatest in the early Holocene. The very high growth rates recorded in the mid-Holocene are thought to be anomalous, as, based on the petrography of the core sample, it appears that much of this section of the speleothem grew on the floors of a series of small pools, implying quite different depositional processes. The two-step increase in growth rate observed at the beginning of the Holocene may be caused by an initial increase due to increased calcium ion concentration, presumably related to a soil temperature increase. The second step can be explained by an increase in flow rate over the speleothem at ca. 13,000 cal yr B.P., as argued in chapter 7. Aside from the mid-Holocene section of the core, growth rate changes are consistent with calcium ion concentration being the predominant influence on growth rate, with water flow rate increases having a secondary influence.

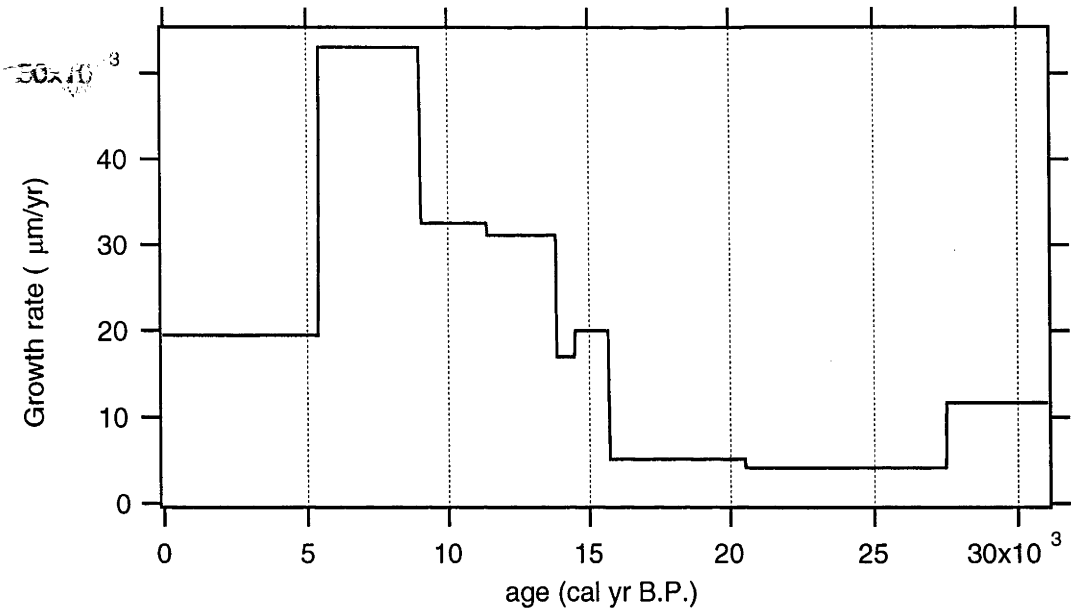

Fig 9.1. Growth rate vs. age, core MD3. The record is limited by the resolution of the dates, and does not attempt to take their errors into account. The very high mid-Holocene growth rate may be anomalous, the physical characteristics of this section of the core indicating it may potentially have grown beneath a series of shallow pools on the flowstone surface.

$\delta^{18}O$ variations and STF movement in the Tasman Sea

Of interest in the MD3 $\delta^{18}O$ record as indicators of local palaeoclimate, are the seven short positive excursions highlighted in figure 6.4, referred to as MD3/1 through MD3/7. From the results section above, these excursions are likely to have resulted from northward migrations of the STF in the Tasman Sea, which would cause stronger westerly winds and lower temperatures in central and southern New Zealand (McGlone *et al.*, 1993). It has been shown that in historic times, stronger westerly atmospheric circulation over the Tasman Sea favours snowline lowering and glacial advance in the western South Island (Fitzharris *et al.*, 1992). There is also considerable evidence, from records of dust flux, marine $\delta^{18}O$ and pollen, that during the LGM westerly winds over the South Island were considerably stronger and more prevalent than today (Moar and Suggate, 1996; Nelson *et al.*, 1994; Thiede, 1979). Thus northward migration of the STF and westerly wind belt may be considered a mechanism strongly linked to both South Island glacial advances and to the MD3 isotope excursions.

Comparison with existing glacier advance records

The correlation of the positive excursions in the MD3 $\delta^{18}O$ record with known South Island glacial advances is excellent, in particular for the three best-dated major advances (fig. 6.4). These are the Waiho Loop advance of the Franz Josef Glacier (Denton and Hendy, 1994), and the Aurora 2 and Aurora 3 advances in Fiordland (Williams, 1996). The Kumara 2_2 glaciation (Suggate, 1965; Suggate and Moar, 1969), while not as well dated as the above records, began shortly before the eruption of the well-dated Kawakawa Tephra, coinciding with the onset of the MD3/7 isotope excursion (fig. 6.4). The fits to MD3 $\delta^{18}O$ of the Kumara 3 glaciation, and of another widely-quoted South Island glacial advance record from the Waimakariri Valley (Gellatly *et al.*, 1988), are also good, although less certain due to less precise dating of the glacial deposits. The fit of the MD3 $\delta^{18}O$ record to the Taranaki quartz loess flux record of Alloway *et al.* (1992), is also very good (fig. 9.2), further

implying that the MD3/5, MD3/6, and MD3/7 oxygen isotope excursions coincide with periods of intensified westerly atmospheric circulation.

Table 9.1 shows a summary of the seven MD3 positive $\delta^{18}O$ excursions, and possible correlations to West Coast and Waimakariri glaciations, based on their reported ages. While Williams (1996) found the Kumara 2_2 advance to coincide with his Aurora 3 advance, it is here considered to pre-date it, in agreement with its reported age (Suggate, 1990). That the Kumara 2_2 advance spanned two of the MD3 excursions is supported by its correlation with the two Blackwater advances in the Waimakariri Valley (Suggate, 1990). Suggate and Moar (1969) considered the Kumara 3 glacial advance to consist of two closely spaced advances, from ca. 20,000—18,900 cal yr B.P. and ca. 17,500—16,700 cal yr B.P., in very good agreement with both the Aurora Cave and MD3 records (fig. 6.4). However, he later reported it (Suggate, 1990) as being two advances between ca. 19,000 and ca. 16,700 cal yr B.P., while cautioning it was not well-dated. Gellatly *et al.* (1988) noted that three New Zealand sites record glacial activity at around 9,000 cal yr B.P., during a period of otherwise low glacial activity from 10,000—6000 cal yr B.P. However, the MD3/2 isotope excursion centred on ca. 9300 cal yr B.P. does not correspond to any convincingly dated glacial advance. The MD3/1 isotope excursion, from ca. 4500 to 3000 cal yr B.P., may correspond to a period of increased glacial activity beginning after ca. 5700 cal yr B.P. (Gellatly *et al.*, 1988). It is here considered significant because of its clarity in both the MD3 and ED1 oxygen isotope records. A younger excursion, not named here, begins at ca. 700 cal yr B.P., and appears to correspond to the Little Ice age (seen in greater detail from a speleothem at nearby Patarau; Wilson *et al.*, 1979).

The relative amplitudes of the MD3 isotope excursions appear to be crudely proportional to those of the glacial advances they correspond to, although there is some ambiguity in defining a baseline from which to measure them. In particular, the MD3/5 excursion, clearly the greatest in magnitude,

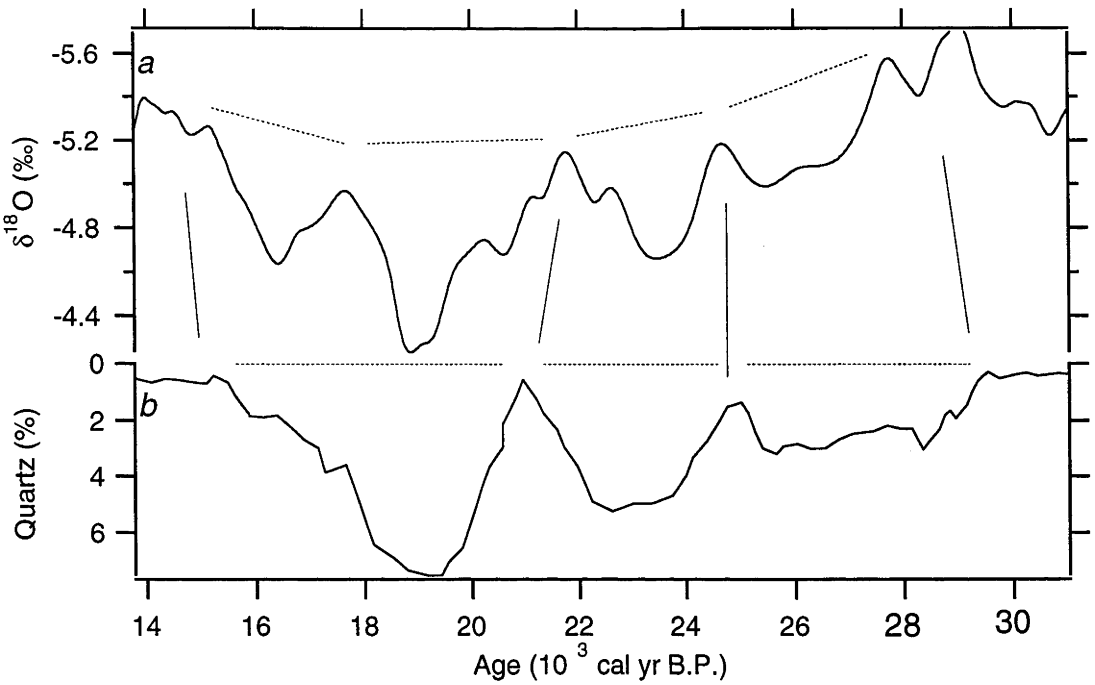

Fig 9.2. A comparison of part of the MD3 $\delta^{18}O$ record with the Taranaki quartz loess flux record of Alloway *et al.* (1992). This illustrates that, within the limitations of their respective chronologies, the two records appear to be in agreement as to the timings, durations and relative intensities of periods of enhanced atmospheric circulation during oxygen isotope stage 2, corresponding to greater $\delta^{18}O$ values in MD3, and increased quartz loess accumulation at Taranaki.

TABLE 9.1. CORRELATIONS OF MD3 ISOTOPE EXCURSIONS TO SOUTH ISLAND GLACIER ADVANCES

Age range (10^3 cal yr B.P.)	Mt Arthur $\delta^{18}O$ excursion	Fiordland glacier advance[a]	Westland glacier advance[b]	Waimakariri glacier advance[c]
4.5 to 3	MD3/1			Arthur's Pass
10.5 to 7.5	MD3/2			McGrath II
13.8 to 11.7	MD3/3	Aurora 1	Waiho Loop	McGrath I
17.5 to 15.5	MD3/4	Aurora 2	Later Kumara 3	Poulter
20 to 18	MD3/5	Aurora 3	Earlier Kumara 3	
24.5 to 22	MD3/6		Kumara 2(2)	Blackwater (II)
27 to 25	MD3/7		Kumara 2(2)	Blackwater (I)

[a] Williams (1996)

[b] Denton and Hendy (1994); Suggate (1965); Suggate and Moar (1969).

[c] The Waimakariri advances (Gellatly *et al.*, 1988; Suggate, 1990) are less certain correlations, having less well-constrained ages.

corresponds to the known timing of the LGM glacial culmination in southwest New Zealand (Williams, 1996). On the central West Coast, the greatest glacial extent (the Kumara 2_2 advance; Suggate, 1990) corresponds to the earlier MD3/6 and MD3/7 excursions, possibly due to the longer duration of these events. The correlation of the well-dated excursions in the MD3 $\delta^{18}O$ record to those South Island glacial advances with tightly constrained ages is excellent, and provides strong support for a common mechanism influencing both glacial advance and the $\delta^{18}O$ of Mt Arthur precipitation.

Utility of speleothems for extending existing glacier records

The apparent correlation between the MD3 isotope excursion record and existing records of South Island glaciation has been explained in terms of broad changes in regional climate. These are likely to lead simultaneously to conditions favourable to glacier advance in the central and southern South Island, and isotopically heavier meteoric water vapours arriving over North-West Nelson. While this model requires more vigorous westerly circulation over the Tasman Sea at times of glacier advance, it does not require simultaneous climate change in the region of Mt Arthur. Indeed the carbon isotope records from Mt Arthur, a proxy for local palaeoenvironmental conditions, do not correlate well with the oxygen isotope records. This implies that local environmental changes may be largely unrelated to those acting further to the south (c.f., Gage, 1965; Moar and Suggate, 1996; Singer *et al.*, 1998; Worthy and Mildenhall, 1989). Noting the good correlation of the MD3 isotope excursions to South Island glacier advances, it is hoped that future extensions of the speleothem record from this location will produce glacier advance records of similar resolution, covering earlier periods for which the glacial history is currently poorly understood.

Was there a Younger Dryas event in New Zealand?

The oxygen isotope results of this study strongly imply that conditions favourable to glacial advance occur synchronously over much of central and

southern New Zealand, and, as proposed by others (Fenner *et al.*, 1992; McGlone *et al.*, 1993; Wright *et al.*, 1995), are generally a result of northward movement of the STF and the westerly wind belt in the Tasman Sea. These latitudinal movements are likely to reflect changes in Southern Hemisphere oceanic circulation and climate. Figure 9.3 shows the MD3 $\delta^{18}O$ record with two other high-resolution isotope records, the GISP $\delta^{18}O$ (Stuiver *et al.*, 1995) and Vostok δD (Lorius *et al.*, 1985) ice core records from the North and South Poles, respectively. The only feature of the MD3 record with apparent equivalents in the polar records is the MD3/3 oxygen isotope excursion, which coincides with the Antarctic Cold Reversal (ACR; Jouzel *et al.*, 1992) in the Vostok and Byrd Ice cores (Blunier *et al.*, 1998), and the Younger Dryas Event in the GISP core. The timing of these events is similar for MD3 (13,800—11,700 cal yr B.P.) and GISP (12,890—11,650 cal yr B.P.), the most precisely dated of the records. The MD3/3 event initiated somewhat before the GISP Younger Dryas, more synchronous with the Older Dryas (14,090 cal yr B.P.) in the GISP record (Stuiver *et al.*, 1995), and with the ACR in the Byrd Ice Core (14,000 cal yr B.P.; Blunier *et al.*, 1998).

The MD3 $\delta^{18}O$ record thus contains further evidence of a significant glacier advance in New Zealand at the time of the Younger Dryas, supporting the finding of Denton and Hendy (1994) that a significant advance of the Franz Josef glacier occurred at this time. McGlone (1995) noted there is no evidence of a temperature drop in New Zealand at this time, and suggested the advance was driven by strengthened westerly winds causing increased precipitation, rather than by lowered temperature. Singer *et al.* (1998) reported similar findings to those of McGlone, interpreting their pollen data as precluding a thermal decline at this time. They instead suggested that any glacier advance at this time reflected a period of increased precipitation, perhaps due to locally increased westerly circulation in the Tasman Sea. The MD3/3 isotope excursion, which began ca. 700 years prior to the Younger

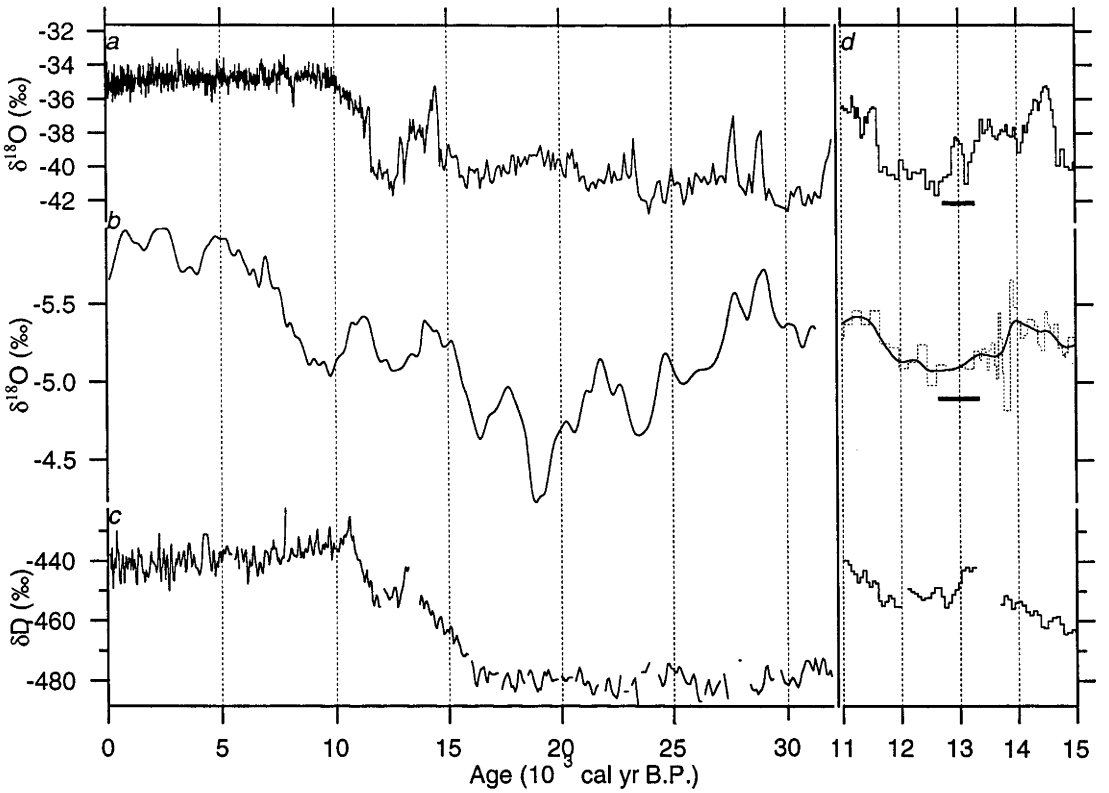

Fig 9.3. *(b)* MD3 $\delta^{18}O$ vs. time shown with δD and $\delta^{18}O$ records from Antarctica (*c*; Vostok; Lorius *et al.*, 1985) and Greenland (*a*; GISP; Stuiver *et al.*, 1995), respectively. *(d)* Expansion of the period 15,000—11,000 cal yr B.P., showing the relative timings of MD3/3, the Younger Dryas, and the Antarctic Cold Reversal. Note that the most recent Antarctic ice core chronologies (Blunier *et al.*, 1998) now show the ACR in the Vostok core lasting from ca. 15,000—12,500 cal yr B.P., pre-dating MD3/3 and the Younger Dryas. The black bars indicate ± 2 sigma age errors for GISP and MD3 at 15,000 years.

Dryas event in Greenland (fig. 9.3) and the glacier advance recorded at Waiho Loop (fig. 6.4; Denton and Hendy, 1994), implies that the latter was not a response to a rapid, global, Younger Dryas event, but instead occurred after some centuries of local conditions favourable to glacier advance.

$\delta^{13}C$ variations and changes in soil ρCO_2

As discussed in chapter 6, the record of $\delta^{13}C$ change versus time from core MD3 appears to predominantly reflect changes in the density and vigour of vegetation growing above the cave, which directly controls the partial pressure of carbon dioxide in the soil atmosphere. An additional possible effect on $\delta^{13}C$ in speleothems, that of changes in flow rate and thus of changes in the relative amount of calcite precipitated from seepage waters on reaching any point on a speleothem surface, was eliminated as a major factor in chapter 7. This was on the basis that any such effect would cause the concentrations of trace elements such as barium to covary with $\delta^{13}C$. That the $\delta^{13}C$ record is predominantly forced by changes in the organic activity of the soil above is strongly supported by its similarity to the record of ultra-violet luminescence from the same speleothem. This is known to be a direct proxy for the production rate of organic acids in the soil (Baker *et al.*, 1996).

Comparisons to existing records

The carbon isotope record from MD3 is fully consistent with other records of palaeovegetation in the region, in particular with those of Pillans *et al.* (1993), Moar and Suggate (1996), Worthy and Mildenhall (1989) and Singer *et al.* (1998). Notably, the extremely rapid return of dense forest cover at 15,000 cal yr B.P., implied by the MD3 $\delta^{13}C$ data, is in very close agreement with that observed from nearby pollen records (Singer *et al.*, 1998). The LGM period of 27,000—15,500 cal yr defined by Pillans *et al.* (1993) for central New Zealand, on the basis of available pollen and geomorphic activity data, exactly coincides with the period of the highest values of $\delta^{13}C$ in MD3 (fig. 6.5). Again as predicted by existing pollen data (McGlone *et al.*, 1993), the early

Holocene appears to have been the most favourable time for forest growth, with conditions degrading gradually through the late Holocene. Such close agreement with established palaeovegetation records for the region must be seen as confirmation that the MD3 $\delta^{13}C$ signal is almost entirely driven by vegetation productivity changes above the cave, or by some very closely related factor.

Utility of $\delta^{13}C$ for enhancing existing records

The finding in chapter 7, that rainfall does not appear to have increased until ca. 13,000 cal yr B.P., significantly after the sudden rise recorded in $\delta^{13}C$ and other variables at 15,000 cal yr B.P., shows that changes in rainfall are unlikely to have played a significant part in the rapid reafforestation inferred at this time. Instead it is assumed, as proposed by Gage (1965), that rainfall in the region was not severely reduced during the last glacial maximum. This is in agreement with the findings from areas to the south of Moar and Suggate (1996), but contrasts with those of Pillans *et al.* (1993), who found the areas to the north and east to be relatively cold and arid at this time. The sudden return of vegetation at 15,000 cal yr B.P., coincident with a massive increase in global methane levels thought to reflect a sharp rise in tropical temperatures (Blunier *et al.*, 1998), is thus found likely to have been predominantly driven by changes in local temperature. Whether this reflects a local warming due to a reduction in cloudiness or wind strength, or a more regional effect, is uncertain, as there is little evidence favouring a synchronous warming across New Zealand at this time (e.g., McGlone *et al.*, 1993).

It is apparent that $\delta^{13}C$ can in at least some speleothems be a direct proxy for organic activity and CO_2 production rates in the soils above, and through this a proxy for temperature. Extreme care should be taken in interpreting such records however, as large changes in rainfall or windiness can also force vegetation changes, as can non-climatic factors such as discussed below. In the case of MD3 it seems that $\delta^{13}C$ is a proxy for temperature variation versus time, presumably with a component of superimposed noise due to other factors. Rainfall, is nevertheless an important factor in vegetation

productivity, and as shown in chapter 7, can be reconstructed using trace element isotopic variation, and magnesium concentration data, and thus its contribution to the $\delta^{13}C$ record constrained to some extent.

A particularly important aspect of $\delta^{13}C$ records from speleothems such as MD3 is their utility in sharply delineating important climatic changes such as termination 1 (fig 6.7), which combined with TIMS U-series dating allows a precise chronology to be placed on these events. A record from The Meltdown of similar nature to MD3, but spanning the last interglacial, is a particularly enticing prospect for the future.

Implications of sudden $\delta^{13}C$ fall at time of human occupation

The very sudden fall in $\delta^{13}C$ at ca. 700 cal yr B.P., implying a shift towards considerably more vigorous forest growth at this time, does not coincide with any known significant climate change. It does however approximately coincide with the first evidence of significant human modification of biota in the Nelson region (McGlone *et al.*, 1994), which may have included direct modification of the forest, in particular by burning it. Whilst burning of the area may have been possible, it seems unlikely that this might lead to a sustained increase in the vigour of forest growth, persistent over the next few centuries. The alternative explanation offered is that vigour of shrubby vegetation growth, and the accumulation rate of leaf litter on the forest floor, greatly increased subsequent to human extermination of the moa (Dinornithiformes), New Zealand's browsing megafauna. The moa, and their extinction, are thought to have had a significant influence on New Zealand forest ecology (Wardle, 1991).

Constraints from MD3 trace element data

As discussed in chapter 7, there are very many mechanisms by which various environmental variables might influence the trace element contents of speleothems. By comparing trace element concentrations with other measured parameters, for which the relationships to environmental factors are

better understood, it has been possible to constrain which of those factors predominantly influence changes in magnesium, strontium, barium, thorium and uranium concentrations. A comprehensive water sampling program, coupled with measurement of environmental variables, such as surface temperature and precipitation, and with analysis of actively forming speleothems, is urgently required before significant further progress is likely to be made in this area.

In addition to the parameters of growth rate, $\delta^{18}O$, $\delta^{13}C$ and ultraviolet luminescence discussed above, two further parameters for which the relationships to environmental variables are relatively well known are strontium and uranium isotope ratios. Increases in initial $\delta^{234}U$ in natural waters are usually interpreted in terms of either increased groundwater residence time (e.g., Osmond and Cowart, 1982), or less aggressive leaching of uranium from source rocks or sediments (e.g., Rosholt, 1982). The rapid fall in $\delta^{234}U(T)$ seen in MD3 postdates by ca. 2000 years the time when seepage waters appear to have become significantly more aggressive. This, and the observation that the uranium content and $\delta^{234}U(T)$ are not correlated in Mt Arthur speleothems, implies that the water residence time is in this case the more important effect. The $^{87}Sr/^{86}Sr$ ratio in groundwaters has also been shown to depend on water residence times (Banner *et al.*, 1996; Banner *et al.*, 1994), through their effect on changes in the relative contributions of strontium derived from soil and host rock end-members. In MD3, strontium isotope variation exhibits no correlation with strontium concentration variation, and is considered in terms of short water residence times favouring a mica-rich soil end-member, and longer residence times leading to a greater contribution from a relatively ^{87}Sr-poor calcite host rock end-member

Magnesium concentration in MD3 exhibits different behaviour from all other continuously measured parameters, showing a gradual decrease throughout the last glacial maximum (fig. 7.2), followed by a sudden drop approximately 13,000 cal yr B.P. After (Roberts *et al.*, 1998), this is interpreted as being due to a water residence time effect on magnesium concentration, whereby progressively more magnesium-rich carbonate phases are dissolved with

time. The strong correlation of magnesium concentration with strontium and uranium isotope ratio variation confirms this mechanism (fig. 7.7), indicating that rainfall at Mt Arthur did not reach Holocene optimum values until ca. 13,000 cal yr B.P., some 2000 years after the sudden increase in forest productivity noted above. Magnesium concentration has no apparent relationship to the changes in the intensity of westerly circulation inferred from the MD3 $\delta^{18}O$ record, implying such changes have little impact on rainfall in North-West Nelson. The sudden increase in precipitation at ca. 13,000 years may instead reflect an increase in temperature in the precipitation source area in the southern Tasman Sea or the Southern Ocean.

Thorium, by nature of its insolubility in natural waters, is found in speleothem as a detrital phase, confirmed by its covariation with aluminium concentration measured by laser ablation ICPMS. In core MD3, high-thorium calcite samples have been found on dissolution to contain significant amounts of white mica, which is interpreted as indicating an airborne origin for the contamination. Whilst changes in cave airflow or humidity might alter the flux of airborne dust onto the flowstone surface, it is here assumed that the flux is constant, and that changes in thorium concentration can be considered an inverse proxy for speleothem growth rate. This suggests a use in some instances for laser-ablation ICPMS analysis of thorium as a rapid means of establishing rough relative growth rates, and of targeting areas for U-series dating

Strontium and barium, while poorly understood, appear to vary primarily in response to changes in the concentration of CO_2 in the soil atmosphere, on the basis of their strong covariance in MD3 with $\delta^{13}C$, ultra-violet luminescence, and growth rate changes. Possible causes of this behaviour are numerous, as described in chapter 7. As discussed above, understanding of these elements is unlikely to improve without thorough characterisation of their behaviour in cave seepage waters. Barium may be of use as a proxy for $\delta^{13}C$ in some speleothems as, although being of a more qualitative nature, it is considerably more easily measured. The processes governing uranium behaviour are also poorly understood, although it strongly covaries with strontium and barium

during the Holocene, implying that similar chemical processes control these three trace elements. Prior to 15,000 cal yr. B.P., the behaviour of uranium was very different, again implying significant changes in soil and groundwater chemistry to have occurred at this time. The change in behaviour of uranium could indicate a greater proportion of soluble U^{+6} to have existed in the waters prior to 15,000 cal yr B.P., due to relatively oxidising soil conditions at this time.

Conclusions additional to isotope record inferences

Trace element data from core MD3 have been of two principal uses. They illustrate that the drastic change seen in $\delta^{13}C$, centred on 15,000 cal yr B.P., was accompanied by significant changes in groundwater chemistry, and confirm that it was driven by significant palaeoenvironmental changes associated with the termination of the last glacial maximum. The trace element data also strongly indicate that there was not a similar sudden increase in rainfall at this time, but that this occurred almost 2000 years later, at which time there was no significant effect on vegetation above the cave. From this, it is deduced that the changes which occurred at 15,000 cal yr B.P. were predominantly associated with a sudden temperature increase at that time, and thus $\delta^{13}C$ can, in at least some speleothems, be an important proxy indicator for palaeotemperature change.

Utility of very high-resolution LA-ICPMS analysis methods

The principal conclusion of this investigation into the viability of laser-ablation ICPMS analysis for producing very high-resolution trace element records from speleothems, is that any such record must be interpreted with extreme care, due to the fine-scale heterogeneities in calcite trace element distribution. Very high-resolution analyses of core sample MD3 give results that are fully repeatable for any single ablation track, but which rarely agree with records from closely spaced parallel tracks. A curious aspect of the method is that slower sample traverse rates, relative to the size of the ablating spot, produce results in better agreement with those from parallel ablation

tracks and with solution-introduction ICPMS analyses of the same samples, than do rapid ablation methods. Because results from the rapid ablation methods are still fully repeatable for any given track, this effect cannot be attributed entirely to improved counting statistics for slower sample traverse rates. A more detailed characterisation of the three-dimensional structure of fine-scale heterogeneities in speleothems is required before this can be explained, although it may be related to micro-inclusions of impurity phases within the calcite, as predicted by Angus *et al.* (1979).

LA-ICPMS has considerable potential as a rapid exploratory technique for speleothem analysis. For flowstones and stalagmites, it is likely that the best results will be obtained by using a spot size of several hundred μm diameter, giving the best compromise between achieving a high spatial resolution and avoiding interference from the fine-scale structural variations discussed above. A number of parallel tracks should demonstrate good agreement before results are taken as representative of variation versus time in a given speleothem. It is likely that solution-introduction ICPMS, with its fully quantitative nature, and with the three-dimensional spatial averaging inherent to the milling of solid samples, will in most cases give more accurate results.

A laser-ablation ICPMS method with excellent potential is the sample rastering method described in chapter 8, for producing images of trace element concentrations over the surfaces of solid carbonate samples. Once sample ablation becomes sufficiently automated this method offers promise as a means, using two-dimensional filtering techniques, of delineating banding due to palaeoclimatic forcing of trace elements far more accurately than is possible using one-dimensional axial scans. A raster scan of a section of sample AM1.2 clearly confirms that millimetre-scale trace element variations occur which are independent of growth layering, and thus which are likely to degrade any time series analysed at high spatial resolutions. Even so, growth bands can clearly be seen cutting across these structures (fig 8.6), interpreted as being caused by crystal face zoning effects (Reeder and Grams, 1987). The averaging of 5 cubic millimetres of speleothem for each sample analysed

seems to have minimised the impact of this effect on MD3 samples measured by solution-introduction ICPMS, illustrated by the close agreement of these results with those measured from other variables.

LA-ICPMS measurement of straw speleothems

Because straw speleothems cannot be physically sampled at high enough resolution to give the desired annually resolved records, microprobe analytical methods remain particularly important for this application. A significant advantage of laser ablation ICPMS analysis over all other methods, such as ion microprobe analysis, is that samples do not need to be finished to a planar surface before analysis. This procedure was argued in chapter 8 to invalidate the assumption that sample age increases consistently with distance from the straw tip. Whilst initial results from a Tasmanian straw speleothem show that parallel ablation tracks can give significantly different results for the same straw (J. Desmarchelier, unpublished data), it is still possible to accurately determine annual extension rates from any given ablation track. Independent estimates for the age of the oldest band in a Tasmanian straw (fig. 8.5) are 1779 AD from interpretation of the barium and magnesium data from a single ablation track, and 1777±2 AD from several repeat counts of the surface bands (J. Desmarchelier, pers. comm.) Two-dimensional raster analyses of straw surfaces may allow significance to be attached to year-to-year changes in the concentrations of individual trace elements along straw samples, although this method can realistically only be used to produce tracks of up to 2 mm in width, due to the curvature of straw surfaces. Pending this, it is likely that palaeoclimatic significance can be attached to changes in annual extension rate measured using LA-ICPMS. Preliminary analysis of LA-ICPMS results from a straw sample from Frankcombe Cave, Tasmania indicates that extension during the severe drought year of 1983 was the lowest for any year in the previous century.

Implications of Mt Arthur records for global palaeoclimate

Speleothem results from Mt Arthur (generalised in fig. 9.4) may be used to derive largely independent proxy records of changes in relative temperature, and changes in relative rainfall, for North-West Nelson. That oxygen isotope records from the same speleothems have little in common with the rainfall and temperature records implies that they are modulated by regional atmospheric effects, and thus may not be directly representative of local climate. However, they clearly delineate past periods favourable to glacier advance in Fiordland and the Southern Alps, which presumably were at times of enhanced atmospheric circulation over the Tasman Sea. Whilst changes in North-West Nelson temperature and rainfall, and in the intensity of Tasman Sea atmospheric circulation, are almost certainly interrelated, they are considered independently in the discussion below.

North-West Nelson relative temperature record

Broadly, from the EDI $\delta^{13}C$ record, temperature at Mt Arthur appears to have been somewhat warmer during oxygen isotope stage 5a than at any time between then and the Holocene. Conditions during oxygen isotope stage 3 were intermediate to those during the LGM and the Holocene, in good agreement with pollen records from North Westland (Moar and Suggate, 1996). Stage 3 interstadial conditions terminated at ca. 27,000 cal yr B.P., and LGM conditions ended abruptly at 15,000 cal yr B.P., both in full agreement with the results of Pillans *et al.* (1993) for central and southern North Island. Treeline and snowline lowering constraints indicate that the LGM temperature on the surface above Nettlebed was only 3—4°C colder than today, consistent with the important role the area is thought to have played as a glacial refuge for many plant and animal species. A gradual warming from 19,000 to 15,500 cal yr B.P. is inferred to have immediately preceded a very sudden temperature rise of several degrees, to Holocene optimum levels, inferred to be ca. 1°C warmer than today (McGlone *et al.*, 1993). There is no

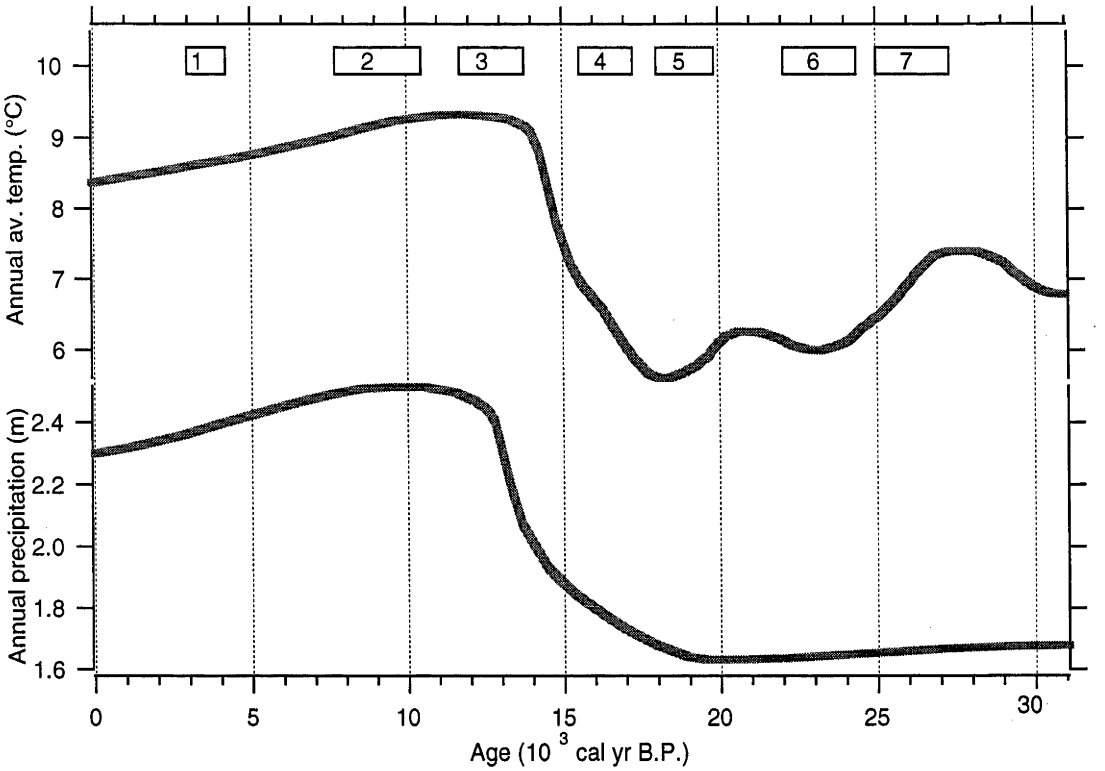

Fig. 9.4. Summary of important palaeoclimatological results from this study, showing the 7 MD3 oxygen isotope excursions thought to indicate periods of enhanced westerly winds, as well as relative precipitation and temperature curves for the last 31,000 cal yr B.P.. The temperature and rainfall data, composed from the various proxy records discussed in the text, are not on absolute scales – the y axis labelling is "best guess" only, and should be interpreted as such, rather than as an attempt to produce quantitative data.

evidence for a Younger Dryas-aged cooling at this time, in agreement with the results of McGlone (1995) and Singer *et al.* (1998).

The warming at 15,000 cal yr B.P. is interpreted as a response to low-latitude warming of the Southern Hemisphere, in excellent agreement with other comparably detailed records covering this period, for mid latitudes in both hemispheres (particularly the records of Bard *et al.*, 1997; Blunier *et al.*, 1998; Chappellaz *et al.*, 1993; Charles *et al.*, 1996; Linsley, 1996; Stuiver *et al.*, 1995). Antarctica and the Southern Ocean do not exhibit a sudden warming at this time, but a considerably more gradual warming, over the period from 19,000 to 12,000 cal yr B.P. (Blunier *et al.*, 1998; Charles *et al.*, 1996). This is in good agreement with the apparent gradual increase in temperature at Mt Arthur over this period (although the increase in vegetation activity from which this is inferred may have instead been a response to the gradually increasing rainfall at this time; see below). This suggests that central New Zealand responded to a gradual high-latitude Southern Hemisphere warming before being affected by a very much stronger event influencing much of the earth.

The absence of a Younger Dryas-aged cooling at Mt Arthur contributes to the ongoing uncertainty as to the global extent of this event (in particular, the question of its effect, if any, in the Southern Hemisphere is a contentious issue; Broecker and Denton, 1989; Clapperton *et al.*, 1997; Denton and Hendy, 1994; Harvey, 1989; Singer *et al.*, 1998). The recent finding by Blunier *et al.* (1998) that the Younger Dryas was related to, and significantly postdated, the Antarctic Cold Reversal was immediately challenged by White and Steig, (1998), who observed that the short-duration Antarctic events may have covaried with those in Greenland, but with an inverse phase relationship. The Mt Arthur speleothem data cannot be used to discriminate between these models, but they do add to the growing body of evidence against the orthodox view of Quaternary climate change, that changes initiate in high northern latitudes and are propagated into the Southern Hemisphere by the "oceanic conveyor." It appears, for maritime regions, that the Northern Hemisphere, the tropics, and the mid-latitude Southern Hemisphere all

experienced sudden warming at 15,000 cal yr B.P., requiring an atmospheric connection for this event (c.f., Charles *et al.*, 1996). In contrast, the Younger Dryas does not appear to have a strong global signature, perhaps indicating an origin proximal to the North Atlantic (e.g., Dansgaard *et al.*, 1989)

North-West Nelson relative precipitation record

Broadly, trace element data, and strontium and uranium isotope ratios from core MD3 imply that rainfall was relatively constant from 31,000 to ca. 17,000 cal yr B.P., at which time it began to gradually increase, until ca. 13,000 cal yr B.P., when it increased rapidly to early Holocene values. Precipitation may have later reduced slightly, over the late Holocene. The changes in rainfall bear little relationship to the record of South Island glacier advance, and while broadly similar to changes in Mt Arthur temperatures, the precipitation record lags by ca. 2000 years. A mechanism by which rainfall can increase without significantly affecting other variables is through increased source region temperature, leading to increased evaporation and transport of water vapour. The precipitation record described above is very similar to the revised Antarctic temperature records of Blunier *et al.* (1998), and to the high-latitude ocean surface temperature record of Charles *et al.* (1996), suggesting that warmer surface conditions in the Southern Ocean might lead to increased South Island rainfall.

A period of increased precipitation may have contributed to the Waiho Loop advance (Denton and Hendy, 1994) of the Franz Josef Glacier, in response to a rapid increase in Southern Ocean temperatures at this time, following the end of the Antarctic Cold Reversal. An increase in precipitation at this time, (supported by a maximum in MD3 magnesium concentration), would have coincided with conditions already favourable to glacier advance, indicated by the MD3/3 isotope excursion at that time. Such circumstances would have lead to a significant glacier surge despite relatively mild temperatures at the time (in agreement with McGlone, 1995). A Uranium isotope datum from core ED1 implies that Mt Arthur precipitation rates were above Holocene values at ca. 79,000 cal yr B.P., the culmination of oxygen isotope stage 5a.

This is in good agreement with the increased effective precipitation inferred for South Australia at that time by Ayliffe *et al.* (1998), and suggests that relatively warm Southern Ocean waters, coupled with enhanced westerly atmospheric circulation, may have been responsible.

South Island glacier advance record

The glacier advance chronology derived from the MD3 $\delta^{18}O$ record is of local advances of mountain glaciers, in response to enhanced regional atmospheric circulation. The earliest four of the MD3 isotope excursions coincided with the global cold period of oxygen isotope stage 2, and thus gave rise to significant glacier advances. Advances associated with the later MD3 isotope excursions were considerably less extensive, due to warmer temperatures working against the effects of increased westerly circulation. If the periods of increased westerly atmospheric circulation inferred from this record can be attributed to regional or hemispheric climatic factors, such as changes in the intensity of the equatorial Walker Circulation, they may have important implications for the understanding of past variability in climatic parameters. These include the El Niño/Southern Oscillation, the past activity of which remains an area of considerable interest. The closest modern analogues to the conditions inferred to have characterised the MD3 isotope excursions are found during El Niño years, which cause increased cloudiness and precipitation in western New Zealand, and cause South Island glaciers to advance (Chinn, 1995; Gordon, 1985).

The MD3/2 isotope excursion appears to be anomalous, as from its magnitude and duration a significant glacier advance is inferred to have occurred at that time, yet there is no evidence of such an advance (Gellatly *et al.*, 1988; Singer *et al.*, 1998). A possible explanation is that the section of core MD3 in question is unsuitable for stable isotope analysis, due to the rapid speed at which it grew. This explanation is not well supported however, as core ED1, for which there is no question of such effects having operated, exhibits similarly elevated $\delta^{18}O$ values at that time. A more convincing explanation is that the excursion instead reflects elevated temperatures in the

water vapour source region at that time. From isotope modelling based on the work of Johnsen *et al.* (1989), it is calculated that for each 1°C increase in source region temperature, the initial water vapour produced there would have been 0.1‰ heavier. Elevated source temperatures are implied by Antarctic stable isotope records (Blunier *et al.*, 1998) and the Mt Arthur precipitation amount record (fig. 9.4).

Concluding Remarks

The results of this study demonstrate that by measuring many variables versus time in a speleothem, and comparing them with each other and with existing palaeoenvironmental records, it is possible to constrain which environmental parameters each variable has changed in response to. Using this approach, it is shown that $\delta^{18}O$ changes in speleothems from Mt Arthur appear to have been in part a response to changes in the intensity of zonal atmospheric circulation in the Tasman Sea, and through this are a proxy for periods of glacier advance in the South Island. Speleothem $\delta^{13}C$ is shown to respond to changes in vegetation productivity above the caves, primarily driven by temperature variation, as are changes in speleothem growth rate, and in concentrations of barium, strontium and organic acids. Changes in strontium and uranium isotopic ratios, and in the concentration of magnesium, are found to primarily reflect changes in groundwater residence time, and thus form a proxy for changes in the amount of rainfall at Mt Arthur.

The resulting climate records show that conditions favourable to glacier advance in the South Island of New Zealand occur during periods of enhanced westerly atmospheric circulation. Such periods result in significant glacier advances when they coincide with reduced global temperatures, or with periods of increased water vapour transport over the Tasman Sea (in response to relatively warm Southern Ocean temperatures). A large and sudden temperature rise at Mt Arthur corresponds to a similar rise observed over much of the northern hemisphere, implying the climate of maritime mid latitudes of the Southern Hemisphere to be more closely associated with that

of Greenland than of Antarctica. Conversely, the absence of any cooling at Mt Arthur associated with the Younger Dryas is consistent with that event having been centred in high northern latitudes, driven by ice sheet dynamics there. Precipitation at Mt Arthur, while not thought to have varied significantly over the last 30,000 years, appears to have been influenced by changes in sea surface temperature in the Southern Ocean, corresponding to changes in Antarctic air temperature.

The findings above have been assisted by comparison of the speleothem data to many existing records of palaeoenvironmental change covering the last few tens of thousands of years, with which they are generally in good agreement. Whilst it is uncertain how many of the relationships between the speleothem variables and palaeoenvironmental changes discussed above are specific to this site or region, these findings can be put to good use in the future by applying them to older speleothems from within the same caves. It is likely that flowstones can be found in Nettlebed Cave spanning much of the last 500,000 years, the age range over which they can be accurately dated by the U-series method. In particular, the precise timings of previous glacial terminations, such as the oxygen isotope stage 6/stage 5e boundary, are of considerable global interest.

Finally, to further advance the understanding the significance of trace element concentration changes in speleothems, an important priority for the future must be a rigorous investigation of the relationships between environmental parameters and cave seepage water trace element concentrations. As well as allowing a greater degree of certainty to be attached to findings such as those above, such studies will show to what extent these relationships are site-specific, and to what extent they can be applied to speleothem records from other regions.

References cited

Allison, V. C. (1923). The growth of stalagmites and stalactites. *Journal of Geology* **31,** 106—125.

Alloway, B. V., Pillans, B. J., Sandhu, A. S., and Westgate, J. A. (1993). Revision of the marine chronology in the Wanganui Basin, New Zealand, based on the isothermal plateau fission-track dating of tephra horizons. *Sedimentary Geology* **82,** 299—310.

Alloway, B. V., Stewart, R. B., Neall, V. E., and Vucetich, C. G. (1992). Climate of the last glaciation in New Zealand, based on aerosolic quartz influx in an andesitic terrain. *Quaternary Research* **38,** 170—179.

Angus, J. G., Raynor, J. B., and Robson, M. (1979). Reliability of experimental partition coefficients in carbonate systems: evidence for inhomogeneous distribution of impurity cations. *Chemical Geology* **27,** 181—205.

Atkinson, T. C., Lawson, T. J., Smart, P. L., Harmon, R. S., and Hess, J. W. (1986). New data on speleothem deposition and palaeoclimate in Britain over the last forty thousand years. *Journal of Quaternary Science* **1,** 67—72.

Atkinson, T. C., Smart, P. L., Harmon, R. S., and Waltham, A. C. (1978). Palaeoclimatic and geomorphic implications of $^{230}Th/^{234}U$ dates on speleothems from Britain. *Nature* **272,** 24—28.

Ayliffe, L. K., Marianelli, P. C., Moriarty, K. C., Wells, R. T., McCulloch, M. T., Mortimer, G. E., and Hellstrom, J. C. (1998). 500 ka precipitation record from southeastern Australia; evidence for interglacial relative aridity. *Geology (Boulder)* **26,** 147—150.

Baker, A., Barnes, W. L., and Smart, P. L. (1996). Speleothem luminescence intensity and spectral characteristics; signal calibration and a record of palaeovegetation change. *Chemical Geology* **130,** 65—76.

Baker, A., Genty, D., Dreybrodt, W., Barnes, W. L., Mockler, N. J., and Grapes, J. (1998). Testing theoretically predicted stalagmite growth rate with recent annually laminated samples; implications for past stalagmite deposition. *Geochimica et Cosmochimica Acta* **62,** 393—404.

Baker, A., Ito, E., Smart, P. L., and McEwan, R. F. (1997). Elevated and variable values of ^{13}C in speleothems in a British cave system. *Chemical Geology* **136,** 263—270.

Baker, A., Smart, P. L., and Edwards, R. L. (1995). Paleoclimatic implications of mass spectrometric dating of a British flowstone. *Geology* **23,** 309—312.

Baker, A., Smart, P. L., Edwards, R. L., and Richards, D. A. (1993a). Annual growth banding in a cave stalagmite. *Nature* **364,** 518—520.

Baker, A., Smart, P. L., and Ford, D. C. (1993b). Northwest European paleoclimate as indicated by growth frequency variations of secondary calcite deposits. *Palaeogeography, Palaeoclimatology, Palaeoecology* **100,** 291—301.

Banner, J. L., and Kaufman, J. (1994). The isotopic record of ocean chemistry and diagenesis preserved in non-luminescent brachiopods from Mississippian carbonate rocks, Illinois and Missouri. *Geological Society of America Bulletin* **106,** 1074—1082.

Banner, J. L., Musgrove, M., Asmerom, Y., Edwards, R. L., and Hoff, J. A. (1996). High-resolution temporal record of Holocene ground-water chemistry: Tracing links between climate and hydrology. *Geology* **24,** 1049—1053.

Banner, J. L., Musgrove, M., and Capo, R. C. (1994). Tracing ground-water evolution in a limestone aquifer using Sr Isotopes: effects of multiple sources of dissolved ions and mineral-solution reactions. *Geology* **22,** 687—690.

Bar-Matthews, M., and Ayalon, A. (1997). Late Quaternary paleoclimate in the eastern Mediterranean region from stable isotope analysis of speleothems at Soreq Cave, Israel. *Quaternary Research* **47,** 155—168.

Bard, E., Arnold, M., Fairbanks, R. G., and Hamelin, B. (1993). ^{230}Th-^{234}U and ^{14}C ages obtained by mass spectrometry on corals. *Radiocarbon* **35,** 191—199.

Bard, E., Arnold, M., Maurice, P., Duprat, J., Moyes, J., and Duplessy, J.-C. (1987). Retreat velocity of the North Atlantic polar front during the last deglaciation determined by ^{14}C accelerator mass spectrometry. *Nature* **328,** 791—794.

Bard, E., Hamelin, B., Fairbanks, R. G., and Zindler, A. (1990). Calibration of the ^{14}C timescale over the past 30,000 years using mass spectrometric U-Th ages from Barbados corals. *Nature* **345,** 405—410.

Bard, E., Rostek, F., and Sonzogni, C. (1997). Interhemispheric synchrony of the last deglaciation inferred from alkenone palaeothermometry. *Nature* **385,** 707—710.

Bartlein, P. J., Edwards, M. E., Shafer, S. L., and Barker, E. D. (1995). Calibration of radiocarbon ages and the interpretation of paleoenvironmental records. *Quaternary Research* **44,** 417—424.

Belkin, I. M., and Gordon, A. L. (1996). Southern Ocean fronts from the Greenwich meridian to Tasmania. *Journal of Geophysical Research* **101,** 3675—3696.

Benedetti, M. F., Riemsdijk, W. H. V., Koopal, L. K., Kinniburgh, D. G., Gooddy, D. C., and Milne, C. J. (1996). Metal ion binding by natural organic matter: From the model to the field. *Geochimica a et Cosmochimica Acta* **60,** 2503—2513.

Berger, G. W., Pillans, B. J., and Palmer, A. S. (1992). Dating loess up to 800 ka by thermoluminescence. *Geology* **20,** 403—406.

Beu, A. G., and Edwards, A. R. (1984). New Zealand Pleistocene and late Pliocene glacio-eustatic cycles. *Palaeogeography, Palaeoclimatology, Palaeoecology* **46,** 119—142.

Bird, M. I., Chivas, A. R., and Head, J. (1996). A latitudinal gradient in carbon turnover times in forest soils. *Nature* **381,** 143—146.

Bischoff, J. L., and Fitzpatrick, J. A. (1991). U-series dating of impure carbonates: An isochron technique using total-sample dissolution. *Geochimica et Cosmochimica Acta* **55,** 543—554.

Black, K. P., Nelson, C. S., and Hendy, C. H. (1988). A spectral analysis procedure for dating Quaternary deep-sea cores and its application to a high-resolution Brunhes record from the southwest Pacific. *Marine Geology* **83,** 21—30.

Blanchon, P., and Shaw, J. (1995). Reef drowning during the last deglaciation: Evidence for catastrophic sea-level rise and ice-sheet collapse. *Geology* **23,** 4—8.

Blunier, T., Chappellaz, J., Schwander, J., Dällenbach, A., Stauffer, B., Stocker, T. F., Raynaud, D., Jouzel, J., Clausen, H. B., Hammer, C. U., and Johnsen, S. J. (1998). Asynchrony of Antarctic and Greenland climate change during the last glacial period. *Nature* **394,** 739—743.

Bond, G., Broecker, W., Johnsen, S., McManus, J., Labeyrie, L., Jouzel, J., and Bonani, G. (1993). Correlations between climate records from North Atlantic sediments and Greenland Ice. *Nature* **365,** 143—147.

Bowen, R. (1988). "Isotopes in the Earth Sciences." Elsevier Applied Science, London.

Broecker, W. S. (1986). Oxygen Isotope constraints on surface ocean temperatures. *Quaternary Research* **26,** 121—134.

Broecker, W. S. (1994). Massive iceberg discharges as triggers for global climate change. *Nature* **372,** 421—424.

Broecker, W. S., and Denton, G. H. (1989). The role of ocean-atmosphere reorganisations in glacial cycles. *Geochimica et Cosmochimica Acta* **53,** 2465—2501.

Broecker, W. S., Olson, E. A., and C, O. P. (1960). ^{14}C measurements and annual rings in cave formations. *Nature* **185,** 93—94.

Broecker, W. S., Peteet, D. M., and Rind, D. (1985). Does the ocean-atmosphere system have more than one stable mode of operation? *Nature* **315,** 21—26.

Brook, G. A., Burney, D. A., and Cowart, J. B. (1990). Desert paleoenvironmental data from cave speleothems with examples from the Chihuahuan, Somali-Chalbi, and Kalahari deserts. *Palaeogeography, Palaeoclimatology, Palaeoecology* **76,** 311—329.

Buchardt, B., and Fritz, P. (1980). Environmental isotopes as environmental and climatological Indicators. *In* "Handbook of Environmental Geochemistry." (P. Fritz, and J. C. Fontes, Eds.), pp. 473—504. Elsevier, Amsterdam.

Burns, S. J., and Matter, A. (1995). Geochemistry of carbonate cements in surficial alluvial conglomerates and their paleoclimatic implications, Sultanate of Oman. *Journal of Sedimentary Research* **A65,** 170—177.

Burrows, C. J. (1979). A Chronology for cool-climate episodes in the Southern Hemisphere 12,000-1000 Yr B.P. *Palaeogeography, Palaeoclimatology, Palaeoecology* **27,** 287—347.

Burton, E. A., and Walter, L. M. (1991). The effects of pCO_2 and temperature on magnesium incorporation in calcite in seawater and $MgCl_2$—$CaCl_2$ solutions. *Geochimica et Cosmochimica Acta* **55,** 777—785.

Cerling, T. E., Quade, J., Wang, Y., and Bowman, J. R. (1989). Carbon Isotopes in soils and paleosols as ecology and palaeoecology indicators. *Nature* **341,** 138—139.

Chappell, J. (1983). A revised sea-level record for the last 300,000 years from Papua New Guinea. *Search* **14,** 99-101.

Chappell, J., Omura, A., Esat, T., McCulloch, M., Pandolfi, J., Ota, Y., and Pillans, B. (1996). Reconciliation of late Quaternary sea levels derived from coral terraces at Huon Peninsula with deep sea oxygen isotope records. *Earth and Planetary Science Letters* **141,** 227—236.

Chappell, J., and Polach, H. (1991). Post-glacial sea-level rise from a coral record at Huon Peninsula, Papua New Guinea. *Nature* **349,** 147—149.

Chappell, J., and Shackleton, N. J. (1986). Oxygen isotopes and sea level. *Nature* **324,** 137—140.

Chappellaz, J., Blunier, T., Raynaud, D., Barnola, J. M., Schwander, J., and Stauffer, B. (1993). Synchronous changes in atmospheric CH^4 and Greenland climate between 40 and 8 kyr BP. *Nature* **366,** 443—445.

Charles, C. D., Lynch-Stieglitz, J., Ninnemann, U. S., and Fairbanks, R. G. (1996). Climate connections between the hemisphere revealed by deep sea sediment core/ice core correlations. *Earth and Planetary Science Letters* **142,** 19—27.

Chen, J. H., Edwards, R. L., and Wasserburg, G. J. (1986). ^{238}U, ^{234}U and ^{232}Th in seawater. *Earth and Planetary Science Letters* **80,** 241—251.

Cherdyntsev, V. V. (1971). "Uranium-234." Israel Program for Scientific Translations, Jerusalem.

Cherdyntsev, V. V., Kazachevskii, I. V., and Kuzmina, Y. A. (1965). Age of Pleistocene carbonate determined from the isotopes of thorium and uranium. *Geochemistry international* **2,** 749—756.

Chinn, T. J. H. (1981). Use of rock weathering-rind thickness for Holocene absolute-age dating in New Zealand. *Arctic and Alpine Research* **13,** 33—45.

Chinn, T. J. H. (1995). Glacier fluctuations in the Southern Alps of New Zealand determined from snowline elevations. *Arctic and Alpine Research* **27,** 187-198.

Clapperton, C. M., Hall, M., Mothes, P., Hole, M. J., Still, J. W., Helmens, K. F., Kuhry, P., and Gemmell, A. M. D. (1997). A Younger Dryas icecap in the equatorial Andes. *Quaternary Research* **47,** 13—28.

Cody, A. D. (1981). Nettlebed Cave (Pearse Valley, Nelson) - a New Zealand record. *Geological Society of New Zealand Newsletter* **52,** 18—20.

Craig, H. (1957). Isotopic standards for carbon and oxygen and correction factors for mass-spectrometric analysis of carbon dioxide. *Geochimica et Cosmochimica Acta* **12,** 113—149.

Craig, H. (1961a). Isotopic variations in meteoric waters. *Science* **133,** 1702—1703.

Craig, H. (1961b). Standard for reporting concentrations of deuterium and oxygen-18 in natural water. *Science* **133,** 1833—1834.

Dansgaard, W. (1964). Stable isotopes in precipitation. *Tellus* **XVI,** 436—468.

Dansgaard, W., Johnsen, S. J., Clausen, H. B., Dahl-Jensen, D., Gundestrup, N. S., Hammer, C. U., Hvidberg, C. S., Steffensen, J. P., Sveinbjörnsdottir, A. E., Jouzel, J., and Bond, G. (1993). Evidence for general instability of past climate from a 350-kyr ice-core record. *Nature* **364,** 218—220.

Dansgaard, W., White, J. W. C., and Johnsen, S. J. (1989). The abrupt termination of the Younger Dryas climate event. *Nature* **339,** 532—534.

Deines, P. (1980). The isotopic composition of reduced organic carbon. *In* "Handbook of Environmental Geochemistry." (P. Fritz, and J. C. Fontes, Eds.), pp. 329—406. Elsevier, Amsterdam.

Dennis, P. F., Rowe, P. J., and Atkinson, T. C. (1996). Isotopic composition of palaeoprecipitation and palaeogroundwaters from speleothem fluid inclusions. *In* "Climate Change: The Karst Record." (S.-E. Lauritzen, Ed.), pp. 20—22. Karst Waters Institute, Bergen.

Denniston, R. F., and Gonzalez, L. A. (1997). Microsampling and isotopic analysis of adjacent fluorescent/ non-fluorescent band couplets in a Midwestern speleothem. *In* "Geological Society of America, North-Central Section, 31st annual meeting." (Anonymous, Ed.), pp. 12. Abstracts with Programs - Geological Society of America. Geological Society of America (GSA), Boulder, CO, United States.

Denton, D. H., and Hendy, C. H. (1994). Younger Dryas age advance of the Franz Josef Glacier in the Southern Alps of New Zealand. *Science* **264,** 1434—1437.

Dodson, J. R., Enright, N. J., and McLean, R. F. (1988). A late Quaternary vegetation history of far northern New Zealand. *Journal of Biogeography* **15,** 647—656.

Dorale, J. A., González, L. A., Reagan, M. K., Pickett, D. A., Murrell, M. T., and Baker, R. G. (1992). A high-resolution record of Holocene climate change in speleothem calcite from Cold Water Cave, Northeast Iowa. *Science* **258,** 1626—1630.

Dörr, H., and Münnich, K. O. (1986). Annual variations of the ^{14}C content of soil. *Radiocarbon* **28,** 338—345.

Dörr, H., and Münnich, K. O. (1989). Downward movement of soil organic matter and its influence on trace element transport (^{210}Pb, ^{137}Cs) in the soil. *Radiocarbon* **31,** 655—663.

Drever, J. I., and Vance, G. F. (1994). Role of soil organic acids in mineral weathering processes. *In* "Organic Acids in Geological Processes." (E. D. Pittman, and M. D. Lewan, Eds.), pp. 138—161. Sringer-Verlag, Berlin.

Dreybrodt, W. (1981). The kinetics of calcite precipitation from thin films of calcareous solutions and the growth of speleothems: revisited. *Chemical Geology* **32,** 237—245.

Dreybrodt, W. (1982). A possible mechanism for growth of calcite speleothems without participation of biogenic carbon dioxide. *Earth and Planetary Science Letters* **58,** 293—299.

Dreybrodt, W., Lauckner, J., Zaihua, L., Svensson, U., and Buhmann, D. (1996). The kinetics of the reaction $CO_2 + H_2O \rightarrow H^+ + HCO_3^-$ as one of the rate limiting steps for the dissolution of calcite in the system H_2O-CO_2-$CaCO_3$. *Geochimica et Cosmochimica Acta* **60,** 3375—3381.

Dulinski, M., and Rozanski, K. (1990). Formation of $^{13}C/^{12}C$ isotope ratios in speleothems: a semi-dynamic model. *Radiocarbon* **32,** 7—16.

Duplessy, J. C., Labeyrie, J., Lalou, C., and Nguyen, H. V. (1970). Continental climatic variations between 130,000 and 90,000 years BP. *Nature* **226,** 631—633.

Edwards, R. L., Beck, J. W., Burr, G. S., Donahue, D. J., Chappell, J. M. A., Bloom, A. L., Druffel, W. R. M., and Taylor, F. W. (1993). A large drop in Atmospheric $^{14}C/^{12}C$ and reduced melting in the Younger Dryas, documented with ^{230}Th ages of corals. *Science* **260,** 962—968.

Edwards, R. L., Chen, J. H., and Wasserburg, G. J. (1987). ^{238}U-^{234}U-^{230}Th-^{232}Th systematics and the precise measurement of time over the past 500,000 years. *Earth and Planetary Science Letters* **81,** 175—192.

Eggins, S. M., Kinsley, L. P. J., and Shelly, J. M. (1997a). Deposition and fractionation processes during atmospheric pressure laser sampling for analysis by ICP-MS. *Applied Surface Science* **127—129,** 278—286.

Eggins, S. M., Woodhead, J. D., Kinsley, L. P. J., Mortimer, G. E., Sylvester, P., McCulloch, M. T., Hergt, J. M., and Handler, M. R. (1997b). A simple method for the precise determination of ≥40 trace elements in geological samples by ICPMS using enriched isotope internal standardisation. *Chemical Geology* **134,** 311—326.

Falguères, C., Lumley, H., and Bischoff, J. L. (1992). U-series dates for Stalagmitic Flowstone E (Riss/Würm Interglaciation) at Grotte du Lazaret, Nice, France. *Quaternary Research* **38,** 227—233.

Fantidis, J., and Ehhalt, D. H. (1970). Variations of the carbon and oxygen isotopic composition in stalagmites and stalactites: evidence of non-equilibrium isotopic fractionation. *Earth and Planetary Science Letters* **10,** 136—144.

Fenner, J., Carter, L., and Stewart, R. (1992). Late Quaternary paleoclimatic and paleoceanographic change over northern Chatham Rise, New Zealand. *Marine Geology* **108,** 383—404.

Ferronsky, V. I., and Brezgunov, V. S. (1989). Stable isotopes and ocean dynamics. *In* "Handbook of Environmental Geochemistry." (P. Fritz, and J. C. Fontes, Eds.), pp. 1—27. Elsevier, Amsterdam.

Fitzharris, B. B., Hay, J. E., and Jones, P. D. (1992). Behaviour of New Zealand glaciers and atmospheric circulation changes over the past 130 years. *The Holocene* **2,** 97—106.

Fontes, J. C. (1980). Environmental isotopes in groundwater hydrology. *In* "Handbook of Environmental Geochemistry." (P. Fritz, and J. C. Fontes, Eds.), pp. 75—140. Elsevier, Amsterdam.

Ford, D. C., Lundberg, J., Palmer, A. N., Palmer, M. V., Dreybrodt, W., and Schwarcz, H. P. (1993). Uranium-series dating of the draining of an aquifer: the example of Wind Cave, Black Hills, South Dakota. *Geological Society of America Bulletin* **105,** 421—250.

Froggatt, P. C. (1983). Toward a comprehensive Upper Quaternary tephra and ignimbrite stratigraphy in New Zealand using electron microprobe analysis of glass shards. *Quaternary Research* **19,** 188—200.

Froggatt, P. C., and Lowe, D. J. (1990). A review of late Quaternary silicic and some other tephra formations from New Zealand: their stratigraphy, nomenclature, distribution, volume and age. *New Zealand Journal of Geology and Geophysics* **33,** 89—109.

Gage, M. (1965). Some characteristics of Pleistocene cold climates in New Zealand. *Transactions of the Royal Society of New Zealand: Geology* **3,** 11—21.

Gage, M. (1985). Glaciation in New Zealand - the first century of research. *Quaternary Science Reviews* **4,** 189—214.

Gage, M., and Suggate, R. P. (1958). Glacial chronology of the New Zealand Pleistocene. *Bulletin of the Geological Society of America* **69,** 589—598.

Garnier, B. J. (1958). "The Climate of New Zealand." Edward Arnold Ltd, London.

Gascoyne, M. (1982). Geochemistry of the actinides and their daughters. *In* "Uranium Series Disequilibrium: Applications to environmental problems." (M. Ivanovich, and R. S. Harmon, Eds.), pp. 33—55. Clarendon Press, Oxford.

Gascoyne, M. (1983). Trace-element partition coefficients in the calcite-water system and their paleoclimatic significance in cave studies. *Journal of Hydrology* **61,** 213—222.

Gascoyne, M. (1984). Twenty years of uranium-series dating of cave calcites: a review of results, problems and new directions. *Studies in Speleology* **5,** 15—30.

Gascoyne, M. (1992). Palaeoclimate determination from cave calcite deposits. *Quaternary Science Reviews* **11,** 609—632.

Gascoyne, M., Benjamin, G. J., Schwarcz, H. P., and Ford, D. C. (1979). Sea-level lowering during the Illinoian Glaciation: evidence from a Bahama "Blue Hole". *Science* **205,** 806—809.

Gascoyne, M., Ford, D. C., and Schwarcz, H. P. (1981). Late Pleistocene chronology and paleoclimate of Vancouver Island determined from cave deposits. *Canadian Journal of Earth Sciences* **18,** 1643—1652.

Gascoyne, M., Schwarcz, H. P., and Ford, D. C. (1980). A palaeotemperature record for the mid-Wisconsin in Vancouver Island. *Nature* **285,** 474—476.

Gat, J. R. (1980). The isotopes of hydrogen and oxygen in precipitation. *In* "Handbook of Environmental Geochemistry." (P. Fritz, and J. C. Fontes, Eds.), pp. 21—47. Elsevier, Amsterdam.

Gellatly, A. F., Chinn, T. J., and Röthlisberger, F. (1988). Holocene glacier variations in New Zealand: a review. *Quaternary Science Reviews* **7,** 227—242.

Gellatly, A. F., and Norton, D. A. (1984). Possible warming and glacier recession in the South Island, New Zealand. *New Zealand Journal of Science* **27,** 381—388.

Genty, D., Baker, A., Barnes, W., and Massault, M. (1996). Growth rate, grey level and luminescence of stalagmite laminae. *In* "Climate Change: The Karst Record." (S.-E. Lauritzen, Ed.), pp. 36—39. Karst Waters Institute, Bergen.

Geyh, M. A., and Henning, G. J. (1986). Multiple dating of a long flowstone profile. *Radiocarbon* **28,** 503—509.

Goede, A. (1994). Continuous early Last Glacial paleoenvironmental record from a Tasmanian speleothem based on stable isotope and minor element variations. *Quaternary Science Reviews* **13,** 283—291.

Goede, A., Green, D. C., and Harmon, R. S. (1982). Isotopic composition of precipitation, cave drips and actively forming speleothems at three Tasmanian cave sites. *Helictite* **20,** 17—27.

Goede, A., Green, D. C., and Harmon, R. S. (1986). Late Pleistocene palaeotemperature record from a Tasmanian speleothem. *Australian Journal of Earth Sciences* **33,** 333—342.

Goede, A., Veeh, H. H., and Ayliffe, L. K. (1990). Late Quaternary palaeotemperature records for two Tasmanian speleothems. *Australian Journal of Earth Sciences* **37,** 267—278.

Goede, A., and Vogel, J. C. (1991). Trace element variations and dating of a late Pleistocene Tasmanian speleothem. *Palaeogeography, Palaeoclimatology, Palaeoecology* **88,** 121—131.

González, L. A., Carpenter, S. J., and Lohmann, K. C. (1992). Inorganic calcite morphology: roles of fluid chemistry and fluid flow. *Journal of Sedimentary Petrology* **62,** 382—399.

Gordon, N. D. (1985). The Southern Oscillation: a New Zealand perspective. *Journal of the Royal Society of New Zealand* **15,** 137—155.

Greenland Ice-core Project Members. (1993). Climate instability during the last interglacial period recorded in the GRIP ice core. *Nature* **364,** 203—207.

Grindley, G. W. (1961). Sheet 13-Golden Bay. Geological Map of New Zealand 1:250,000. Department of Scientific and Industrial Research, Wellington.

Guilderson, T. P., Fairbanks, R. G., and Rubenstone, J. L. (1994). Tropical temperature variations since 20,000 years ago: Modulating interhemispheric climate change. *Science* **263,** 663—665.

Hansen, B. C. S. (1995). A review of lateglacial pollen records from Ecuador and Peru with reference to the Younger Dryas event. *Quaternary Science Reviews* **14,** 853—865.

Harmon, R. S., Ford, D. C., and Schwarcz, H. P. (1977). Interglacial chronology of the Rocky and Mackenzie Mountains based upon ^{230}Th-^{234}U dating of calcite speleothems. *Canadian Journal of Earth Sciences* **14,** 2543—2552.

Harmon, R. S., Land, L. S., Mitterer, R. M., Garrett, P., Schwarcz, H. P., and Larson, G. J. (1981). Bermuda sea level during last interglacial. *Nature* **289,** 481—483.

Harmon, R. S., and Schwarcz, H. P. (1981). Changes of ^{2}H and ^{18}O enrichment of meteoric water and Pleistocene glaciation. *Nature* **290,** 125—128.

Harmon, R. S., Schwarcz, H. P., and Ford, D. C. (1978a). Stable isotope geochemistry of speleothems and cave waters from the Flint Ridge-Mammoth Cave system, Kentucky: implications for terrestrial climate change during the period 230,000 to 100,000 years B.P. *Journal of Geology* **86,** 373—384.

Harmon, R. S., Schwarcz, H. P., and O'Neil, J. R. (1979). D/H ratios in fluid inclusions: a guide to variations in the isotopic composition of meteoric precipitation? *Earth and Planetary Science Letters* **42,** 254—266.

Harmon, R. S., Thompson, P., Schwarcz, H. P., and Ford, D. C. (1978b). Late Pleistocene paleoclimates of North America as inferred from stable isotope studies of speleothems. *Quaternary Research* **9,** 54—70.

Harvey, L. D. D. (1989). Modelling the Younger Dryas. *Quaternary Science Reviews* **8,** 137—149.

Hays, J. D., Imbrie, J., and Shackleton, N. J. (1976). Variations in the Earth's orbit: pacemaker of the ice ages. *Science* **194,** 1121—1132.

Head, P. S., and Nelson, C. S. (1994). A high-resolution oxygen isotope record for the past 6.4 million years at DSDP Site 593, Challenger Plateau, southern Tasman Sea. *In* "Evolution of the Tasman Sea." (G. J. v. d. Linden, K. M. Swanson, and R. J. Muir, Eds.), pp. 159—179. A A Balkema, Rotterdam.

Heath, R. A. (1985). A review of the physical oceanography of the seas around New Zealand - 1982. *New Zealand Journal of Marine and Freshwater Research* **19,** 79—124.

Heinrich, H. (1988). Origin and consequences of cyclic ice rafting in the northeast Atlantic Ocean during the past 130,000 years. *Quaternary Research* **29,** 142—152.

Henderson, L. M., and Kracek, F. C. (1927). The fractional precipitation of barium and radium chromates. *Journal of the American Chemical Society* **49,** 739—749.

Hendy, C. H. (1970). The use of C^{14} in the study of cave processes. *In* "Radiocarbon Variations and Absolute Chronology." (I. U. Olsson, Ed.), pp. 419—423. Almqvist & Wiksell, Stockholm.

Hendy, C. H. (1971). The isotope geochemistry of speleothems-I. The calculation of the effects of different modes of formation on the isotopic composition of speleothems and their applicability as palaeoclimatic indicators. *Geochimica et Cosmochimica Acta* **35,** 801—824.

Hendy, C. H., and Hendy, I. L. (1997). The role of Antarctica in Pleistocene glacial history - Wilson's Ice Age theory revisited. *In* "Sixth Australian-New Zealand Environmental Isotope Conference.". Institute of Geological and Nuclear Sciences, Lower Hutt, New Zealand.

Hendy, C. H., and Wilson, A. T. (1968). Palaeoclimatic data from speleothems. *Nature* **219,** 48—51.

Henning, G. J., Grün, R., and Brunnacker, K. (1983). Speleothems, travertines, and paleoclimates. *Quaternary Research* **20,** 1—29.

Hercman, H., and Walanus, A. (1996). Randomisation as a method of frequency histogram construction. *In* "Climate Change: The Karst Record." (S.-E. Lauritzen, Ed.), pp. 56—58. Karst Waters Institute, Charles Town.

Hessell, J. W. D. (1983). Climatic effects on the recession of the Franz Josef Glacier. *New Zealand Journal of Science* **26,** 315—320.

Heusser, C. J., and Rabassa, J. (1987). Cold climatic episode of Younger Dryas age in Tierra del Fuego. *Nature* **328,** 609—611.

Heusser, L. E., and Van De Geer, G. (1994). Direct correlation of terrestrial and marine paleoclimatic records from four glacial-interglacial cycles - DSDP Site 594 Southwest Pacific. *Quaternary Science Reviews* **13,** 273—282.

Hill, C., and Forti, P. (1997). "Cave minerals of the world." National Speleological Society, Huntsville, AL, United States.

Holdaway, R. N. (1996). Arrival of rats in New Zealand. *Nature* **384,** 225—226.

Hughen, K. A., Overpeck, J. T., Lehman, S. J., Kashgarian, M., Southon, J., Peterson, L. C., Alley, R., and Sigman, D. M. (1998). Deglacial changes in ocean circulation from an extended radiocarbon calibration. *Nature* **391,** 65—68.

Imbrie, J., Berger, A., Boyle, E. A., Clemens, S. C., Duffy, A., Howard, W. R., Kukla, G., Kutzbach, J., Martinson, D. G., McIntyre, A., Mix, A. C., Molfino, B., Morley, J. J., Peterson, L. C., Pisias, N. G., Prell, W. L., Raymo, M. E., Shackleton, N. J., and Toggweiler, J. R. (1993a). On the structure and origin of major glaciation cycles 2. The 100,000-year cycle. *Paleoceanography* **8,** 699—735.

Imbrie, J., Boyle, E. A., Clemens, S. C., Duffy, A., Howard, W. R., Kukla, G., Kutzbach, J., Martinson, D. G., McIntyre, A., Mix, A. C., Molfino, B., Morley, J. J., Peterson, L. C., Pisias, N. G., Prell, W. L., Raymo, M. E., Shackleton, N. J., and Toggweiler, J. R. (1992). On the structure and origin of major glaciation cycles 1. Linear responses to Milankovitch forcing. *Paleoceanography* **7,** 701—738.

Imbrie, J., Hays, J. D., Martinson, D. G., McIntyre, A., Mix, A. C., Morley, J. J., Pisias, N. G., Prell, W. L., and Shackleton, N. J. (1984). The orbital theory of Pleistocene climate: Support from a revised chronology of the marine $\delta^{18}O$ record. *In* "Milankovitch and Climate." (A. L. Berger, Ed.), pp. 269—305. D. Reidel Publishing Company.

Imbrie, J., Mix, A. C., and Martinson, D. G. (1993b). Milankovitch theory viewed from Devils Hole. *Nature* **363,** 531—533.

Ivanovich, M. (1982). Uranium series disequilibria applications in geochronology. *In* "Uranium Series Disequilibrium: Applications to environmental problems." (M. Ivanovich, and R. S. Harmon, Eds.), pp. 56—78. Clarendon Press, Oxford.

Johnsen, S. J., Clausen, H. B., Dansgaard, W., Fuhrer, K., Gundestrup, N., Hammer, C. U., Iversen, P., Jouzel, J., Stauffer, B., and Steffensen, J. P. (1992). Irregular glacial interstadials recorded in a new Greenland ice core. *Nature* **359,** 311—313.

Johnsen, S. J., Dansgaard, W., and White, J. W. C. (1989). The origin of Arctic precipitation under present and glacial conditions. *Tellus* **41B,** 452—468.

Johnston, M. R. (1973). Geology of the Mount Arthur district, North-West Nelson. *New Zealand Journal of Geology and Geophysics* **17,** 75—92.

Jones, M. C., Gonzalez, L. A., Hanson, L., Allabastro, A. J., Reagan, M. K., Thorson, W. P., Jaumann, P. J., and Baker, R. G. (1995). A 6000 year stalagmite growth banding record for Cold Water Cave, northeastern Iowa; annual and seasonal precipitation changes. *In* "Geological Society of America, 1995 annual meeting." (Anonymous, Ed.), pp. 55. Abstracts with Programs - Geological Society of America. Geological Society of America (GSA), Boulder, CO, United States.

Jouzel, J. (1998). Water isotopes in precipitation: Data/model comparison for present-day and past climates. *In* "Past Global Climates and their Significance for the Future." (B. Marcolli, Ed.), pp. 24. IGBP PAGES, London.

Jouzel, J., Barkov, N. I., Barnola, J. M., Bender, M., Chappellaz, J., Genthon, G., Kotlyakov, V. M., Lipenkov, V., Lorius, C., Petit, J. R., Raynaud, D., Raisbeck, G., Ritz, C., Sowers, T., Stievenard, M., Yiow, F., and Yiow, P. (1993). Extending the Vostok ice-core record of palaeoclimate to the penultimate glacial period. *Nature* **364,** 407—412.

Jouzel, J., Lorius, C., Petit, J. R., Genthon, C., Barkov, N. I., Kotlyakov, V. M., and Petrov, V. M. (1987). Vostok ice core: a continuous isotope temperature over the last climatic cycle (160,000 years). *Nature* **329,** 403—408.

Jouzel, J., Petit, J. R., Barkov, N. I., Barnola, J. M., Chappellaz, J., Ciais, P., Kotkyakov, V. M., Lorius, C., Petrov, V. N., Raynaud, D., and Ritz, C. (1992). The last deglaciation in Antarctica: further evidence of a "Younger Dryas" type climatic event. *In* "The last deglaciation: absolute and radiocarbon chronologies." (E. Bard, and W. S. Broecker, Eds.), pp. 231—266. Springer-Verlag, Berlin.

Jouzel, J., Waelbroeck, C., Malaize, B., Bender, M., Petit, J. R., Stievenard, M., Barkov, N. I., Barnola, J. M., King, T., Kotlyakov, V. M., Lipenkov, V., Lorius, C., Raynaud, D., Ritz, C., and Sowers, T. (1996). Climatic interpretation of the recently extended Vostok ice records. *Climate Dynamics* **12,** 513—521.

Juillet-Leclerc, A., Jouzel, J., Labeyrie, L., and Joussaume, S. (1997). Modern and last glacial maximum sea surface $\delta^{18}O$ derived from an Atmospheric General Circulation Model. *Earth and Planetary Science Letters* **146,** 591—605.

Kaufman, A., and Broecker, W. S. (1965). Comparison of ^{230}Th ages and ^{14}C ages for carbonate materials from lakes Lahontan and Bonneville. *Journal of Geophysical Research* **70,** 4039.

Keigwin, L. D., Curry, W. B., Lehman, S. J., and Johnsen, S. (1994). The role of the deep ocean in North Atlantic climate change between 70 and 130 kyr ago. *Nature* **371,** 323—326.

Keigwin, L. D., and Jones, G. A. (1994). Western North Atlantic evidence for millennial-scale changes in ocean circulation and climate. *Journal of Geophysical Research* **99,** 12,397—12410.

Koç, N., and Jansen, E. (1994). Response of the high-latitude Northern Hemisphere to orbital climate forcing: Evidence from the Nordic Seas. *Geology* **22,** 523—526.

Kukla, G. (1987). Loess stratigraphy in central China. *Quaternary Science Reviews* **6,** 191—219.

Latham, A. G., Schwarcz, H. P., Ford, D. C., and Pearce, G. W. (1979). Palaeomagnetism of stalagmite deposits. *Nature* **280,** 383—385.

Lauritzen, S.-E. (1995). High-resolution Paleotemperature proxy record for the last interglaciation based on Norwegian speleothems. *Quaternary Research* **43,** 133—146.

Lauritzen, S.-E., Haugen, J. E., Løvlie, R., and Gilje-Nielsen, H. (1994). Geochronological potential of isoleucine epimerization in calcite speleothems. *Quaternary Research* **41,** 52—58.

Lauritzen, S.-E., Løvlie, R., Moe, D., and Østbye, E. (1990). Paleoclimate deduced from a multidisciplinary study of a half-million-year-old stalagmite from Rana, Northern Norway. *Quaternary Research* **34,** 306—316.

Lauritzen, S.-E., and Lundberg, J. (1998). Rapid temperature variations and volcanic events during the Holocene from a Norwegian speleothem record. *In* "Past Global Climates and their Significance for the Future." (B. Marcolli, Ed.), pp. 88. IGBP PAGES, London.

Lebron, I., and Suarez, D. L. (1996). Calcite nucleation and precipitation kinetics as affected by dissolved organic matter at 25°C and pH > 7.5. *Geochimica et Cosmochimica Acta* **60,** 2765—2776.

Lebron, I., and Suárez, D. L. (1998). Kinetics and mechanisms of precipitation of calcite as affected by pCO2 and organic ligands at 25°C. *Geochimica et Cosmochimica Acta* **62,** 405—416.

Lewis, K., and Carter, L. (1994). When and how did Cook Strait form? *In* "Evolution of the Tasman Sea." (G. J. v. d. Linden, K. M. Swanson, and R. J. Muir, Eds.), pp. 119—137. A A Balkema, Rotterdam.

Li, W. X., Lundberg, J., Dickin, A. P., Ford, D. C., Schwarcz, H. P., McNutt, R., and Williams, D. (1989). High-precision mass-spectrometric uranium-series dating of cave deposits and implications for palaeoclimate studies. *Nature* **339,** 534—536.

Lindstrom, D. R., and MacAyeal, D. R. (1993). Death of an ice sheet. *Nature* **365,** 214—215.

Linsley, B. K. (1996). Oxygen-isotope record of sea level and climate variations in the Sulu Sea over the past 150,000 years. *Nature* **380,** 234—237.

Lorens, R. B. (1981). Sr, Cd, Mn and Co distribution coefficients in calcite as a function of calcite precipitation rate. *Geochimica et Cosmochimica Acta* **45,** 553—561.

Lorius, C., Jouzel, J., Ritz, C., Merlivat, L., Barkov, N. I., Korotkevich, Y. S., and Kotlyakov, V. M. (1985). A 150,000-year climate record from Antarctic ice. *Nature* **316,** 591—596.

Ludwig, K. R., Simmons, K. R., Szabo, B. J., Winograd, I. J., Landwehr, J. M., Riggs, A. C., and Hoffman, R. J. (1992). Mass-spectrometric ^{230}Th-^{234}U-^{238}U dating of the Devils Hole calcite vein. *Science* **258,** 284—287.

Luo, S., and Ku, T.-L. (1991). U-series isochron dating: A generalized method employing total-sample dissolution. *Geochimica et Cosmochimica Acta* **55,** 555—564.

Lyons, R. G. (1996). The elusive Blake: a record of paleomagnetically reversed deposits in New Zealand post 120ka. *Quaternary Science Reviews* **15,** 719—726.

Martinson, D. G., Pisias, N. G., Hays, J. D., Imbrie, J., Moore, T. C., and Shackleton, N. J. (1987). Age dating and the orbital theory of the ice ages: Development of a high-resolution 0 to 300,000-year chronostratigraphy. *Quaternary Research* **27,** 1—29.

McCulloch, M., Mortimer, G., Esat, T., Xianhua, L., Pillans, B., and Chappell, J. (1996). High resolution windows into early Holocene climate: Sr/Ca coral records from the Huon Peninsular. *Earth and Planetary Science Letters* **138,** 169—178.

McGlone, M. S. (1988). New Zealand. *In* "Vegetation History." (B. Huntly, and T. Web III, Eds.), pp. 557—599. Kluwer Academic Publishers, Dordrecht.

McGlone, M. S. (1995). Lateglacial landscape and vegetation change and the Younger Dryas climatic oscillation in New Zealand. *Quaternary Science Reviews* **14,** 867—881.

McGlone, M. S., Anderson, A. J., and Holdaway, R. N. (1994). An ecological approach to the Polynesian settlement of New Zealand. *In* "The Origins of the First New Zealanders." (D. G. Sutton, Ed.), pp. 136—163. Auckland University Press, Auckland.

McGlone, M. S., Salinger, M. J., and Moar, N. T. (1993). Paleovegetation studies of New Zealand's climate since the last glacial maximum. *In* "Global climates since the last glacial maximum." (H. E. Wright, J. E. Kutzbach, T. Webb III, W. F. Ruddiman, F. A. Street-Perrott, and P. J. Bartlein, Eds.), pp. 294—317. University of Minnesota Press, Minneapolis.

McIntosh, P. D., Eden, D. N., and Burgham, S. J. (1990). Quaternary deposits and landscape evolution in northeast Southland, New Zealand. *Palaeogeography, Palaeoclimatology, Palaeoecology* **81,** 95—113.

McManus, J. F., Bond, G. C., Broecker, W. S., Johnsen, S., Labeyrie, L., and Higgens, S. (1994). High-resolution climate records from the North Atlantic during the last interglacial. *Nature* **371,** 326—329.

McSaveney, M. J., and Whitehouse, I. E. (1989). An early Holocene glacial advance in the Macaulay River valley, central Southern Alps, New Zealand. *New Zealand Journal of Geology and Geophysics* **32,** 217—223.

Merlivat, L., and Jouzel, J. (1979). Global climatic interpretation of the deuterium-oxygen 18 relationship for precipitation. *Journal of geophysical research* **84,** 5029—5033.

Milankovitch, M. (1930). "Mathematische Klimalehre und Astronomische Theorie der Klimaschwankungen." Gebruder Borntraeger, Berlin.

Millen, T. M., and Dickey, D. N. (1987). A stable isotopic investigation of waters and speleothems in Wind Cave, South Dakota: an application of isotope paleothermometry. *National Speleological Society Bulletin* **49,** 10—14.

Miller, E. K., Blum, J. D., and Friedland, A. J. (1993). Determination of soil exchangeable-cation loss and weathering rates using Sr isotopes. *Nature* **362,** 438—441.

Miller, G. H., Magee, J. W., and Jull, A. J. T. (1997). Low-Latitude glacial cooling in the Southern Hemisphere from amino-acid racemization in emu eggshells. *Nature* **385,** 241—244.

Moar, N. T., and Suggate, R. P. (1996). Vegetation history from the Kaihinui (Last) Interglacial to the present, West Coast, South Island, New Zealand. *Quaternary Science Reviews* **15,** 521—547.

Moore, G. W. (1952). Speleothem - a new cave term. *National Speleological Society News* **10,** 2.

Moore, G. W. (1956). Aragonite speleothems as Indicators of palaeoclimate. *American Journal of Science* **254,** 746—753.

Moore, G. W. (1962). The growth of stalactites. *National Speleological Society Bulletin* **24,** 95—106.

Morinaga, H., Inokuchi, H., and Yaskawa, K. (1985). Paleomagnetism and paleotemperature of a stalagmite. *Journal of Geomagnetism and Geoelectricity* **37,** 823—828.

Morse, J. W., and Bender, M. L. (1990). Partition coefficients in calcite: Examination of factors influencing the validity of experimental results and their application to natural systems. *Chemical Geology* **82,** 265—277.

Morse, J. W., Shanbhag, P. M., Saito, A., and Choppin, G. R. (1984). Interaction of uranyl ions in carbonate media. *Chemical Geology* **42,** 85—99.

Nelson, C. S., Cooke, P. J., Hendy, C. H., and Cuthbertson, A. M. (1993). Oceanographic and climatic changes over the past 160,000 years at Deep Sea Drilling Project site 594 off southeastern New Zealand, southwest Pacific Ocean. *Paleoceanography* **8,** 435—458.

Nelson, C. S., Hendy, C. H., and Cuthbertson, A. M. (1994). Oxygen isotope evidence for climatic contrasts between Tasman Sea and Southwest Pacific Ocean during the late Quaternary. *In* "Evolution of the Tasman Sea." (G. J. v. d. Linden, K. M. Swanson, and R. J. Muir, Eds.), pp. 181—197. A A Balkema, Rotterdam.

Nelson, C. S., Hendy, C. H., Cuthbertson, A. M., and Jarrett, G. R. (1986). Late Quaternary carbonate and isotope stratigraphy, subantarctic site 594, Southwest Pacific. *Initial reports of the Deep Sea Drilling Project* **90,** 1425—1436.

Nelson, C. S., Hendy, C. H., Jarrett, G. R., and Cuthbertson, A. M. (1985). Near-synchroneity of New Zealand alpine glaciations and Northern Hemisphere continental glaciations during the past 750 kyr. *Nature* **318,** 361—363.

Ohde, S., and Kitano, Y. (1984). Coprecipitation of strontium with marine Ca-Mg carbonates. *Geochemical Journal* **18,** 143—146.

Osmond, J. K. (1980). Uranium series disequilibrium in hydrologic studies. *In* "Handbook of Environmental Geochemistry." (P. Fritz, and J. C. Fontes, Eds.), pp. 259—282. Elsevier, Amsterdam.

Osmond, J. K., and Cowart, J. B. (1982). Ground water. *In* "Uranium Series Disequilibrium: Applications to environmental problems." (M. Ivanovich, and R. S. Harmon, Eds.), pp. 202—245. Clarendon Press, Oxford.

Petit, J. R., Briat, M., and Royer, A. (1981). Ice age aerosol content from East Antarctic ice core samples and past wind strength. *Nature* **293,** 391-394.

Pillans, B. (1983). Upper Quaternary marine terrace chronology and deformation, South Taranaki, New Zealand. *Geology* **11,** 292—297.

Pillans, B. (1991). New Zealand Quaternary stratigraphy: an overview. *Quaternary Science Reviews* **10,** 405—418.

Pillans, B. (1994). Direct marine-terrestrial correlations, Wanganui Basin, New Zealand: the last 1 million years. *Quaternary Science Reviews* **13,** 189—200.

Pillans, B., Kohn, B. P., Berger, G., Froggatt, P., Duller, G., Alloway, B., and Hesse, P. (1996). Multi-Method dating comparison for Mid-Pleistocene Rangitawa Tephra, New Zealand. *Quaternary Science Reviews* **15,** 641—653.

Pillans, B., McGlone, M., Palmer, A., Mildenhall, D., Alloway, B., and Berger, G. (1993). The last glacial maximum in central and southern North Island, New Zealand: a paleoenvironmental reconstruction using the Kawakawa Tephra Formation as a chronostratigraphic marker. *Palaeogeography, Palaeoclimatology, Palaeoecology* **101,** 283—304.

Pillans, B., and Wright, I. (1990). 500,000-year paleomagnetic record from New Zealand loess. *Quaternary Research* **33,** 178—187.

Pillans, B. J. (1988). Loess chronology in Wanganui Basin, New Zealand. *In* "Loess." (Eden, and Furkert, Eds.), pp. 175—191. Balkema, Rotterdam.

Pillans, B. J., Roberts, A. P., Wilson, G. S., Abbott, S. T., and Alloway, B. V. (1994). Magnetostratigraphic, lithostratigraphic and tephrostratigraphic constraints on Lower and Middle Pleistocene sea-level changes, Wanganui Basin, New Zealand. *Earth and Planetary Science Letters* **121,** 81—98.

Pisias, N. G., Martinson, D. G., Moore, T. C., Shackleton, N. J., Prell, W., Hays, J., and Boden, G. (1984). High resolution stratigraphic correlation of benthic oxygen isotope records spanning the last 300,000 years. *Marine Geology* **56,** 119—136.

Polyak, V. J., Karlsson, H. R., Browning, J. M., and Cokendolpher, J. C. (1996). A fresh look at stalagmites as paleoclimatic indicators. *In* "Geological Society of America, 28th annual meeting." (Anonymous, Ed.), pp. 307. Abstracts with Programs - Geological Society of America. Geological Society of America (GSA), Boulder, CO, United States.

Porter, S. C., and An, Z. (1995). Correlation between climate events in the North Atlantic and China during the last glaciation. *Nature* **375,** 305—309.

Qing, H., Barnes, C. R., Buhl, D., and Veizer, J. (1998). The strontium isotopic composition of Ordovician and Silurian brachiopods and conodants: Relationships to geological events and implications for coeval seawater. *Geochimica et Cosmochimica Acta* **62,** 1721—1733.

Ramseyer, K., Miano, T. M., D, O. V., Wildberger, A., Wagner, T., and Geister, J. (1997). Nature and origin of organic matter in carbonates from speleothems, marine cements and coral skeletons. *Organic Geochemistry* **26,** 361—378.

Ravens, J. M. (1986). Nettlebed Cave. New Zealand Speleological Society, Wellington.

Ravens, J. M. (1992). The Ellis Basin Cave System. New Zealand Speleological Society, Wellington.

Reeder, R. J. (1996). Interaction of divalent cobalt, zinc, cadmium and barium with the calcite surface during layer growth. *Geochimica et Cosmochimica Acta* **60,** 1543—1552.

Reeder, R. J., and Grams, J. C. (1987). Sector zoning in calcite cement crystals: Implications for trace element distributions in carbonates. *Geochimica et Cosmochimica Acta* **51,** 187—194.

Richards, D. A., Smart, P. L., and Edwards, R. L. (1994). Maximum sea levels for the last glacial period from U-series ages of submerged speleothems. *Nature* **367,** 357—360.

Roberts, M. S., Smart, P. L., and Baker, A. (1998). Annual trace element variations in a Holocene speleothem. *Earth and Planetary Science Letters* **154,** 237—246.

Roberts, M. S., Smart, P. L., Perkins, W. T., Pearce, N. J. G., and Hawkesworth, C. J. (1996). Trace elements in Holocene speleothems. *In* "Climate Change: The Karst Record." (S.-E. Lauritzen, Ed.), pp. 138—139. Karst Waters Institute, Bergen.

Rosholt, J. N. (1982). Mobilization and weathering. *In* "Uranium Series Disequilibrium: Applications to environmental problems." (M. Ivanovich, and R. S. Harmon, Eds.), pp. 167—180. Clarendon Press, Oxford.

Rosholt, J. N., and Antal, P. S. (1962). Evaluation of the $^{231}Pa/U$-$^{230}Th/U$ method for dating Pleistocene carbonate rocks. *United States Geological Survey Professional Paper* **450,** E108—111.

Rowe, P., Dennis, P., Atkinson, T., Lauritzen, S.-E., and Lundberg, J. (1998). A high resolution deuterium record from fluid inclusions in a late Holocene speleothem from S.W. Britain. *In* "Past Global Climates and their Significance for the Future." (B. Marcolli, Ed.), pp. 88. IGBP PAGES, London.

Salinger, M. J. (1983). New Zealand climate: the last 5 million years. *In* "Late Cainozoic palaeoclimates of the Southern Hemisphere." (J. C. Vogel, Ed.), pp. 131—150. Balkema, Rotterdam.

Salinger, M. J., Heine, M. J., and Burrows, C. J. (1983). Variations of the Stocking (Te Wae Wae) Glacier, Mount Cook, and climatic relationships. *New Zealand Journal of Science* **26,** 321—338.

Schwarcz, H. P. (1986). Geochronology and isotopic geochemistry of speleothems. *In* "Handbook of environmental isotope geochemistry." (P. Fritz, and J. C. Fontes, Eds.), pp. 271—303. Elsevier.

Schwarcz, H. P. (1989). Uranium series dating of quaternary deposits. *Quaternary International* **1,** 7—17.

Schwarcz, H. P., Harmon, R. S., Thompson, P., and Ford, D. C. (1975). Stable isotope studies of fluid inclusions in speleothems and their paleoclimatic significance. *Geochimica et Cosmochimica Acta* **40,** 657—665.

Scott, M. R. (1982). The chemistry of U- and Th-series nuclides in rivers. *In* "Uranium Series Disequilibrium: Applications to environmental problems." (M. Ivanovich, and R. S. Harmon, Eds.), pp. 181—201. Clarendon Press, Oxford.

Shackleton, N. J. (1987). Oxygen isotopes, ice volume and sea level. *Quaternary Science Reviews* **6,** 183—190.

Shackleton, N. J., and Opdyke, N. D. (1973). Oxygen isotope and Palaeomagnetic stratigraphy of Equatorial Pacific Core V28—238: Oxygen isotope temperatures and ice volumes on a 10^5 year and 10^6 year scale. *Quaternary Research* **3,** 39—55.

Sharp, D. W. A. (1983). Dictionary of Chemistry. Penguin Books, Harmondsworth.

Shaw, T. R. (1992). "History of Cave Science." Sydney Speleological Society, Sydney.

Shopov, Y. Y. (1996). Speleothem records of environmental changes in the past - potential in comparison with the other palaeoenvironmental archives and related UIS international programs. *In* "Climate Change: The Karst Record." (S.-E. Lauritzen, Ed.), pp. 148—149. Karst Waters Institute, Bergen.

Shopov, Y. Y., Ford, D. C., and Schwarcz, H. P. (1994). Luminescent microbanding in speleothems: High-resolution chronology and paleoclimate. *Geology* **22,** 407—410.

Siegel, F. R., and Dort, W. (1966). Calcite-aragonite speleothems from a hand-dug cave in north-east Kansas. *International Journal of Speleology* **2,** 165—169.

Sinclair, D. J., Kinsley, L. P. J., and McCulloch, M. T. (1998). High resolution analysis of trace elements in corals by laser ablation ICP-MS. *Geochimica et Cosmochimica Acta* **62,** 1889—1901.

Singer, C., Shulmeister, J., and McLea, B. (1998). Evidence against a significant Younger Dryas cooling event in New Zealand. *Science* **281,** 812—814.

Slowey, N. C., Henderson, G. M., and Curry, W. B. (1996). Direct U-Th dating of marine sediments from the two most recent interglacial periods. *Nature* **383,** 242—244.

Soons, J. M. (1979). Late Quaternary environments in the central South Island of New Zealand. *New Zealand Geographer* **35,** 16—23.

Spalding, R. F., and Mathews, T. D. (1972). Stalagmites from caves in the Bahamas: Indicators of low sea level stand. *Quaternary Research* **2,** 470—472.

Stanton, B. R. (1973). Circulation along the Eastern Boundary of the Tasman Sea. *In* "Oceanography of the South Pacific 1972." (R. Fraser, Ed.), pp. 141—147. New Zealand National Commission for UNESCO, Wellington.

Stirling, C. H. (1996). "High-Precision U-series Dating of Corals from Western Australia: Implications for Last Interglacial Sea-Levels." Unpublished PhD thesis, Australian National University.

Stirling, C. H., Esat, T. M., McCulloch, M. T., and Lambeck, K. (1995). High-precision U-series dating of corals from Western Australia and implications for the timing and duration of the last interglacial. *Earth and Planetary Science Letters* **135,** 115—130.

Stuiver, M., Grootes, P. M., and Braziunas, T. F. (1995). The GISP2 $\delta^{18}O$ climate record of the past 16,500 years and the role of the sun, ocean and volcanoes. *Quaternary Research* **44,** 341—354.

Stuiver, M., and Reimer, P. J. (1993). Extended ^{14}C data base and revised Calib 3.0 ^{14}C age calibration program. *Radiocarbon* **35,** 215—230.

Sturman, A. P., and Tapper, N. J. (1996). "The weather and climate of Australia and New Zealand." Oxford University Press, Melbourne.

Suggate, R. P. (1965). Late Pleistocene geology of the northern part of the South Island, New Zealand. *Bulletin of the New Zealand Geological Survey* **77.**

Suggate, R. P. (1990). Late Pliocene and Quaternary glaciations of New Zealand. *Quaternary Science Reviews* **9,** 175—197.

Suggate, R. P., and Moar, N. T. (1969). Revision of the chronology of the late Otira glacial. *New Zealand Journal of Geology and Geophysics* **13,** 742—746.

Suggate, R. P., Stevens, G. R., and Te Punga, M. T. (1978). The Geology of New Zealand, pp. 820. Government Printer, Wellington.

Szabo, B. J., and Rosholt, J. N. (1982). Surficial continental sediments. *In* "Uranium Series Disequilibrium: Applications to environmental problems." (M. Ivanovich, and R. S. Harmon, Eds.), pp. 246—267. Clarendon Press, Oxford.

Talma, A. S., and Vogel, J. C. (1992). Late Quaternary paleotemperatures derived from a speleothem from Cango Caves, Cape Province, South Africa. *Quaternary Research* **37,** 203—213.

Taylor, C. B. (1990). Stable isotope compositions of monthly precipitation samples collected in New Zealand and Rarotonga. Department of Scientific and Industrial Research.

Tesoriero, A. J., and Pankow, J. F. (1996). Solid solution partitioning of Sr^{2+}, Ba^{2+}, and Cd^{2+} to calcite. *Geochimica et Cosmochimica Acta* **60,** 1053—1063.

Thiede, J. (1979). Wind regimes over the late Quaternary southwest Pacific Ocean. *Geology* **7,** 259—262.

Thompson, L. G. (1998). Ice core evidence for climate change in the Tropics: Implications for our future. *In* "Past Global Changes and their Significance for our Future." (B. Marcolli, Ed.), pp. 5. IGBP PAGES, London.

Thompson, L. G., Mosley-Thompson, E., Davis, M. E., Lin, P.-N., Henderson, K. A., Cole-Dai, J., Bolzan, J. F., and Liu, K.-b. (1995). Late Glacial stage and Holocene tropical ice core records from Huascarán, Peru. *Science* **269,** 46—50.

Thompson, P., Schwarcz, H. P., and Ford, D. C. (1974). Continental Pleistocene climatic variations from speleothem age and isotopic data. *Science* **184,** 893—895.

Thompson, P., Schwarcz, H. P., and Ford, D. C. (1976). Stable isotope geochemistry, geothermometry and geochronology of speleothems from West Virginia. *Geological Society of America Bulletin* **87,** 1730—1738.

Thunell, R., Anderson, D., Gellar, D., and Miao, Q. (1994). Sea-surface temperature estimates for the tropical western Pacific during the last glaciation and their implications for the Pacific Warm Pool. *Quaternary Research* **41,** 255—264.

Trumbore, S. E., Chadwick, O. A., and Amundson, R. (1996). Rapid exchange between soil carbon and atmospheric carbon dioxide driven by temperature change. *Science* **272,** 393—396.

Waelbroeck, C., Jouzel, J., Labeyrie, L., Lorius, C., Labracherie, M., Stiévenard, M., and Barkov, N. I. (1995). A comparison of the Vostok ice deuterium record and series from Southern Ocean core MD 88-770 over the last two glacial-interglacial cycles. *Climate Dynamics* **12,** 113—123.

Wardle, P. (1991). "Vegetation of New Zealand." Cambridge University Press, Cambridge.

White, J. W. C., and Steig, E. J. (1998). Timing is everything in a game of two hemispheres. *Nature* **394,** 717—718.

White, W. B., Smailer, S. A., and Brennan, E. (1995). Fulvic and humic acids in cave calcite deposits; characterization, luminescence, and paleoclimatic implications. *In* "Geological Society of America, 1995 annual meeting." (Anonymous, Ed.), pp. 323. Abstracts with Programs - Geological Society of America. Geological Society of America (GSA), Boulder, CO, United States.

Wigley, T. M. L., and Brown, M. C. (1976). The Physics of Caves. *In* "The Science of Speleology." (T. D. Ford, and C. M. D. Cullingford, Eds.), pp. 229—358. Academic Press, New York.

Williams, P. W. (1982). Speleothem dates, Quaternary terraces and uplift rates in New Zealand. *Nature* **298,** 257—260.

Williams, P. W. (1996). A 230ka record of glacial and interglacial events from Aurora Cave, Fiordland, New Zealand. *New Zealand Journal of Geology and Geophysics* **39,** 225—241.

Wilson, A. T., and Hendy, C. H. (1971). Past wind strength from isotope studies. *Nature* **234,** 344—345.

Wilson, A. T., Hendy, C. H., and Reynolds, C. P. (1979). Short-term climate change and New Zealand temperatures during the last millennium. *Nature* **279,** 315—317.

Winograd, I. J., Coplen, T. B., Landwehr, J. M., Riggs, A. C., Ludwig, K. R., Szabo, B. J., Kolesar, P. T., and Revesz, K. M. (1992). Continuous 500,000-year climate record from Vein Calcite in Devils Hole, Nevada. *Science* **258,** 255—260.

Wintle, A. G. (1978). A Thermoluminescence dating study of some Quaternary calcite: potential and problems. *Canadian Journal of Earth Science* **15,** 1977—1986.

Wohlfarth, B. (1996). The chronology of the last termination: a review of radiocarbon-dated, high-resolution terrestrial stratigraphies. *Quaternary Science Reviews* **15,** 267—284.

Worthy, T. H., and Mildenhall, D. C. (1989). A late Otiran-Holocene paleoenvironment reconstruction based on cave excavations in Northwest Nelson, New Zealand. *New Zealand Journal of Geology and Geophysics* **32,** 243—253.

Wright, A. C. (1981). Aspects of the geology and hydrology of Nettlebed Cave, Nelson, New Zealand. *Journal of the Royal Society of New Zealand* **12,** 143—157.

Wright, I. C., McGlone, M. S., Nelson, C. S., and Pillans, B. J. (1995). An integrated latest Quaternary (Stage 3 to present) paleoclimatic and Paleoceanographic record from offshore northern New Zealand. *Quaternary Research* **44,** 283—293.

Appendix 1. Publication in press, *Quaternary Research*

Page proofs

The following paper, titled "A Detailed 31,000-Year Record of Climate and Vegetation Change, from the Isotope Geochemistry of Two New Zealand Speleothems," by John Hellstrom, Malcolm McCulloch, and John Stone, was submitted to *Quaternary Research* in November 1997. It is scheduled to appear in the September 1998 issue of the journal. Included in this appendix are the page proofs received from Academic Press in August 1998, and details of the corrections made to them.

QUATERNARY RESEARCH 50, 000–000 (1998)
ARTICLE NO. QR981991

A Detailed 31,000-Year Record of Climate and Vegetation Change, from the Isotope Geochemistry of Two New Zealand Speleothems

John Hellstrom, Malcolm McCulloch, and John Stone[1]

Research School of Earth Sciences, The Australian National University, Canberra, ACT 0200 Australia

Received December 1, 1997

Uranium-series dating and stable isotope analyses of two speleothems from northwest Nelson, New Zealand, record changes in regional climate and local forest extent over the past 31,000 years. Oxygen isotope variation in these speleothems primarily represents changes in the meteoric waters falling above the caves, possibly responding to latitudinal changes in the position of the Subtropical Front in the Tasman Sea. Seven positive excursions can be identified in the oxygen isotope record, which coincide with periods of glacier advance, known to be sensitive to northward movement of the Subtropical Front. Four glacier advances occurred during oxygen isotope stage 2, with the most extreme glacial conditions centered on 19,000 cal yr B.P.[2] An excursion in the oxygen isotope record from 13,800 to 11,700 cal yr B.P. provides support for a previously identified New Zealand glacier advance at the time of the Younger Dryas Stade, but suggests it began slightly before the Younger Dryas as recorded in Greenland ice cores. Carbon isotope variations in the speleothems record changes in forest productivity, closely matching existing paleovegetation records. On the basis of vegetation changes, stage 2 glacial climate conditions terminated abruptly in central New Zealand, from 15,700 to 14,200 cal yr B.P. Evidence of continuous speleothem growth at one site suggests that depression of the local treeline was limited to 600–700 m below its present altitude, throughout the last 31,000 years.

*Key Words:*New Zealand Quaternary climate; oxygen and carbon isotopes; speleothem climate records; Subtropical Front; isotope paleovegetation record.

INTRODUCTION

Investigation of the global cycles of Pleistocene glaciation has focused on high northern latitudes, especially the North Atlantic region, for which there are now detailed records of marine and terrestrial paleoclimate. Records from other Northern Hemisphere regions have also been tied to the resulting framework of glacial–interglacial changes. However, climatic changes in the Southern Hemisphere during this period are less-well-constrained, as the relevant marine and terrestrial records are mostly of comparatively low resolution. The only continuous high-resolution records are from Antarctic ice cores (e.g., Lorius *et al.*, 1985), which indicate that Antarctic climate broadly co-varied with North Atlantic climate over the last glacial cycle, but did not undergo the short-duration events seen there, implying that the Antarctic is buffered from transient shifts in Northern Hemisphere climate (Dansgaard *et al.*, 1993).

This leaves open the question of whether Pleistocene climate change in central southern latitudes is more closely related to that in the Northern Hemisphere or in Antarctica, an understanding of which is crucial to our knowledge of the mechanisms behind Quaternary climate change (Broecker *et al.*, 1985). In trying to determine the global extent of the well-documented northern climate change sequence, and through this reach some understanding of the mechanisms driving global climate (Denton and Hendy, 1994), attention has focused on the Younger Dryas Stade, a distinctive cold event centered in the North Atlantic region from 12,900 to 11,700 cal yr B.P. (Stuiver *et al.*, 1995). Another event that can be identified in many climate records is Termination I, the end of the last glaciation, the relative timing of which around the world is likewise of critical importance.

There is a clear need for high-resolution, well-dated records of climate change in the largely marine Southern Hemisphere. Results from Southern Hemisphere continental landmasses show temperatures to have been considerably lower during the last glacial maximum (LGM) than they are today (Miller *et al.*, 1997; Thompson *et al.*, 1995), but the extent to which continental climate was influenced by local factors, such as greatly increased aridity, is unclear. In contrast, records from maritime regions might be expected to show variations more representative of marine, and thus hemispheric, climate change generally.

The islands of New Zealand are well positioned to record the effects of mid-latitude climate change. They lie across 13° of

[1] Current address: Department of Geological Sciences and Quaternary Research Center, Box 351310, University of Washington, Seattle, WA 98195.

[2] All ages reported or cited in this paper are in calendar years before present, expressed as "cal yr B.P." With the exception of the U-series dates of Williams (1996), all ages cited for events in New Zealand were reported by the sources cited as radiocarbon ages. In this paper, these radiocarbon ages have been corrected to calendar years before present using the 1993 calibration data set of Stuiver and Reimer (1993), or, for ages of greater than 19,000 ^{14}C yr B.P., by the addition of 4000 yr, on the basis of data in Bard *et al.* (1993).

0033-5894/98 $25.00

latitude, including the Subtropical Front (STF), south of which westerly airflow is stronger and more dominant, and associated with greater rainfall and lower temperatures. New Zealand's weather is dominated by the westward movement of weather systems over the Tasman Sea, and is sensitive to changes in the nature of this movement (McGlone *et al.*, 1993), such as in the latitudinal position of the STF. Records of terrestrial environmental change in New Zealand, then, should reflect changes in Tasman Sea weather patterns, in turn influenced by changes in mid-latitude ocean circulation and climate. Here we present continuous high-resolution stable isotope records of environmental change in New Zealand from speleothems that grew over the last 31,000 yr.

SPELEOTHEMS AS RECORDERS OF ENVIRONMENTAL CHANGE

Speleothems, secondary calcite deposits formed in caves, have long been used to infer climate histories based on variations in chemical and stable isotopic compositions deposited through time. Among recorders of terrestrial paleoclimate, a particular advantage of speleothems is that they can be accurately dated using uranium-series disequilibrium methods (Li *et al.*, 1989), thereby allowing geochemical and isotopic measurements to be placed into a precise chronological framework. Generally, speleothems will only form beneath soils where sufficient vegetation exists to elevate soil CO_2 levels, and where water is able to seep to a cave below. As water sinks through the soil, it absorbs CO_2, forming carbonic acid, and so is able to dissolve some of the carbonate rock between the surface and the cave. On reaching the cave, some CO_2 is lost from solution, causing precipitation of calcite from the seepage waters as speleothem.

Most attempts to reconstruct paleoclimate from speleothems have relied on oxygen isotope measurements ($\delta^{18}O$). Oxygen isotope fractionation between speleothem calcite and the dripwater from which it formed is sensitive to temperature, and under ideal conditions can record cave temperature changes at a rate of $-0.24‰/°C$ (Hendy and Wilson, 1968). However, changes in depositional conditions, and in the $\delta^{18}O$ of meteoric waters (and therefore the cave seepage waters), also influence the $\delta^{18}O$ of speleothem calcite, and in many situations are likely to obscure the temperature-controlled signal. These other effects may, however, record important climatic information in their own right.

Carbon isotope ($\delta^{13}C$) variation in speleothems is commonly interpreted as a response to changes in the relative abundance of plants above the cave that use the C_4 photosynthetic pathway. In several cases, it has been assumed that the resultant variations in soil $\delta^{13}C$ will be directly reflected in the speleothem calcite (e.g., Dorale *et al.*, 1992). The validity of this approach was recently challenged by Baker *et al.* (1997), who observed that inorganic processes acting on soil CO_2 during transport and speleothem formation can have greater effects on $\delta^{13}C$ than can C_3/C_4 vegetation changes, which may be completely masked. These inorganic effects include changes in the partial pressure of soil CO_2 and the rate of seepage water flow over the speleothem surface (Dulinski and Rozanski, 1990), and may themselves vary in response to environmental changes, providing important information via the speleothem $\delta^{13}C$ record.

SETTING

Mt. Arthur (1795 m), in the northwestern corner of New Zealand's South Island (Fig. 1), is underlain by many known cave systems, the two largest and deepest being Exhaleair and Nettlebed (Ravens, 1986), 1992), the caves used for this study. The two sampled speleothems are at elevations of 390 m (core MD3, Nettlebed) and 685 m (core ED1, Exhaleair). Both are located ca. 200 m beneath the surface, under the eastern and southern flanks of the mountain, respectively (Fig. 2). These sites are at least 500 m from the nearest known entrance, and are free of active streamflow or vigorous airflow. Due to the fractured nature of the host marble, it is assumed that the water feeding the speleothems is derived from the land surface approximately above each site. The surface above both sites is forested, predominantly by *Nothofagus*. The treeline lies at 1200–1300 m, above which is alpine scrub, grassland, and bare rock.

Mt. Arthur receives precipitation predominantly from westerly airflow (Garnier, 1958) that first crosses 50 km of mountainous country from the coast, including the Arthur Range at ca. 1600 m. Annual precipitation in the region is >2500 mm, and annual average temperature at sea level nearby is 12°C (Garnier, 1958). The climate of the Mt. Arthur area is also influenced by the proximity of Cook Strait, the only break in the 1600 km length of New Zealand's main islands. Here the southwesterly winds, dominant to the north and south, are replaced by northwesterly winds as the westerly airflow funnels between the islands.

SAMPLES AND METHODS

A 50-mm-diameter core sample was recovered from each site by drilling into gently sloping flowstones (massive sheet speleothems which form on cave walls and floors). Examination of core MD3 from Nettlebed Cave, the main focus of this research, showed it to consist, over most of its 587 mm length, of large crystals of clouded calcite, with faint growth banding defined by layers of fine fluid inclusions. The basal 105 mm is of clearer (with fewer fluid inclusions) parallel, elongated crystals of calcite. From 100 to 290 mm depth in the core, the calcite crystals are irregular and elongated (growth banding is still defined by fluid inclusions, but the layering is irregular). It appears (Fig. 2) that the parallel elongate crystals correspond to the period of slowest growth rate, and the irregular elongate crystals to the period of fastest growth rate in the core.

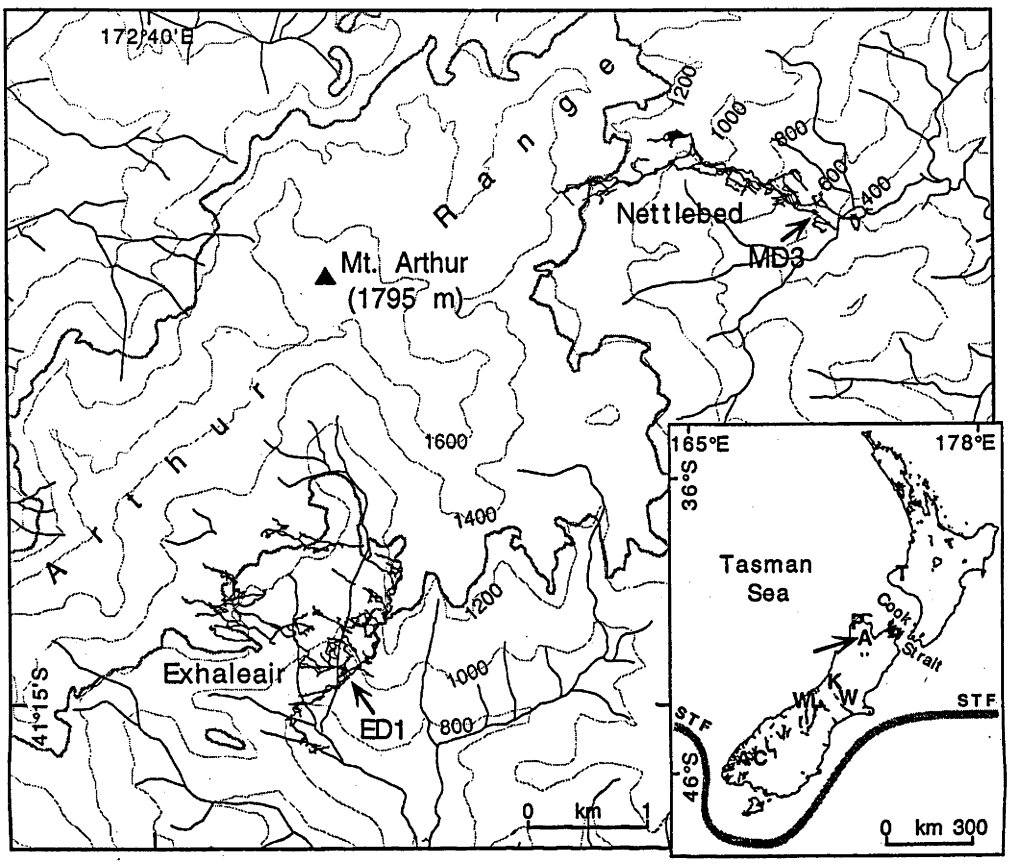

FIG. 1. Map of the Mt. Arthur study area, showing the relationship of surface relief and modern treeline (thick gray line) to the cave systems (Ravens, 1986, 1992). Sample sites (arrowed) underlie forested areas, as do all known actively growing flowstones. Inset: Outline map of New Zealand, showing locations mentioned in text. STF, present position of Subtropical Front; T, Taranaki loess record; A, Mt. Arthur (arrowed); K, Kumara glacial sequence; W, Waimakariri glacial sequence; WL, Waiho Loop moraine; AC, Aurora Cave; P, Patarau.

Whereas a possible growth hiatus, a very sharp, light-brown band, was identified at 457 mm depth, dates immediately above and below it (samples MD3A7 and MD3A9) showed it not to represent a measurable break in speleothem deposition, strongly implying that MD3 contains no significant hiatus. The consistently large crystal size, preservation of growth layering, and clean nature of MD3 precludes any post-depositional alteration of the speleothem. The Exhaleair core, ED1 (235 mm long), was found to have several hiatuses below 172 mm. Above this, the core consists entirely of large clouded crystals similar to those in MD3, except with a faint orange coloration. Core ED1 also shows no sign of post-depositional alteration.

Core sample MD3 was dated at nine points, using the mass-spectrometric ^{238}U-^{234}U-^{230}Th method (Li *et al.*, 1989). The procedure closely followed that of Stirling *et al.* (1995), except the thorium measurements were made using a peak-hopping method on the secondary electron multiplier of a Finnigan MAT 261 mass spectrometer. Five-gram samples of calcite were used, representing 2–3 mm increments of core. Core ED1 was dated at three points. Stable isotope data were obtained from homogenized adjacent increments of the cores, integrating 1, 2, or 5 mm of growth for low-, medium-, and high-growth-rate sections, respectively. Portions of each homogenized sample (150 μg) were run on a Finnigan MAT 251 mass spectrometer equipped with a Kiel carbonate-extraction device, and are reported relative to the PDB standard.

RESULTS

Uranium-Series Dating

The activity ratios and calculated ages for the U-series dates are shown in Table 1. Figure 2 shows depth versus age for

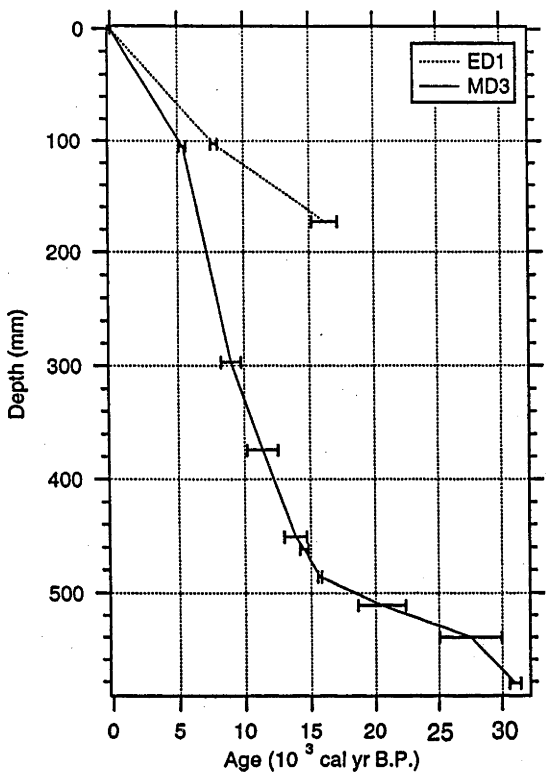

FIG. 2. Age vs depth below speleothem surface, for cores ED1 and MD3 (2σ errors shown). The age/depth models used in this paper are obtained by linear interpolation between the dates, as shown.

cores ED1 and MD3, and the age/depth models used in this study. Both speleothems are still growing today, illustrated by incorporation of boot prints into the calcite since the discovery of the caves. Core MD3 grew continuously from 31,000 cal yr B.P. to the present, covering all of oxygen isotope stages 2 and 1. During this time, its growth rate ranged from 6 to 60 μm per year, illustrating the importance of dating multiple points along a speleothem. Core ED1 ceased growth between 73,000 and 16,000 cal yr B.P., and then grew continuously to the present.

Oxygen Isotope Record

The speleothems from both caves show similar patterns of oxygen isotope variation over the last 16,000 yr (Fig. 3).). Total variation of $\delta^{18}O$ in the Nettlebed flowstone over the last 31,000 yr is 1.8‰, generally increasing from −5.5‰ at 31,000 cal yr B.P. to −4.2‰ at 19,000 cal yr B.P., then decreasing to ca. −6.0‰ by 7000 cal yr B.P. Seven short (1000–2000 yr) positive excursions in $\delta^{18}O$, of up to 0.6‰ in magnitude, are identified along the record. Summer temperature of 8.3°C was measured at the MD3 site; the ED1 site (which is 300 m higher) is noticeably colder. If $\delta^{18}O$ variations in the speleothems were controlled primarily by cave temperature, the ED1 record should then be displaced from MD3 in a positive sense. In fact, over much of its length, it is displaced in a negative sense, by 0.6‰, suggesting that variations in the $\delta^{18}O$ of these speleothems instead predominantly reflect changes in the $\delta^{18}O$ of the meteoric waters falling above the caves.

Kinetic fractionation during speleothem deposition can in some circumstances introduce an unpredictable bias to the isotopic record. Hendy (1971) noted that it causes co-variation of $\delta^{13}C$ and $\delta^{18}O$, and suggested testing for kinetic fractionation in speleothems by measuring this co-variance (preferably

TABLE 1
U-Series Data and Calculated Ages for Mt. Arthur Speleothems

Sample	U (ppm)	Depth (mm)	$^{234}U/^{238}U$ activity	$^{230}Th/^{238}U$ activity	Age (yr)[a]	$^{230}Th/^{232}Th$ activity	Corrected age (yr)[b]
MD3A1	0.052	105	1.370 (0.044)	0.067 (0.003)	5401 (275)	82	5380
MD3A5	0.049	297	1.355 (0.004)	0.108 (0.009)	9018 (782)	10	8140
MD3A6	0.091	374	1.362 (0.007)	0.136 (0.013)	11,382 (1157)	564	11,370
MD3A7	0.113	451	1.410 (0.013)	0.169 (0.010)	13,850 (878)	177	13,790
MD3A9	0.081	462	1.402 (0.007)	0.176 (0.004)	14,499 (322)	260	14,450
MD3A19	0.092	486	1.413 (0.005)	0.191 (0.001)	15,699 (145)	193	15,620
MD3A10	0.113	511	1.405 (0.005)	0.244 (0.020)	20,533 (1868)	103	20,350
MD3A11	0.106	540	1.386 (0.057)	0.313 (0.021)	27,469 (2417)	173	27,330
MD3.11C2	0.107	581	1.376 (0.003)	0.345 (0.004)	31,012 (442)	85	30,700
ED1A1	0.073	103	1.246 (0.010)	0.086 (0.003)	7786 (239)	15	7260
ED1A2	0.068	173	1.225 (0.030)	0.170 (0.009)	16,216 (980)	22	15,490
ED1A4	0.040	179	1.178 (0.005)	0.583 (0.014)	72,777 (2501)	42	71,520

[a] Two-sigma errors (bracketed) are propagated by Monte Carlo simulation, and can be considered symmetrical for young samples such as these.

[b] Ages recalculated to allow for the effect of detrital thorium, by assuming $^{230}Th/^{232}Th$ activity was equal to 1 at time of formation. Corrected ages are not used in the text of this paper, as, with the exception of samples MD3A5 and ED1A4, the correction is not significant, and it introduces additional assumptions to the dating technique.

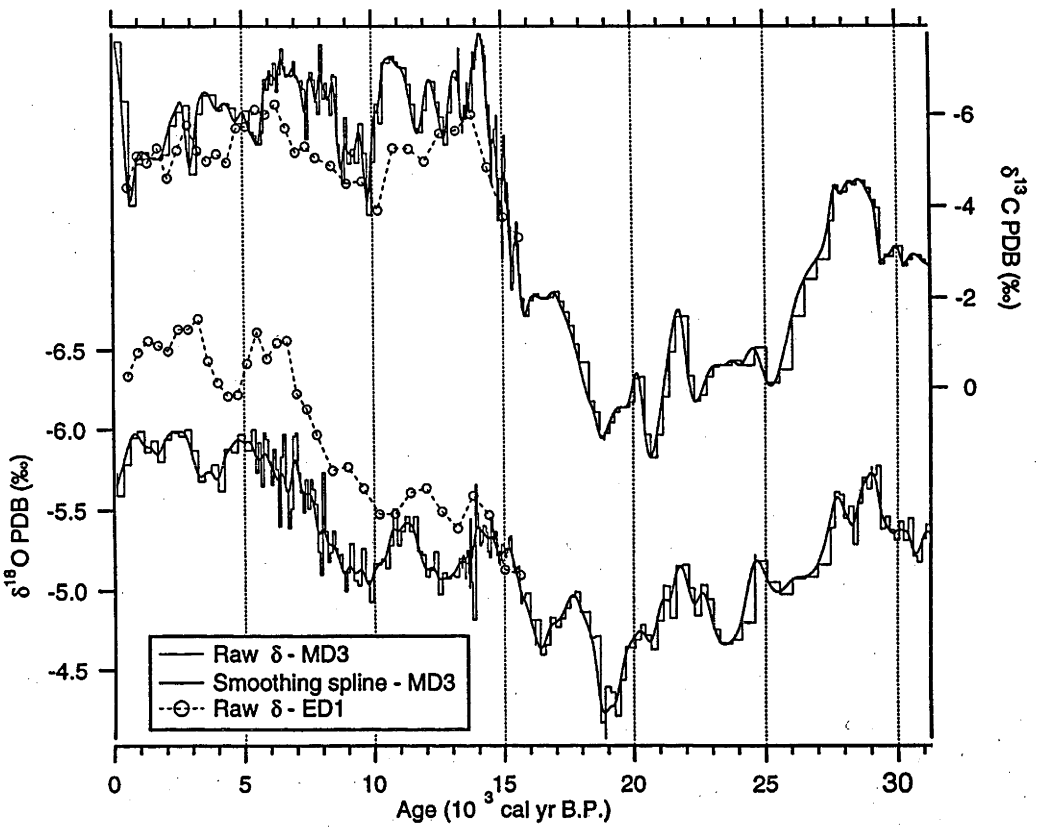

FIG. 3. The $\delta^{13}C$ and $\delta^{18}O$ vs time, for adjacent increments of cores MD3 and ED1. Repeat measurements of a number of samples indicated an external precision of better than 0.1‰. Subsequent figures use the smoothing splines shown here.

along growth layers, which is unfortunately not feasible for a core sample of only 50 mm diameter). While the $\delta^{18}O$ and $\delta^{13}C$ signals in MD3 do broadly co-vary, this is explained below in terms of both signals responding to related environmental changes. If the relative humidity in a cave falls below 100%, evaporation of water can also bias speleothem $\delta^{18}O$, increasing it; however, this is unlikely given the cold and wet nature of these caves. That the MD3 and ED1 $\delta^{18}O$ records co-vary further implies that site-specific depositional effects are not significant.

The $\delta^{18}O$ of rainwater falling above a cave is dependent on local temperature, and on the $\delta^{18}O$ of the water vapor arriving in the region (Dansgaard, 1964). The $\delta^{18}O$ in modern New Zealand precipitation generally has a temperature dependence of ca. +0.19‰/°C (the average of the temperature dependencies from five moderate-to high-rainfall sites; Taylor, 1990). Thus, at least for modern times, this temperature effect largely cancels the speleothem temperature dependence of −0.24‰/°C. If the temperature dependence of $\delta^{18}O$ in precipitation was also 0.19‰/°C during the LGM, and this was 5°C colder than today (McGlone, 1988; Soons, 1979), the net effect of local temperature could account for ca. −0.25‰ of the observed −1.8‰ change in MD3 $\delta^{18}O$ since the LGM.

Much of the variation in MD3 $\delta^{18}O$ may be due to changes in conditions at the source area of the water vapor arriving above the cave, including changes in the $\delta^{18}O$ of the bulk oceans and changes in the configuration of oceanic water masses. Such variations would affect ED1 and MD3 by the same amount, because due to their proximity they share the same distal water vapor source. Changes in source temperature, humidity, and ocean-surface roughness could affect the $\delta^{18}O$ of the initial water vapor by as much as −0.5, 0.5, and 0.5‰, respectively (Johnsen *et al.*, 1989; Merlivat and Jouzel, 1979).

Deuterium excess, d, can be used to identify the type of oceanic water source from which precipitation was derived (Dansgaard, 1964; Johnsen *et al.*, 1989). In modern New Zealand precipitation, d indicates a gradation from a subtropical source (d = 10.2 ± 0.7‰; Taylor, 1990) in the north

of New Zealand, to a windy, sub-Antarctic source (d = 4.5 ± 1.5‰; Taylor, 1990) in the south. This difference in source is associated with a gradation in season of precipitation in western New Zealand, from a winter maximum to the north of the STF to a summer maximum to the south (Garnier, 1958). If, as seems very likely (McGlone *et al.*, 1993; T. Barrows, unpublished data), the STF and westerly wind belt moved north in the Tasman Sea during the LGM, the sub-Antarctic component would have become more dominant in Mt. Arthur meteoric water, presumably coupled with a move toward summer maximum precipitation (consistent with Gage, 1965). Such a change could result in average meteoric water ca. 0.5‰ heavier during the LGM.

The $\delta^{18}O$ of precipitation depends on the altitude of the site at which it falls, typically changing at between −0.15 and −0.5‰ per 100 m increase in altitude (Gat, 1980). The strength of this effect is site specific, depending on local climate and topography (Gat, 1980), and so may vary as local climate changes. A modern speleothem at Patarau, near sea level on the coast 70 km northwest of Mt. Arthur, has a $\delta^{18}O$ of ca. −3.5‰ (Wilson *et al.*, 1979), compared to ca. −6.0‰ and ca. −6.5‰ for MD3 (surface above at 600 m) and ED1 (900 m), respectively. The offset between the two latter records, presumably due to an increase in the local altitude effect, increases from 16,000 to 6000 cal yr B.P. (Fig. 3). This parallels post-LGM sea-level rise (e.g., Blanchon and Shaw, 1995), perhaps reflecting changes in the local lapse rate as the coastline retreated and Cook Strait submerged.

All of the effects discussed above are cumulative, and so isolating the change due to any one of them is not feasible. Broadly, the MD3 $\delta^{18}O$ signal corresponds to the 1.2‰ global ice volume signal seen in records from ocean cores, but superimposed on this are a number of excursions toward higher $\delta^{18}O$ values, which may have been caused by any of a number of mechanisms. That these records reflect events external to the cave environment is very strongly supported by the similarity of the MD3 and ED1 signals, despite different growth rates of the speleothems and their physical separation in different cave systems. The excursions are too rapid to be attributed to changes in sealevel or global ice volume, and so must be considered due to changes in local and Tasman Sea climate, considered here as being driven by latitudinal movement of the STF in the Tasman sea.

Carbon Isotope Record

The MD3 and ED1 carbon isotope records broadly co-vary (Fig. 3), but do not show the same degree of agreement as the oxygen records, perhaps due to localized vegetation changes. Total variation of MD3 $\delta^{13}C$ over the last 31,000 yr is almost 10‰, generally increasing from −4‰ at 31,000 cal yr B.P. to +2‰ at 21,000 cal yr B.P., then rapidly decreasing to −8‰ by 14,000 cal yr B.P. The greatest single change in $\delta^{13}C$ was at ca. 700 cal yr B.P. With only two exceptions (both salt-tolerant lowland species), no plant species native to New Zealand are known to use the C_4 photosynthetic pathway (Wardle, 1991). The 10‰ total variation in the MD3 carbon isotope record must therefore be explained in terms of inorganic processes acting on soil carbon dioxide derived from C_3 plants.

Lower water-flow rates over a speleothem surface will cause more calcite to have been precipitated from the fluid at any given point on that speleothem, producing heavier calcite at that point (Dulinski and Rozanski, 1990). This effect is consistent with the elevated values in core MD3 during the LGM, thought to have been drier than today (Pillans *et al.*, 1993). The effect of lowered soil atmosphere CO_2 levels is to raise speleothem $\delta^{13}C$ (Dulinski and Rozanski, 1990), which is seen during the LGM in core MD3, and which is consistent with the known sparser vegetation during these times (McGlone *et al.*, 1993). That the growth rate, linked to the CO_2 flux from soil to cave, was low during the LGM further implies soil CO_2 levels are the predominant effect forcing this record.

From the above, it would be expected that speleothem calcite growing beneath wet, dense lowland forest will be significantly depleted in ^{13}C, compared to calcite formed beneath sparse sub-alpine forest. The MD3 $\delta^{13}C$ record is consistent with low forest productivity lasting from 27,000 to 16,000 cal yr B.P., followed by a very rapid increase in forest productivity in the Mt Arthur region, centered on 15,000 cal yr B.P.

DISCUSSION

Modern flowstones at Mt. Arthur are present beneath forested areas, but are not known beneath areas of alpine scrub and grassland (Fig. 1). The continuous growth of MD3 over the last 31,000 yr thus implies that forest cover of some kind persisted on the surface above the MD3 site over this period, giving a maximum local treeline lowering of 600–700 m at the LGM. Similarly, the dated hiatus in core ED1 implies that from 73,000 to 16,000 cal yr B.P. the treeline was locally at least 300–400 m below its present altitude.

Existing records of late Quaternary glaciation in New Zealand are mostly in the form of glacial deposits on South Island, and are generally poorly dated and fragmentary (Pillans, 1991). The mountainous regions were extensively glaciated during oxygen isotope stage 2, but the moraines are not easily dated, and correlation even between adjacent valleys is difficult. The most widely quoted general chronology over this period is that of Suggate and Moar (1969), which subdivides stage 2 events into the Kumara 2_2 and Kumara 3 advances. Williams (1996) used the stratigraphy of glacial deposits in Aurora Cave, in the southwestern part of South Island, to infer periods of major glacier advance, dating these advances by U-series analysis of interbedded speleothems.

Episodes of loess deposition have also been used to infer times of glacial climate in New Zealand, in particular on North Island where extensive and well-dated tephras permit accurate dating and regional correlation of Quaternary deposits (Pillans, 1991). Alloway *et al.* (1992) were able to obtain a high-

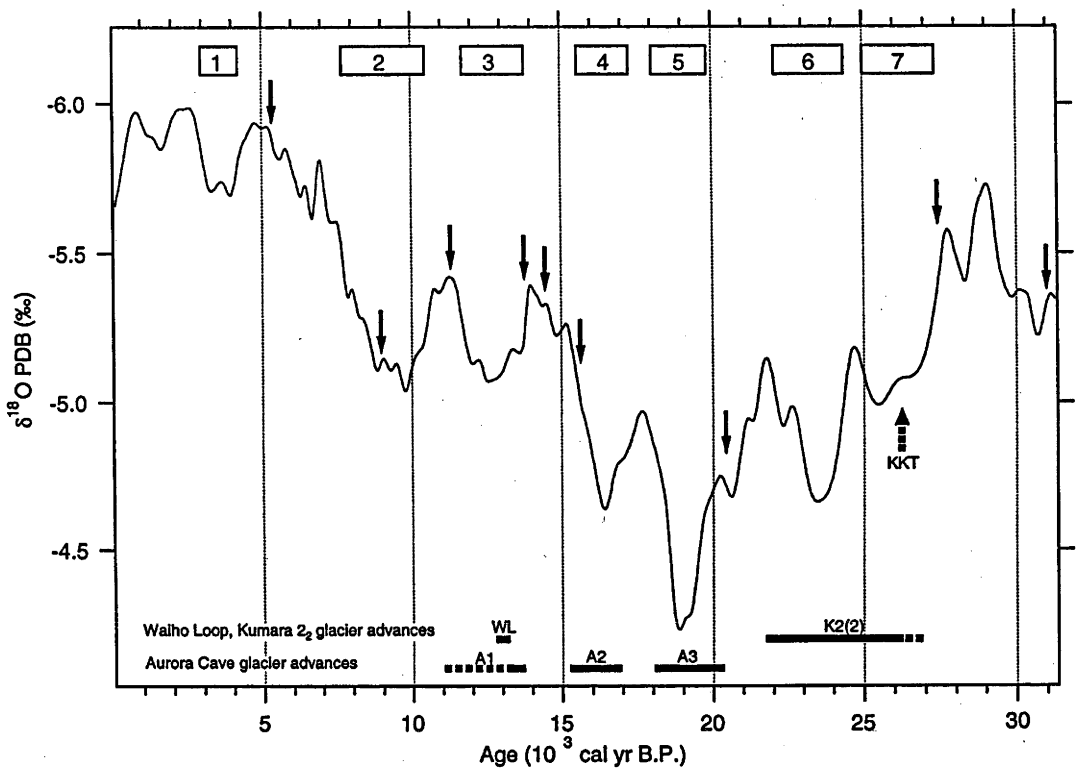

FIG. 4. The MD3 $\delta^{18}O$ record, showing the positive isotope excursions MD3/1 to MD3/7 (numbered). The locations of U-series dates are arrowed. Also shown is the age of the Kawakawa Tephra (Pillans *et al.*, 1993), and the known time ranges of major South Island glacier advances (Denton and Hendy, 1994; Suggate, 1990; Williams, 1996).

resolution record of loess accumulation rate during oxygen isotope stage 2 by examining the quartz (loess) content of andesitic airfall tephra beds in Taranaki, in south-western North Island. Many records of pollen accumulation have been obtained covering stage 1, and to a lesser extent stage 2, in New Zealand. Although these records often have insufficient dating control, there is currently a good understanding of New Zealand vegetation changes since the LGM (McGlone *et al.*, 1993). A very important marker for the LGM in New Zealand is the Kawakawa Tephra, erupted 26,300 cal yr B.P., which is present near the base of stage 2 in many late Quaternary deposits, and which allows accurate correlation between them (Pillans*et al.*, 1993).

Of interest in the MD3 $\delta^{18}O$ record as indicators of local paleoclimate are the seven short positive excursions highlighted in Figure 6, referred to as MD3/1 through MD3/7. These excursions are interpreted as being a response to northward migrations of the STF in the Tasman Sea, which would cause stronger westerly winds and lower temperatures in central and southern New Zealand (McGlone *et al.*, 1993), and which in historic times has favored snowline lowering and glacier advance in western South Island (Fitzharris *et al.*, 1992). Records of dust flux, marine $\delta^{18}O$, and pollen show that during the LGM westerly winds over South Island were considerably stronger and more prevalent than today (Moar and Suggate, 1996; Nelson *et al.*, 1994; Thiede, 1979). Thus, northward migration of the STF and the associated westerly wind belt is a plausible mechanism linking South Island glacier advances to the MD3 isotope excursions.

The correlation of the positive excursions in the MD3 $\delta^{18}O$ record with known South Island glacier advances is excellent, especially for the three best-dated major advances (Fig. 4), the Waiho Loop advance of the Franz Josef Glacier (Denton and Hendy, 1994) and the Aurora 2 and Aurora 3 advances in Fiordland (Williams, 1996). In particular, the MD3/5 excursion, clearly the greatest in magnitude, exactly corresponds to the known timing of the LGM culmination in southwestern New Zealand (Williams, 1996). The Kumara 2_2 glaciation (Suggate and Moar, 1969), although not as well-dated as the above events, began somewhat before 26,000 cal yr B.P.,

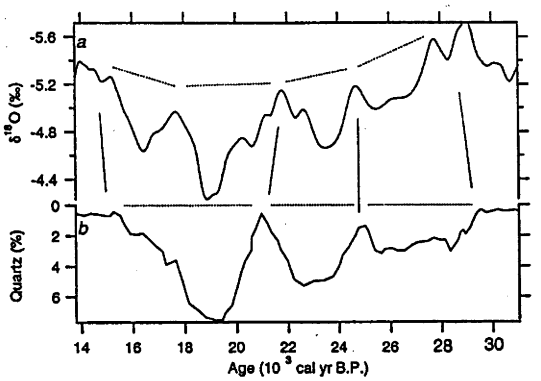

FIG. 5. Comparison of the MD3 $\delta^{18}O$ record (*a*) with the Taranaki quartz accumulation record (*b*) of Alloway *et al.* (1992). The MD3 isotope excursions show close agreement in both magnitude and duration with periods of increased atmospheric dust flux at Taranaki, southwestern North Island.

coinciding with the onset of the MD3/7 isotope excursion (Fig. 4). The fits to the MD3 $\delta^{18}O$ record of the Kumara 3 glaciation, and to another widely quoted South Island glacier advance record from the Waimakariri Valley (Gellatly *et al.*, 1988), are also good, although less certain due to less precise dating of the glacial deposits. The fit of the MD3 $\delta^{18}O$ record to the Taranaki quartz loess flux record of Alloway *et al.* (1992) is also very good (Fig. 5), further implying that the MD3/5, MD3/6, and MD3/7 oxygen isotope excursions coincide with periods favorable to glacier advance.

Table 2 shows a summary of the seven MD3 positive $\delta^{18}O$ excursions, and possible correlations of West Coast and Waimakariri glaciations, based on their reported ages. Whereas Williams (1996) inferred that the Kumara 2_2 advance coincided with his Aurora 3 advance, it is here considered to pre-date that advance, in agreement with its reported age (Suggate, 1990). That the Kumara 2_2 advance spanned two of the MD3 excursions is supported by its correlation with the two Blackwater advances in the Waimakariri Valley (Suggate, 1990). Suggate and Moar (1969) considered the Kumara 3 glacier advance to consist of two closely spaced advances, from ca. 20,000 to 18,900 and ca. 17,500 to 16,700 cal yr B.P., in very good agreement with both the Aurora Cave and MD3 records (Fig. 4). However, (Suggate, 1990) later reported it as being two advances between ca. 19,000 and ca. 16,700 cal yr B.P., while cautioning that it was not well dated.

Gellatly *et al.* (1988) noted that three New Zealand sites record glacier activity at ca. 9000 cal yr B.P., during a period of otherwise low glacier activity from 10,000–6000 cal yr B.P. However, the MD3/2 isotope excursion centered on ca. 9300 cal yr B.P. does not correspond to any convincingly dated glacier advance. The MD3/1 isotope excursion, from ca. 4500 to 3000 cal yr B.P., may correspond to a period of increased glacier activity beginning after ca. 5700 cal yr B.P. (Gellatly *et al.*, 1988), and is here considered significant because of its clarity in both the MD3 and ED1 oxygen isotope records. A younger unnamed excursion, which may correspond to the Little Ice Age, begins at ca. 700 cal yr B.P. and is seen in greater detail from a speleothem at nearby Patarau (Wilson *et al.*, 1979).

The correlation of oxygen isotope results of this study with existing glacier advance records strongly implies that conditions favorable to glacier advance occur synchronously over much of central and southern New Zealand, and, as proposed by others (Fenner *et al.*, 1992; McGlone *et al.*, 1993; Wright *et al.*, 1995), are generally a result of northward movement of the STF and the westerly wind belt in the Tasman Sea. These latitudinal movements are likely to reflect changes in Southern Hemisphere ocean circulation and climate. Figure 6 shows the MD3 $\delta^{18}O$ record with two other high-resolution isotope records, the GISP2 $\delta^{18}O$ (Stuiver *et al.*, 1995) and Vostok δD (Lorius *et al.*, 1985) ice core records from the north and south polar regions, respectively. The only feature of the MD3 record with apparent equivalents in the polar records is the MD3/3 oxygen isotope excursion, which coincides with the Antarctic Cold Reversal (Jouzel *et al.*, 1992) in the Vostok core, and the Younger Dryas interval in the GISP2 core. The timing of these events is very similar for MD3 (13,800–11,700 cal yr B.P.) and GISP2 (12,890–11,650 cal yr B.P.), the most precisely dated of the records, although the MD3/3 event begins somewhat before the GISP2 Younger Dryas. This is further evidence of a glacier advance on South Island at the time of the Younger Dryas, as suggested by Denton and Hendy (1994).

The MD3 carbon isotope record of the last 31,000 years (Fig. 7) is interpreted as a proxy for forest extent through time in the Mt. Arthur area. Seen in this light, this record is remarkably consistent with other records of paleovegetation in the region, (e.g., Moar and Suggate, 1996; Pillans *et al.*, 1993). In particular, the extremely rapid return of dense forest cover at

TABLE 2
Correlation of MD3 Isotope Excursions to South Island Glacial Advances

Age range (10^3 yr)	Mt. Arthur $\delta^{18}O$ excursion	Fiordland glacier advance[a]	Westland glacier advance[b]	Waimakariri glacier advance[c]
4.5 to 3	MD3/1		Arthur's Pass	
10.5 to 7.5	MD3/2		McGrath II	
13.8 to 11.7	MD3/3	Aurora 1	Waiho Loop	McGrathI
17.5 to 15.5	MD3/4	Aurora 2	Later Kumara 3	Poulter
20 to 18	MD3/5	Aurora 3	Earlier Kumara 3	
24.5 to 22	MD3/6	Kumara 2_2	Blackwater (II)	
27 to 25	MD3/7	Kumara 2_2	Blackwater (I)	

[a] Williams (1996).
[b] Denton and Hendy (1994); Suggate and Moar (1969).
[c] The Waimakariri advances (Gellatly *et al.*, 1988; Suggate, 1990) are less certain correlations, due to less-well-constrained ages.

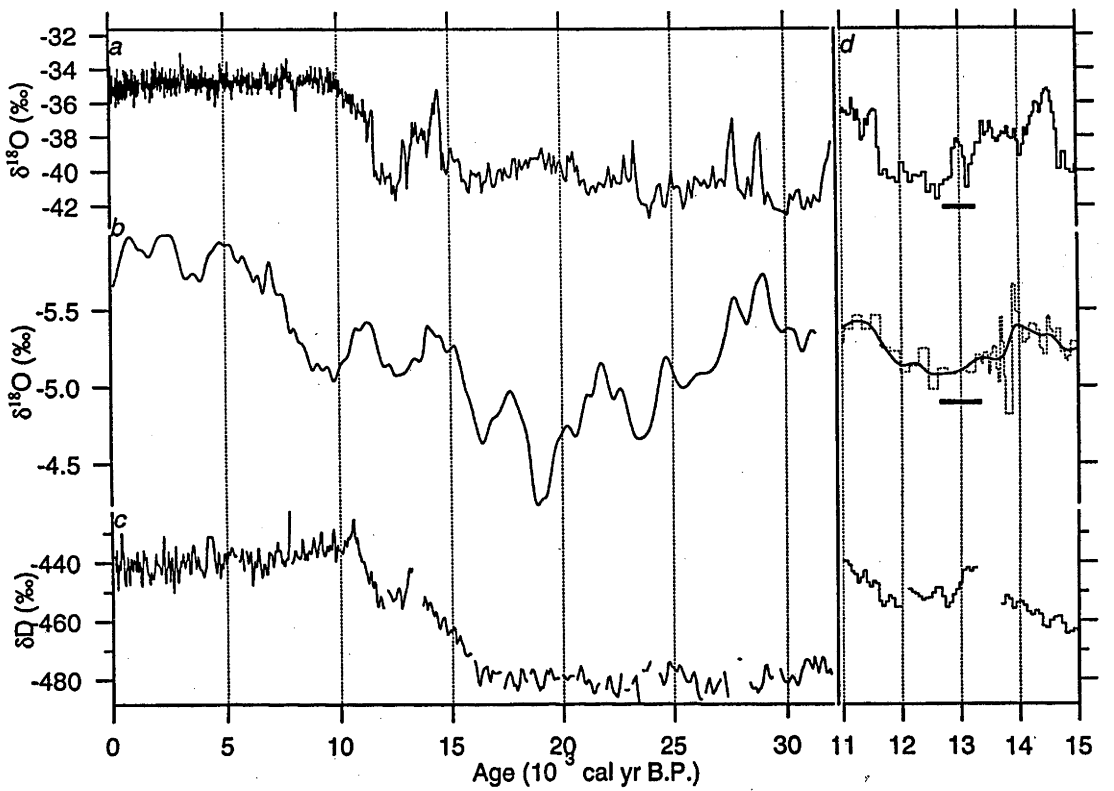

FIG. 6. A comparison of the MD3 $\delta^{18}O$ record (*b*) to the GISP2 ice core $\delta^{18}O$ record (*a*; Stuiver *et al.*, 1995) and the Vostok ice core δD record (*c*; Lorius *et al.*, 1985). (*d*) Detail of the period 11,000–15,000 cal yr B.P. Black bars show $\pm 2\sigma$ age errors at 13,000 cal yr B.P. for the GISP2 and MD3 records.

15,000 cal yr B.P. implied by the MD3 $\delta^{13}C$ data, also coinciding with a sudden increase in MD3 growth rate and the resumption of growth of ED1 (Fig. 2), is in very close agreement with changes observed in nearby pollen records (W. McLea, C. Singer, and J. Shulmeister, unpublished data). The LGM period of 27,000–15,500 cal yr B.P. defined by Pillans *et al.* (1993) for central New Zealand on the basis of available pollen and geomorphic data exactly coincides with the period of the highest values of $\delta^{13}C$ in MD3 (Fig. 9) in Pillans *et al.*, (1993). Again, as predicted by existing pollen data (McGlone *et al.*, 1993), the early Holocene appears to have been the most favorable time for forest growth, with conditions becoming gradually less favorable through the late Holocene.

Reinforcing the likelihood that soil conditions driven by vegetation changes are the dominant forcing factor for the $\delta^{13}C$ record is the very sudden rise in $\delta^{13}C$ at ca. 700 cal yr B.P., a time at which drastic climate-driven forest expansion seems unlikely, but which coincides with the first signs of human modification of the New Zealand environment (McGlone *et al.*, 1994). The sudden change to more-vigorous forest growth indicated at this time is perhaps a result of the human extermination of New Zealand's browsing megafauna, thought to have had a major impact on the forest ecology (Wardle, 1991).

CONCLUSIONS

Speleothem sample MD3 from Nettlebed cave grew continuously over the last 31,000 years, allowing construction of high-resolution paleoenvironmental records covering this period. The continuous growth of the speleothem implies that forest was present above the cave throughout this period, and thus that the LGM treeline was locally no more then 600–700 m below its modern position. A growth hiatus in a second speleothem, ED1, similarly implies that the local treeline was at least 300–400 m below its modern position for the period 73,000–16,000 cal yr B.P.

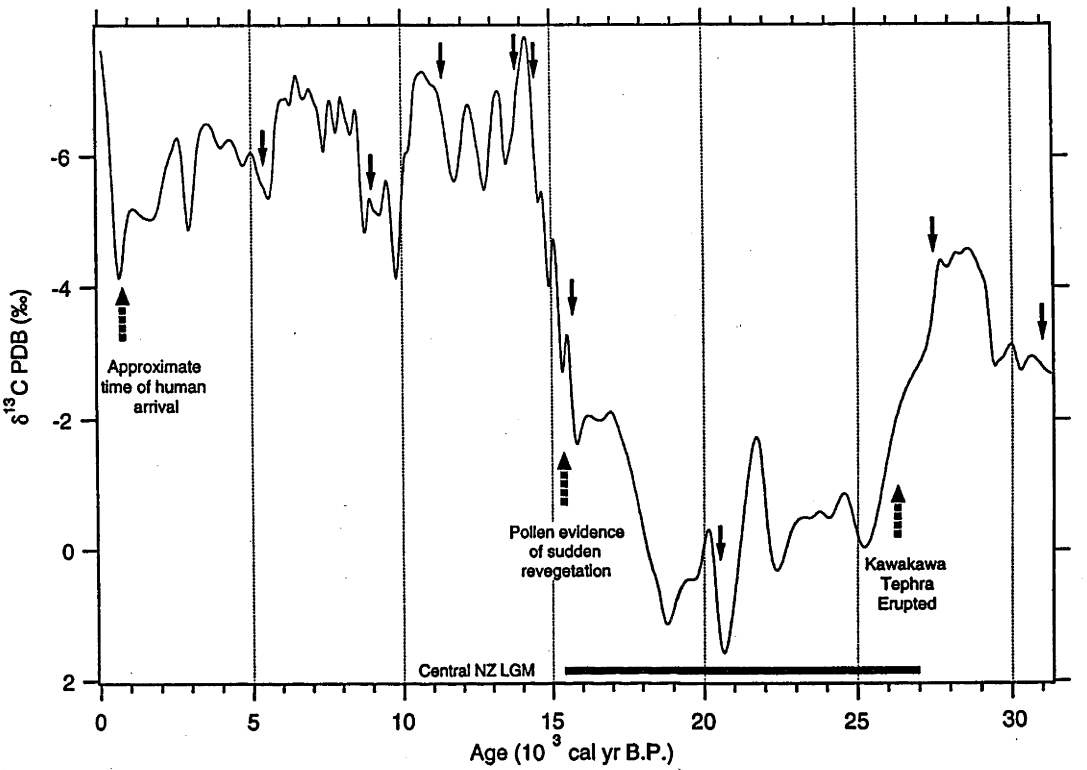

FIG. 7. MD3 $\delta^{13}C$ record (locations of U-series dates arrowed). Shown are the timings of the Kawakawa Tephra (Pillans *et al.*, 1993), the sudden reafforestation observed from pollen records near Mt. Arthur (W. McLea, C. Singer, and J. Shulmeister, unpublished data), and the likely time of the first significant human modification of the South Island forest environment (McGlone *et al.*, 1994). The timing of the central New Zealand LGM is from Pillans *et al.*, (1993).

The 1.8‰ total variation in the $\delta^{18}O$ record from MD3 over the last 31,000 yr must be explained predominantly in terms of variation in the $\delta^{18}O$ of local meteoric waters, rather than in terms of temperature. Seven short-duration excursions to heavier values in the MD3 $\delta^{18}O$ record are interpreted as recording northward movements of the Subtropical Front (STF) in the Tasman Sea, expected to coincide with periods of increased westerly winds in western South Island and thus with periods of increased glacier activity. Supporting this interpretation are the excellent fits to MD3 $\delta^{18}O$ excursions of the best-dated major South Island glacier advances. Based on this relationship, there were four glacier advances on South Island during oxygen isotope stage 2 (27,000–15,500 cal yr B.P.), including early and late events in both the Kumara 2_2 and the Kumara 3 advances. The most extreme glacial conditions appear to have occurred at 19,000 yr B.P. in agreement with earlier U-series dating in southwestern New Zealand. An isotope excursion from 13,800 to 11,700 cal yr B.P. coincides with the Waiho Loop advance, and is taken as further evidence of a glacier advance in southern New Zealand at the time of the Younger Dryas Stade in northern Europe, although the earlier onset of the New Zealand advance suggests the two events may not be directly related.

The $\delta^{13}C$ record in MD3 is interpreted in terms of inorganic processes acting on carbon derived purely from C_3 plants, and appears to be closely related to changes in soil CO_2 concentration above the cave. As such, it is considered an excellent proxy for forest productivity above the cave, a conclusion strongly supported by its similarity to pollen-based records of forest extent in the region. Notably, an extremely rapid increase in forest cover, coincident with a significant increase in speleothem growth rate, was centered on 15,000 cal yr B.P., marking the end of glacial maximum conditions in the region. A rapid increase in forest productivity at ca. 700 cal yr B.P. is attributed to human modification of the environment, possibly

indirectly by the extermination of New Zealand's browsing megafauna.

ACKNOWLEDGMENTS

The speleothem samples were collected with the permission of the New Zealand Department of Conservation, and with the enthusiastic assistance of members of Wellington Caving Group, Victoria Cavers, and the National University Caving Club. We thank Brad Pillans and John Chappell for their incisive comments, and the referees for constructive reviews.

REFERENCES

Alloway, B. V., Stewart, R. B., Neall, V. E., and Vucetich, C. G. (1992). Climate of the last glaciation in New Zealand, based on aerosolic quartz influx in an andestic terrain. *Quaternary Research* **38,** 170–179.

Baker, A., Ito, E., Smart, P. L., and McEwan, R. F. (1997). Elevated and variable values of ^{13}C in speleothems in a British cave system. *Chemical Geology* **136,** 263–170.

Bard, E., Arnold, M., Fairbanks, R. G., and Hamelin, B. (1993). ^{230}Th-^{234}U and ^{14}C ages obtained by mass spectrometry on corals. *Radiocarbon* **35,** 191–199.

Broecker, W. S., Peteet, D. M., and Rind, D. (1985). Does the ocean-atmosphere system have more than one stable mode of operation? *Nature* **315,** 21–26.

Chappell, J., and Shackleton, N. J. (1986). Oxygen isotopes and sea level. *Nature* **324,** 137–140.

Dansgaard, W. (1964). Stable isotopes in precipitation. *Tellus* **XVI,** 436–468.

Dansgaard, W., Johnsen, S. J., Clausen, H. B., Dahl-Jensen, D., Gundestrup, N. S., Hammer, C. U., Hvidberg, C. S., Steffensen, J. P., Sveinbjörnsdottir, A. E., Jouzel, J., and Bond, G. (1993). Evidence for general instability of past climate from a 350-kyr ice-core record. *Nature* **364,** 218–220.

Denton, D. H., and Hendy, C. H. (1994). Younger Dryas age advance of the Franz Josef Glacier in the Southern Alps of New Zealand. *Science* **264,** 1434–1437.

Dorale, J. A., Gonzâlez, L. A., Reagan, M. K., Pickett, D. A., Murrell, M. T., and Baker, R. G. (1992). A high-resolution record of Holocene climate change in speleothem calcite from Cold Water Cave, Northeast Iowa. *Science* **258,** 1626–1630.

Dulinski, M., and Rozanski, K. (1990). Formation of $^{13}C/^{12}C$ isotope ratios in speleothems: A semi-dynamic model. *Radiocarbon* **32,** 7–16.

Fenner, J., Carter, L., and Stewart, R. (1992). Late Quaternary paleoclimatic and paleoceanographic change over northern Chatham Rise, New Zealand. *Marine Geology* **108,** 383–404.

Fitzharris, B. B., Hay, J. E., and Jones, P. D. (1992). Behaviour of New Zealand glaciers and atmospheric circulation changes over the past 130 years. *The Holocene* **2,** 97–106.

Gage, M. (1965). Some characteristics of Pleistocene cold climates in New Zealand. *Transactions of the Royal Society of New Zealand: Geology* **3,** 11–21.

Garnier, B. J. (1958). "The Climate of New Zealand." Edward Arnold, London.

Gat, J. R. (1980). The isotopes of hydrogen and oxygen in precipitation. *In* "Handbook of Environmental Geochemistry" (P. Fritz and J. C. Fontes, Eds.), pp. 21–47. Elsevier, Amsterdam.

Gellatly, A. F., Chinn, T. J., and Röthlisberger, F. (1988). Holocene glacier variations in New Zealand: A review. *Quaternary Science Reviews* **7,** 227–242.

Hendy, C. H. (1971). The isotope geochemistry of speleothems—I. The calculation of the effects of different modes of formation on the isotopic composition of speleothems and their applicability as palaeoclimatic indicators. *Geochimica et Cosmochimica Acta* **35,** 801–824.

Hendy, C. H., and Wilson, A. T. (1968). Palaeoclimatic data from speleothems. *Nature* **219,** 48–51.

Johnsen, S. J., Dansgaard, W., and White, J. W. C. (1989). The origin of Arctic precipitation under present and glacial conditions. *Tellus* **41B,** 452–468.

Jouzel, J., Petit, J. R., Barkov, N. I., Barnola, J. M., Chappellaz, J., Ciais, P., Kotkyakov, V. M., Lorius, C., Petrov, V. N., Raynaud, D., and Ritz, C. (1992). The last deglaciation in Antarctica: Further evidence of a "Younger Dryas" type climatic event. *In* "The Last Deglaciation: Absolute and Radiocarbon Chronologies" (E. Bard and W. S. Broecker, Eds.), pp. 231–266. Springer-Verlag, Berlin.

Li, W. X., Lundberg, J., Dickin, A. P., Ford, D. C., Schwarcz, H. P., McNutt, R., and Williams, D. (1989). High-precision mass-spectrometric uranium-series dating of cave deposits and implications for palaeoclimate studies. *Nature* **339,** 534–536.

Lorius, C., Jouzel, J., Ritz, C., Merlivat, L., Barkov, N. I., Korotkevich, Y. S., and Kotlyakov, V. M. (1985). A 150,000-year climate record from Antarctic ice. *Nature* **316,** 591–596.

McGlone, M. S. (1988). New Zealand. *In* "Vegetation History" (B. Huntly and T. Web III, Eds.), pp. 557–599. Kluwer Academic, Dordrecht.

McGlone, M. S., Anderson, A. J., and Holdaway, R. N. (1994). An ecological approach to the Polynesian settlement of New Zealand. *In* "The Origins of the First New Zealanders" (D. G. Sutton, Ed.), pp. 136–163. Auckland University Press, Auckland.

McGlone, M. S., Salinger, M. J., and Moar, N. T. (1993). Paleovegetation studies of New Zealand's climate since the Last Glacial Maximum. *In* "Global Climates since the Last Glacial Maximum" (H. E. Wright, J. E. Kutzbach, T. Webb III, W. F. Ruddiman, F. A. Street-Perrott, and P. J. Bartlein, Eds.), pp. 294–317. University of Minnesota Press, Minneapolis.

Merlivat, L., and Jouzel, J. (1979). Global climatic interpretation of the deuterium-oxygen-18 relationship for precipitation. *Journal of Geophysicial Research* **84,** 5029–5033.

Miller, G. H., Magee, J. W., and Jull, A. J. T. (1997). Low-latitude glacial cooling in the Southern Hemisphere from amino-acid racemization in emu eggshells. *Nature* **385,** 241–244.

Moar, N. T., and Suggate, R. P. (1996). Vegetation history from the Kaihinui (Last) Interglacial to the present, West Coast, South Island, New Zealand. *Quaternary Science Reviews* **15,** 521–547.

Nelson, C. S., Hendy, C. H., and Cuthbertson, A. M. (1994). Oxygen isotope evidence for climatic contrasts between Tasman Sea and Southwest Pacific Ocean during the late Quaternary. *In* "Evolution of the Tasman Sea" (G. J. v. d. Linden, K. M. Swanson, and R. J. Muir, Eds.), pp. 181–197. Balkema, Rotterdam.

Pillans, B. (1991). New Zealand Quaternary stratigraphy: An overview. *Quaternary Science Reviews* **10,** 405–418.

Pillans, B., McGlone, M., Palmer, A., Mildenhall, D., Alloway, B., and Berger, G. (1993). The Last Glacial Maximum in central and southern North Island, New Zealand: A paleoenvironmental reconstruction using the Kawakawa Tephra Formation as a chronostratigraphic marker. *Palaeogeography, Palaeoclimatology, Palaeoecology* **101,** 283–304.

Ravens, J. M. (1986). "Nettlebed Cave." New Zealand Speleological Society, Wellington.

Ravens, J. M. (1992). "The Ellis Basin Cave System." New Zealand Speleological Society, Wellington.

Salinger, M. J. (1983). New Zealand climate: The last 5 million years. *In* "Late Cainozoic Palaeoclimates of the Southern Hemisphere" (J. C. Vogel, Ed.), pp. 131–150. Balkema, Rotterdam.

Soons, J. M. (1979). Late Quaternary environments in the central South Island of New Zealand. *New Zealand Geographer* **35,** 16–23.

Stirling, C. H., Esat, T. M., McCulloch, M. T., and Lambeck, K. (1995). High-precision U-series dating of corals from Western Australia and implications for the timing and duration of the last interglacial. *Earth and Planetary Science Letters* **135,** 115–130.

Stuiver, M., Grootes, P. M., and Braziunas, T. F. (1995). The GISP2 $\delta^{18}O$ climate record of the past 16,500 years and the role of the sun, ocean, and volcanoes. *Quaternary Research* **44,** 341–354.

Stuiver, M., and Reimer, P. J. (1993). Extended ^{14}C data base and revised Calib 3.0 ^{14}C age calibration program. *Radiocarbon* **35,** 215–230.

Suggate, R. P., and Moar, N. T. (1969). Revision of the chronology of the late Otira glacial. *New Zealand Journal of Geology and Geophysics* **13,** 742–746.

Suggate, R. P. (1990). Late Pliocene and Quaternary glaciations of New Zealand. *Quaternary Science Reviews* **9,** 175–197.

Taylor, C. B. (1990). "Stable Isotope Compositions of Monthly Precipitation Samples Collected in New Zealand and Rarotonga." Department of Scientific and Industrial Research.

Thiede, J. (1979). Wind regimes over the late Quaternary southwest Pacific Ocean. *Geology* **7,** 259–262.

Thompson, L. G., Mosley-Thompson, E., Davis, M. E., Lin, P.-N., Henderson, K. A., Cole-Dai, J., Bolzan, J. F., and Liu, K.-b. (1995). Late Glacial stage and Holocene tropical ice core records from Huascarán, Peru. *Science* **269,** 46–50.

Wardle, P. (1991). "Vegetation of New Zealand." Cambridge University Press, Cambridge, UK.

Williams, P. W. (1996). A 230ka record of glacial and interglacial events from Aurora Cave, Fiordland, New Zealand. *New Zealand Journal of Geology and Geophysics* **39,** 225–241.

Wilson, A. T., Hendy, C. H., and Reynolds, C. P. (1979). Short-term climate change and New Zealand temperatures during the last millenium. *Nature* **279,** 315–317.

Wright, I. C., McGlone, M. S., Nelson, C. S., and Pillans, B. J. (1995). An integrated latest Quaternary (Stage 3 to present) paleoclimatic and Paleoceanographic record from offshore northern New Zealand. *Quaternary Research* **44,** 283–293.

Corrections to page proofs

Page 1

Address line: Insert a comma, to read: "...*Canberra, ACT 0200, Australia*"

Key Words, line 1: Insert a space, to read: "...*Words:* New..."

Page 2

Column 2, line 12: Delete the extra bracket, to read: "...(Ravens, 1986, 1992),..."

Page 4

Column 2, line 12: Delete the extra bracket and full stop, to read: "...(Fig. 3)."

Table 1 footnote *b*, line 2: Insert ", ED1A1" to read "...samples MD3A5, ED1A1 and ED1A4,..."

Page 5

Column 1, line 15: Insert "temporal " to read: "...of the temporal temperature..."

Column 1, line 18-19: Move line break to place "–0.24‰/°C" on one line.

Column 2, lines 13-14: Replace "–0.5, 0.5, and 0.5‰, respectively" with "+0.6‰" to read "...as much as +0.6‰ (Johnsen..."

Page 6

Column 2, line 16: Insert "that" to read "...implies that soil CO_2..."

Page 7

Column 1, line 13: Insert space to read "(Pillans *et*..."

Page 8

Column 1, line 2: Swap "of" and "to" to read: "...fits of the MD3 $\delta^{18}O$ record to the..."

Column 1, line 24: Move bracket and delete comma, to read "...However, Suggate (1990)..."

Column 2, lines 10-12: Insert "that" and "they" to read "...Zealand, and that, as proposed... ...1995), they are generally..."

Table 2, columns 3-5: Shift "Arthur's Pass", "McGrath II", "Kumara 2_2", "Kumara 2_2", "Blackwater (II)", and "Blackwater (I)" one column to the right.

Table 2, column 5: Text should be flush left

Page 9

Column 1, row 5: Replace "(W. McLea, C. Singer, and J. Shulmeister, unpublished data)." with "(Singer *et al.*, 1998)."

Column 1, rows 9-10: Replace "(Fig. 9) in Pillans *et al.* (1993)" with "(Fig. 7)" to read "...MD3 (Fig. 7). Again, as..."

Page 10

Figure 7 caption, line 1: Replace "sudden" with "rapid" to read: "...1993), the rapid"

Figure 7 caption, line 2: Replace "(W. McLea, C. Singer, and J. Shulmeister, unpublished data)" with "(Singer *et al.*, 1998)"

Figure 7 caption, line 3: Insert "(black bar)" to read: "...Zealand LGM (black bar) is from..."

Column 1, lines 14-15: Replace "including" with "being" to read: "...yr B.P.), being early and late..."

Page 11

Acknowledgments, line 4: Move "and" and insert "Linda Ayliffe" to read: "...thank Brad Pillans, John Chappell, and Linda Ayliffe for their..."

References: Insert new reference in list: "Singer, C., Shulmeister, J., and McLea, B. (1998). Evidence against a significant Younger Dryas cooling event in New Zealand. *Science* **281,** 812–814."

Page 12

References, Column 1, line 18: Insert "Lower Hutt, NZ" to read "...and Industrial Research, Lower Hutt, NZ."

Appendix 2. MD3 Stable isotope and trace element data

Data here are for 117 homogenised increments of core MD3, each of 5 mm in length. See chapters 6 and 7 for unit definitions. Stable isotope data sampled at higher resolutions and reported in chapter 6 will be submitted to internet data archives upon the publication of Hellstrom *et al.* (in press; appendix 1).

Sample Name	Depth (mm)	Age (yr)	$\delta^{13}C$ (‰)	$\delta^{18}O$ (‰)	Mg (ppb)	Sr (ppb)	Ba (ppb)	U ppb	U.V. lum.
MD3B 117	2.5	128.6	-7.51	-5.73	309232	34635	3007	47	166
MD3B 116	7.5	385.8	-6.31	-5.78	337620	35751	3477	59	164
MD3B 115	12.5	643	-4.05	-5.95	380466	36933	2688	34	147
MD3B 114	17.5	900.2	-4.94	-5.99	346218	34541	2579	38	144
MD3B 113	22.5	1157.4	-5.19	-5.86	353446	34337	2820	48	139
MD3B 112	27.5	1414.6	-5.09	-5.93	374855	35625	2871	46	143
MD3B 111	32.5	1671.8	-5.05	-5.80	363656	33711	2633	50	156
MD3B 110	37.5	1929	-5.15	-5.94	350957	33623	2648	50	159
MD3B 109	42.5	2186.2	-5.78	-5.99	346605	37712	3352	56	161
MD3B 108	47.5	2443.4	-6.08	-5.96	345152	37954	3348	60	164
MD3B 107	52.5	2700.6	-6.22	-6.00	328336	35299	3409	62	157
MD3B 106	57.5	2957.8	-4.73	-5.87	395642	35160	2923	55	140
MD3B 105	62.5	3215	-6.03	-5.68	348161	35853	2952	62	153
MD3B 104	67.5	3472.2	-6.45	-5.73	388894	33614	2716	68	145
MD3B 103	72.5	3729.4	-6.46	-5.78	383959	32482	2898	71	128
MD3B 102	77.5	3986.6	-6.12	-5.62	391851	30576	2265	63	121
MD3B 101	82.5	4243.8	-6.26	-5.88	365404	36810	2642	47	111
MD3B 100	87.5	4501	-6.16	-5.86	383130	35236	2561	53	116
MD3B 099	92.5	4758.2	-5.82	-5.97	381389	35570	2527	55	119
MD3B 098	97.5	5015.4	-6.11	-5.87	370975	36936	2742	53	131
MD3B 097	102.5	5272.6	-5.63	-6.00	369381	37972	2672	44	123
MD3B 096	107.5	5448.3	-5.56	-5.73	402816	36675	2601	57	126
MD3B 095	112.5	5542.5	-5.37	-5.92	399451	37216	2677	52	125
MD3B 094	117.5	5636.7	-5.37	-5.65	387262	31120	2366	63	127
MD3B 093	122.5	5730.9	-5.66	-5.92	346788	37261	2711	35	146
MD3B 092	127.5	5825.1	-6.80	-5.94	327765	40146	3498	65	165
MD3B 091	132.5	5919.3	-6.57	-5.80	353233	38488	3174	69	176
MD3B 090	137.5	6013.5	-6.99	-5.66	346098	27246	2209	69	178
MD3B 089	142.5	6107.7	-6.68	-5.88	308853	37312	3078	54	178
MD3B 088	147.5	6201.9	-7.16	-5.75	334409	36191	3094	63	163
MD3B 087	152.5	6296.1	-6.53	-5.40	331327	33591	2927	78	149
MD3B 086	157.5	6390.3	-6.91	-5.83	340811	29038	2301	51	147
MD3B 085	162.5	6484.5	-7.47	-5.97	273873	39479	3180	45	135
MD3B 084	167.5	6578.7	-7.08	-5.62	336232	33371	2935	85	164
MD3B 083	172.5	6672.9	-6.86	-5.39	351446	25806	2055	71	174
MD3B 082	177.5	6767.1	-6.89	-5.51	346283	32704	3014	93	178
MD3B 081	182.5	6861.3	-6.88	-5.96	279316	39307	3102	39	176
MD3B 080	187.5	6955.5	-7.19	-5.98	283766	39454	3396	55	187
MD3B 079	192.5	7049.7	-6.85	-5.73	302043	38867	3572	85	210
MD3B 078	197.5	7143.9	-6.75	-5.61	325469	34841	2796	61	208
MD3B 077	202.5	7238.1	-6.77	-5.49	318953	33977	2715	45	194
MD3B 076	207.5	7332.3	-6.59	-5.69	284866	39511	3264	49	181
MD3B 075	212.5	7426.5	-5.47	-5.51	361005	36243	2870	65	190
MD3B 074	217.5	7520.7	-6.79	-5.69	283138	41170	3219	44	187
MD3B 073	222.5	7614.9	-6.96	-5.63	338063	37895	3425	77	166
MD3B 072	227.5	7709.1	-6.80	-5.54	367742	34726	2709	59	172
MD3B 071	232.5	7803.3	-6.30	-5.24	431624	28380	2338	76	180
MD3B 070	237.5	7897.5	-6.04	-5.10	398927	32984	2386	53	173
MD3B 069	242.5	7991.7	-7.57	-5.73	304814	41879	2768	22	169

Sample Name	Depth (mm)	Age (yr)	$\delta^{13}C$ (‰)	$\delta^{18}O$ (‰)	Mg (ppb)	Sr (ppb)	Ba (ppb)	U ppb	U.V. lum.
MD3B 068	247.5	8085.9	-6.37	-5.37	308167	42387	2957	29	159
MD3B 067	252.5	8180.1	-6.71	-5.18	338957	36870	3177	82	182
MD3B 066	257.5	8274.3	-6.41	-5.24	264721	40831	2981	31	163
MD3B 065	262.5	8368.5	-6.02	-5.37	305285	39120	2899	50	177
MD3B 064	267.5	8462.7	-6.90	-5.26	297481	42961	3477	54	192
MD3B 063	272.5	8556.9	-6.85	-5.21	308826	41519	3488	68	182
MD3B 062	277.5	8651.1	-5.36	-5.23	291911	39976	2691	23	177
MD3B 061	282.5	8745.3	-4.89	-5.12	305689	39456	3048	48	162
MD3B 060	287.5	8839.5	-4.52	-5.00	310696	38449	2953	58	146
MD3B 059	292.5	8933.7	-5.95	-5.11	302384	43789	3572	65	157
MD3B 058	297.5	9034.275	-4.95	-5.29	314910	42687	3081	51	173
MD3B 057	302.5	9187.725	-5.25	-5.06	347896	34634	3368	15	181
MD3B 056	307.5	9341.175	-4.96	-5.03	368670	46893	3042	38	176
MD3B 055	312.5	9494.625	-5.81	-5.26	332397	42314	3166	62	188
MD3B 054	317.5	9648.075	-5.17	-5.06	360399	39507	3087	94	195
MD3B 053	322.5	9801.525	-3.83	-4.93	377868	37355	2619	75	190
MD3B 052	327.5	9954.975	-4.98	-5.17	392891	41260	3307	88	190
MD3B 051	332.5	10108.45	-6.24	-5.16	355254	41391	3581	98	192
MD3B 050	337.5	10261.85	-5.83	-5.20	326015	42522	3612	82	209
MD3B 049	342.5	10415.32	-7.18	-5.14	316485	42811	3829	103	217
MD3B 048	347.5	10568.77	-7.16	-5.28	300201	43749	3822	91	219
MD3B 047	352.5	10722.22	-7.31	-5.51	303482	45878	4436	104	221
MD3B 046	357.5	10875.67	-7.18	-5.28	299201		4311	106	224
MD3B 045	362.5	11029.12	-7.06	-5.37	312707	45156	4493	112	226
MD3B 044	367.5	11182.57	-7.05	-5.46	305391	46459	4625	111	222
MD3B 043	372.5	11336.02	-6.69	-5.37	311851	44426	4364	106	225
MD3B 042	377.5	11491.65	-6.25	-5.46	311824	44731	4196	87	228
MD3B 041	382.5	11651.95	-5.71	-5.25	321903	42300	3965	88	221
MD3B 040	387.5	11812.25	-5.63	-5.22	326026	42535	3767	77	214
MD3B 039	392.5	11972.55	-6.11	-5.09	334960	42580	3958	85	186
MD3B 038	397.5	12132.85	-6.74	-5.13	310960	42434	4095	91	190
MD3B 037	402.5	12293.15	-6.75	-5.24	320062	44803	4347	89	214
MD3B 036	407.5	12453.45	-6.29	-4.98	313606	42631	4098	87	209
MD3B 035	412.5	12613.75	-5.96	-5.11	318330	42323	3991	90	208
MD3B 034	417.5	12774.05	-5.36	-5.07	323230	42415	3950	77	201
MD3B 033	422.5	12934.35	-6.06	-5.10	303654	42713	3878	80	200
MD3B 032	427.5	13094.65	-6.86	-5.08	304991	44803	4257	102	192
MD3B 031	432.5	13254.95	-6.78	-5.20	321539	44276	3854	87	198
MD3B 030	437.5	13415.25	-5.84	-5.15	323488	43819	3540	69	179
MD3B 029	442.5	13575.55	-6.21	-5.25	348671	43809	3598	88	176
MD3B 028	447.5	13735.85	-7.18	-5.47	375134	40272	3384	108	177
MD3B 027	452.5	13938.5	-7.40	-5.49	366472	41932	3712	116	146
MD3B 026	457.5	14233.5	-6.92	-5.42	379201	41718	3633	106	130
MD3B 025	462.5	14522	-5.36	-5.35	381110	43887	3715	87	121
MD3B 024	467.5	14772	-4.24	-5.34	394667	42507	2860	50	155
MD3B 023	472.5	15022	-4.46	-5.33	395507	41659	3028	68	149
MD3B 022	477.5	15272	-2.79	-5.13	425350	39696	2480	49	141
MD3B 021	482.5	15522	-2.51	-5.09	425297	37627	2160	49	117
MD3B 020	487.5	15991	-2.60	-5.26	431452	30694	1809	75	97
MD3B 019	492.5	16957.8	-1.67	-5.24	465659	27642	1638	116	83
MD3B 018	497.5	17924.6	0.38	-4.68	403615	16239	848	140	62
MD3B 017	502.5	18891.4	0.63	-4.45	410851	14498	851	172	62
MD3B 016	507.5	19858.2	0.52	-4.79	455106	20921	1140	125	70
MD3B 015	512.5	20893.62	-0.28	-4.99	489186	21625	1567	135	89
MD3B 014	517.5	22089.47	-0.05	-4.64	470364	17628	1490	184	107
MD3B 013	522.5	23285.32	-0.25	-4.69	469826	16348	1163	164	104
MD3B 012	527.5	24481.17	-0.47	-5.14	500377	22519	1397	105	99
MD3B 011	532.5	25677.02	-1.84	-5.15	515197	28341	1691	91	102
MD3B 010	537.5	26872.85	-3.48	-5.33	508139	28167	2019	121	122
MD3B 009	542.5	27684.85	-4.26	-5.46	507717	30569	2364	134	133
MD3B 008	547.5	28116.95	-4.66	-5.52	520489	30805	2323	124	137
MD3B 007	552.5	28549.05	-4.48	-5.57	521994	30847	2322	118	132

Sample Name	Depth (mm)	Age (yr)	$\delta^{13}C$ (‰)	$\delta^{18}O$ (‰)	Mg (ppb)	Sr (ppb)	Ba (ppb)	U ppb	U.V. lum.
MD3B 006	557.5	28981.15	-3.64	-5.64	542308	32676	2316	91	129
MD3B 005	562.5	29413.25	-2.85	-5.26	516368	26672	1721	79	128
MD3B 004	567.5	29845.35	-3.12	-5.32	494362	26252	1898	123	127
MD3B 003	572.5	30277.45	-2.67	-5.16	483457	24548	1809	111	134
MD3B 002	577.5	30709.55	-2.72	-5.23	482455	28672	1950	105	128
MD3B 001	582.5	31141.65	-2.48	-5.24	448137	27778	1924	138	104

Appendix 3. Samples collected

All samples collected in the course of this study are listed. See chapter 4 for additional sample details.

SAMPLE	TYPE	DESCRIPTION	LOCATION	DATE
AM1	Calcite fragment	300gm orange calcite with white crust	Mullamullang Cave main breakdown passage, Nullarbor Plain	Dec-94
AM2	Contaminated calcite fragment	2 mm white crust on 7 mm brick red layer	Mullamullang Cave main breakdown passage, Nullarbor Plain	Dec-94
AT1	Flowstone fragment	30 mm planar banded calcite, cream-brown bands	Thampana rockhole, Nullarbor plain	Dec-94
AW1	Flowstone fragments	2 small fragments, cream, banded	Witches Cave, Nullarbor Plain	Dec-94
AW2	Contaminated flowstone fragment	Small piece, brown banded calcite	Witches Cave, Nullarbor Plain	Dec-94
AX1	Calcite lump	Cream calcite, small crystals on surface	Unknown, Nullarbor Plain	Dec-94
CF1	Vein Calcite fragment	Orange-white calcite, large crystals	Karst surface, Cliefden Caves	Jun-95
ED1	50 mm calcite core	400 mm in 8 sections	Flowstone, downstream passage, Exhale Air	Jan-96
EK1	Arthur Marble fragment	20 mm*50 mm core, grey marble	Eyles Creek, Pearse Resurgence	Aug-94
HS1	20 mm flowstone core	130 mm in 6 sections	Flowstone below Headsnapper Squeeze, Nettlebed	Aug-94
HS2	20 mm flowstone core	52 mm in 2 sections	Flowstone below Headsnapper Squeeze, Nettlebed	Aug-94
HS3	20 mm flowstone core	73 mm in 2 sections	Flowstone below Headsnapper Squeeze, Nettlebed	Aug-94
JN1	Calcite fragments	Flowstone chips from track cutting	Main tourist cave, Jenolan	Apr-95
MD1	20 mm flowstone core	≥190 mm, in 3 sections	Flat flowstone floor at bottom of main Meltdown flow, Nettlebed	Aug-94
MD10	50 mm calcite core	650 mm in 10 sections	Base of main Meltdown flowstone	Feb-96
MD2	20 mm flowstone core	195 mm in 4 sections	Flat flowstone floor at bottom of main Meltdown flow	Aug-94
MD3	50 mm flowstone core	1.1 m, in 17 pieces, includes silt near base	Top of Coredrop Pitch, The Meltdown, Nettlebed	Mar-95
MD4	Acidified water sample	1 litre for U-series analysis	Drip from roof onto base of main meltdown flow	Mar-95
MD5	Acidified water sample	125 ml for ICPMS	Drip from roof onto base of main meltdown flow	Sep-95
MD6	Water sample	125 ml for stable isotope analysis	Drip from roof onto base of main meltdown flow	Jun-95
MD7	Silt	Grey silt from passage floor	Near base of Meltdown, Nettlebed	Mar-95

SAMPLE	TYPE	DESCRIPTION	LOCATION	DATE
MD8	50 mm flowstone core	25 cm, in 7 pieces	Top of Coredrop Pitch, The Meltdown, Nettlebed	Mar-95
MD9	Active straws	6 straws in up to 5 sections each	Meltdown passage, Nettlebed	Mar-96
OB1	Acidified water sample	125 ml for ICPMS	Crystal pool, Oubliette oxbow, Nettlebed	Oct-95
OB2	Water sample	125 ml for stable isotope analysis	Crystal pool, Oubliette oxbow, Nettlebed	May-95
OB3	Pool Crystals	Handfull of medium crystals from pool wall	Oubliette oxbow, Nettlebed	Mar-95
OB4	Stalactites	2* 15cm white.	Oubliette oxbow, Nettlebed	Mar-95
PR1	Acidified water sample	125 ml for ICPMS	Pearse resurgence water	Nov-95
PR2	Water sample	125 ml for stable isotope analysis	Pearse resurgence water	Aug-95
PV1	Straw fragments	Many short broken straws	Portalverst to Honking Holes, Nettlebed	Mar-95
RK1	Stalagmite	White, 20cm*10cm diameter at base	Rockfall K, Nettlebed	Mar-95
SW1	Acidified water sample	1 litre for U-series analysis	Rimstone pool, route to spillway, Nettlebed	Apr-95
SW2	Acidified water sample	125 ml for ICPMS	Rimstone pool, route to spillway, Nettlebed	Dec-95
SW3	Pool Crystals	Handfull of medium crystals from pool wall	Rimstone pools, route to Spillway, Nettlebed	Mar-95
SW4	Water sample	125 ml for stable isotope analysis	Rimstone pool, route to spillway, Nettlebed	Jul-95
SW5	Micro-crystaline flowstone fragments	Grey calcite, grown on flagging tape	Rimstone pools, route to Spillway, Nettlebed	Mar-95
SW6	Shawl fragments	Small pieces of mini-shawls, from white flow	Rimstone pools, route to Spillway, Nettlebed	Mar-95

Appendix 3. U-series Data for Mt Arthur samples

See text of chapter 4 for sample details, and chapter 5 for unit definitions.

Sample	Date run	Weight (g)	del 234U(0)	±del 234U(0)	U(ppm)	±U(ppm)	(230Th/ 238U)act	±(230Th/ 238U)act	(234U/ 238U)act	±(234U/ 238U)act	Age (yr)	±Age (yr)	del 234U(T)	±del 234U(T)	(230Th/ 232Th)act
ED1A1	Sep-96	3.5191	246.4	9.9	0.07298	0.00059	0.0863	0.0025	1.2464	0.0099	7787	245	251.9	9.8	15
ED1A2	Sep-96	5.0844	225.3	29.6	0.06833	0.00229	0.1704	0.0093	1.2253	0.0296	16216	1034	235.9	30.2	22
ED1A3	Sep-96	4.0852	183.8	6.5	0.01975	0.00004	0.5956	0.0121	1.1838	0.0065	74391	2193	227.0	8.0	99
ED1A4	Sep-96	4.6345	178.2	5.1	0.04004	0.00007	0.5833	0.0144	1.1782	0.0051	72777	2522	219.0	6.1	42
ED1A5	Sep-96	3.4058	98.5	5.4	0.06192	0.00028	0.5688	0.0092	1.0985	0.0054	78251	1937	122.9	6.4	145
ED1A6	Sep-96	4.5082	221.1	7.6	0.02263	0.00009	0.6945	0.0279	1.2211	0.0076	88530	5454	284.1	9.7	595
HS1.2	Nov-94	2.4058	173.5	12.6	0.02178		0.4526	0.0217	1.1735	0.0126	52279	3191	201.2	14.4	85
HS1.4a2	Feb-95	5.3126	99.7	3.3	0.02834		0.6966	0.0051	1.0997	0.0033	106818	1419	135.0	4.2	18
HS1.6	Nov-94	3.0658	99.3	7.6	0.04827		0.8562	0.0295	1.0993	0.0076	157626	12172	155.2	11.6	11
HS2.2	Nov-94	1.8407	120.0	9.2	0.04095		0.7674	0.0284	1.1200	0.0092	121845	8314	169.5	12.5	15
HS3.2a1	Feb-95	4.1376	111.2	5.9	0.03155	0.00012									
MD1.2c1	Feb-95	4.7564	349.9	3.4	0.00011		0.3739	0.0037	1.3499	0.0034	34756	412	386.1	3.5	91
MD10A1	Sep-96	6.0377	362.4	2.0	0.08390	0.00007	0.1385	0.0013	1.3624	0.0020	11609	112	374.5	1.9	170
MD10A2	Sep-96	4.3416	297.9	2.3	0.08300	0.00005	0.5604	0.0048	1.2979	0.0023	59968	686	353.1	2.6	14
MD10A3	Sep-96	5.5560	292.4	2.0	0.08492	0.00003	0.5735	0.0057	1.2924	0.0020	62175	822	348.8	2.3	31
MD2.2a1	Feb-95	5.1803	397.2	3.2	0.08589		0.2357	0.0047	1.3972	0.0032	19922	433	420.3	3.5	13
MD2.4a1	Feb-95	3.1693	346.2	2.0	0.09717		0.3868	0.0121	1.3462	0.0020	36282	1337	383.7	2.5	70
MD3.11c2	May-95	4.8731	375.7	2.5	0.10690		0.3453	0.0043	1.3757	0.0025	31012	444	410.2	2.6	85
MD3.15a1	May-95	2.1901	297.6	3.9	0.04285		0.5895	0.0436	1.2976	0.0039	64110	6301	356.9	7.3	22
MD3A1	Nov-95	7.0729	370.0	43.9	0.05200		0.0665	0.0025	1.3700	0.0439	5401	276	375.7	43.8	82
MD3A10	Nov-95	3.6479	405.2	5.1	0.11318		0.2438	0.0203	1.4052	0.0051	20533	1871	429.5	5.5	103
MD3A11	May-96	4.1266	386.5	56.7	0.10623	0.00648	0.3128	0.0207	1.3865	0.0567	27469	2453	417.7	56.4	173
MD3A13	May-96														
MD3A19	May-96	4.3393	413.0	5.0	0.09193	0.00024	0.1912	0.0015	1.4130	0.0050	15699	142	431.8	5.1	193
MD3a2	Aug-95	4.7720	321.8	37.6											
MD3A26	May-96	2.8139	396.8	7.0	0.09177	0.00047									
MD3A30	May-96	3.6930	358.2	4.0	0.08171	0.00019	0.5170	0.2339	1.3582	0.0040	50904	29126	413.8	33.4	641
MD3a4	Dec-95														
MD3A5	Nov-95	6.7475	354.9	4.1	0.04854		*0.1082*	*0.0090*	1.3549	*0.0041*	9018	781	364.1	4.2	10
MD3A6	Nov-95	4.2301	362.0	7.0	0.09143		0.1359	0.0131	1.3620	0.0070	11382	1150	373.8	7.0	564
MD3A7	Nov-95	3.3604	409.5	12.9	0.11333		0.1695	0.0100	1.4095	0.0129	13850	885	425.9	12.6	177
MD3A8	Nov-95	4.7110	401.0	24.0	0.10466		0.2353	0.1015	1.4010	0.0240	19824	9287	424.2	27.7	12
MD3A9	Nov-95	4.8313	402.1	6.6	0.08139		0.1760	0.0036	1.4021	0.0066	14499	320	419.0	6.5	260
MD8.7c2	Dec-95	2.5717	350.5	3.5	0.08542										
OB3.1		4.4621	130.1	1.2	0.13685	0.00006	0.0180	0.0132	1.1301	0.0012	1745	1295	130.7	1.3	
RK1.2	May-95	2.1584	-36.3	2.0	0.36590		0.0158	0.0007	0.9637	0.0020	1800	83	-36.5	2.0	177

Appendix 4. YB1 standard age determinations

U-series data for repeat measurements of the YB1 speleothem standard, by J. Hellstrom (JCH) and J. Desmarchelier (JD). See text of chapter 5 for unit definitions.

Sample	Date run	Del 234U	±del 234U	U (ppm)	(230 Th/ 238U) act	±(230 Th/ 238U) act	(234 U/ 238U) act	Age (yr)	±Age(yr)	(230 Th/ 232Th)Act
YB1 17/8/96 (JCH)	Sep-96	744	2	0.115	0.429	0.003	1.744	30059	263	399
YB1 9/6/96-1(JCH)	Jun-96	745	18	0.116						
YB1 9/6/96-2(JCH)	Jun-96	752	10	0.113						
YB1 9/6/96-3(JCH)	Jun-96	747	8	0.114						
YB1 9/6/96-4(JCH)	Jun-96	742	10	0.113						
YB-1 STD (JD)	Sep-96	757	4	0.113	0.435	0.017	1.758	30255	1374	286
YB1-STD-JD#4	Jun-97	751	5	0.145	0.438	0.008	1.751	30665	664	445
YB1-STD-JD#5	Jul-97	753	3	0.153	0.429	0.006	1.753	29920	496	237
YB1-STD-JD#8	Nov-97	751	3	0.153	0.416	0.018	1.751	28959	1390	357
Average of all samples		749		0.126	0.429		1.752	29972		345